



## **Phase II Report: Investigation of the Wind Resistance of Asphalt Shingle Roof Coverings**

**Project Principal Investigator:  
Forrest J. Masters, Ph.D., P.E. (FL)**

This material is based upon work supported by the U.S. Department of Homeland Security under U.S. Department of Energy Interagency Agreement 43WT10301. The views and conclusions contained in this document are those of the authors and should not be interpreted as necessarily representing the official policies, either expressed or implied, of the U.S. Department of Homeland Security.

**SERRI Project:  
Investigation of the Wind Resistance of  
Asphalt Shingle Roof Coverings**

Authors

*Craig R. Dixon, Ph.D. Candidate, Department of Civil and Coastal Engineering  
Forrest J. Masters, Ph.D., P.E. (FL), Associate Professor of Civil and Coastal Engineering  
David O. Prevatt, Ph.D., P.E. (MA), Assistant Professor of Civil and Coastal Engineering  
Kurtis R. Gurley, Ph.D., Associate Professor of Civil and Coastal Engineering*



Date Published:  
June 16, 2013

Prepared for  
U.S. Department of Homeland Security  
under U.S. Department of Energy Interagency Agreement 43WT10301

Prepared by  
OAK RIDGE NATIONAL LABORATORY  
Oak Ridge, Tennessee 37831-6283  
managed by  
UT-BATTELLE, LLC  
for the  
U.S. DEPARTMENT OF ENERGY  
under contract DE-AC05-00OR22725



## **ACKNOWLEDGEMENTS**

This research was funded by the Southeast Region Research Initiative (SERRI), which is managed by Oak Ridge National Laboratory for the U.S. Department of Homeland Security. Additional support was provided by the Florida Building Commission (FBC) through the State of Florida Department of Business and Professional Regulation. The authors would like to thank the program managers from both programs, Dr. Ben Thomas (SERRI), Mr. Rick Dixon (FBC) and Mr. Mo Modani (FBC), for their gracious assistance. The authors would also like to extend their appreciation to the industry and government stakeholders that served on the oversight committee and provided valuable feedback.

Any opinions, findings, and conclusions or recommendations expressed in this paper are those of the authors and do not necessarily reflect the views of the sponsors, partners and contributors.

# CONTENTS

ACKNOWLEDGEMENTS.....	v
LIST OF FIGURES.....	ix
LIST OF TABLES.....	xvii
ACRONYMS.....	xx
SOUTHEAST RESEARCH REGION RESEARCH INITIATIVE .....	xxiii
EXECUTIVE SUMMARY .....	xxv
1. INTRODUCTION.....	1
1.1 Asphalt Shingle Roof Systems .....	1
1.2 Asphalt Shingle Wind Test Standards.....	1
1.3 Project Overview.....	1
1.4 Project Timeline .....	4
1.5 Public Dissemination.....	4
1.6 Summary .....	5
2. AGING EFFECTS ON ASPHALT SHINGLE WIND RESISTANCE.....	6
2.1 Introduction.....	6
2.2 Wind Load Resistance of Heat Aged ASTM D7158 Class H Three-Tab Asphalt Shingles .....	7
2.2.1 Introduction .....	7
2.2.2 Experiment Overview.....	7
2.2.3 Results.....	10
2.3 Wind Load Resistance of ASTM D7158 Class H Three-Tab Asphalt Shingles Exposed to Cycles of Heat, Ultraviolet Light, and Water Spray.....	33
2.3.1 Introduction .....	33
2.3.2 Experimental Procedure.....	33
2.3.3 Results.....	37
2.3.4 Findings .....	43
2.4 Wind Load Resistance of Naturally-Aged Asphalt Shingles .....	44
2.4.1 Introduction .....	44
2.4.2 Portable Mechanical Uplift Apparatus.....	45
2.4.3 Experimental Procedure.....	45
2.4.4 Results.....	48
2.4.5 Findings .....	51

2.4.6	Future Work .....	52
2.5	Survey of Existing Asphalt Shingle Roofs for Unsealed Asphalt Shingles.....	53
2.5.1	Introduction.....	53
2.5.2	Survey Procedure.....	54
2.5.3	Analysis Procedures .....	56
2.5.4	Results .....	57
2.5.5	Findings.....	68
2.5.6	Future Work .....	70
3.	ASSESSMENT OF THE ASPHALT SHINGLE WIND LOAD MODEL.....	71
3.1	Introduction .....	71
3.2	Characterization of Velocity above the Roof Plane .....	76
3.2.1	Model-Scale Measurement of Near Roof Surface Wind Flow .....	76
3.2.2	Full-Scale Measurement of Near Roof Surface Wind Flow .....	77
3.2.3	Findings and Recommendations .....	79
3.3	Validation and Extension of the Shingle Wind Uplift Model.....	82
3.3.1	Overview.....	82
3.3.2	Experimental Methods.....	82
3.3.3	Preliminary Results .....	97
3.3.4	Preliminary Findings.....	123
4.	SYSTEM-LEVEL WIND RESISTANCE OF ASPHALT SHINGLES .....	125
4.1	Introduction .....	125
4.2	IBHS Research Center.....	126
4.3	Experimental Methods .....	128
4.3.1	Experiment Overview .....	128
4.3.2	Construction of Asphalt Shingle Roof Specimens .....	130
4.3.3	Conditioning Phase Temperature Profiles.....	134
4.3.4	Base Structure.....	137
4.3.5	Installation of Asphalt Shingle Roof Specimens.....	139
4.3.6	Test Sequence Procedure .....	141
4.4	Results.....	147
4.4.1	Field, Eave, and Rake Shingle Performance.....	147
4.4.2	Hip and Ridge Shingle Performance.....	161
4.4.3	Estimated Roof Repair Costs.....	168

4.5 Findings and Recommendations .....	173
5. REFERENCES .....	178
APPENDIX A. SUMMARY OF MEASURED WIND FORCES .....	A-1
APPENDIX B. APPRAISAL OF ROOF SPECIMENS TESTED IN THE IBHS RESEARCH CENTER .....	B-1

## LIST OF FIGURES

Fig. 1. UTM used for ASTM D6381 mechanical uplift testing.....	9
Fig. 2. (a) ASTM D6381 Procedure A and (b) ASTM D6381 Procedure B mechanical uplift testing.....	9
Fig. 3. TT-101 mean ( $\pm$ 95% confidence interval) ASTM D6381 mechanical uplift resistance versus thermal aging time.....	12
Fig. 4. TT-102 mean ( $\pm$ 95% confidence interval) ASTM D6381 mechanical uplift resistance versus thermal aging time.....	14
Fig. 5. TT-103 mean ( $\pm$ 95% confidence interval) ASTM D6381 mechanical uplift resistance versus thermal aging time.....	16
Fig. 6. Comparison of TT-101, -102, and -103 mean ( $\pm$ 95% confidence intervals) ASTM D6381 Procedure A mechanical uplift resistance versus thermal aging time.....	18
Fig. 7. Scatterplot comparing TT-103's ASTM D6381 Procedure A mechanical uplift resistance results versus the estimated sealant strip surface area of each ASTM D6381 Procedure A specimen.....	19
Fig. 8. Comparison of TT-101, -102, and -103 mean ( $\pm$ 95% confidence interval) ASTM D6381 Procedure B mechanical uplift resistance versus thermal aging time. ....	21
Fig. 9. Uplift forces generated on an asphalt shingle (Figure: ASTM D7158).....	23
Fig. 10. Mean ASTM D7158 total uplift resistance versus thermal aging time. Note: TT-102's manufacturer did not provide its product's ASTM D7158 uplift coefficients, therefore, TT-101's ASTM D7158 uplift coefficients were used to develop the total load equation for TT-102.....	25
Fig. 11. Cohesive failure in the adherend.....	26
Fig. 12. Adhesive failure mode. ....	26
Fig. 13. Combined (mixed-modal). ....	27
Fig. 14. Distribution of failure modes versus thermal aging time for TT-101 – Procedure A.	29
Fig. 15. Distribution of failure modes versus thermal aging time for TT-101 – Procedure B.	29
Fig. 16. Distribution of failure modes versus thermal aging time for TT-102 – Procedure A.	30
Fig. 17. Distribution of failure modes versus thermal aging time for TT-102 – Procedure B.	30
Fig. 18. Distribution of failure modes versus thermal aging time for TT-103 – Procedure A.	31
Fig. 19. Distribution of failure modes versus thermal aging time for TT-103 – Procedure B.	31
Figure 20. Test interval schedule for Heat, Ultraviolet Light and Water Spray experiment. .	33
Fig. 21. Exterior view of the accelerated aging chamber.....	34
Fig. 22. Interior view of the accelerated aging chamber. ....	35
Fig. 23. Distribution of irradiance output from UVA 340 lamps along the centerline of the accelerated aging chamber. ....	36
Fig. 24. Temperature time history of one aging cycle with T = 0-300 minutes as heat and ultraviolet light followed by 15 minutes of water spray.....	37
Fig. 25. TT-101 mean ( $\pm$ 95% confidence interval) ASTM D6381 mechanical uplift resistance for UV+Heat+Water and thermal aging versus accelerated aging time. ....	38

Fig. 26. TT-102 mean ( $\pm$ 95% confidence interval) ASTM D6381 mechanical uplift resistance for UV+Heat+Water and thermal aging versus accelerated aging time.....	40
Fig. 27. Comparison of ASTM D7158 mean total uplift resistance between Thermal and UV+Heat+Water Spray accelerated aging regimes vs. accelerated aged time. ....	43
Fig. 28. UF's custom Portable Mechanical Uplift Apparatus capable of performing in-situ ASTM D6381 mechanical uplift tests (controlling computer not shown in figure).....	45
Fig. 29. Test specimens prepared for in-situ ASTM D6381 mechanical uplift testing (a) Procedure A specimen and (b) Procedure B specimen.....	46
Fig. 30. The Portable Test Apparatus performing in-situ ASTM D6381 mechanical uplift tests: (a) Procedure A and (b) Procedure B. ....	47
Fig. 31. The Portable Test Apparatus performing in-situ ASTM D6381 Procedure A mechanical uplift tests.....	47
Fig. 32. Example of failure modes for mechanically uplifted shingles: (a) cohesive failure in the adherend (ORM-01) and (b) combined cohesive failures in the sealant and adherend (ORG-01).....	50
Fig. 33. Distribution of failure modes for in-situ ASTM D6381 mechanical uplift tests. ....	51
Fig. 34. Patterns of partially unsealed asphalt shingles reported in Marshall et al. (2010). ...	54
Fig. 35. Locations of the unsealed asphalt shingle surveys conducted in Florida. ....	54
Fig. 36. UF investigators conducting an unsealed shingle survey: (a) unsealed field shingle and (b) unsealed ridge shingle.....	55
Fig. 37. Example of unsealing patterns for (a) racked three-tab system with 86% unsealing and (b) diagonally installed laminate system with 39% unsealing.....	58
Fig. 38. Example of unsealing patterns for (a) diagonally installed laminate system with 17% unsealing and (b) diagonally installed laminate system with 1% unsealing. ....	59
Fig. 39. Typical unsealing pattern of three-tab shingles that are vertically installed.....	60
Fig. 40. Typical unsealing pattern of laminate shingles showing a transition between diagonal directions. ....	60
Fig. 41. All unsealed shingles near the end joint failed cohesively within the sealant strip, suggesting that shingles were previously adhered.....	61
Fig. 42. Percent of unsealed shingle strips located in the field of the roof (hip and ridge shingles not included) verses roof age at the time of investigation.....	64
Fig. 43. Boxplot of unsealed shingle strips located in the field of the roof verses roof age at the time of investigation.....	64
Fig. 44. Typical partially unsealed ridge and hip shingle conditions: (a) fully unsealed ridge shingle due to lack of sealant strip below cap and (b) poor adhesion on edges of shingle....	66
Fig. 45. Percent of partially unsealed cap shingles verses roof age at the time of investigation. (Note: 100% unsealed ridge shingles represent a lack of sealant strips below the caps).....	68
Fig. 46. Wind uplift forces on asphalt shingles are generated from the separation of wind over the shingle's leading edge.....	72
Fig. 47. ASTM D7158 test deck arrangement and pressure tap layout. (1 in = 25.4 mm).....	73

Fig. 48. (a) Particle Image Velocimetry test setup and (b) downwind view of Particle Image Velocimetry test setup components.....	76
Fig. 49. (a) Aerial view of the test building and (b) roof plan with near roof surface wind measurement locations and experiments wind directions shown.....	77
Fig. 50. Wind velocity and direction measured at the eave height of the subject home. ....	78
Fig. 51. Particle Image Velocimetry measured “speed-up” factor ( $x / U$ ) compared to Peterka et al. (1997) factor ( $x / U^*$ ).....	79
Fig. 52. Comparison of peak speed-up ( $x / U$ ) versus mean speed-up ( $X / U$ ) over the full-scale building roof tested in the IBHS Research Center and wind tunnel modeling results performed by Peterka et al. (1997). ....	79
Fig. 53. Particle Image Velocimetry measured mean velocity field (top plot) and measured peak velocity field (bottom plot). ....	80
Fig. 54. Low-pass filtered (10 Hz) velocity record of Location 57 compared to approach flow measured at eave height.....	81
Fig. 55. Rendering of the Dynamic Flow Simulator componentry.....	83
Fig. 56. Dynamic Flow Simulator, as constructed.....	83
Fig. 57. Test specimen in the Dynamic Flow Simulator test section with upstream turbulence grid shown.....	84
Fig. 58. a) Six-axis load cell measured: b) three forces and c) three moments. ....	85
Fig. 59. TFI Cobra Probe measuring wind velocity inside the DFS during testing.....	86
Fig. 60. Plan view of the test specimens: a) three-tab and b) laminate asphalt shingle system. (1 in = 25.4 mm) .....	87
Fig. 61. Wood test deck with laminate test shingle installed (light colored shingle).....	88
Fig. 62. Plan view, 3-tab asphalt shingle with six fasteners per strip. (1 in = 25.4 mm) .....	89
Fig. 63. Plan view, laminate shingle with six fasteners per strip. (1 in = 25.4 mm).....	89
Fig. 64. Installation and wind test procedure. (Note: Three-tab shingle system shown. Laminate shingle system follows same procedure).....	91
Fig. 65. Load cell measurement locations for three-tab, six fastener test shingle (L1-R2 = sealant strip measurement) (1 in = 25.4 mm).....	92
Fig. 66. Load cell measurement locations for laminate, six fastener test shingle (L, M, R = sealant strip measurement) (1 in = 25.4 mm).....	92
Fig. 67. Connection detail to measure the six-axis wind loads on an asphalt shingle’s tab sealant. Note: A differential pressure was measured in the test section causing the plastic sheeting to displace upwards and imparting a load on the load cell. This inappropriate load was experimentally estimated and described in further detail in Section 3.3.3.3. ....	93
Fig. 68. Epoxied steel flat bars on (a) underside of three-tab test shingle and (b) underside of laminate test shingle.....	93
Fig. 69. Laminate test specimen deck and test shingle installation procedure: (a) lower deck with load cells, (b) closer view of load cell arrangement, (c) top deck with cutout for load cells shown and (d) test shingle placed over the cutout to produce a complete test specimen. ....	94

Fig. 70. Load cell locations for a) three-tab system and b) laminate system. (1 in = 2.54 mm) The load cells were placed at the center of each measurement location (black nodes along the sealant strip on figure).....	95
Fig. 71. Wind azimuths.....	96
Fig. 72. Wind test sequence for each wind angle of attack.....	96
Fig. 73. Vertical profile of mean longitudinal wind speeds. Note: wind speeds were adjusted during testing to match target wind speeds measured at 25 mm (1 in) above the shingle surface.....	98
Fig. 74. Lateral mean wind speed profiles for High (red) and Low (black) Wind Levels on three-tab specimens. ....	99
Fig. 75. Lateral mean wind speed profiles for High (red) and Low (black) Wind Levels on laminate specimens.....	99
Fig. 76. Example wind speed time-history for Low Wind Level test. ....	100
Fig. 77. Example wind speed time-history for High Wind Level test. ....	101
Fig. 78. Force time-history record for Measurement Location C2 on fully sealed three-tab Test Shingle Specimen 3 - 90° wind azimuth - High Wind Level. ....	102
Fig. 79. Example of temperature effects on load cell output - force time-history record for Measurement Location C2 on fully sealed three-tab Test Shingle Specimen 3 - 45° wind azimuth - High Wind Level. ....	103
Fig. 80. In-plane force orientation for six-axis load cells. ....	104
Fig. 81. Connection detail for specimen's sealant strip to six-axis load cell. ....	107
Fig. 82. Static pressure test specimens: (a) laminate, (b) three-tab, and (c) no shingle. ....	107
Fig. 83. Static pressure test setup. ....	108
Fig. 84. Force measurements of six-axis load cell attached to laminate shingle specimen in response to static pressure.....	109
Fig. 85. Pressure tap layout for static pressure test on laminate shingles.....	110
Fig. 86. Measured static pressures on top and bottom surface of laminate shingle. (1 psf = 47.8 Pa).....	111
Fig. 87. Mean uplift force coefficient for laminate shingle specimens versus wind azimuth. Note: blue dashed line is uplift component only. ....	113
Fig. 88. Progressive unsealing observed on partially unsealed laminate shingle specimen. ....	116
Fig. 89. Mean total force coefficient for laminate shingle specimens versus wind azimuth. ....	116
Fig. 90. Mean uplift force coefficient for three-tab specimens versus wind azimuth.....	118
Fig. 91. Lifting of the unsealed portion of a three-tab specimen increased the uplift force on the sealed portion of the tab. ....	120
Fig. 92. Mean total force coefficient for three-tab specimens versus wind azimuth. ....	121
Fig. 93. Post-storm observations of shingle roof systems: (a) rake edge shingle blow off [Photo from FEMA (2011)], (b) hip shingle blow off [Photo from FEMA (2011)], (c) rake shingle and underlayment blow off [Photo from FEMA (2005a)], and (d) eave shingle blow off [Photo from FEMA (2009)].....	126

Fig. 94. Google Earth image of the IBHS Research Center with shingle roof specimens located at conditioning site (shown on right)..... 127

Fig. 95. IBHS Research Center (a) exterior view showing the fan arrays and (b) interior of test chamber with test specimen installed on the base structure..... 127

Fig. 96. Test building with hip roof specimen. The blue marks note the location of partially/fully unsealed shingles. .... 129

Fig. 97. Test building with gable roof specimen. .... 130

Fig. 98. Aerial view of the completed asphalt shingle roof sections at the IBHS Research Center. The roofs were located at this field site throughout their 11 month conditioning phase..... 131

Fig. 99. (a) - (c) Construction of the mono-slope gable roof sections. (d) Completed mono-slope gable roof section..... 132

Fig. 100. (a) - (c) Construction of the hip roof sections. (d) Completed hip roof section..... 133

Fig. 101. (a) Omega copper-constantan thermocouple was sandwiched between two shingles and recorded thermal loads encountered during conditioning period. (b) Thermocouple data loggers were installed in PVC housing and secured to roof trusses for weather protection..... 135

Fig. 102. Empirical cumulative distribution function (CDF) for measured roof temperatures during the condition phase. .... 136

Fig. 103. Example temperature time history generated from thermocouples embedded between shingles during the conditioning phase. The peak observed temperature during the conditioning phase is shown. .... 137

Fig. 104. The base structure construction consisted of (a) modifications to the existing steel structural framing, (b) installation of a permanent gable end 6:12 roof and (c) installation of wood-framed exterior walls secured to the steel frame..... 138

Fig. 105. Hip roof installation procedure: the roof was (a) carried from the conditioning site with crane and rigging, then (b) driven inside the test chamber and (c) hoisted onto the base structure. A survey for the presence of unsealed shingles (following ERP #6) was conducted before testing (d) and blue painter’s tape was used to mark the location of unsealed shingles. .... 140

Fig. 106. Similar to the hip roof sections, each mono-slope gable section was (a) individually installed on the base structure to form a (b) complete gable roof section..... 141

Fig. 107. Wind directions for (a) - (c) gable roof sections and (d) through (f) hip roof sections. .... 142

Fig. 108. Test sequence flowchart. (Note: Exposure C wind profile for all wind tests)..... 142

Fig. 109. Wind monitor (shown in red circle)..... 143

Fig. 110. Example wind speed time history (first 200 s) for Wind Levels 1-3 used for LAM-201 – Roofs 1-3..... 144

Fig. 111. Example wind speed time history (first 200 s) for Wind Levels 1-3 used for LAM-201 – Roofs 4-6, LAM-202 – Roofs 1-6, and TT-201 – Roofs 1-5. .... 145

Fig. 112. Wind speed time history for Wind Level 4. .... 146

Fig. 113. Pull-through of the starter strip around fasteners on LAM-201 – Roof 6. The fasteners were placed approximately 102 mm (4 in) from the butt edge of the starter strip. .... 150

Fig. 114. Pull-through of the starter strip around fasteners on LAM-201 – Roof 2. The fasteners were placed approximately 127 mm (5 in) from the butt edge of the starter strip. .... 150

Fig. 115. Pre-test roof survey of LAM-202 – Roof 2 found five partially unsealed shingles along the windward rake. The blue tape was placed on the leading edge where shingles were found unsealed prior to the wind testing. The cause of the partial unseal is unknown. .... 151

Fig. 116. Progressive lifting of pre-test unsealed shingles and eave near windward edge for LAM-202 – Roof 2..... 152

Fig. 117. Crack on pre-test unsealed shingle caused by the shingle lifting during wind testing..... 152

Fig. 118. Pre-wind test unsealed shingles (marked with blue tape) for LAM-202 – Roof 3 (a) windward rake and (b) interior edge of shingle specimen. .... 153

Fig. 119. Pre-wind test unsealed rake shingle with an adhesive failure mode – LAM-202 – Roof 3. .... 153

Fig. 120. Shingle with 711 mm (28 in) of unsealed length (a) located on the third course on the interior of the roof section. (b) The non-sealing was caused by a transfer of the release tape onto the sealant strip. This shingle remained on the roof during wind testing and no surface cracks were observed following the test. .... 154

Fig. 121. LAM-202 – Roof 3 pre-test unsealed shingles: (a) loss of shingle during wind tests, (b) and (c) pre-test unsealed shingles that lifted during wind testing, (d) crack formed on shingle surface due to pre-test unsealed shingle lifting during wind test..... 155

Fig. 122. Pull-through of the shingle system’s eave starter strips around the fasteners on LAM-202 – Roof 2. The fasteners were placed approximately 127 mm (5 in) from the butt edge of the starter strip. .... 156

Fig. 123. TT-201 – Roof 5 pre-test unsealing was caused by a cohesive failure in the tab sealant for both (a) partially and (b) fully unsealed shingles. .... 157

Fig. 124. Unsealed shingles found on TT-201 – Roof 5 prior to wind testing. Blue marks denote the location of full/partially unsealed shingle. .... 158

Fig. 125. Progression of shingles lifting, folding, and blowing off during wind testing of TT-201 – Roof 5. .... 158

Fig. 126. Post-Level 4 wind test photo of TT-201 – Roof 5..... 159

Fig. 127. TT-201 – Roof 5 (a) blow off of shingles caused by a group of pre-test unsealed shingles. (b) Horizontal crack formed by lifting of the unsealed tab during wind testing. . 159

Fig. 128. Progression of shingle blow off for TT-201 – Roof 3. Fasteners placed further from the roof’s edges than recommended by ARMA (2006)..... 160

Fig. 129. TT-201 – Roof 3 with blown off shingles caused by eave and rake shingles that pulled-through their edge fasteners. Note: The location of fasteners was not within ARMA (2006) specification. .... 160

Fig. 130. Example of partially unsealed hip shingles (marked with blue tape): (a) LAM-201 – Roof 6 (10% unsealed) and (b) LAM-202 – Roof 4 (31 % unsealed) ..... 163

Fig. 131. Example of unsealed hip shingle on LAM-201 – Roof 5. The shingle was unadhered at the edge of the hip shingle and adhered closer to the center of the hip line. (Note: this photo was taken after wind testing.) ..... 163

Fig. 132. Progression of hip shingle blow off through the wind test sequence for specimen LAM-201 – Roof 4. .... 165

Fig. 133. Typical hip shingle blow off for 0° wind azimuth (photo of LAM-201 – Roof 4 specimen). .... 166

Fig. 134. Typical hip shingle blow off for 45° wind azimuth (photo of LAM-202 – Roof 5 specimen). .... 166

Fig. 135. Typical hip shingle blow off for 90° wind azimuth (photo of LAM-201 – Roof 6 specimen). .... 167

Fig. 136. Underlayment wrapped over hip line: (a) likely water-resistant (LAM-201 – Roof 4) and (b) torn underlayment likely due to roof installers cutting field shingles at the hip line causing exposure of hip line to moisture intrusion (LAM-202 – Roof 6). .... 167

Fig. 137. Pull-through eave starter strip shingles at fasteners causing cracking to the surface of first and second shingle courses (LAM-201 – Roof 6). .... 169

Fig. 138. Estimated cost of roof repairs in Miami, FL versus wind direction. (Costs estimated using Xactware 2012 software and October 2012 price list) ..... 172

Fig. 139. (a) Shingle blow off obtained from system-level performance test caused by pre-test non-bonded shingles and (b) blown off shingles observed by FEMA after Hurricane Charley [Photo from FEMA (2011)] ..... 174

Fig. 140. (a) Shingle blow off observed during System-Level wind tests caused by pull-through of edge details at their fasteners. (b) Roof from FEMA post-storm assessment teams after Hurricane Katrina [Photo from FEMA (2011)]. .... 175

Fig. 141. FEMA P-499 recommended installation method for rake details. Further work is necessary to define wind resistance of this method and to ensure long-term performance of asphalt roof cement. [Figure from FEMA (2012)] ..... 176

Fig. 142. FEMA P-499 Technical Fact Sheet 7.3 – new construction installation guideline for enhanced hip and ridge shingle wind resistance. Further work is necessary to define wind resistance of this method and to ensure long term performance of asphalt roof cement. [Figure from FEMA (2012)] ..... 177



**LIST OF TABLES**

Table 1. Oversight Committee ..... 3

Table 2. Test interval schedule for thermal aging experiment..... 8

Table 3. Summary of results and comparison statistics – TT-101 – Procedure A..... 12

Table 4. Summary of results and comparison statistics – TT-101 – Procedure B ..... 13

Table 5. Summary of results and comparison statistics – TT-102 – Procedure A..... 14

Table 6. Summary of results and comparison statistics – TT-102 – Procedure B ..... 15

Table 7. Summary of results and comparison statistics – TT-103 – Procedure A..... 16

Table 8. Summary of results and comparison statistics – TT-103 – Procedure B ..... 17

Table 9. Statistical comparison of ASTM D6381 Procedure A mean uplift resistance data.... 20

Table 10. Mean surface area coverage of the sealant strip for ASTM D6381 Procedure A specimens..... 20

Table 11. Statistical comparison of ASTM D6381 Procedure B mean uplift resistance data... 22

Table 12. TT-101 ASTM D7158 Test Results ..... 23

Table 13. TT-103 ASTM D7158 Test Results ..... 23

Table 14. Comparison statistics for UV + Heat + Water Spray verses Heat only accelerated aging TT-101 – Procedure A..... 39

Table 15. Comparison statistics for UV + Heat + Water Spray verses Heat only accelerated aging TT-101 – Procedure B ..... 39

Table 16. Comparison statistics for UV + Heat + Water Spray verses Heat only accelerated aging TT-102 – Procedure A..... 41

Table 17. Comparison statistics for UV + Heat + Water Spray verses Heat only accelerated aging TT-102 – Procedure B ..... 41

Table 18. ASTM D7158 mean total wind uplift resistance for TT-101 and TT-102 subjected to UV+Heat+Water and Thermal aging methods compared to ASTM D7158 Class H requirement ..... 42

Table 19. Summary of results for in-situ ASTM D6381 mechanical uplift tests ..... 49

Table 20. Estimated ASTM D7158 total uplift resistances for ORM-02 and ORM-03..... 49

Table 21. City locations for each identification code ..... 57

Table 22. Summary of results from unsealed asphalt shingle survey – unsealed field shingles ..... 63

Table 23. Statistical comparison between grouped roof ages..... 65

Table 24. Summary of results from unsealed asphalt shingle survey – unsealed ridge and hip shingles ..... 67

Table 25. ASTM D7158 test result from shingle product TT-101 in the Thermal Aging experiment..... 74

Table 26. Six-axis load cell sensing ranges and resolutions..... 85

Table 27. Sealed and partially unsealed asphalt shingle test matrix .....	95
Table 28. Comparison of raw wind speed record vs. filtered wind speed record.....	97
Table 29. ASTM D7158 mean uplift pressure coefficients for laminate and three-tab test shingles.....	105
Table 30. Static pressure in DFS test section 25 mm (1 in) above the test shingle specimen.	106
Table 31. Static pressure induced force measurements normalized by static pressure .....	109
Table 32. Laminate – measured mean uplift (combined).....	114
Table 33. Laminate – measured mean total force (combined).....	117
Table 34. Three-Tab – measured mean uplift force (combined).....	119
Table 35. Three-Tab – measured mean total force (combined).....	122
Table 36. Comparison of measured force coefficients above ASTM D7158 prediction .....	123
Table 37. Asphalt shingle roof specimen test matrix .....	129
Table 38. Summary of recorded asphalt shingle temperatures during the 11 month conditioning phase.....	136
Table 39. Statistical summary for Wind Levels 1-3 used on LAM-201 – Roofs 1-3 .....	144
Table 40. Statistical summary for Wind Levels 1-3 used on LAM-201 – Roofs 4-6, LAM-202 – Roofs 1-6, and TT-201 – Roofs 1-5.....	145
Table 41. Summary of test parameters for Wind Level 4 used on LAM-201 – Roofs 4-6, LAM-202 – Roofs 1-6, and TT-201 – Roofs 1-5.....	146
Table 42. Summary of field, eave, rake, and underlayment wind resistance – LAM-201 and LAM-202.....	148
Table 43. Summary of field, eave, rake, and underlayment wind resistance – TT-201.....	162
Table 44. Summary of ridge and hip shingle pre-test adhesion condition and resulting wind resistance .....	164
Table 45. Summary of estimated repair and replacement costs – LAM-201 and LAM-202 ..	170
Table 46. Summary of estimated repair and replacement costs – TT-201.....	171
Table A-1. Comparison of measured forces versus ASTM D7158 predicted uplift results for Fully Sealed Laminate Specimen 1 .....	A-2
Table A-2. Comparison of measured forces versus ASTM D7158 predicted uplift results for Fully Sealed Laminate Specimen 2 .....	A-3
Table A-3. Comparison of measured forces versus ASTM D7158 predicted uplift results for Fully Sealed Laminate Specimen 3 .....	A-4
Table A-4. Comparison of measured forces versus ASTM D7158 predicted uplift results for Partially Sealed Laminate Specimen 1 .....	A-5
Table A-5. Comparison of measured forces versus ASTM D7158 predicted uplift results for Partially Sealed Laminate Specimen 2 .....	A-6
Table A-6. Comparison of measured forces versus ASTM D7158 predicted uplift results for Partially Sealed Laminate Specimen 3 .....	A-7

Table A-7. Comparison of measured forces versus ASTM D7158 predicted uplift results for Fully Sealed Three-Tab Specimen 1 .....A-8

Table A-8. Comparison of measured forces versus ASTM D7158 predicted uplift results for Fully Sealed Three-Tab Specimen 2 .....A-9

Table A-9. Comparison of measured forces versus ASTM D7158 predicted uplift results for Fully Sealed Three-Tab Specimen 3 .....A-10

Table A-10. Comparison of measured forces versus ASTM D7158 predicted uplift results for Partially Sealed Three-Tab Specimen 1 .....A-11

Table A-11. Comparison of measured forces versus ASTM D7158 predicted uplift results for Partially Sealed Three-Tab Specimen 2 .....A-12

Table A-12. Comparison of measured forces versus ASTM D7158 predicted uplift results for Partially Sealed Three-Tab Specimen 3 .....A-13

Table B-1. Estimated Roof Costs for LAM-201 – Roof 1 (Gable) – Miami, FL ..... B-1

Table B-2. Estimated Roof Costs for LAM-201 – Roof 2 (Gable) – Miami, FL ..... B-1

Table B-3. Estimated Roof Costs for LAM-201 – Roof 3 (Gable) – Miami, FL ..... B-1

Table B-4. Estimated Roof Costs for LAM-201 – Roof 4 (Hip) – Miami, FL ..... B-1

Table B-5. Estimated Roof Costs for LAM-201 – Roof 5 (Hip) – Miami, FL ..... B-2

Table B-6. Estimated Roof Costs for LAM-201 – Roof 6 (Hip) – Miami, FL ..... B-2

Table B-7. Estimated Roof Costs for LAM-202 – Roof 1 (Gable) – Miami, FL ..... B-2

Table B-8. Estimated Roof Costs for LAM-202 – Roof 2 (Gable) – Miami, FL ..... B-3

Table B-9. Estimated Roof Costs for LAM-202 – Roof 3 (Gable) – Miami, FL ..... B-3

Table B-10. Estimated Roof Costs for LAM-202 – Roof 4 (Hip) – Miami, FL ..... B-3

Table B-11. Estimated Roof Costs for LAM-202 – Roof 5 (Hip) – Miami, FL ..... B-4

Table B-12. Estimated Roof Costs for LAM-202 – Roof 6 (Hip) – Miami, FL ..... B-4

Table B-13. Estimated Roof Costs for TT-201 – Roof 1 (Gable) – Miami, FL ..... B-4

Table B-14. Estimated Roof Costs for TT-201 – Roof 2 (Gable) – Miami, FL ..... B-5

Table B-15. Estimated Roof Costs for TT-201 – Roof 3 (Gable) – Miami, FL ..... B-5

Table B-16. Estimated Roof Costs for TT-201 – Roof 4 (Hip) – Miami, FL ..... B-5

Table B-17. Estimated Roof Costs for TT-201 – Roof 5 (Hip) – Miami, FL ..... B-6

## ACRONYMS

ARMA	Asphalt Roofing Manufacturers Association
ASCE	American Society of Civil Engineers
ASTM	ASTM International (formerly the American Society for Testing and Materials)
COV	Coefficient of Variation
CSU	Colorado State University
DAQ	Data Acquisition System
DFS	Dynamic Flow Simulator
ERP	Experimental Research Plan
ESDU	Engineering Science and Data Unit
FBC	Florida Building Commission
FEMA	Federal Emergency Management Agency
IBHS	Insurance Institute for Business & Home Safety
ID	Identification
MAT	FEMA Mitigation Assessment Team
ORNL	Oak Ridge National Laboratory
OSB	Oriented Strand Board
Pa	Pascal

PC	Personal Computer
PLA	Pressure Loading Actuator
PI	Principal Investigator
PIV	Particle Image Velocimetry
PMUA	Portable Mechanical Uplift Apparatus
PVC	Polyvinyl Chloride
RCI	RCI, Inc. (formerly the Roof Consultants Institute)
RICOWI	Roofing Industry Committee on Weather Issues
RMS	Risk Management Solutions
SARA	Saturates, Aromatics, Resins, and Asphaltene
SERRI	Southeast Region Research Initiative
TFI	Turbulent Flow Instrumentation
TI	Turbulence Intensity
TR-PIV	Time-Resolved Particle Image Velocimetry
UF	University of Florida
UL	Underwriters Laboratories
US	United States
UTM	Universal Testing Machine

UV

Ultraviolet

UWO

University of Western Ontario

## **SOUTHEAST REGION RESEARCH INITIATIVE**

In 2006, the U.S. Department of Homeland Security commissioned UT-Battelle at the Oak Ridge National Laboratory (ORNL) to establish and manage a program to develop regional systems and solutions to address homeland security issues that can have national implications. The project, called the Southeast Region Research Initiative (SERRI), is intended to combine science and technology with validated operational approaches to address regionally unique requirements and suggest regional solutions with potential national implications. As a principal activity, SERRI will sponsor university research directed toward important homeland security problems of regional and national interest.

SERRI's regional approach capitalizes on the inherent power resident in the southeastern United States. The project partners, ORNL, the Y-12 National Security Complex, the Savannah River National Laboratory, and a host of regional research universities and industrial partners, are all tightly linked to the full spectrum of regional and national research universities and organizations, thus providing a gateway to cutting-edge science and technology unmatched by any other homeland security organization.

As part of its mission, SERRI supports technology transfer and implementation of innovations based upon SERRI-sponsored research to ensure research results are transitioned to useful products and services available to homeland security responders and practitioners.

For more information on SERRI, go to the SERRI Web site: [www.serri.org](http://www.serri.org).



## EXECUTIVE SUMMARY

### Summary of Findings

Asphalt shingle systems are the most popular roof covering for residential construction, including coastal regions susceptible to hurricanes. These systems are relatively low cost and have been shown to perform well in many environments. Investigations after recent landfalling hurricanes reveal that in some cases, asphalt shingle roofs provided excellent performance, remaining intact and preventing the intrusion of rain water into the living space. These successes are tempered by other cases where wind damaged shingle roofs permitted water intrusion, resulting in significant costs for repair and temporary relocation of the residents.

Asphalt shingle roofing represents over 80% of the residential roofing inventory, and it is likely that the market share for future construction will be similar. The potential for excellent performance demonstrated in recent hurricanes presents an opportunity to dramatically reduce the vulnerability of residential housing to the hurricane hazard. If this excellent performance transitions from the noted success to the rule, the reduced cost of repair, remediation, relocation, and down time would improve the economic sustainability of coastal communities.

The precise mechanisms and contributing factors that result in asphalt shingle loss of resilience in high winds have not been well established. This knowledge gap inhibits the cost effective refinement of product development, installation, maintenance / replacement scheduling, inspection and certification test standards that are necessary to improve the reliability of asphalt shingle roof systems.

This report presents the results of a two-year study on the wind resistance of asphalt shingle roofs. The intention is to bridge the knowledge gap between expected performance based on existing standardized wind resistance test protocols and the actual in-service performance of new and aged asphalt shingle roofs. Seven interrelated experimental research plans were conceived, publicly vetted by outside experts and stakeholders, and carried out using technology customized for these applications. Experiments included: field surveys of real homes to characterize age and weather-related effects on shingle roofing, evaluations of mechanical property transitions during simulated aging experiments, characterization of turbulent airflow near the roof and the resultant loads on shingles, and full-scale testing of asphalt shingle roofs in a large wind tunnel that simulated hurricane wind and rain conditions. The remainder of this summary presents a brief overview of findings.

As wind passes over the shingle roof, uplift forces are produced on the shingle's surface. The sealant strip located near the shingle's leading edge is designed to prevent lifting of the leading edge and provide a path for wind load transfer to the shingle below. The wind load is ultimately transferred to the roof deck via the nails along the back edge of the tab and back edge of the shingle. Additional stress is placed on the nails at the nail-to-shingle interface when the sealant strip does not adhere or becomes unadhered. The upward displacement of the shingle's leading edge on an unadhered shingle causes a deformation that increases the wind load. The integrity of the sealant strip therefore represents a significant contributor to acceptable long term shingle performance in high winds.

The prevalence and spatial patterns of unsealed shingles on existing homes were investigated in this study. An inspection of every shingle on 27 Florida homes revealed

systemic patterns of partially unsealed asphalt shingles. It was observed that the percentage of shingles that were unsealed was correlated to the age of the roof, with fewer occurrences of unsealed sealant strips on newer roofs and more on older roofs. The percentage of shingles with unsealed sealant strips was as high as 79% in old roofing systems. The observed spatial patterns of unsealed shingles in many cases were similar to patterns of blown off shingles reported in post-hurricane reports. This suggests a strong correlation between the patterns of unsealed shingles and the shingle damage that occurs in high winds. The observed unseal patterns on the 27 inspected homes were not random, but rather the likely result of a systemic issue related to long term weather exposure and the resultant differential shear stresses on the sealant strips.

Shingle products are required by building codes (e.g., Florida Building Code 2010) to pass performance tests prior to being certified for use. These evaluation tests are conducted on new shingle systems, and cannot predict the effects of material degradation over time. The effects of aging / weathering on the uplift capacity of shingles were evaluated in this project via two industry accepted accelerated aging protocols: shingle specimens exposed to heat-only and to heat + ultraviolet light + water spray. Both aging protocols produced statistically significant changes in uplift resistance relative to the non-aged baseline. However, the mean uplift capacities all remained well above their ASTM D7158 wind resistant certification load requirements. Three failure modes were observed on the mechanically uplifted shingles: adhesive, cohesive in the adherend and combined (mixed-modal). An interesting observation from this experiment was the percentage of adhesive failures increased in one manufacturer's product as the shingle aged or its exposure to weathering increased. Furthermore, the two mechanical uplift test procedures produced dissimilar dominant failure modes for each product. This has implications for design of the shingle's composite structure to resist wind throughout its service life, as the in-service failure mode may not be captured during ASTM D6381 mechanical uplift tests.

Wind load modeling on the shingle system was also studied. One model-scale and one full-scale experiment were performed to determine the peak instantaneous gust wind speeds just above the roof surface relative to the mean speed of the wind approaching the building (speed-up ratio). Model and full-scale measurements indicated that the currently specified speed-up ratio of 2.5 is appropriately conservative for shingle design on hip and gable roof structures.

Experiments were also conducted to directly measure the mean wind uplift loads generated along the sealant strip line. This is a refinement to the surface point measurements specified in ASTM D7158. Six-axis load cells were used to measure the wind uplift forces for three wind speeds and five wind azimuths. Results showed that in-plane forces were greater than out-of-plane forces in both laminate and three-tab shingles. The mean total load along a fully sealed shingle strip was greater than predicted by ASTM D7158 in over 25% of the cases. Partially unsealed specimens were also tested because such shingles were observed in the roof survey investigation, and these tests produced loads on three-tab shingles that were greater than those found on fully sealed shingles, whereas partially unsealed laminate shingles were equivalent to fully sealed. The results showed the increased potential of partially unsealed three-tab shingles to further unsealing in wind. An example of this progressive unsealing was observed on one laminate specimen near the unsealed portion of the specimen at the interface between the load cell measurement bar and the shingle's bottom surface. This suggests a stress concentration that causes a progressive unsealing of the sealant strip. These results highlight a potentially important

deficiency within ASTM D7158, as point measurements on the shingle's surface at below design-level wind speeds may not properly characterize wind uplift forces along the shingle's primary wind load path for shingles that are partially unsealed. Additional wind tunnel work is planned to validate these results.

The final component of this research was a wind performance evaluation of laminate and three-tab asphalt shingles at the Insurance Institute for Business and Home Safety (IBHS) Research Center. This work subjected a series of shingled gable and hip roofs to a controlled and repeatable simulated hurricane wind and wind-driven rain environment. Both the building specimens and wind speeds were at full-scale. This study linked pre-storm roof condition, in-storm progression of the roof's condition, and resultant post-storm condition. Performance was compared between one three-tab shingle system and two laminate systems that were installed by a professional roofing contractor on three hip and three gable style roof replicates for each shingle product for a total of eighteen roofs. Post-wind test examination of the roof sections revealed shingle roof installation practices that did not conform to the manufacturer and building code standards set forth in the experimental design. The discussion of results in Section 4 notes where non-conformance occurred.

The roofs were conditioned outdoors for eleven months at the Insurance Institute for Business and Home Safety Research Center in Richburg, South Carolina, followed by testing of each roof specimen installed on a base structure that formed a complete one-story residential building. All tests utilized an open-country boundary layer profile and each test consisted of three 30-minute wind records of increasing magnitude, with the largest peak gust approach wind speed near 64 m/s (120 mph). This was followed by a 17-minute ramp and hold low-turbulence test with peak approach wind speeds also approaching 64 m/s (120 mph). For each shingle product, peak wind speeds were below their ASTM D7158 Class H design-level. Roof inspections conducted prior to each test established the pre-test condition of the shingle's sealant strips, and high-definition video recorded the progression of shingle unsealing or blowoff (if any) throughout testing. Results showed that the roofs having fully-sealed field shingles before testing remained fully-sealed, while roofs with partially and fully-unsealed shingles consistently sustained surface cracking and blow off that frequently impacted adjacent sealed shingles. Lifting of shingles along the roof's eaves and rakes were consistently observed in all three systems, initiated by eave and rake shingle pull-through around fasteners heads that were located further from the roof edge than manufacturers' specifications (i.e., installation error). Lifting of the edge shingles was localized in the laminate systems, but propagated to widespread blow off of field shingles in the three-tab specimens. This finding emphasizes the importance of installations performed in accordance with building code requirements and manufacturer recommendations. Hip shingle performance suffered from partially unsealed hip shingles, echoing comments made above and post-hurricane reports. At present, an asphalt shingle's wind resistance is defined at the beginning of the product's life and only addresses shingles installed in the field of the roof, and not the complete system resistance, which includes eave, hip, rake, and ridge shingles. The findings of this experiment highlight the need for shingles to maintain proper adhesion throughout their service-life and the critical role of roof system componentry that extends beyond the evaluation methods in current wind test standards.

## Summary of Critical Recommendations

The following recommendations were developed from the findings of this research and represent the most critical steps on the path towards improving the wind resistance of asphalt shingle roofing.

1. Address the cause and develop retrofit solutions for partially unsealed field shingles  
Partially unsealed field shingle patterns were observed in roof surveys (Section 2.5) and correlate to blow off patterns observed in post-hurricane reports. This indicates that partially unsealed shingles existing on the roof before a wind event may be responsible for in-storm blow off of shingles in the field of the roof. Given the relationship of the roof's age to the quantity of partial unsealed shingles, natural weathering is the most likely source of partial unsealing. Future work should:

- a. Define the precise mechanism(s) causing partial unsealing
- b. Apply the knowledge gained from (a) to improve the long-term adhesion performance of new shingle products
- c. Quantify the extent of this issue on existing roofs in other US climates
- d. Develop durable and reliable retrofit solutions to reseal partially unsealed shingles on existing roofs

2. Address the cause and develop retrofit solutions for partially unsealed hip and ridge shingles

Hip shingles were frequently blown off on the hip roof systems evaluated in the system-level wind tunnel tests (Section 4). Blow off primarily initiated from partially unsealed hip shingles that were discovered prior to wind testing. This partial unsealing was also frequently observed during the roof surveys of existing residential structures. The survey results indicate that hip and ridge shingles have poor adhesion on the downslope edges of their sealant strip, most likely caused by the action of folding the shingle over the roofline. This leaves the edges of the hip and ridge shingles exposed to wind flow under their surface, which increases the total wind load on the shingle. Retrofit guidelines for existing homes with this specific unsealing are available in FEMA P-499 (2012); however, further work is necessary to validate the performance improvement and long-term durability of this retrofit method. Additional attention should be given towards the current manufacturing and installation methods for hip and ridge shingle products in order to improve new products introduced to the market.

3. Validate the wind resistance of rake and eave details

Rake and eave shingle pull-through at attachment points were observed on nearly all roofs evaluated during the system-level wind tunnel tests (Section 4). This was typically initiated by installation error (i.e., nails placed outside of manufacturer specification). However, edge details are prescriptively specified by shingle manufacturers and/or local building codes, rather than directly evaluated through performance testing methods (e.g., ASTM, UL, etc.). It is therefore difficult to assess

proper installation guidelines for rake and eave attachment details. 'Enhanced' edge details, such as the addition of asphalt roof cement along the rake and eave, are available, but, to the authors' knowledge, their performance has not been measured. Further research is necessary to validate the wind resistance of current edge attachment methods and to assess the improved wind resistance of 'enhanced' edge details.

4. Implement a Load and Resistance Factor Design (LRFD) methodology for shingle performance

From ASTM D7158, a shingle's mean total wind uplift resistance must be greater than or equal to its predicted design-level wind forcing. Wind loads are computed for a worst-case near roof wind speed location (i.e., the greatest peak roof wind speed to mean approach speed), whereas wind resistance is defined as a shingle's non-factored resistance to ASTM D6381 mechanical uplift tests. A new design methodology for defining resistance, following the LRFD concept, should be implemented to account for the inherent variability of a shingle's ultimate resistance to wind forces along its sealant strip.

5. Increase education of shingle roof installation contractors

The quality of installation will play a large contributing role in the wind resistance of the shingle roof system. Knowledge transfer to shingle contractors should emphasize basic wind load mechanics and the importance of their installation methods on the system's overall wind performance.



## 1. INTRODUCTION

### 1.1 Asphalt Shingle Roof Systems

Today, asphalt shingles are the most popular roof covering for steep-slope residential buildings largely due to their light weight, relatively inexpensive installation cost, and adaptability to a wide range of roof geometries (Noone and Blanchard, 1993). A 2009 study of the county property tax appraiser databases in Florida found that over 80% of all single family homes have asphalt shingle roofs (Engineering Team Report, 2009). Outside of Florida, asphalt shingle roofs are even more dominant.

Despite recent improvements to shingle wind resistance test standards (Corbin, 2000), post-storm reports (FEMA 2005a, FEMA 2005b, FEMA 2006, FEMA 2009) have consistently observed damage to shingles in below-design level wind events. This damage ranged from surface cracking due to unsealed shingles folding backwards to blow off of both individual shingles and larger sections of shingle roofing in the field off the roof and on associate components (e.g., hip and ridge shingles). The purpose of this research is to fill critical knowledge gaps that limit our ability to relate product evaluation and installation procedures to the observed performance of shingle roof systems in wind events.

### 1.2 Asphalt Shingle Wind Test Standards

Installation methods, product approvals, building codes, and standardized wind test methods have evolved significantly since the 1980s. Today, the primary wind test procedures asphalt shingles are ASTM D3161 and ASTM D7158/UL 2390. ASTM D3161 was first published in 1972, while UL 2390 and the equivalent ASTM D7158 were published in 2003 and 2005, respectively. The wind test method(s) (if any) to which the shingles in Sections 2.4 and 2.5 were evaluated by is unknown. It can be assumed, however, that all shingles installed prior to 2003 were not evaluated by the UL2390/ASTM D7158 test standard. Further information on the evolution and background to the wind test methods can be found in Dixon et al. (2012).

### 1.3 Project Overview

In August 2010, the University of Florida (UF) initiated a two-year research program to identify and address critical knowledge gaps in asphalt shingle performance in high winds. The major emphases of this work are described in the Experimental Research Plans (ERP), which were created for each of the project's experimental components. Seven ERPs were written (four in Phase I and three in Phase II). All but one was carried out during this project. The ERPs provided background information, described materials and methods, and presented the starting point for the analysis. This scope of this project addressed three main thrusts, which are organized into separate sections in this report:

#### 1. The Effects of Aging on Asphalt Shingle Wind Resistance - Section 2

- a. Wind Load Resistance of Heat Aged ASTM D7158 Class H Three-Tab Asphalt Shingles (ERP #1)

- b. Wind Load Resistance of ASTM D7158 Class H Three-Tab Asphalt Shingles Exposed to Cycles of Heat, Ultraviolet Light, and Water Spray (ERP #5)
  - c. Wind Load Resistance of Naturally-Aged Roof Systems
  - d. The Survey of Existing Asphalt Shingle Roofs for Unsealed Asphalt Shingles (ERP #6)
- 2. Assessment of the Asphalt Shingle Wind Load Model - Section 3**
- a. Characterization of Velocity above the Roof Plane (ERP #3)
  - b. Assessment of the Peterka Shingle Wind Uplift Model (ERP #7)
- 3. System-Level Wind Resistance of Asphalt Shingles - Section 4**
- a. System-Level Wind Resistance of Asphalt Shingles (ERP #2)

An Oversight Committee was formed to review research plans and findings. The committee members represented stakeholder groups from product manufacturing, product testing, homebuilding, catastrophe modeling, wind engineering, architecture, insurance, building code enforcement, and emergency management. Table 1 lists the committee members and their affiliations. The committee was given at least two weeks to comment on ERPs and was encouraged to crowdsource the document with other industrial and organizational partners.

**Table 1. Oversight Committee**

<b>Name</b>	<b>Affiliation</b>
Peter Vickery, Ph.D., P.E.	Applied Research Associates
Bill Coulbourne, P.E.	Applied Technology Council
Michael Fischer	Asphalt Roofing Manufacturers Association
Jon Peterka, Ph.D., P.E.	Cermak Peterka Petersen, Inc.
John Minor, CGC (FL)	Complete General Contractors, Inc.
Leslie Chapman-Henderson Tim Smail	Federal Alliance for Safe Homes
John Plisich Andrew Herseth, P.E., S.E. Thomas Smith, A.I.A., R.R.C. <sup>a</sup>	FEMA
Rick Dixon Mo Madani	Florida Building Commission
Miles Anderson	Florida Division of Emergency Management
Jack Glenn	Florida Home Builders Association
Anne Cope, Ph.D., P.E. Tim Reinhold, Ph.D., P.E.	Insurance Institute of Business & Home Safety
Michael Young, P.E. Peter Datin, Ph.D.	Risk Management Solutions, Inc. (RMS)
Walter Rossiter, Ph.D.	RCI (formally the Roof Consultants Institute)
Jim Baker	Roofing Industry Committee on Weather Issues (RICOWI)
Benjamin Thomas Jr., Ph.D.	Southeast Region Research Initiative
Tom Nichols	U.S. Polyco Inc.
Julie Serakos	BMS Intermediaries, Inc.

<sup>a</sup>Mr. Smith also works as a consultant for TlSmith Consulting Inc.

## 1.4 Project Timeline

The project was funded in two phases:

### Phase I (August 2010 – August 2011)

- Formation of Oversight Committee
- Identification of critical knowledge gaps
- Creation of public domain website to detail project goals and results
- Publishing of peer-reviewed magazine article on the history of asphalt shingle wind resistance
- Development and approval of four ERPs
- Commencement of three experiments

### Phase II (September 2011 – October 2012)

- Development and approval of three additional ERPs
- Commencement of three additional experiments
- Completion of six experiments

Following completion of Phase I, a report detailing the accomplishments of Phase I and progress towards Phase II was generated (see the SERRI Phase I Report on [www.serri.org](http://www.serri.org)). For the purposes of this report, the experiments detailed in Section 3.2 will refer to the SERRI Phase I Report for further detail on the experiment's methodologies and results. This document may be viewed as a complete overview of the two-year project, including experimental methods, results, and discussion of key findings from each experiment.

## 1.5 Public Dissemination

Project activities and findings were made public through a project website ([asphaltshingles.windengineer.org](http://asphaltshingles.windengineer.org)), multiple conference proceedings and presentations, and one peer-reviewed journal article (the content of this report will be recast into at least three more papers). The website provided public access to the project's scope, ERPs, project updates, and historical information on the wind resistance of asphalt shingles. The website was developed and maintained by UF and served as the official knowledge base for the project. This website will continue to be maintained in order to serve the public interest.

The first peer-review journal article was published in the May/June 2012 issue of RCI's *Interface* magazine, titled "A historical perspective on the wind resistance of asphalt shingles." The article provided a comprehensive overview of the evolution of asphalt shingles wind resistance and introduced the SERRI projects goals of solving the outstanding performance issues. A similar document can also be found in the SERRI Phase I Report and the reader is directed to either article for detailed background information. Additional peer-

reviewed journal articles will be submitted in spring 2013, subject to the review of the contents of this report:

C.R. Dixon, F.J. Masters, D.O. Prevatt, and K.R. Gurley. "Unsealed naturally aged asphalt shingles and their vulnerability in hurricane winds." *Journal of Wind Engineering and Industrial Aerodynamics*. (In Preparation)

C.R. Dixon, F.J. Masters, and K.R. Gurley (2013). "Wind uplift resistance of naturally and artificially aged asphalt shingles." *Building and Environment*. (In Preparation)

C.R. Dixon, F.J. Masters, K.R. Gurley, and D.O. Prevatt (2013). "Three-dimensional measurements of wind uplift force on asphalt shingles." *Journal of Wind Engineering and Industrial Aerodynamics*. (In Preparation)

## 1.6 Summary

This document reports the methodology and outcomes of a two-year research program to identify and address the knowledge gaps in asphalt shingle performance in high winds. Section 2 addresses the effect of aging on the wind resistance of asphalt shingles. Section 3 covers experimental work that evaluated two parameters of the wind load model for asphalt shingles. Finally, Section 4 details full-scale experimental work that assessed the system-level wind resistance of asphalt shingle roofs subjected to hurricane strength wind. Each section:

1. Identifies the knowledge gaps
2. Provides pertinent background information with cited sources
3. Outlines the experimental methods
4. Presents relevant results
5. Highlights significant findings, recommendations and proposals for future work

## 2. AGING EFFECTS ON ASPHALT SHINGLE WIND RESISTANCE

### 2.1 Introduction

Post-storm assessments of shingle roofing suggest that wind-induced damage to asphalt shingles may increase with age of the shingle roof (e.g., Liu et al., 2010); however, the effects of aging are not well understood (Baskaran, 1999). Moreover, the primary asphalt shingle wind performance test standards, ASTM D7158/UL 2390 and ASTM D3161, do not address aging effects, and limited information is available in the literature that links aging to shingle wind resistance. Furthermore, it is unknown if newer products, such as those with polymer-modified asphalt blends in the shingle's matrix and/or sealant strip adhesive will show the similar aging trends as non-modified products.

Terrenzio et al. (1997) and Shiao et al. (2003a) have shown that physical properties of asphalt shingles change over time (e.g., stiffening of the shingle matrix and molecular changes in the shingle matrix). Yet, applying this knowledge to characterize the wind resistance of a shingle over time is not straightforward in large part because the shingle's sealant strip (i.e., tab sealant) adhesion performance over time is not well understood. The sealant strip serves as the primary restraint preventing the shingle's leading edge from lifting in the wind. Once lifted, the aerodynamic force on the shingle increases (Peterka et al., 1997), thereby causing an increased vulnerability of the shingle to damage in the form of surface cracking arising from folding action or blow off of the shingle from the roof surface. The sealant strip has traditionally consisted of an asphalt based resin, but polymer-modified products have recently increased in market share (Nichols, 2010). The adhesive performance of both resin and polymer modified-based sealant strips throughout their lifecycle remains unknown.

This section presents four experiments directed at the aging of asphalt shingles via artificial (accelerated) and natural processes:

- Section 2.2      Wind Load Resistance of Heat Aged ASTM D7158 Class H Three-Tab Asphalt Shingles
- Section 2.3      Wind Load Resistance of ASTM D7158 Class H Three-Tab Asphalt Shingles Exposed to Ultraviolet Light, Heat, and Water Spray
- Section 2.4      Wind Load Resistance of Naturally-Aged Asphalt Shingles
- Section 2.5      Survey of Existing Asphalt Shingle Roofs for Unsealed Asphalt Shingles

## 2.2 Wind Load Resistance of Heat Aged ASTM D7158 Class H Three-Tab Asphalt Shingles

### 2.2.1 Introduction

Terrenzio et al. (1997) and Shiao et al. (2003a) performed the first publicly available studies of the aging kinetics of asphalt shingles. Their work primarily focused on the characterization of physical and chemical changes within the shingle matrix to define aging. This research component continues their work by investigating how a shingle's mechanical uplift resistance changes over time using conventional accelerated heat aging as a proxy for natural aging.

Accelerated aging involves the artificial aging of a material in order to increase the rate of aging of a product while still maintaining a similar reaction behavior. Accelerated aging methods have been performed extensively on other asphalt products, such as pavements (Hubard and Decker, 1995), and are standardized within ASTM International. Aging in this context is generally defined as a change in physical or chemical properties as a result of exposure to weathering elements known to cause these changes (i.e. heat, ultraviolet (UV) light, and rain).

Under their definition of aging, Terrenzio et al. (1997) and Shiao et al. (2003a) demonstrated that heat was the primary cause of asphalt shingle aging with UV light and rain-induced thermal shock playing a secondary role. Thermal loads caused a pronounced increase in the shingle's molecular weight and asphaltene content, while at the same time causing a decrease in the shingle's naphthenic aromatic content. The increased molecular structuring of the asphalt produced a stiffer (i.e., embrittled) shingle. The rate at which this chemical change occurred was proportional to the temperature in the aging chamber.

### 2.2.2 Experiment Overview

Following the Terrenzio et al. and Shiao et al. studies, an experiment was designed to evaluate the effects of thermal loads on the wind uplift performance of ASTM D7158 Class H three-tab asphalt shingles produced by three manufacturers. The tested three-tab (TT) products will henceforth be referred to as TT-101, TT-102, and TT-103. Shingle products TT-102 and TT-103 were purchased from a Gainesville, Florida, contract supply store, while TT-101 was obtained directly from the shingle manufacturer's plant. Specimens were created sequentially from the purchased bundles with their location in the thermal aging oven and the time interval at which they were tested randomized. Specimens were placed inside a forced-air dark oven (ASTM E145, Type IIB) and subjected to a continuous 70°C (158°F) heat for up to a 5376 h (32 week) period. The shingles were loose-laid in the oven and the sealant strip's adhesive was activated while heated in the oven, bonding the upper portion of specimen to the lower. The temperature of the oven and the total duration of aging were selected upon recommendations of the Oversight Committee members. The shingles were removed from the oven at the time intervals shown in Table 2, and tested for their mechanical uplift resistance following ASTM D6381. In practice, ASTM D6381 is utilized within ASTM D7158 in order to determine the wind uplift capacity of a shingle, and requires that shingle specimens be conditioned for a period of 16 hours at 60°C (140°F) inside a forced-air dark oven prior to the mechanical uplift test. This experiment compared the mechanical uplift performance of a shingle at its 16 hour "conditioned" state at 70°C

(158°F) to the mechanical uplift performance of shingles subjected to longer-term thermal aging.

**Table 2. Test interval schedule for thermal aging experiment**

Experiment Phase	Time Interval	Duration	
		Hours	Weeks
1	1	16	0.1
	2	84	0.5
	3	168	1
	4	252	1.5
	5	336	2
	6	504	3
	7	840	5
	8	1176	7
	9	1512	9
	10	2016	12
	11	2688	16
	12	3360	20
2	13	4032	24
	14	4368	26
	15	4704	28
	16	5040	30
	17	5376	32

The ASTM D6381 test consists of two test procedures (A and B) that simulate the individual wind loading components of asphalt shingles. The individual results of each test are combined using an empirical equation within ASTM D7158 to generate the total wind uplift capacity of a shingle. Both tests utilized a Universal Testing Machine (UTM) to subject the shingle specimens to a constant uplift displacement rate of 127 mm/min (5 in/min) (Figure 1). Procedure A simulates a peel-type loading of the shingle’s sealant strip (Figure 2a), while Procedure B simulates a direct tensile loading of the shingle’s sealant strip (Figure 2b). Specimens were prepared in accordance with ASTM D6381 and placed inside the thermal aging oven on metal racks. Oven temperature was continuously monitored and recorded with four Omega model 5TC-GG-T-24-72 constantan-copper (Type T) thermocouples vertically distributed inside the oven and the data were recorded using a National Instruments C-DAQ module and laptop computer. Ten specimens for each mechanical uplift test procedure per manufacturer were tested at each test interval, with exception of the final test interval where all remaining test specimens inside the oven were tested (a maximum of 20 specimens for each manufacturer per test procedure).

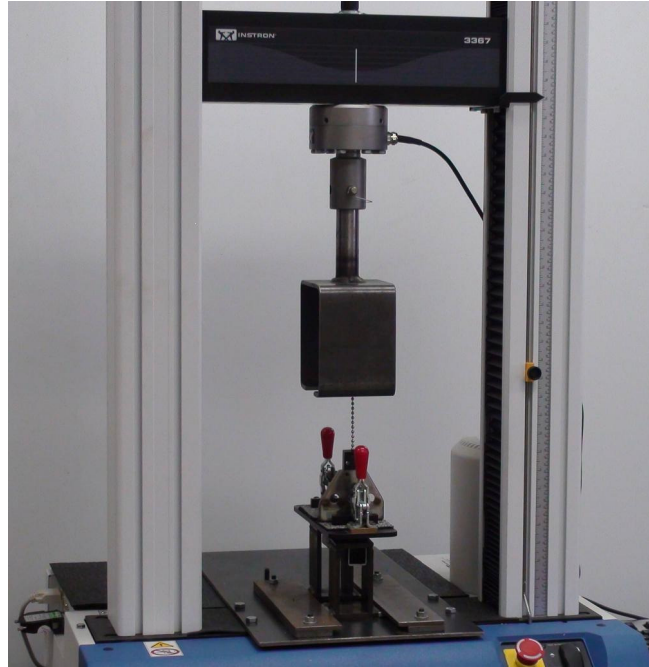


Fig. 1. UTM used for ASTM D6381 mechanical uplift testing.

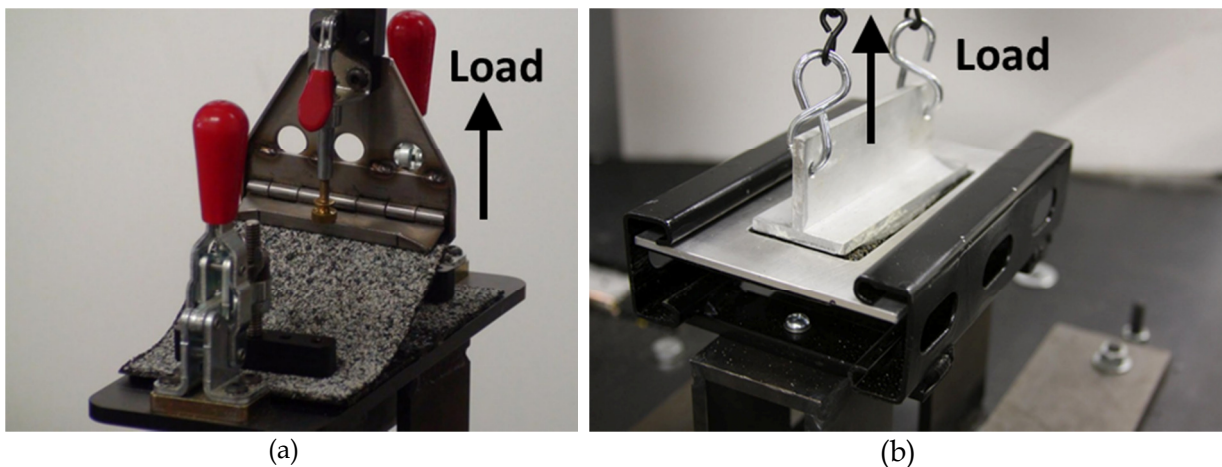


Fig. 2. (a) ASTM D6381 Procedure A and (b) ASTM D6381 Procedure B mechanical uplift testing.

This experiment was performed in two phases that aligned with the performance periods of the project. Phase I evaluated the mechanical uplift performance of shingles subjected up to 20 weeks of thermal aging and commenced in January 2011. Results from Phase I were also reported in this project's Phase I report. Phase II began in June 2011 and extended the thermal aging experiment to 32 weeks. TT-103 was not used in Phase II due to the product's relatively short distance between the sealant strip and the leading edge of the shingle, resulting in inherent issues with the ASTM D6381 Procedure A clamp fixture.

During Phase I, two chemical (SARA Fraction and Gel Permeation Chromatography), similar to those performed by Terrenzio et al. (1997), and one rheological test (Dynamic Shear Rheometer) were conducted on thermally aged shingle specimens by PRI Asphalt

Technologies, Inc. at their Tampa, FL laboratory. The results will not be discussed in this report due to ongoing analysis of the results.

### 2.2.3 Results

The ASTM D6381 mechanical uplift results presented herein are stratified by heat exposure time. The purpose of the analysis presented below was to:

1. Determine statistically significant changes in mean mechanical uplift resistance throughout the thermal aging process. Section 2.2.3.1 outlines the method for this analysis.
2. Quantify the dominant mode of failure at each test interval in order to correlate transitions in dominant failure mode to changes in uplift capacity.
3. Compare the thermally aged test specimen's ASTM D7158 predicted mean uplift capacity to the ASTM D7158 required mean wind uplift capacity.

As predicted by Shiao et al. (2003b), the mean uplift capacity of the shingle's sealant strip to Procedure B uplift was higher than Procedure A for the three products evaluated at all time intervals. Mechanical uplift test results are presented first for each manufacturer in Sections 2.2.3.2 through 2.2.3.4. Uplift resistance over thermal aging time is then compared by each mechanical uplift test procedure (Procedure A - Section 2.2.3.5 and Procedure B - Section 2.2.3.6), and by the ASTM D7158 total wind uplift resistance calculation procedure (Section 2.2.3.7). Finally, Section 2.2.3.8 presents a summary of failure modes observed during mechanical uplift testing.

#### 2.2.3.1 Data Analysis Methods

The primary data analysis statistically compared the mean uplift resistance of "new" shingles (heat exposure = 16 h) to the mean uplift resistance of "aged" shingles (heat exposure > 16 h). The variance of the uplift data was different at each time interval, therefore, statistically significant changes in mean uplift resistance were established using Welch's *t* test assuming unequal variance between the two sample sets at a 95% confidence level (i.e.,  $\alpha = 0.05$ ) (Ott and Longnecker, 2004). The 95% confidence intervals shown in Figures 3 - 8 were constructed using Equations (1) - (3), assuming a normal distribution of uplift resistances at each time interval.

$$\text{Upper 95\% Limit} = \bar{x} + (SE * 1.96) \quad (1)$$

and

$$\text{Lower 95\% Limit} = \bar{x} - (SE * 1.96) \quad (2)$$

where:

$$SE = \frac{s}{\sqrt{n}} \quad (3)$$

where:

$\bar{x}$  = sample mean

$SE$  = standard error of the sample

$s$  = standard deviation of the sample

$n$  = size (number of observations) of the sample

### 2.2.3.2 TT-101 - Aged Asphalt Shingle Mechanical Uplift Resistance

Stratifying the ASTM D6381 Procedures A and B test data by thermal exposure time, shingle product TT-101 had a statistically significant reduction in mean uplift capacity as exposure time increased. At the 16 h exposure (i.e., 'new' specimens), the mean uplift resistance ( $\bar{x}$ ) of TT-101's Procedure A specimens was 105.0 N (23.6 lbf) with a sample standard deviation ( $s$ ) of 10.9 N (2.5 lbf) (Figure 3 and Table 3). The next time interval (84 h) produced a mean uplift resistance ( $\bar{x}$  = 94.3 N) that was statistically significantly lower than the new shingle's. Tests following this at 168, 252, 336, and 840 h were, however, statistically similar to the 16 h baseline. The main reduction in Procedure A uplift resistance was observed in specimens exposed for greater than 1176 h. From 1176 h through the final time interval at 5376 h, the mean Procedure A uplift resistance of the aged shingles was statistically lower than the new shingles, with  $t$  test p-values ranging from 0.000 to 0.013 ( $\alpha$  = 0.05). The largest reduction in mean uplift capacity was 43.3 N (9.7 lbf) occurring at the 4704 h test interval (see Figure 3), corresponding to a 41% loss in uplift resistance. The sample standard deviation across all test intervals ranged from 6.0 N (3360 h) to 27.2 N (4032 h), producing a coefficient of variation (COV) range of 7-36%.

The long-term reduction in uplift capacity of ASTM D6381 Procedure B specimens (Figure 3 and Table 4) was less dramatic than Procedure A's, but statistically significant reductions in mean uplift resistance were observed on 3 out of the 16 (19%) time intervals. The first significant reduction occurred after 2016 h, producing a 27.5 N (6.2 lbf) reduction in mean uplift capacity. However, as the aging progressed past 2688 h, mean uplift resistance regained its similarity to the 16 h mean capacity. By the final uplift time interval (5376 h) the mean uplift resistance of the aged specimens was statistically lower than the new shingle specimens, resulting in a 29.3 N (6.6 lbf) loss of uplift capacity (15% reduction).

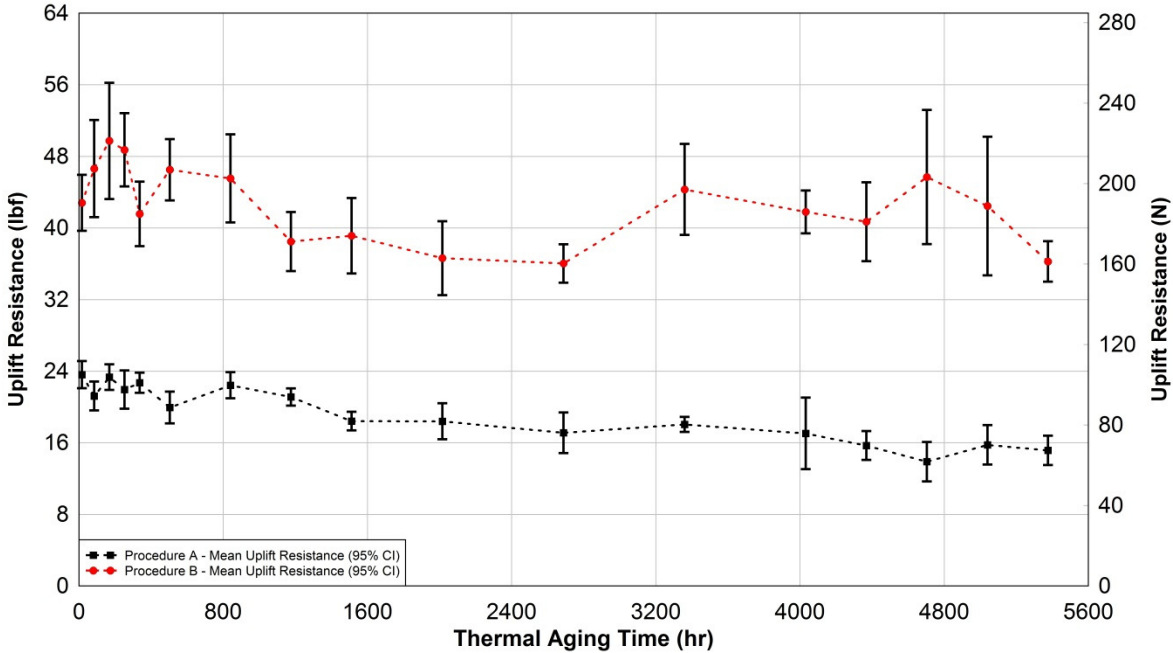


Fig. 3. TT-101 mean ( $\pm$  95% confidence interval) ASTM D6381 mechanical uplift resistance versus thermal aging time.

Table 3. Summary of results and comparison statistics - TT-101 - Procedure A

Thermal Aging Time (h)	Mean Uplift Resistance (N)	Standard Deviation (N) [COV]	Change in Mean Uplift Resistance From 16 h Mean Resistance (N)	Statistically Different from 16 h Mean Resistance? (Yes/No) [P-Value <sup>a</sup> ]
16	105.0	10.9 [10%]	--	--
84	94.4	11.6 [12%]	-10.6	Yes [0.049]
168	103.8	10.2 [10%]	-1.2	No [0.798]
252	97.6	15.3 [16%]	-7.4	No [0.228]
336	100.9	8.1 [8%]	-4.0	No [0.358]
504	88.7	12.7 [14%]	-16.3	Yes [0.007]
840	99.7	10.5 [10%]	-5.3	No [0.283]
1176	93.9	6.9 [7%]	-11.1	Yes [0.015]
1512	81.9	7.5 [9%]	-23.1	Yes [0.000]
2016	81.8	14.4 [18%]	-23.2	Yes [0.001]
2688	76.1	16.3 [21%]	-28.9	Yes [0.000]
3360	80.3	6.0 [8%]	-24.7	Yes [0.000]
4032	75.8	27.2 [36%]	-29.2	Yes [0.013]
4368	69.5	11.0 [16%]	-35.2	Yes [0.000]
4704	61.8	15.8 [26%]	-43.3	Yes [0.000]
5040	70.1	15.0 [21%]	-34.9	Yes [0.000]
5376	67.4	17.0 [25%]	-37.6	Yes [0.000]

<sup>a</sup>Welch's two-Sided *t* test Assuming unequal variances ( $\alpha = 0.05$ )

**Table 4. Summary of results and comparison statistics - TT-101 - Procedure B**

Thermal Aging Time (h)	Mean Uplift Resistance (N)	Standard Deviation (N) [COV]	Change in Mean Uplift Resistance From 16 h Mean Resistance (N)	Statistically Different from 16 h Mean Resistance? (Yes/No) [P-Value <sup>a</sup> ]
16	190.4	22.5 [12%]	--	--
84	207.4	38.9 [19%]	17.0	No [0.251]
168	221.2	46.6 [21%]	30.8	No [0.083]
252	216.7	29.4 [14%]	26.4	Yes [0.038]
336	184.9	25.9 [14%]	-5.5	No [0.619]
504	206.8	24.6 [12%]	16.4	No [0.136]
840	202.5	35.3 [17%]	12.1	No [0.374]
1176	171.1	23.7 [14%]	-19.3	No [0.078]
1512	174.0	30.3 [17%]	-16.4	No [0.188]
2016	162.9	28.1 [17%]	-27.5	Yes [0.033]
2688	160.3	15.3 [10%]	-30.1	Yes [0.003]
3360	197.1	32.6 [17%]	6.7	No [0.632]
4032	185.9	17.1 [9%]	-4.5	No [0.620]
4368	181.0	28.3 [16%]	-9.4	No [0.456]
4704	203.2	51.1 [25%]	12.8	No [0.501]
5040	188.8	35.2 [19%]	-1.6	No [0.937]
5376	161.2	20.5 [13%]	-29.2	Yes [0.004]

<sup>a</sup>Welch's two-Sided *t* test Assuming unequal variances ( $\alpha = 0.05$ )

### 2.2.3.3 TT-102 - Aged Asphalt Shingle Mechanical Uplift Resistance

Unlike TT-101, the results of TT-102 indicate that the sealant strip's bond strengthened as thermal exposure time increased. This strengthening was observed on 6 out of the 16 time intervals for ASTM D6381 Procedure A specimens, while statistically significant increases in Procedure B mean uplift resistance were observed on 14 out of the 16 time intervals. For Procedure A, the specimens uplift capacity increased from an initial mean uplift resistance of 78.1 N (17.6 lbf) [ $s = 25.8$  N (5.8 lbf)] to a peak mean resistance of 116 N (26 lbf) [ $s = 11.6$  N (2.6 lbf)] at the 840 h test interval. The mean capacity reduced from this peak capacity for specimens exposed to 1176 through 4032 h of thermal aging, but strengthened again to a statistically significant level on time intervals at 4368, 4704, and 5376 h. The mean uplift capacity at the final test interval was 25% greater than the initial 16 h mean capacity ( $p$ -value = 0.048).

Procedure B specimens exhibited greater strengthening through the aging process than Procedure A's. The first two time intervals (84 h and 168 h) saw significant increase in mean uplift capacity with a high confidence ( $p$ -values = 0.003 and 0.000, respectively). Only 2 out of the following 14 time intervals did not show significant increases in mean uplift capacity. The specimen's resistance to Procedure B uplift increased 47% between the initial and final time intervals ( $p$ -value = 0.000).

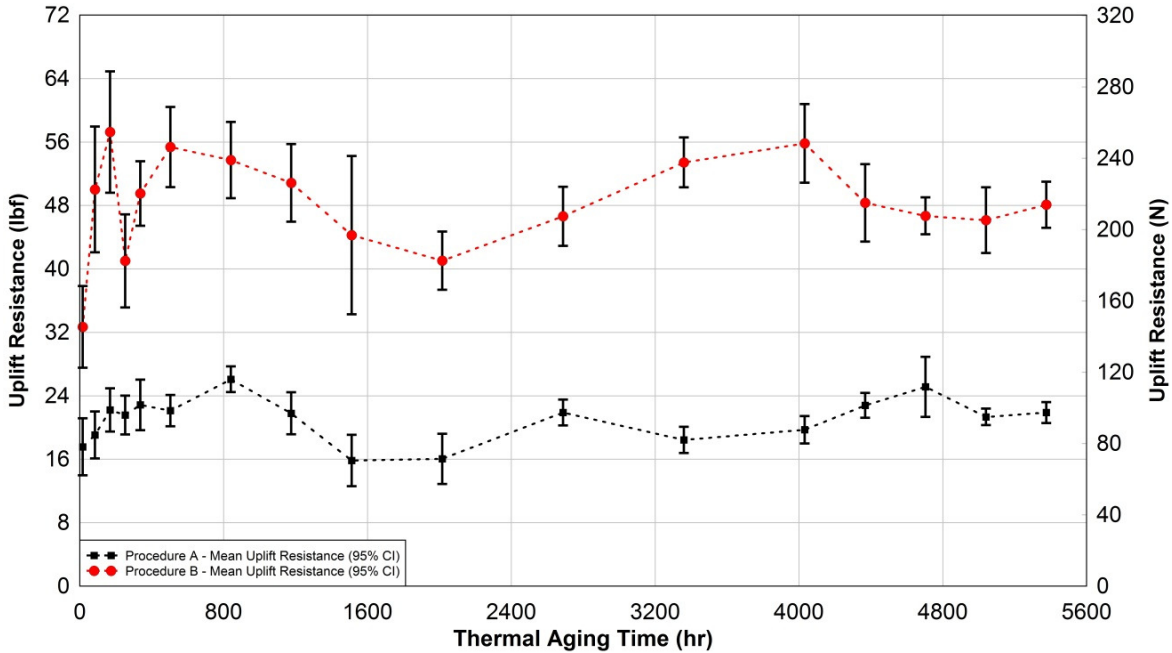


Fig. 4. TT-102 mean ( $\pm$  95% confidence interval) ASTM D6381 mechanical uplift resistance versus thermal aging time.

Table 5. Summary of results and comparison statistics - TT-102 - Procedure A

Thermal Aging Time (h)	Mean Uplift Resistance (N)	Standard Deviation (N) [COV]	Change in Mean Uplift Resistance From 16 h Mean Resistance (N)	Statistically Different from 16 h Mean Resistance? (Yes/No) [P-Value <sup>a</sup> ]
16	78.1	25.8 [33%]	--	--
84	84.8	21.2 [25%]	6.7	No [0.534]
168	98.8	19.5 [20%]	20.7	No [0.059]
252	96.0	17.6 [18%]	17.9	No [0.089]
336	101.6	22.8 [22%]	23.5	Yes [0.045]
504	98.4	14.2 [14%]	20.3	Yes [0.046]
840	116.0	11.6 [10%]	37.9	Yes [0.001]
1176	96.9	19.0 [20%]	18.8	No [0.081]
1512	70.4	23.2 [33%]	-7.7	No [0.494]
2016	71.4	22.7 [32%]	-6.7	No [0.544]
2688	97.4	11.7 [12%]	19.3	No [0.051]
3360	82.0	11.8 [14%]	3.9	No [0.670]
4032	87.7	12.4 [14%]	9.6	No [0.308]
4368	101.4	10.6 [10%]	23.3	Yes [0.022]
4704	111.7	25.8 [23%]	33.7	Yes [0.011]
5040	94.9	7.1 [7%]	16.8	No [0.074]
5376	97.4	12.7 [13%]	19.3	Yes [0.048]

<sup>a</sup>Welch's two-Sided *t* test Assuming unequal variances ( $\alpha = 0.05$ )

Table 6. Summary of results and comparison statistics - TT-102 - Procedure B

Thermal Aging Time (h)	Mean Uplift Resistance (N)	Standard Deviation (N) [COV]	Change in Mean Uplift Resistance From 16 h Mean Resistance (N)	Statistically Different from 16 h Mean Resistance? (Yes/No) [P-Value <sup>a</sup> ]
16	145.4	37.0 [25%]	--	--
84	222.5	56.9 [26%]	77.1	Yes [0.003]
168	254.7	54.9 [22%]	109.3	Yes [0.000]
252	182.4	42.2 [23%]	37.0	No [0.052]
336	220.2	29.3 [13%]	74.8	Yes [0.000]
504	246.3	36.3 [15%]	100.9	Yes [0.000]
840	238.9	34.5 [14%]	93.5	Yes [0.000]
1176	226.2	35.1 [16%]	80.8	Yes [0.000]
1512	196.8	71.6 [36%]	51.4	No [0.064]
2016	182.5	25.0 [14%]	37.1	Yes [0.020]
2688	207.4	23.9 [12%]	62.0	Yes [0.001]
3360	237.6	23.6 [10%]	92.3	Yes [0.000]
4032	248.3	35.6 [14%]	102.9	Yes [0.000]
4368	214.9	33.2 [15%]	69.6	Yes [0.000]
4704	207.7	17.5 [8%]	62.3	Yes [0.000]
5040	205.3	26.6 [13%]	59.9	Yes [0.001]
5376	213.9	24.4 [12%]	68.5	Yes [0.000]

<sup>a</sup>Welch's two-Sided *t* test Assuming unequal variances ( $\alpha = 0.05$ )

#### 2.2.3.4 TT-103 - Aged Asphalt Shingle Mechanical Uplift Resistance

The response of TT-103 specimens to thermal aging was characterized by no significant changes in mean uplift capacity for Procedure A and significant increases in Procedure B mean capacity on 5 out of the 11 time intervals. The 95% confidence intervals for Procedure A, visually represented in Figure 5, show that the statistical variability at 16 h nearly captures the 95% confidence intervals of all subsequent time intervals. The variability of data from tests conducted at time intervals less than 840 h was most likely influenced by the reduced number of successful tests performed in the early exposures. Due to the close location of the sealant strip to the shingle's leading edge, the Procedure A clamp could not be fixed to the shingle's leading edge as specified by ASTM D6381. Therefore, TT-103's specimens were tested using the modified test setup detailed in ASTM D6381 Section 7.7.3. Unfortunately, the epoxy bond between the modified test piece and the specimen's top surface frequently failed before the sealant strip failed during Procedure A testing. When premature failure occurred, the corresponding uplift resistance was not reported and the specimen was discarded. The Procedure A clamp fixture issue was the primary reason for discontinuing the thermal aging of TT-103 after the conclusion of Phase I.

Tests conducted beyond 1176 h of thermal exposure produced less variable results within each time interval and the mean values on the longer-term exposures were within

10.8 N (2.4 lbf) of one another. Procedure B's initial (16 h) test produced less variable data than Procedure A's (Figure 5) and the first statistically significant increase in mean uplift resistance was observed after 504 h of thermal exposure. The final time interval produced a mean uplift capacity of 325.2 N (73 lbf), compared to the initial mean uplift capacity of 243 N (54.6 lbf). This 34% increase in mean uplift resistance between the new and aged was statistically significant (p-value = 0.003).

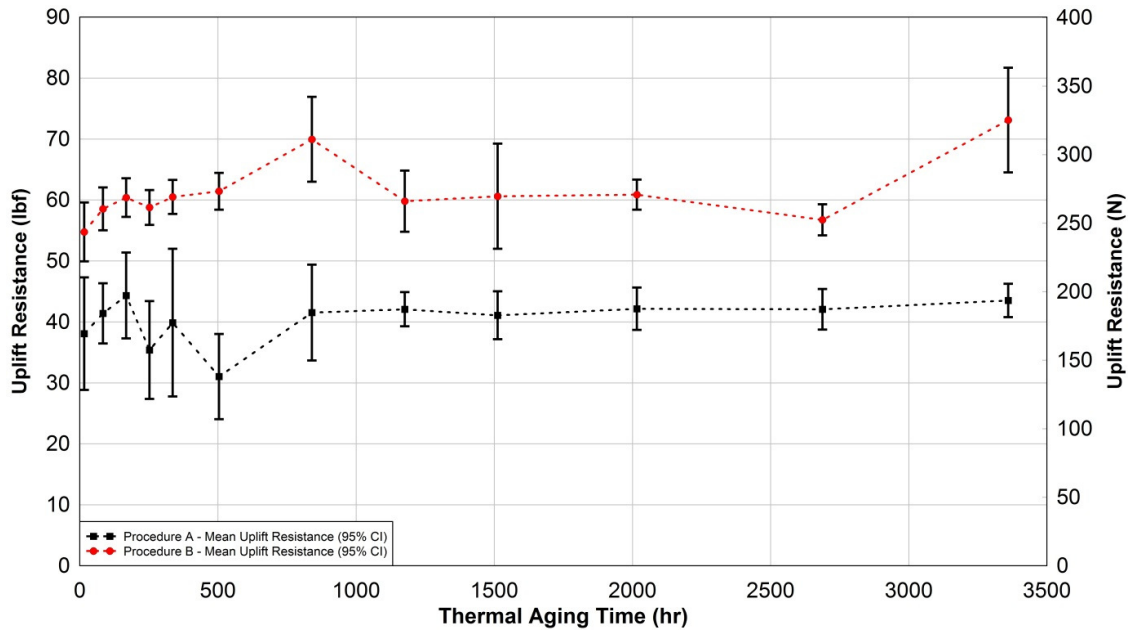


Fig. 5. TT-103 mean ( $\pm$  95% confidence interval) ASTM D6381 mechanical uplift resistance versus thermal aging time.

Table 7. Summary of results and comparison statistics - TT-103 - Procedure A

Thermal Aging Time (h)	Mean Uplift Resistance (N)	Standard Deviation (N) [COV]	Change in Mean Uplift Resistance From 16 h Mean Resistance (N)	Statistically Different from 16 h Mean Resistance? (Yes/No) [P-Value <sup>a</sup> ]
16	169.5	66.2 [39%]	--	--
84	184.1	31.7 [17%]	14.8	No [0.545]
168	197.2	48.0 [24%]	27.8	No [0.307]
252	157.4	48.1 [31%]	-11.9	No [0.673]
336	177.4	67.3 [38%]	8.0	No [0.822]
504	138.0	42.0 [30%]	-31.3	No [0.252]
840	184.7	56.4 [31%]	15.3	No [0.584]
1176	187.1	15.6 [8%]	17.8	No [0.435]
1512	182.7	25.3 [14%]	13.4	No [0.568]
2016	187.5	24.9 [13%]	18.1	No [0.434]
2688	187.1	20.0 [11%]	17.7	No [0.443]
3360	193.6	19.6 [10%]	24.2	No [0.292]

<sup>a</sup>Welch's two-Sided *t* test Assuming unequal variances ( $\alpha = 0.05$ )

Table 8. Summary of results and comparison statistics – TT-103 – Procedure B

Thermal Aging Time (h)	Mean Uplift Resistance (N)	Standard Deviation (N) [COV]	Change in Mean Uplift Resistance From 16 h Mean Resistance (N)	Statistically Different from 16 h Mean Resistance? (Yes/No) [P-Value <sup>a</sup> ]
16	243.6	32.8 [13%]	--	--
84	260.4	25.2 [10%]	16.8	No [0.233]
168	268.6	22.7 [8%]	25.0	No [0.076]
252	261.4	20.6 [8%]	17.8	No [0.184]
336	269.1	20.0 [7%]	25.6	No [0.064]
504	273.2	21.6 [8%]	29.6	Yes [0.038]
840	311.1	49.4 [16%]	67.6	Yes [0.003]
1176	266.0	36.0 [14%]	22.4	No [0.173]
1512	269.6	58.7 [22%]	26.0	Yes [0.268]
2016	270.8	17.7 [7%]	27.2	Yes [0.047]
2688	252.4	18.3 [7%]	8.9	No [0.488]
3360	325.2	61.6 [19%]	81.6	Yes [0.003]

<sup>a</sup>Welch's two-Sided *t* test Assuming unequal variances ( $\alpha = 0.05$ )

### 2.2.3.5 Comparison of ASTM D6381 Procedure A Mechanical Uplift Results

A comparison of each manufacturer's ASTM D6381 Procedure A results show that, across all time intervals, TT-103's resistance to Procedure A uplift was statistically greater than TT-101 and TT-102 (Figure 6 and Table 9). For TT-101 and TT-102, mean Procedure A uplift resistance was statistically similar on 59% of the time intervals with a statistically significant difference in strength (TT-102 > TT-101) observed on thermal exposures greater than 4368 h (Table 9). The 95% confidence intervals given in Figure 6 depict the high variability of uplift test results within TT-103, relative to TT-101 and TT-102, especially on lower exposure samples. As stated before, this is likely due to a reduced number of successful TT-103 – Procedure A tests in the early time intervals due to repeated epoxy failures of the modified Procedure A setup required for TT-103. There are three possible reasons for TT-103 having the greatest resistance to Procedure A uplift:

1. The sealant used on TT-103's sealant strip has the highest adhesive strength per unit surface area.
2. TT-103 has the shortest distance between the shingle's leading edge and its sealant strip.
3. The mean sealant strip contact surface area of TT-103 is the highest of the three manufacturers.

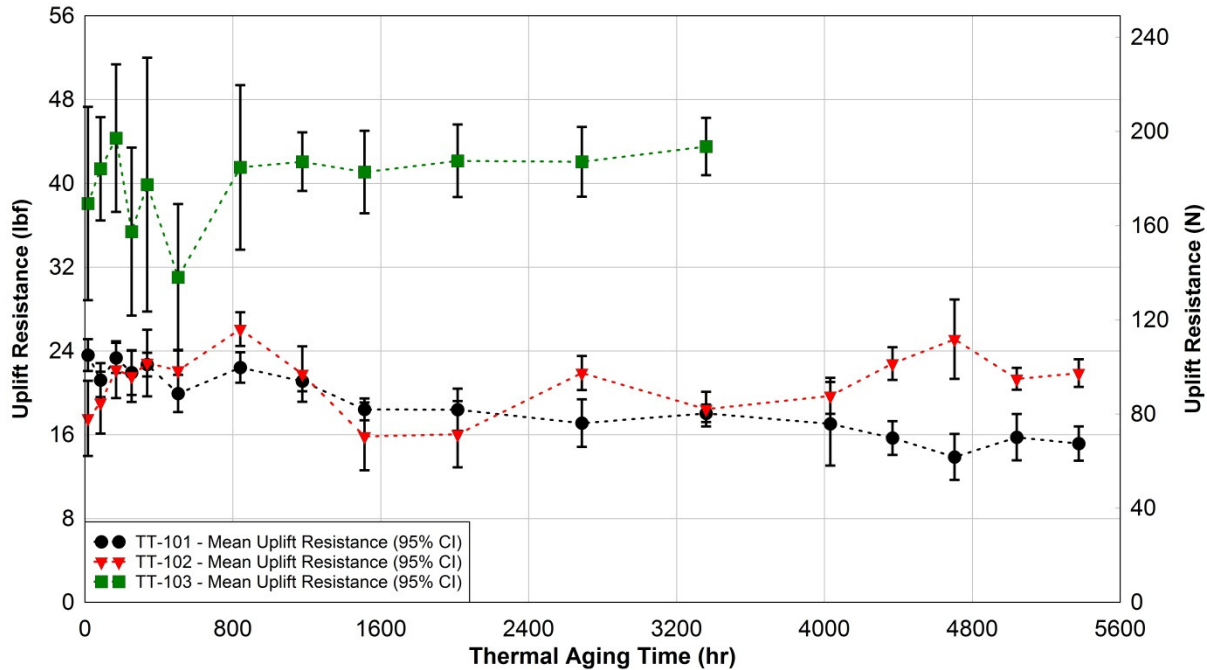


Fig. 6. Comparison of TT-101, -102, and -103 mean ( $\pm$  95% confidence intervals) ASTM D6381 Procedure A mechanical uplift resistance versus thermal aging time.

From Shiao et al. (2003b) a shingle's sealant strip has less resistance to peel stress than tensile stress. The distance between TT-103's sealant strip and leading edge was less than the distance on TT-101 and TT-102's specimens. Therefore, the moment arm between the application of Procedure A load at the leading edge and the sealant strip (i.e., the load path) of TT-103 was less than TT-101 and TT-102's. This decreased moment arm lead to a reduction in peel stress and an increase tensile stress in TT-103's specimens, thereby, leading to an increased resistance to Procedure A loading.

As stated above, the mean sealant strip area of TT-103 was greater than TT-101 and TT-102. Cullen (1960) proposed a correlation between the contact surface area of the sealant strip and the uplift resistance of sealant strip (i.e., increasing surface area leads to increasing wind uplift resistance). To evaluate the effect of sealant strip contact area on Procedure A uplift capacity, 25 samples each from TT-101 and TT-102 and 100 samples of TT-103 were digitally analyzed for the sealant strip coverage on ASTM D6381 Procedure A samples using a pixel counting algorithm performed in MATLAB 2010. Results show that the mean sealant strip coverage of TT-103 was, on average over the 9.5 cm (3.75 in) specimen width, 4.46 cm<sup>2</sup> (0.69 in<sup>2</sup>) greater than TT-101 and 1.55 cm<sup>2</sup> (0.24 in<sup>2</sup>) greater than TT-102 (Table 10).

The uplift capacity of each TT-101 - Procedure A specimen was then plotted against its estimated sealant strip area, as shown in Figure 7. The data used in this figure represents 81% of TT-103's uplift data with a roughly even distribution of specimens evaluated at all time intervals. Visually, the results indicate no correlation between ASTM D6381 Procedure A uplift resistance and sealant strip surface area. This was also confirmed statistically by estimating both linear and non-linear (exponential, power, and logarithmic) regression lines through the data. The coefficient of determination ( $R^2$ ) of all regression estimations were less than 0.03, an indication of poor fit between the data and estimated regression. In contrast to Cullen's (1960) observation, the results indicate that sealant strip surface area cannot be

used as an independent estimation for uplift resistance to the Procedure A peel-type loading. Future work will evaluate the effect of sealant strip surface area on Procedure B tensile loading.

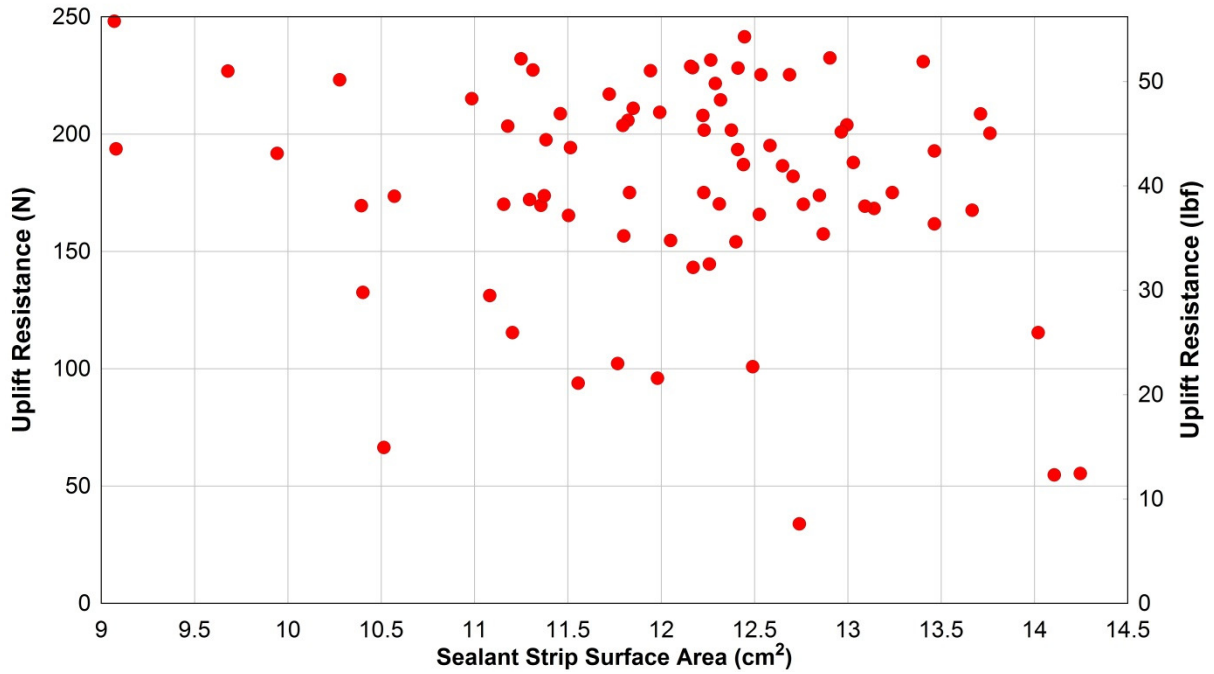


Fig. 7. Scatterplot comparing TT-103's ASTM D6381 Procedure A mechanical uplift resistance results versus the estimated sealant strip surface area of each ASTM D6381 Procedure A specimen.

**Table 9. Statistical comparison of ASTM D6381 Procedure A mean uplift resistance data**

Thermal Aging Time (h)	Statistically Significant Difference Between Mean ASTM D6381 Procedure A Uplift Resistances? (Yes/No) [P-Value] <sup>a</sup>		
	TT-101 vs. TT-102	TT-101 vs. TT-103	TT-102 vs. TT-103
16	Yes (TT-101 > TT-102) [0.01]	Yes (TT-103 > TT-101) [0.013]	Yes (TT-103 > TT-102) [0.002]
84	No [0.231]	Yes (TT-103 > TT-101) [0.000]	Yes (TT-103 > TT-102) [0.000]
168	No [0.488]	Yes (TT-103 > TT-101) [0.000]	Yes (TT-103 > TT-102) [0.000]
252	No [0.832]	Yes (TT-103 > TT-101) [0.016]	Yes (TT-103 > TT-102) [0.014]
336	No [0.932]	Yes (TT-103 > TT-101) [0.039]	Yes (TT-103 > TT-102) [0.039]
504	No [0.123]	Yes (TT-103 > TT-101) [0.020]	Yes (TT-103 > TT-102) [0.047]
840	Yes (TT-102 > TT-101) [0.004]	Yes (TT-103 > TT-101) [0.001]	Yes (TT-103 > TT-102) [0.000]
1176	No [0.643]	Yes (TT-103 > TT-101) [0.000]	Yes (TT-103 > TT-102) [0.000]
1512	No [0.165]	Yes (TT-103 > TT-101) [0.000]	Yes (TT-103 > TT-102) [0.000]
2016	No [0.238]	Yes (TT-103 > TT-101) [0.000]	Yes (TT-103 > TT-102) [0.000]
2688	Yes (TT-102 > TT-101) [0.004]	Yes (TT-103 > TT-101) [0.000]	Yes (TT-103 > TT-102) [0.000]
3360	No [0.683]	Yes (TT-103 > TT-101) [0.000]	Yes (TT-103 > TT-102) [0.000]
4032	No [0.254]	-	-
4368	Yes (TT-102 > TT-101) [0.000]	-	-
4704	Yes (TT-102 > TT-101) [0.000]	-	-
5040	Yes (TT-102 > TT-101) [0.000]	-	-
5376	Yes (TT-102 > TT-101) [0.000]	-	-

<sup>a</sup>Welch's two-Sided *t* test Assuming unequal variances ( $\alpha = 0.05$ )

**Table 10. Mean surface area coverage of the sealant strip for ASTM D6381 Procedure A specimens**

Shingle Product	Number of Specimens	Mean Sealant Strip Surface Area Over the 9.5 cm (3.75 in) Width (cm <sup>2</sup> ) [in <sup>2</sup> ]	Standard Deviation Over the 9.5 cm (3.75 in) Width (cm <sup>2</sup> ) [in <sup>2</sup> ]
TT-101	25	7.48 [1.16]	1.23 [0.19]
TT-102	25	10.39 [1.61]	1.03 [0.16]
TT-103	100	11.94 [1.85]	1.10 [0.17]

### 2.2.3.6 Comparison of ASTM D6381 Procedure B Mechanical Uplift Results

Similar to Procedure A's observations, the mean Procedure B uplift capacity of TT-103 was statistically greater than TT-101 on all time intervals and statistically greater than TT-102 on 75% of all comparable time intervals. TT-102's mean uplift capacity was statistically greater than TT-101 at 65% of the time intervals, and interestingly, the behavior of their mean resistances followed a similar trend through the thermal aging process (Figure 8). From tests after 504 h through 4368 h, changes in mean uplift resistance (either positive or negative) occur at similar time intervals and by similar amounts. However, the statistical significance of these changes in mean resistances varied across this same time and, therefore, the fluctuations observed in Figure 8 may not be representative of the population.

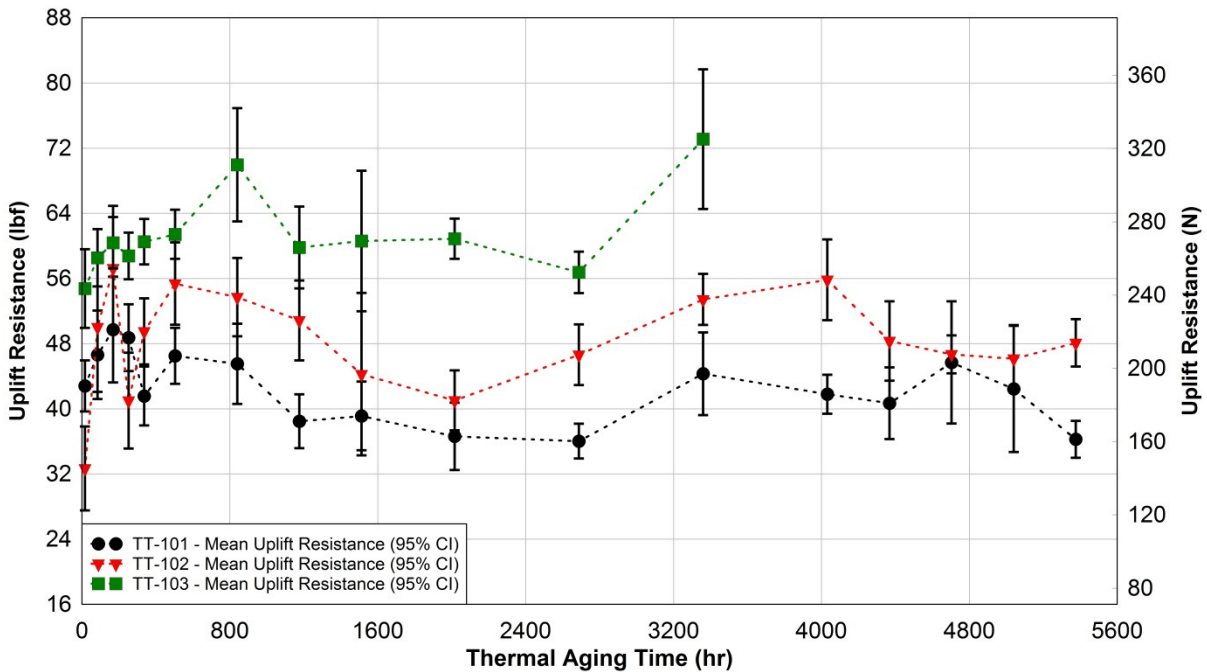


Fig. 8. Comparison of TT-101, -102, and -103 mean ( $\pm$  95% confidence interval) ASTM D6381 Procedure B mechanical uplift resistance versus thermal aging time.

**Table 11. Statistical comparison of ASTM D6381 Procedure B mean uplift resistance data**

Thermal Aging Time (h)	Statistically Significant Difference Between Manufactures' Mean ASTM D6381 Procedure A Uplift Resistances? (Yes/No) [P-Value] <sup>a</sup>		
	TT-101 vs. TT-102	TT-101 vs. TT-103	TT-102 vs. TT-103
16	Yes (TT-101 > TT-102) [0.005]	Yes (TT-103 > TT-101) [0.001]	Yes (TT-103 > TT-102) [0.000]
84	No [0.500]	Yes (TT-103 > TT-101) [0.002]	No [0.077]
168	No [0.160]	Yes (TT-103 > TT-101) [0.013]	No [0.473]
252	No [0.051]	Yes (TT-103 > TT-101) [0.011]	Yes (TT-103 > TT-102) [0.000]
336	Yes (TT-102 > TT-101) [0.011]	Yes (TT-103 > TT-101) [0.000]	Yes (TT-103 > TT-102) [0.000]
504	Yes (TT-102 > TT-101) [0.012]	Yes (TT-103 > TT-101) [0.000]	No [0.062]
840	Yes (TT-102 > TT-101) [0.032]	Yes (TT-103 > TT-101) [0.000]	Yes (TT-103 > TT-102) [0.002]
1176	Yes (TT-102 > TT-101) [0.001]	Yes (TT-103 > TT-101) [0.000]	Yes (TT-103 > TT-102) [0.022]
1512	No [0.137]	Yes (TT-103 > TT-101) [0.001]	Yes (TT-103 > TT-102) [0.027]
2016	Yes (TT-102 > TT-101) [0.000]	Yes (TT-103 > TT-101) [0.000]	Yes (TT-103 > TT-102) [0.000]
2688	Yes TT-102 > TT-101) [0.011]	Yes (TT-103 > TT-101) [0.000]	Yes (TT-103 > TT-102) [0.001]
3360	Yes (TT-102 > TT-101) [0.000]	Yes (TT-103 > TT-101) [0.000]	Yes (TT-103 > TT-102) [0.001]
4032	Yes (TT-102 > TT-101) [0.038]	-	-
4368	No [0.809]	-	-
4704	Yes (TT-102 > TT-101) [0.000]	-	-
5040	No [0.448]	-	-
5376	Yes (TT-102 > TT-101) [0.000]	-	-

<sup>a</sup>Welch's two-Sided *t* test Assuming unequal variances ( $\alpha = 0.05$ )

### 2.2.3.7 ASTM D7158 Total Wind Uplift Resistance of Thermally Aged Shingles

The uplift resistance of a shingle is determined from ASTM D6381 and ASTM D7158. Wind pressure uplift is resolved into two forces that act on the windward ( $F_F$ ) and leeward side ( $F_B$ ) of the shingle's sealant strip (Figure 9). The forces are product-specific due to the variations in the shape and seal location between products. The required total wind uplift resistance of the sealant strip ( $R_T$ ) is determined from ASTM D6381 Procedures A and B. If  $F_F$  is significantly greater than  $F_B$  (i.e., the windward force is greater than the leeward force), then the main wind loading mechanism on the sealant strip will be a peel-type loading. Therefore, more weight will be given to the mean mechanical uplift resistance of the shingle determined by ASTM D6381 Procedure A.

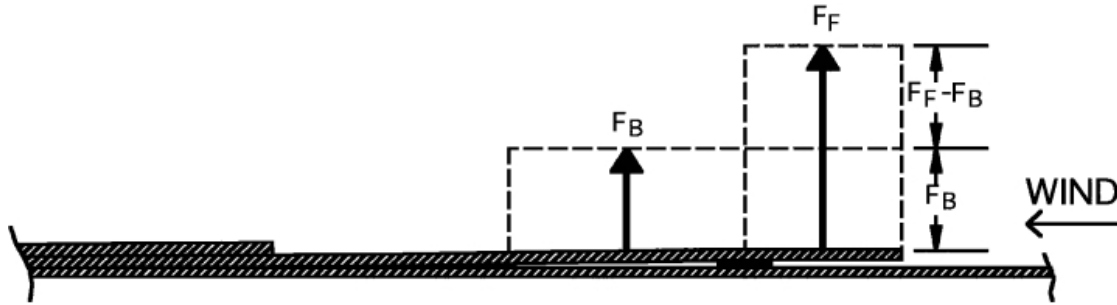


Fig. 9. Uplift forces generated on an asphalt shingle (Figure: ASTM D7158).

In order to convert the ASTM D6381 test results into ASTM D7158 total uplift resistance values, ASTM D7158 pressure coefficient test results were obtained for TT-101 (Table 12) and TT-103 (Table 13). Pressure coefficient data for TT-102 were not provided by the manufacturer. The ASTM D7158 results from TT-101 will be used in the conversion of TT-102's ASTM D6381 data as it represents a more conservative (i.e., higher) uplift value. An example of the conversion of TT-101's ASTM D6381 test results to ASTM D7158 total uplift resistance is given below in Equations (4) through (6).

Table 12. TT-101 ASTM D7158 Test Results

Test No.	Windward Side			Leeward Side		
	$P_{top} - P_{bottom}$ (Pa)	V (m/s)	DCp1	$P_{top} - P_{bottom}$ (Pa)	V (m/s)	DCp2
1	-56.5	14	-0.45	-10.5	14	-0.09
2	-73.3	15	-0.51	-26.8	15	-0.19
<b>Average</b>			<b>-0.48</b>			<b>-0.14</b>

Table 13. TT-103 ASTM D7158 Test Results

Test No.	Windward Side			Leeward Side		
	$P_{top} - P_{bottom}$ (Pa)	V (m/s)	DCp1	$P_{top} - P_{bottom}$ (Pa)	V (m/s)	DCp2
1	-79.5	15	-0.57	-12.4	15	-0.09
2	-74.2	14.7	-0.54	-10.5	14.7	-0.07
3	-68.0	15	-0.48	-13.9	15	-0.10
4	-74.7	15.6	-0.51	-14.8	15.6	-0.10
<b>Average</b>			<b>-0.53</b>			<b>-0.09</b>

From ASTM D7158-11:

$F_F > F_B$  Therefore, use ASTM D7158-11 Calculation Case 1:

$$R_T = \left[ \frac{F_F - F_B}{F_T} \right] \times R_A + \left[ \frac{2 \times F_B}{F_T} \right] \times R_B \quad (4)$$

Where,

$R_T$  = the total mechanical uplift resistance of an asphalt shingles tab sealant

$F_F$  = the expected uplift force generated on the forward edge of a shingles tab  
 = -17 N (-3.84 lbf) [TT-101] *NOTE: This value will vary between shingle products*

$F_B$  = the expected uplift force generated on the leeward side of a shingles tab  
 = -7.5 N (-1.68 lbf) [TT-101] *NOTE: This value will vary between shingle products*

$F_T$  = the expected total uplift force generated on a shingle's tab sealant  
 = -24.5 N (-5.52 lbf) [TT-101] *NOTE: This value will vary between shingle products*

$R_A$  = the uplift resistance of a shingles tab sealant as determined by ASTM D6381 Procedure A

$R_B$  = the uplift resistance of a shingles tab sealant as determined by ASTM D6381 Procedure B

Therefore,

$$R_T [TT - 101] = \left[ \frac{(-17) - (-7.5)}{(-24.5)} \right] \times R_A + \left[ \frac{2 \times (-7.5)}{(-24.5)} \right] \times R_B \quad (5)$$

and,

$$R_T [TT - 101] = [0.39] \times R_A + [0.61] \times R_B \quad (6)$$

The ASTM D7158 mean total uplift resistance of the thermally aged asphalt shingles is given in Figure 10 along with the required total uplift resistance to meet ASTM D7158 Class H wind resistance based on data from TT-101 (24.5 N [5.52 lbf]) and TT-103 (20.0 N [4.5 lbf]). All three manufacturers exceed the ASTM D7158 Class H wind resistance requirements across all time intervals. A statistically significant reduction in TT-101's uplift resistance was observed during ASTM D6381 Procedures A and B testing, but the mean total uplift resistance was still roughly five times the ASTM D7158 Class H minimum requirement. Note that these values represent the mean values of the sampled population and the method outlined in ASTM D7158 and performed on the data presented herein does not account for outliers – beyond their inclusion within the mean data calculation.

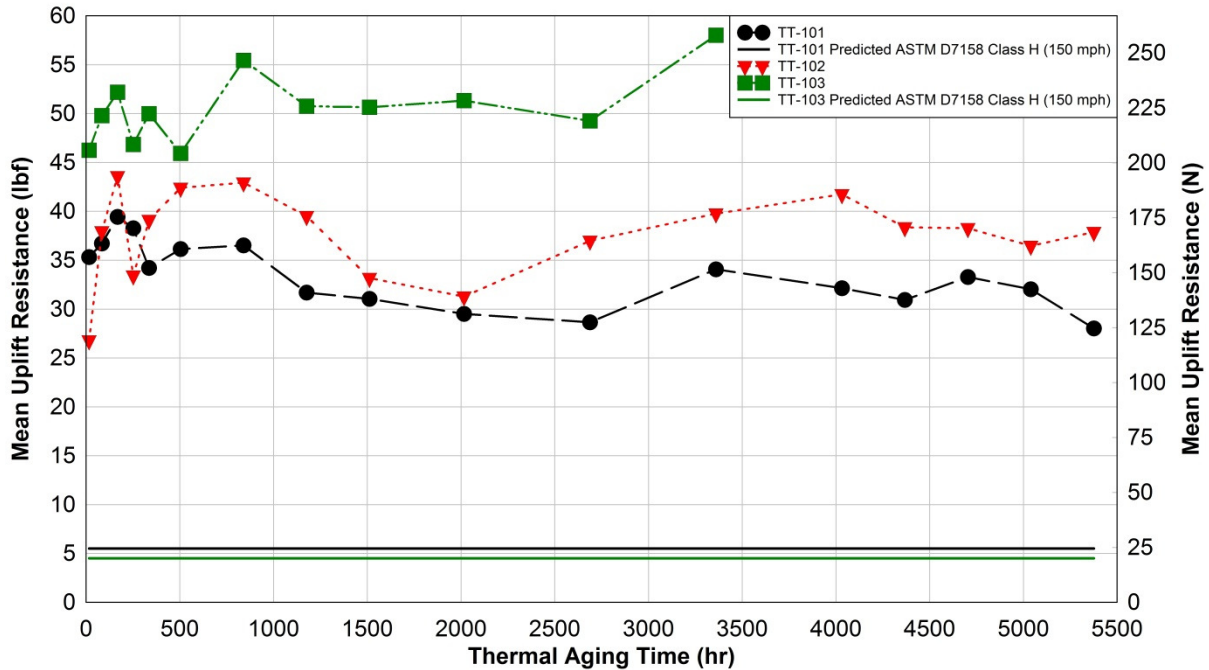
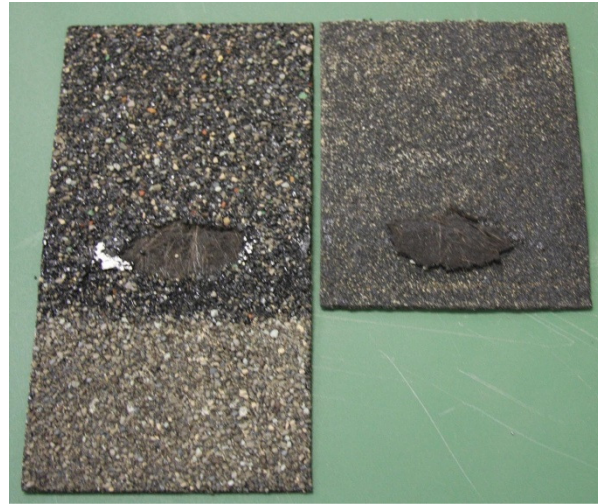
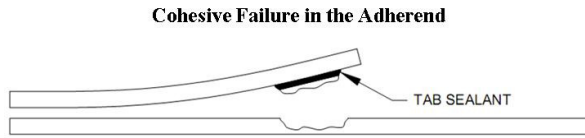


Fig. 10. Mean ASTM D7158 total uplift resistance versus thermal aging time. Note: TT-102’s manufacturer did not provide its product’s ASTM D7158 uplift coefficients, therefore, TT-101’s ASTM D7158 uplift coefficients were used to develop the total load equation for TT-102.

### 2.2.3.8 Observed Failure Modes for Mechanically Uplifted Shingles

Transitions in the dominate failure mode for mechanically uplifted shingles over time may signal that changes are occurring within the bonded composite. Three failure modes were observed during this experiment (Figures 11 through 13). Using the terminology set forth in Shiao et al. (2003b), these modes were:

1. Cohesive in the shingle (adherend): This failure mode occurs when the tab’s adhesive strength is greater than the cohesive strength of the shingle matrix. The asphalt coated fiberglass mats are located near the midpoint of the shingle thickness. When the shingle unseals from uplift force, the sealant remains bonded to the shingle, and the shingle separates cohesively via the asphalt matrix separating from the fiberglass mat.



**Fig. 11. Cohesive failure in the adherend.**

2. Adhesive: This occurs when the adhesive bond between the top and bottom shingle loses adhesion in the plane between the top surface of the adhesive and the bottom side of the top shingle.

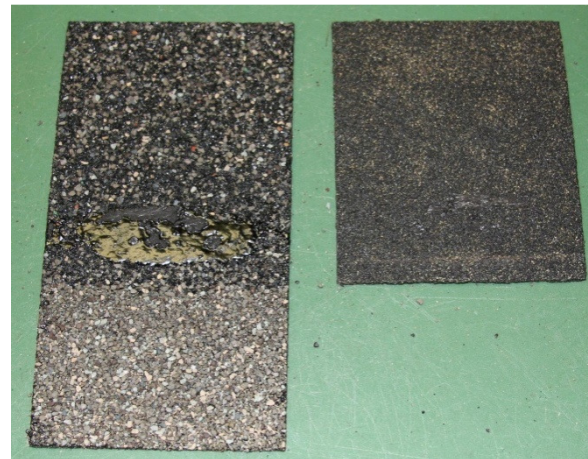
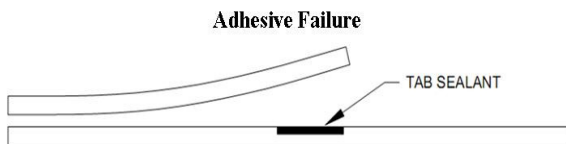


**Fig. 12. Adhesive failure mode.**

3. Combined: This is a mixed-mode failure whereby partial cohesive failure in the adherend and partial adhesive failure are observed on the mechanically uplifted specimen. No attempt to quantify the relative contribution of each failure mode has been made for this report.



**Fig. 13. Combined (mixed-modal).**

A fourth failure mode corresponding to a cohesive failure within the sealant was observed in the mechanical uplift tests performed on naturally aged shingle specimens (Section 2.4), but was not observed in this experiment. The distribution of failure modes stratified by thermal aging time for each manufacturer and ASTM D6381 test procedure is given in Figures 14 through 19. Findings are summarized below:

1. A reduction in sealant adhesive strength over time was observed for TT-101 - Procedure A specimens (Figure 14): A transition in dominant failure mode occurs at 1512 hours of aging; which correlates to an observed reduction in shingle uplift resistance. Combined failures and cohesive failures within the adherend account for approximately 80% of the observed failure modes in the first 1176 hours of aging. This suggests that the adhesive bond between the two shingles was generally stronger than the cohesive bond within the bottom shingle itself. At 1512 hours, the dominant failure mode transitions to adhesive failures, which account for 90% of the observed failures modes. A decrease in mean uplift resistance also occurs. Therefore, it is postulated that during the aging process, a reduction in bond strength occurred for TT-101 - Procedure A specimens.
2. An increase in sealant adhesive strength over time was observed for TT-103 - Procedure A specimens: While this conclusion is in contrast to the observation made above for TT-103, examination of the failure modes and uplift resistance plots reveals that failure mode transitions may signal uplift performance changes. For this set of specimens, adhesive failures dominate the early time intervals (16 - 840 hours). After 840 hours, cohesive failures in the adherend dominate the observed failure modes. Between 504 hours and 840 hours adhesive failures reduced from 50% of the observation to 10%. At this same time period a 44.5 N (10 lbf) increase in mean uplift resistance occurs, and overall, the uplift performance of this specimen set increases over aging time. The transition from mostly adhesive failures to mostly cohesive failures in the adherend combined with uplift performance gains suggests that sealant strengthening occurred throughout the aging process.

3. For all manufacturers, the dominant failure modes observed in Procedure A do not match the dominant failure modes observed in Procedure B. An example of this conclusion is given by examining the failure modes reported for TT-101 specimens. Cohesive failures in the adherend dominate Procedure B test specimens across all aging time intervals (Figure 15). However, for Procedure A specimens, cohesive failures in the adherend occurred less often. Furthermore, the failure mode trends are not visible in the corresponding Procedure B failure mode data. Recall that the two test methods in the ASTM D6381 test procedure were developed with the intent of simulating the partial peel-type and partial direct tension loading that exists during actual wind uplift. With the two test methods producing different failure limit states (i.e., loss of adhesion in the sealant strip bond or loss of adhesion within the shingle matrix); it is possible that the true in-service limit state may not be defined with the current ASTM D6381 test procedure.

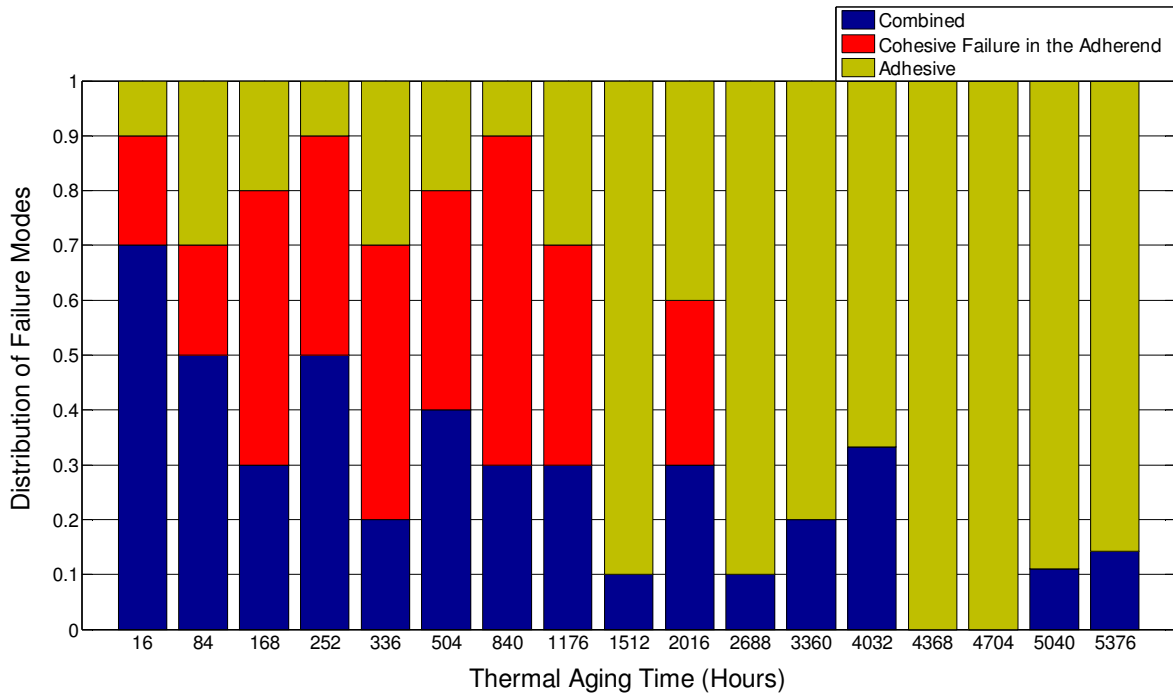


Fig. 14. Distribution of failure modes versus thermal aging time for TT-101 - Procedure A.

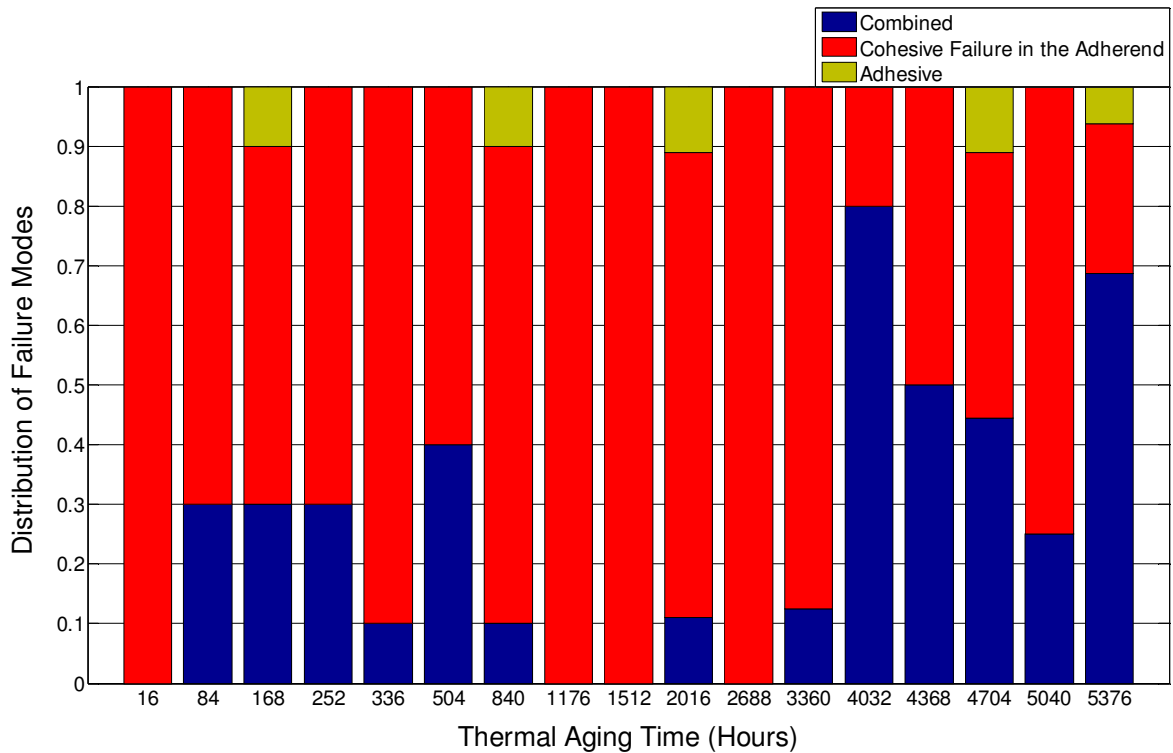


Fig. 15. Distribution of failure modes versus thermal aging time for TT-101 - Procedure B.

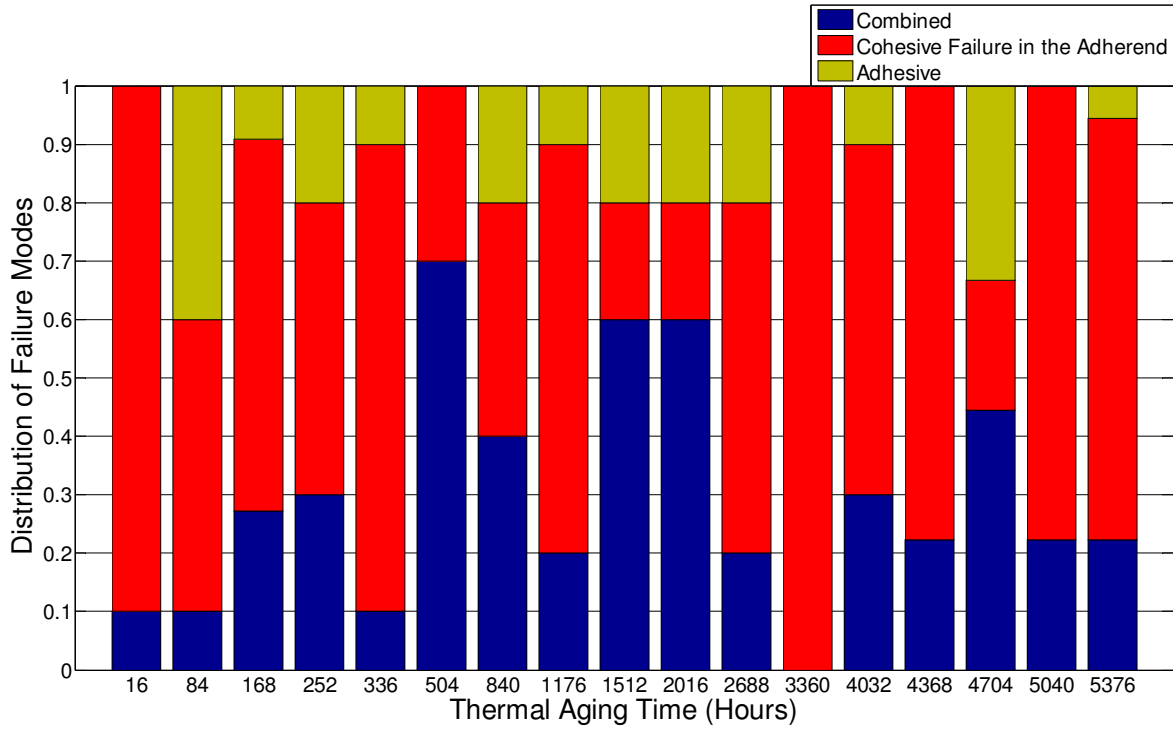


Fig. 16. Distribution of failure modes versus thermal aging time for TT-102 - Procedure A.

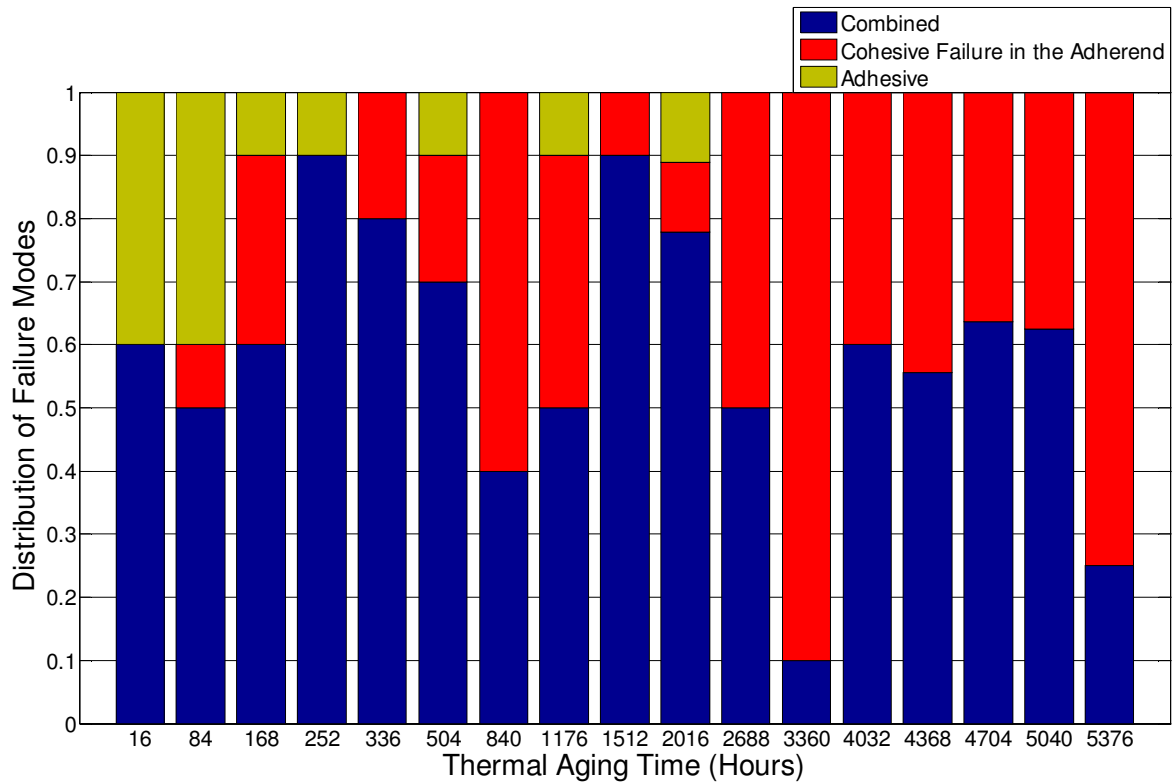


Fig. 17. Distribution of failure modes versus thermal aging time for TT-102 - Procedure B.

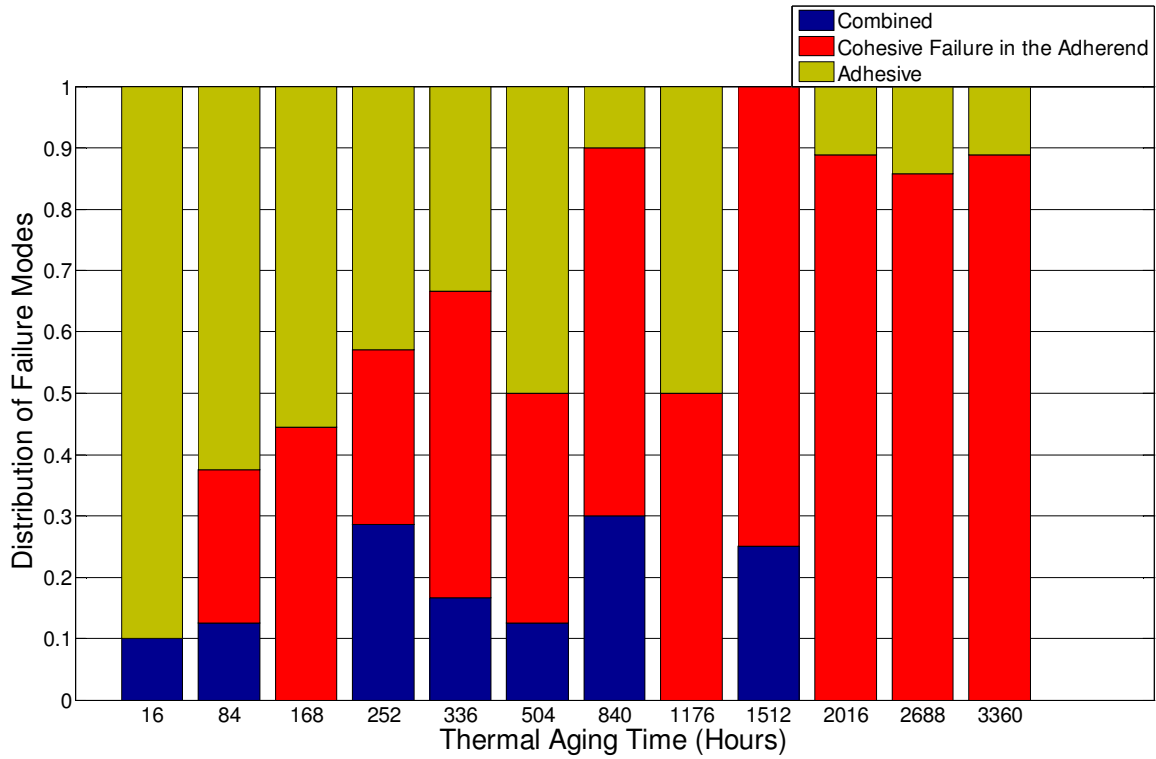


Fig. 18. Distribution of failure modes versus thermal aging time for TT-103 - Procedure A.

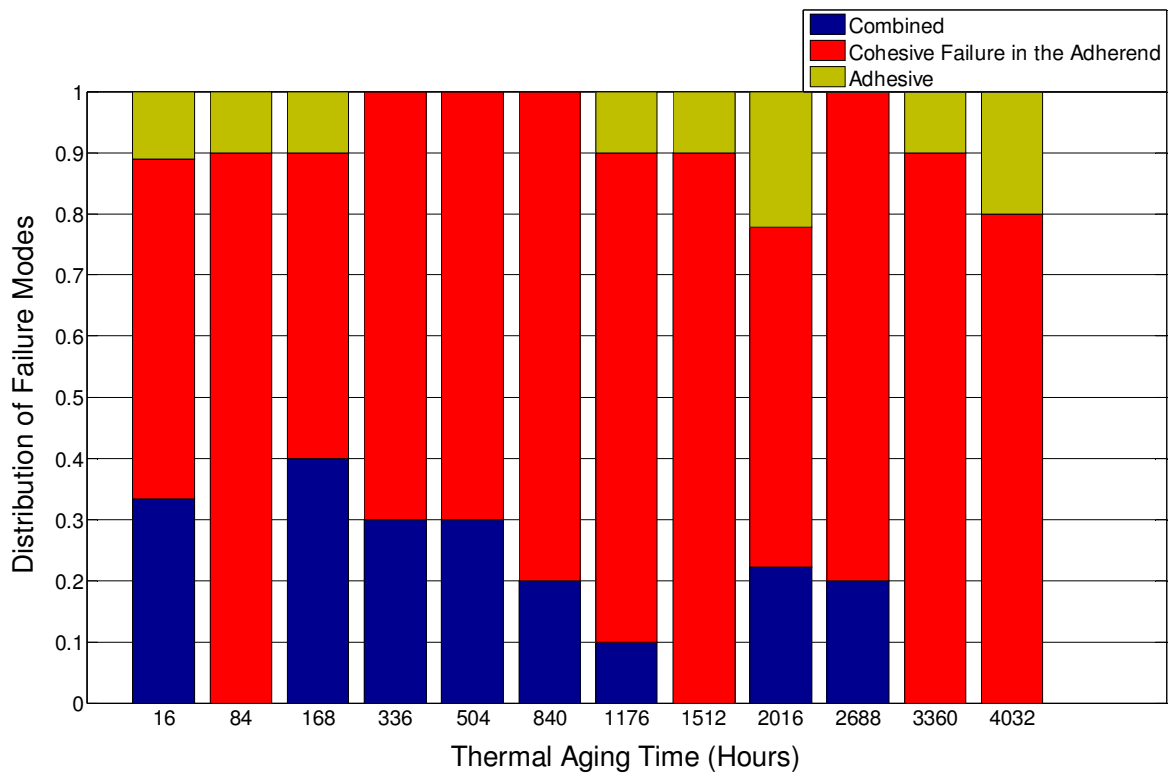


Fig. 19. Distribution of failure modes versus thermal aging time for TT-103 - Procedure B.

### 2.2.3.9 Significant Findings

The following conclusions can be made regarding the wind load resistance of asphalt shingles subjected to thermal aging:

1. Thermal aging caused a statistically significant reduction in the wind load resistance of TT-101's specimens. Analysis of ASTM D6381 Procedure A test specimens showed a failure mode transition towards adhesive failures through the aging process, signaling either a decrease in adhesive strength over aging time or a strengthening of the shingle matrix. Despite this weakening, the estimated wind uplift strength remained over five times greater than TT-101's required minimum ASTM D7158 Class H (150 mph) mean total uplift resistance.
2. Thermal aging caused a statistically significant increase in the wind load resistance of TT-102 and TT-103 on several test intervals. For TT-103 – Procedure A specimens, a correlation between mechanical uplift resistance and dominant failure mode transition was established, suggesting that the adhesive strength of the sealant increased with thermal aging.
3. Based upon conclusions 1 and 2, it is evident that thermal aging may cause a change in a shingle's uplift resistance over time. This change, whether increasing or decreasing, may depend on several design and manufacturing factors, including: sealant strip formulation, reinforcement mat composition, and the strength of the shingle matrix to reinforcement mat interface. At present, there are no standardized test methods to predict the wind uplift performance of aged asphalt shingles. Further work should be conducted to correlate the exposure of shingles in accelerated tests to naturally-aged exposure, this is a difficult endeavor due to the complex nature of asphalt chemistry.
4. Three failure modes were observed: 1) adhesive, 2) cohesive in the adherend, and 3) combined (partial cohesive in the adherend, partial adhesive). Comparisons between test procedures within the same manufacturer's specimens showed no correlation in failure modes between test procedures.
5. The ASTM D6381 test procedure did not identify a failure mode (cohesive within the sealant) that was identified by evaluation of existing houses exposed to actual aging (Section 2.4). The reasons for this revolve around the nature of shingle systems rather than individual shingle-to-shingle loads and are discussed in that section.

## 2.3 Wind Load Resistance of ASTM D7158 Class H Three-Tab Asphalt Shingles Exposed to Cycles of Heat, Ultraviolet Light, and Water Spray

### 2.3.1 Introduction

Asphalt shingles are subjected to daily cycles of temperature, ambient humidity, and sunlight. The sunlight's spectrum ranges from the ultraviolet (UV) (up to approximately 380 nm), visible light (380 nm to 740 nm), and into the infrared (740 nm to 1 mm) wavelengths. The two components of interest for aging are the infrared and UV spectrums. The complete spectrum from the sun causes the roof temperature to rise above ambient conditions. The UV spectrum of sunlight causes bituminous materials, such as the shingle's matrix material, to oxidize on their top surface and become water soluble. Precipitation then washes away the water soluble bituminous layer, and the process begins again (Terrenzio et al., 1997). Shingles are manufactured with opaque granules on their upper (exposed) surface over the asphalt to restrict the infiltration of UV into the shingle matrix. Therefore, granular loss exposes a shingle to the potential of accelerated weathering. Rain can also cause thermal shock on the sealant strip, but its effect on the adhesion of a shingle's sealant strip is not well understood. Terrenzio et al. (1997) hypothesized that the rapid changes in temperature arising from rain showers may compromise the sealant's long-term adhesive performance due to rapid thermally induced stresses that are generated in the adhesive.

The goal of this experiment was to subject two three-tab ASTM D7158 Class H asphalt shingle products, TT-101 and TT-102 from Section 2.2, to laboratory exposure of combined UV, heat and moisture over a 20 week period in order to evaluate their wind uplift performance throughout the aging process. A second goal of the experiment was to compare the results of the thermal aging study (Section 2.2) to the results of this experiment to evaluate the role of UV light and water spray. This experiment utilized an accelerated aging protocol, ASTM D4799, which combined UV fluorescent light, elevated temperatures, and water spray inside of a custom aging chamber designed and built by UF.

### 2.3.2 Experimental Procedure

The accelerated aging protocol conformed to ASTM D4799-08, with components of the aging chamber designed in conformance to ASTM G151-00, and ASTM G154-06. ASTM D6381 Procedures A and B mechanical uplift tests were performed on 20 specimens per test procedure per manufacturer at each of 5 aging intervals (Figure 20). This increase in sampling size was made in response to the high standard error observed in heat only experiment detailed in Section 2.2. Therefore, a total of 400 specimens were prepared in accordance with ASTM D6381 test specimen construction specifications.

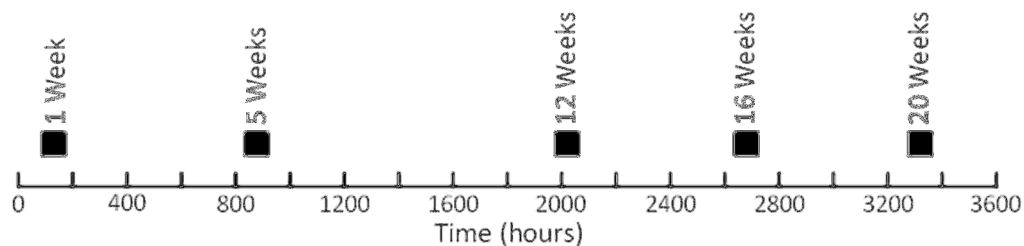


Figure 20. Test interval schedule for Heat, Ultraviolet Light and Water Spray experiment.

Prior to placing the shingle test specimens in the accelerated weathering chamber (Section 2.3.2.1), the specimens were conditioned in a forced air dark oven for 16 hours at 70°C (158°F). This was to ensure that the tab seals activated and bonded the shingles together prior to their exposure to the water spray cycle. All specimens were inspected for adhesion prior to their placement in the chamber. Once inside the chamber, the specimens were subjected to continuous cycles of five hours of 70°C (158°F) heat with UVA-340 ultraviolet light exposure, followed by fifteen minutes of water spray (only).

### 2.3.2.1 Accelerated Aging Chamber

Most accelerated weathering chambers (e.g., the QUV system manufactured by Q-Lab) are significantly smaller than the capacity required for this experiment. Therefore, a larger accelerated weathering chamber was designed and built to conform to the requirements for accelerated weathering of bituminous materials set forth in ASTM D4799-08, ASTM G151-10, and ASTM G154-06 (Figure 21). The chamber had plan dimensions of 1.4 m by 4.9 m (4 ft 6 in by 16 ft) and a water spray retention basin with a chamber height that slopes from 0.30 m to 0.48 m (1 ft to 1 ft 6 in).

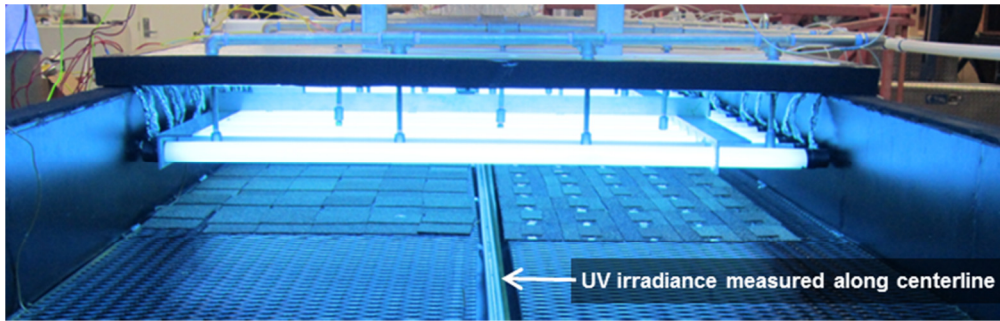


Fig. 21. Exterior view of the accelerated aging chamber.

The project evaluated 400 specimens in five intervals over 20 weeks. The entire specimen inventory could not fit in the chamber at one time; therefore, specimens for Weeks 1, 16, and 20 were placed in the oven first. After extraction of Week 1 specimens, Week 12 specimens were placed in the oven. Following Week 12 extraction, Week 5 specimens were placed in the oven.

Environmental conditions inside chamber were controlled and monitored using a National Instruments Labview 8.5 and a National Instruments CompactDAQ data acquisition system. The UV light system consisted of 1.2 m (4 ft) long UVA 340 lamps, manufactured by Q-Lab, located 102 mm (4 in) above the specimens at an on center spacing of 102 mm (4 in) to ensure irradiance uniformity (Figure 22). The lamps produced peak irradiance at a wavelength of 340 nm, and were powered by fluorescent light ballasts using an overdriving technique to produce maximum irradiance at the specimen level of 0.72 W/m<sup>2</sup> at 340 nm. The irradiance output was 0.04 W/m<sup>2</sup> (at 340 nm) greater than the irradiance of the sun at noon on a clear day (Fedor and Brennan, 1996). The lamps were

supplied with the constant current throughout the experiment, irrespective of the irradiance output.



**Fig. 22. Interior view of the accelerated aging chamber.**

ASTM G151-00 Section 5.1.2 specifies that the irradiance at any point in the specimen area must be within 70% of the maximum irradiance measured in the same area. Irradiance produced by the lamps is inversely correlated to the ambient air temperature near the lamp and, over time, the irradiance output can decrease due to a degradation of lamp's filament. Therefore, the irradiance of the UV light system was periodically recorded at 25 mm (1 in) increments using an Apogee SU-100 radiometer attached to a single-stage gantry affixed to the centerline of the chamber. Prior to the experiment, the Apogee radiometer was calibrated to a Q-Lab CR-10 radiometer. Figure 23 shows a typical irradiance data measurement. Uniformity of the irradiance throughout the chamber (ASTM G151-00 Section 5.1.2) was met during the entire test; however the average irradiance values decreased from 0.72 W/m<sup>2</sup> to 0.20 W/m<sup>2</sup> at the end of the experiment. The uniformity along each lamp's longitudinal axis was also confirmed prior to the initiation of the experiment.

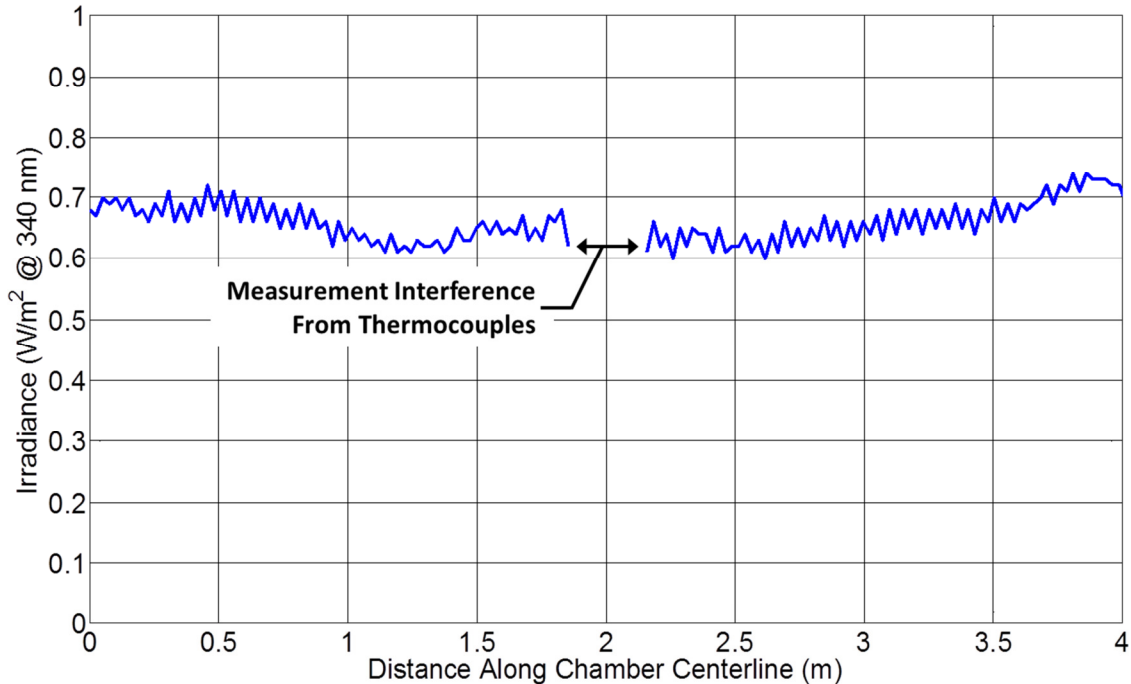


**Fig. 23. Distribution of irradiance output from UVA 340 lamps along the centerline of the accelerated aging chamber.**

To achieve an even distribution of water spray to the specimen area, spray nozzles were located 152 mm (6 in) above the specimen surface between the lighting system at an on center spacing of 305 mm (12 in). The temperature of water spray was approximately 21°C (70°C). In order to meet the water quality requirements specified in ASTM D4799 - Section 5.3.1.1, an in-line water filtration system was used to reduce the concentration of cations, anions, organics, and silica in the water used for the water spray.

Heat was supplied to the chamber's interior via ducting with an in-line blower and duct heater to create a forced-air oven. During the experiment copper-constantan (Type-T) thermocouples, located at the specimen level and distributed as shown in Figure 24, continuously monitored and recorded the chamber temperature. Additional thermocouples were installed above the specimen area in the center of the chamber to provide feedback to the air heating control system. Figure 24 presents a temperature time history of one complete 5 hour 15 minute cycle. Starting at 0 minutes the chamber began to heat after the previous cycle's water spray. Thermocouple 1 (TC1) encountered the highest rate of heating due to its location just below the entrance of the heating duct into the chamber. The entire heating process took approximately 70 minutes to reach temperature stabilization. The chamber then held a constant temperature for the remaining 220 minutes of the heating/light cycle. At 300 minutes into the cycle, the heating and light system was shut off and the water spray cycle began. Once completed, the cycle restarted. The two extreme end thermocouple temperatures of Figure 24, TC1 and TC4, are approximately 10°C and 7 °C less than the TC2 (i.e., the highest temperature measurement). The observation for TC1 is the result of an interaction between the chamber's interior air and the ambient air in the lab due to an opening at the end of the chamber that provides access for the radiometer. Thus, the extreme ends of the specimen area were moved away from the chamber ends to ensure that

the air temperature on the specimens was within  $\pm 3^{\circ}\text{C}$  ( $\pm 5^{\circ}\text{F}$ ) of the set point temperature of  $70^{\circ}\text{C}$  ( $158^{\circ}\text{F}$ ), as required by ASTM G151-00 Section 5.2.8.

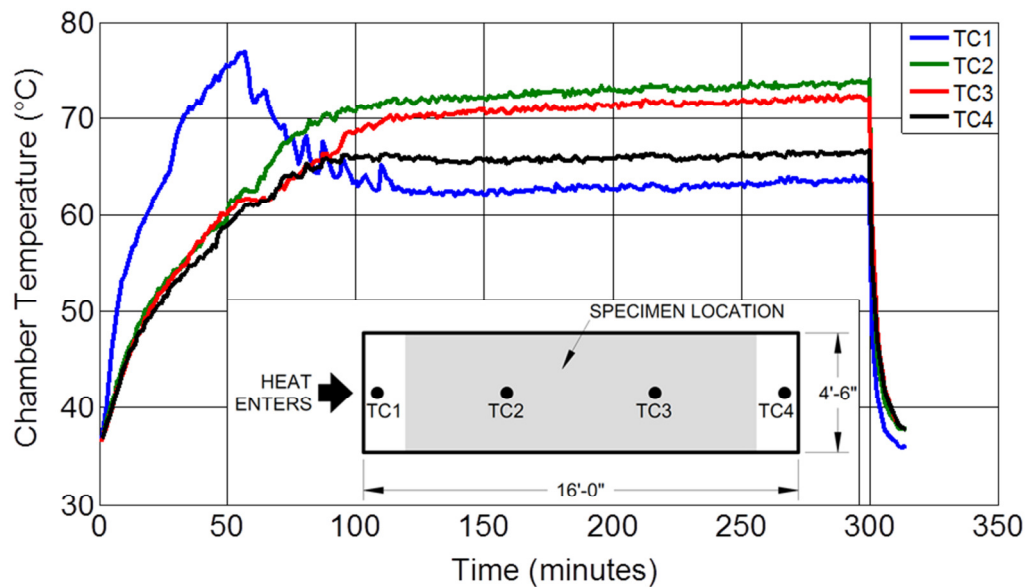


Fig. 24. Temperature time history of one aging cycle with  $T = 0\text{-}300$  minutes as heat and ultraviolet light followed by 15 minutes of water spray.

### 2.3.3 Results

ASTM D6381 mechanical uplift data were stratified by shingle product, test procedure, and exposure time in order to determine if statistical changes in mean uplift resistance occurred between 'new' shingles, measured after 16 h of thermal exposure (Section 2.2.3), and shingles 'aged' within the accelerated aging chamber using the test sequence described above. The same data analysis techniques employed in the thermal aging experiment were used in this experiment and are described above in Section 2.2.3.1. Failure modes of the UV+Heat+Water specimens will not be discussed herein; however, similar failure mode trends noted in the thermal aging experiment (Section 2.2.3.8) were also observed on specimens in this experiment.

#### 2.3.3.1 TT-101 Uplift Resistance

TT-101 specimens artificially aged using the UV+Heat+Water cyclical process experienced statistical reductions between their new and aged mean uplift resistance at four of the five Procedure A time intervals and all five Procedure B time intervals (Figure 25 and Tables 14 and 15). By 3360 h of artificial aging, the mean Procedure A uplift resistance reduced by 39%, while Procedure B reduced by 19%. The statistical strength of this observation is shown in Table 14, whereby, the p-value obtained for the comparison of the mean uplift resistance at 3360 h and 16 h was equal to 0.000 for Procedure A specimens and 0.001 for Procedure B. This is a strong indication that the mean uplift resistances (Procedures A and B) obtained after 16 h of thermal exposure are different from those obtained after 3360 h of cyclical UV+Heat+Water exposure.

When the mean uplift resistances of the two artificial aging methods are compared, the data indicate that mean uplift resistance was statistically different on two of the five Procedure A time intervals and three of the five Procedure B time intervals (Table 14). As shown in Figure 25, the greatest difference between the two aging methods was observed at the 168 h time interval. The cause of the observed difference is unknown; and curiously, the mean uplift resistance increases between the 168 h and 840 h time interval. For Procedure A, mean uplift resistance was statistically similar on tests performed after 840, 2016, and 2688 h of exposure. Specimens artificially aged for 3360 h using the UV+Heat+Water method had a 21% lower Procedure A uplift capacity (p-value = 0.005) and 22% lower Procedure B uplift capacity (p-value = 0.006) when compared to the Thermal aging method.

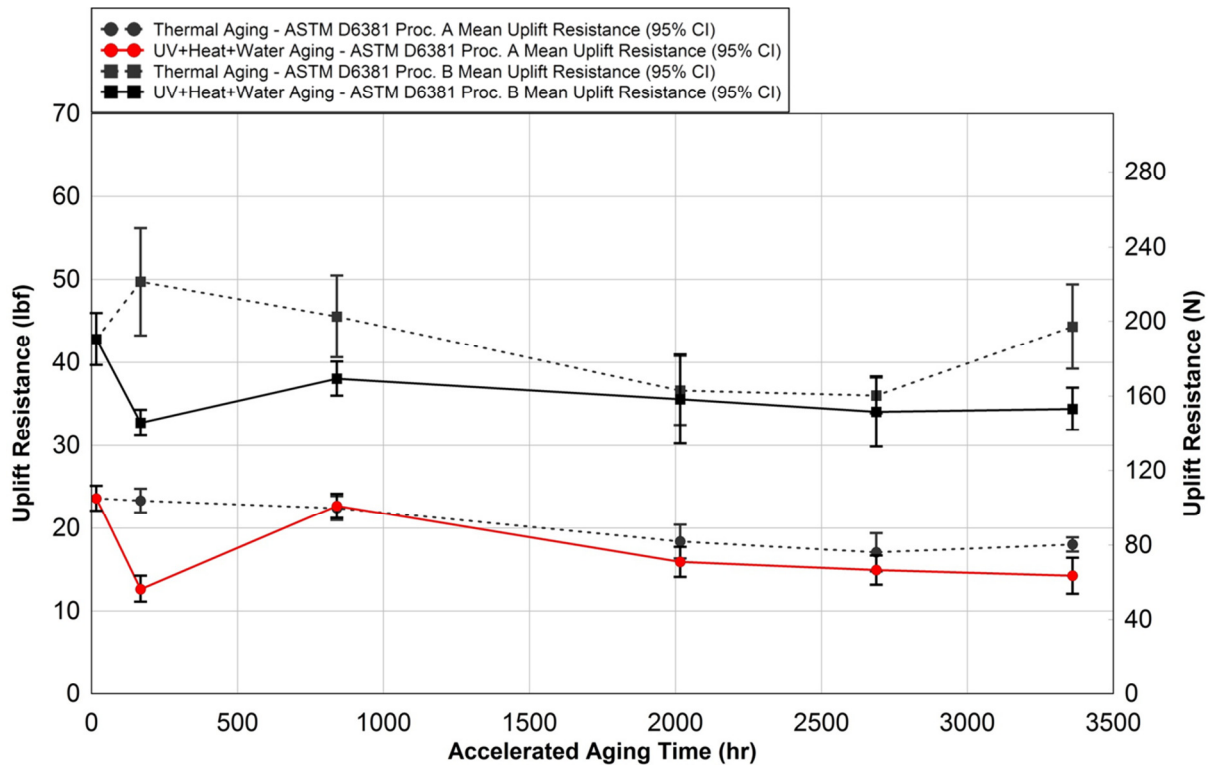


Fig. 25. TT-101 mean ( $\pm$  95% confidence interval) ASTM D6381 mechanical uplift resistance for UV+Heat+Water and thermal aging versus accelerated aging time.

**Table 14. Comparison statistics for UV + Heat + Water Spray verses Heat only accelerated aging TT-101 - Procedure A**

Aged Time (hours)	Mean Uplift Resistance (N) [95% Confidence Interval (N)]		Statistically Significant Differences Between Sample Means ( $\bar{x}$ ) <sup>a</sup> (P-Value)		
	UV+Heat+Water	Thermal	$\bar{x}$ (16 h) [Thermal] and $\bar{x}$ (i) [UV+Heat+Water]	$\bar{x}$ (16 h) [Thermal] and $\bar{x}$ (i) [Thermal]	$\bar{x}$ (i) [Thermal] and $\bar{x}$ (i) [UV+Heat+Water]
16	-	105.0 [6.7]	-	-	-
168	56.6 [7.1]	103.8 [6.4]	Yes [0.000]	No [0.798]	Yes [0.000]
840	100.9 [6.5]	99.7 [6.5]	No [0.396]	No [0.283]	No [0.808]
2016	71.0 [7.9]	81.8 [8.9]	Yes [0.000]	Yes [0.001]	No [0.091]
2688	66.7 [7.8]	76.1 [10.1]	Yes [0.000]	Yes [0.000]	No [0.162]
3360	63.7 [9.5]	80.3 [3.7]	Yes [0.000]	Yes [0.000]	Yes [0.005]

<sup>a</sup>Welch's two-Sided *t* test assuming unequal variances ( $\alpha = 0.05$ )**Table 15. Comparison statistics for UV + Heat + Water Spray verses Heat only accelerated aging TT-101 - Procedure B**

Aged Time (hours)	Mean Uplift Resistance (N) [Standard Error of the Mean]		Statistically Significant Differences Between Sample Means ( $\bar{x}$ ) <sup>a</sup> (P-Value)		
	UV+Heat+Water	Thermal	$\bar{x}$ (16 h) [Thermal] and $\bar{x}$ (i) [UV+Heat+Water]	$\bar{x}$ (16 h) [Thermal] and $\bar{x}$ (i) [Thermal]	$\bar{x}$ (i) [Thermal] and $\bar{x}$ (i) [UV+Heat+Water]
16	-	190.4 [13.9]	-	-	-
168	145.8 [6.9]	221.2 [28.9]	Yes [0.000]	No [0.083]	Yes [0.001]
840	169.2 [9.1]	202.5 [21.9]	Yes [0.023]	No [0.374]	Yes [0.017]
2016	158.3 [23.7]	162.9 [18.4]	Yes [0.030]	Yes [0.033]	No [0.765]
2688	151.6 [18.8]	160.3 [9.5]	Yes [0.003]	Yes [0.003]	No [0.427]
3360	153.1 [11.3]	197.1 [22.6]	Yes [0.001]	No [0.632]	Yes [0.006]

<sup>a</sup>Welch's two-Sided *t* test assuming unequal variances ( $\alpha = 0.05$ )

### 2.3.3.2 TT-102 Uplift Resistance

Similar to the thermally aged TT-102 specimens, mean uplift resistance statistically increased in TT-102 specimens subjected UV+Heat+Water artificial aging, as shown in Figure 26 and Tables 16 and 17. Three out of the five time intervals in Procedure A and all of time intervals in Procedure B had statistically higher mean uplift capacity than their 16 h thermal exposure mean uplift resistance. By the last time interval (3360 h), the mean Procedure A uplift capacity increased by 29% (p-value = 0.022), while mean Procedure B uplift capacity increased by 40% (p-value = 0.001).

Significant differences between the two artificial aging methods were observed in Procedure A and B, but particularly in Procedure B where mean uplift resistance was statistically dissimilar at all comparable time intervals. Procedure B mean uplift resistance was statistically lower in the UV+Heat+Water specimens than the Thermal on four of the five time intervals. However, the mean uplift was statistically greater than the 'unaged' 16 h resistance for both aging methods on all time intervals. Therefore, while the two methods produced dissimilar mean values in Procedure B, the overall increase in mean uplift resistance was observed in both aging methods. For Procedure A, the mean uplift capacities on the Thermal and UV+Heat+Water specimens were statistically similar at the 168 h, 840 h, and 2688 h time intervals. The data indicate that both artificial aging methods produced a similar increase in mean uplift capacity as exposure time increased. Thus, the general response of the shingle's adhesive bond was captured by both aging methods.

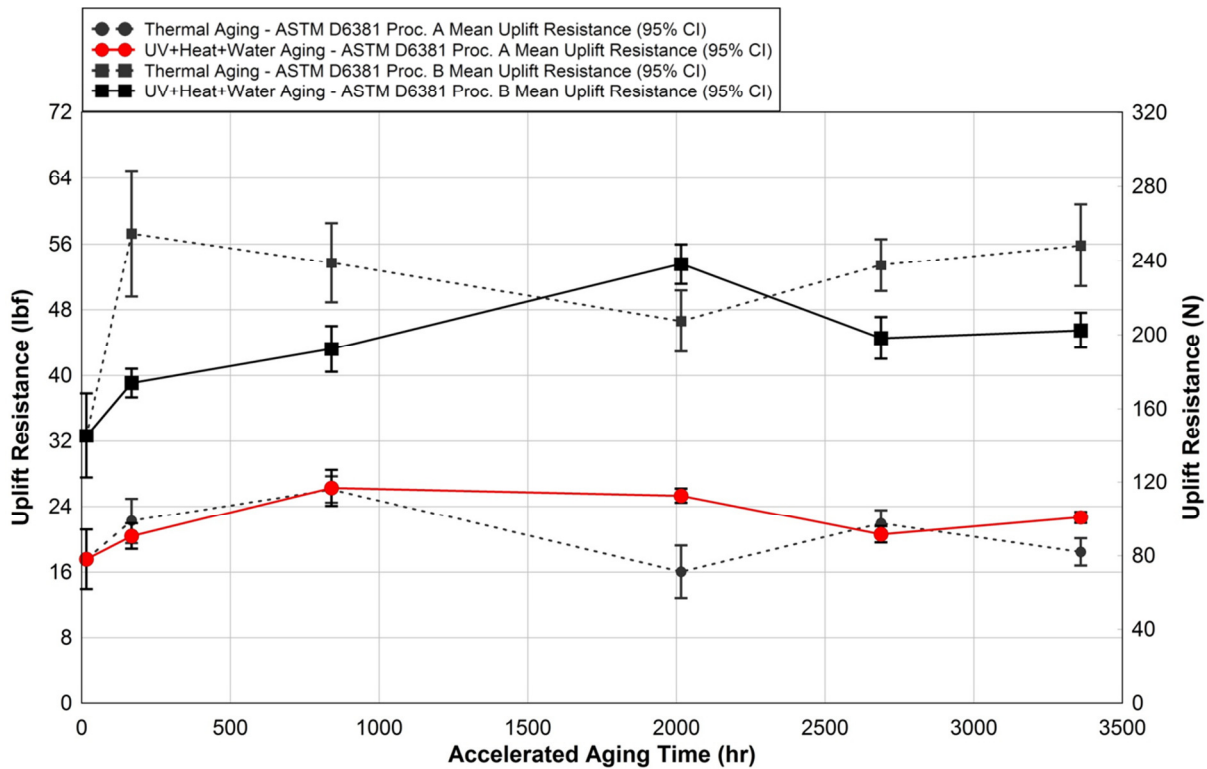


Fig. 26. TT-102 mean ( $\pm$  95% confidence interval) ASTM D6381 mechanical uplift resistance for UV+Heat+Water and thermal aging versus accelerated aging time.

**Table 16. Comparison statistics for UV + Heat + Water Spray verses Heat only accelerated aging TT-102 - Procedure A**

Aged Time (hours)	Mean Uplift Resistance (N) [Standard Error of the Mean]		Statistically Significant Differences Between Sample Means ( $\bar{x}$ ) <sup>a</sup> (P-Value)		
	UV+Heat+Water	Thermal	$\bar{x}$ (16 h) [Thermal] and $\bar{x}$ (i) [UV+Heat+Water]	$\bar{x}$ (16 h) [Thermal] and $\bar{x}$ (i) [Thermal]	$\bar{x}$ (i) [Thermal] and $\bar{x}$ (i) [UV+Heat+Water]
16	-	78.1 [16.0]	-	-	-
168	90.5 [6.8]	98.8 [12.1]	No [0.187]	No [0.059]	No [0.260]
840	116.8 [9.8]	116.0 [7.2]	Yes [0.001]	Yes [0.001]	No [0.900]
2016	112.6 [3.8]	71.4 [14.1]	Yes [0.002]	No [0.544]	Yes [0.000]
2688	91.5 [4.3]	97.4 [7.2]	No [0.144]	No [0.051]	No [0.188]
3360	100.7 [3.1]	82.0 [7.3]	Yes [0.022]	No [0.670]	Yes [0.001]

<sup>a</sup>Welch's two-Sided *t* test assuming unequal variances ( $\alpha = 0.05$ )**Table 17. Comparison statistics for UV + Heat + Water Spray verses Heat only accelerated aging TT-102 - Procedure B**

Aged Time (hours)	Mean Uplift Resistance (N) [Standard Error of the Mean]		Statistically Significant Differences Between Sample Means ( $\bar{x}$ ) <sup>a</sup> (P-Value)		
	UV+Heat+Water	Thermal	$\bar{x}$ (16 h) [Thermal] and $\bar{x}$ (i) [UV+Heat+Water]	$\bar{x}$ (16 h) [Thermal] and $\bar{x}$ (i) [Thermal]	$\bar{x}$ (i) [Thermal] and $\bar{x}$ (i) [UV+Heat+Water]
16	-	145.4 [22.9]	-	-	-
168	173.9 [7.7]	254.7 [34.0]	Yes [0.041]	Yes [0.000]	Yes [0.001]
840	192.3 [12.3]	238.9 [21.4]	Yes [0.003]	Yes [0.000]	Yes [0.002]
2016	238.2 [10.7]	207.4 [16.6]	Yes [0.000]	Yes [0.001]	Yes [0.009]
2688	198.3 [11.3]	237.6 [14.0]	Yes [0.001]	Yes [0.000]	Yes [0.000]
3360	202.4 [9.4]	248.3 [22.1]	Yes [0.001]	Yes [0.000]	Yes [0.003]

<sup>a</sup>Welch's two-Sided *t* test assuming unequal variances ( $\alpha = 0.05$ )

### 2.3.3.3 ASTM D7158 Total Wind Uplift Resistance of UV+Heat+Water Aged Shingles

The ASTM D7158 mean total wind uplift capacity of the UV+Heat+Water specimens was calculated using the same methods presented in Section 2.2.3.7. Recall, ASTM D7158 pressure coefficient data were not available for TT-102, therefore, TT-101 coefficient data were used in the calculation procedure of TT-102. A comparison of the UV+Heat+Water and Thermal mean wind uplift capacities at each time interval are provided in Table 18 and Figure 27. Results indicate that the mean resistance of TT-101 and TT-102 specimens exceeded Class H requirements in both artificial aging methods at every time interval. TT-101's mean wind uplift capacity after 3360 h of UV+Heat+Water exposure was nearly five times its Class H requirement, whereas, TT-102 specimens after the same exposure were over six times more resistance than TT-101's ASTM D7158 Class H requirement. The mean wind uplift resistance of specimens artificially aged by the UV+Heat+Water method was lower than the thermally aged resistance at all of TT-101's time intervals and four of the five time intervals of product TT-102. However, the statistical significance of this observation cannot be quantified due to the ASTM D7158 calculation procedure.

**Table 18. ASTM D7158 mean total wind uplift resistance for TT-101 and TT-102 subjected to UV+Heat+Water and Thermal aging methods compared to ASTM D7158 Class H requirement**

Aged Time (hours)	Mean Total Uplift Resistance (N) [lbf]				ASTM D7158 Class H Requirement
	TT-101		TT-102		
	UV+Heat+Water	Thermal	UV+Heat+Water	Thermal	
168	111 [25]	175 [39]	141 [32]	194 [44]	24.4 [5.5] (TT-101)
840	142 [32]	162 [37]	163 [37]	191 [43]	
2016	124 [28]	131 [30]	189 [43]	154 [35]	
2688	119 [27]	127 [29]	157 [35]	183 [41]	
3360	118 [27]	152 [34]	163 [37]	184 [41]	

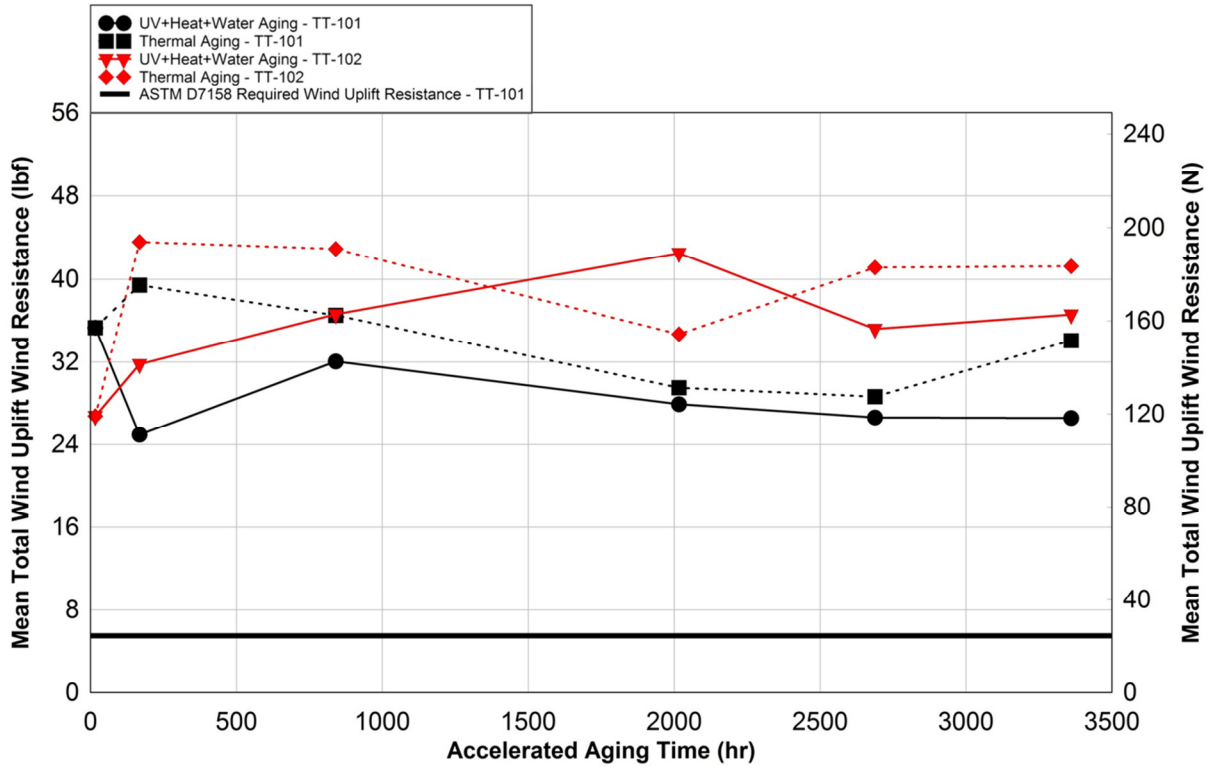


Fig. 27. Comparison of ASTM D7158 mean total uplift resistance between Thermal and UV+Heat+Water Spray accelerated aging regimes vs. accelerated aged time.

### 2.3.4 Findings

This experiment quantified the ASTM D6381 Procedure A and B mechanical uplift resistance of shingle products TT-101 and TT-102 as they were artificially aged with continuous cycles of UV light, heat, and water spray (UV+Heat+Water). Mechanical uplift tests were performed at five aging time intervals with the last time interval occurring after 3360 h of artificial aging. The primary objective of the experiment was to evaluate the effect of UV light and intermittent water spray on a shingle’s wind uplift capacity as it is artificially aged. This was achieved by comparing the results of the UV+Heat+Water aging experiment to the Thermal aging experiment (Section 2.2) at the five comparable time intervals (168, 840, 2016, 2688, and 3360 h).

When uplift test data were stratified by time interval, the results indicated that the UV+Heat+Water specimens of product TT-101 were statistically lower than TT-101’s thermally aged specimens at two of the five time intervals for Procedure A tests, and at three of the five time intervals for Procedure B tests. The remaining time intervals for TT-101 were statistically equivalent. In contrast, mean uplift data from product TT-102’s UV+Heat+Water specimens were lower than, equivalent to, or greater than TT-102’s thermally aged data at the five time intervals. TT-102’s UV+Heat+Water Procedure A and B mean uplift resistances were statistically greater than the thermally aged resistances at the 2016 h time interval. Given this, it is difficult to conclude that the addition of UV light and water spray reduce the mean uplift capacity of the shingle when compared to a continuous application of heat only.

Other factors potentially influencing this comparison include the sourcing of the shingle specimens in the two experiments. For each shingle product, the shingle specimens created for the two experiments were sourced from a single pallet of shingles. Therefore, the two experiments most likely used shingles that had similar sealant strip and asphalt coating formulations. However, shingles specimens in the thermal aging experiment were prepared in January 2011 from three bundles per product, while in the 2012 UV+Heat+Water experiment, two different bundles each for TT-101 and TT-102 were used to create test specimens. The variability of uplift resistance between shingle bundles is unknown and future work may be necessary to characterize this effect.

Despite the observation of reductions in mean uplift capacity between the 16 h and artificially aged TT-101 specimens, the ASTM D7158 mean total wind uplift resistance remained nearly five times the ASTM D7158 Class H required wind uplift resistance at all time intervals. TT-102's mean total wind uplift resistance was also greater than TT-101's Class H required at all time intervals. Recall that this comparison can only be made for mean uplift values and a prediction of the lower bound wind uplift resistance cannot be made by the current ASTM D7158 calculation procedure. Failure modes of the UV+Heat+Water specimens were not discussed herein; however, initial analysis of the data indicate similar trends summarized in Section 2.2.3.8 of the thermal aging experiment.

## **2.4 Wind Load Resistance of Naturally-Aged Asphalt Shingles**

### **2.4.1 Introduction**

This report has focused, thus far, on the uplift performance of asphalt shingles subjected to accelerated aging methods. While these techniques provide valuable insight into wind performance of aged asphalt shingles, the correlation of accelerated aging to natural aging is not well understood. Accelerated aging can, at best today, be used as a diagnostic tool to evaluate whether a material is affected by the aging parameters set within the test protocol. Even if a material shows signs of degradation due to accelerated aging, the time at which the material would show this behavior in the natural state remains elusive. An effective method for evaluating a material's ability to resist weathering is a combination of accelerated and natural weathering test procedures. The objective of this experiment was to evaluate wind uplift performance of naturally-aged roofs in order to provide a benchmark for the observations made during the accelerated aging test previously discussed.

The ASTM D6381 mechanical uplift test is a laboratory test method that utilizes a non-field deployable UTM apparatus (Figure 1). To evaluate the wind uplift resistance of naturally-aged asphalt shingles, UF designed and constructed a custom UTM capable of performing ASTM D6381 tests on shingle roofs installed on existing homes. Section 2.4.2 details the test apparatus. Mechanical uplift tests were performed in 2011 and 2012 on four existing homes in Central Florida; acquired by UF through the Florida Department of Emergency Management (FDEM). The homes resided in flood-prone areas and were slated for demolition. The list of the homes is given in Table 19, along with their respective shingle roof age and shingle type. The products evaluated in this experiment were manufactured prior the adoption of the ASTM D7158 test standards; therefore, the shingles wind resistance was likely evaluated using the ASTM D3161 test standard.

## 2.4.2 Portable Mechanical Uplift Apparatus

The Portable Mechanical Uplift Apparatus, henceforth PMUA, consists of a Tritex TLM20 electric linear actuator mounted to a lightweight aluminum frame (Figure 28). The PMUA can achieve a maximum uplift force of 836 N (188 lb) at a maximum speed of 0.287 m/s (11.3 in/s). For ASTM D6381 tests, the actuator was set to the specified constant displacement rate of 0.0021 m/s (5 in/min). The actuator was powered by a 48 Volt power supply that was located in a separate weather tight container. An 890 N (200 lb) Futek low profile load cell was connected in series with the actuator to provide force feedback. An electrical box bolted to the aluminum frame housed a National Instruments 6211 data acquisition card for simultaneous measurement of position and velocity from the actuator and force measurement from the load cell. A RS-485 converter, also in the electrical box, allowed calibration adjustments to be made to the actuator using Exlar's proprietary software. The test series was loaded using National Instruments Labview 2010 on an Xplore Technologies rugged tablet PC. The total weight of the PMUA was approximately 111 N (25 lbf). Two people are required to run the uplift tests: one to hold the apparatus and one to operate the test program.

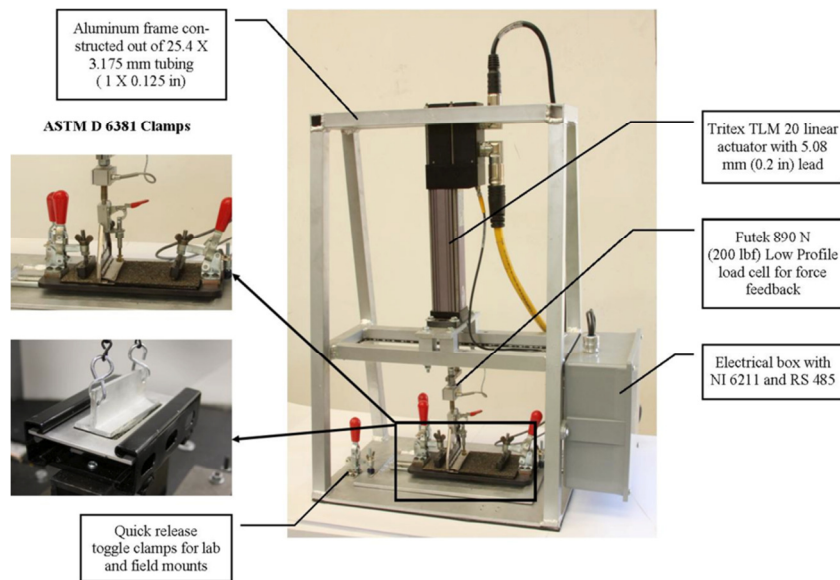


Fig. 28. UF's custom Portable Mechanical Uplift Apparatus capable of performing in-situ ASTM D6381 mechanical uplift tests (controlling computer not shown in figure).

## 2.4.3 Experimental Procedure

The experimental procedure for in-situ ASTM D6381 mechanical uplift tests:

1. Specimens were randomly selected for either ASTM D6381 Procedure A or Procedure B uplift testing.
  - a. Procedure A specimens were made using a hook blade knife to cut two 114 mm (4.5 in) vertical lines (upslope) into the upper shingle strip

starting from the leading edge of the shingle's strip (Figure 29a). Care was taken not to disturb the sealed specimen. Additional vertical cuts were made in the adjacent shingles to prevent interference during uplift testing.

- b. Procedure B specimens were made using a hook blade knife to cut two 38 mm (1.5 in) vertical lines (upslope) into the upper shingle strip starting from the leading edge of the shingle's strip. The two vertical lines were 95 mm (3.75 in) apart. The top portion of the shingle specimen was then isolated from the surrounding shingle by 95 mm (3.75 in) horizontal cut along the top of the vertical cut lines. Once the 38 mm (1.5 in) by 95 mm (1.5 in) sealed specimen was isolated, an ASTM D6381 specified aluminum tee was epoxied to the specimen and allowed to cure overnight prior to uplift testing (Figure 29b).



(a)



(b)

**Fig. 29. Test specimens prepared for in-situ ASTM D6381 mechanical uplift testing (a) Procedure A specimen and (b) Procedure B specimen.**

2. ASTM D6381 Procedure A tests were conducted by first placing the PMUA over the specimen such that only the specimen was exposed through the bottom plate of the apparatus. The ASTM D6381 Procedure A specified test clamp, attached to the actuator's arm, was then secured to the leading edge of the specimen for mechanical uplift testing (Figures 30a and 31). Using the test program, the actuator's arm was raised until the slack in the chain connecting the clamp to the actuator was removed. The load cell reading was zeroed in the test program, followed by the initiation of the mechanical uplift test. Once a test was complete, the investigator visually inspected and recorded the failure mode of the test specimen.

- Similar to Procedure A tests, ASTM D6381 Procedure B tests were conducted by first placing the PMUA over the specimen such that only the specimen was exposed through the bottom plate of the apparatus. The aluminum tee was then connected to the actuator via two chains hooked into either side of the tee. Using the test program, the actuator's arm was raised until the slack in the chains was removed (Figure 30b). The load cell reading was zeroed in the test program, followed by the initiation of the mechanical uplift test. Once a test was complete, the operator visually inspected and recorded the failure mode of the test specimen.



(a)



(b)

Fig. 30. The Portable Test Apparatus performing in-situ ASTM D6381 mechanical uplift tests: (a) Procedure A and (b) Procedure B.



Fig. 31. The Portable Test Apparatus performing in-situ ASTM D6381 Procedure A mechanical uplift tests.

#### 2.4.4 Results

The discussion of experimental results will begin with the results of in-situ ASTM D6381 mechanical uplift tests. Table 19 presents a summary of ASTM D6381 test results from the four homes investigated. ASTM D6381 Procedure A tests were not performed on ORG-01 due to the location of the sealant strip near the leading edge of the shingle, which prevented the Procedure A clamp from fully grasping the bottom and top portion of the shingles leading edge. The modified Procedure A clamp pieces detailed in ASTM D6381 Section 7.7.3 were not available onsite. ASTM D6381 Procedure B tests were not conducted on ORM-1 due to time constraints. The lowest Procedure A mean uplift resistance was obtained on the oldest roof in the data set, ORM-01.

Uplift resistances of the naturally-aged homes were compared to the resistances of shingle product TT-101 at the 5376 h time interval of the thermal aging experiment – representing the lowest mean resistance values at the longest accelerated aging time period. This serves as a comparison between a currently produced product aged in an artificial environment and naturally-aged shingles. The mean uplift resistance for ORM-01 is 56 N (12.5 lbf) less than the mean uplift resistance of TT-101 – Procedure A after 5376 h of thermal exposure. This difference in mean uplift was statistically significant when evaluated using Welch’s *t* test at a 95% confidence level (*p*-value = 0.000). The mean Procedure A uplift resistances for ORM-02 and ORM-03 were within 11 N (2.4 lbf) and 3 N (0.6 lbf), respectively, of TT-101’s Procedure A mean uplift resistance after 5376 h of thermal exposure. Using the same Welch *t* test as above, the difference in mean uplift resistance for ORM-02 was statistically lower than TT-101’s, while there was no statistical difference between ORM-03’s mean Procedure A uplift resistance and TT-101’s at the 5376 h time interval.

The mean uplift resistances for all three roofs tested by Procedure B were within 20 N (4.5 lbf) of each other. The mean Procedure B uplift resistance for ORM-02 was statistically greater than TT-101’s Procedure B, while ORM-03 and ORG-01 were statistically similar to the mean uplift TT-101. The COVs for all data sets were over 25%. This is slightly higher than, yet still within range of, the COVs observed on thermally aged shingle mean uplift resistance data. The COV for ORM-01 was 60%; however, the COV is significantly more sensitive to fluctuations about this lower mean uplift resistance value than the other, higher, uplift resistance.

**Table 19. Summary of results for in-situ ASTM D6381 mechanical uplift tests**

House ID	Roof Age (years)	Shingle Type	ASTM D6381 Test Procedure	Number of Specimens	Mean Uplift Resistance <sup>a</sup> (N) [lbf]	COV (%)
ORG-01	9	Laminate	B	81	165 [37]	32
ORM-01	13+	Three-Tab	A	25	11 [2.5]	60
ORM-02	13	Three-Tab	A	40	53 [12]	25
			B	40	185 [41.5]	29
ORM-03	10	Three-Tab	A	41	64 [14.5]	38
			B	40	171 [38.5]	42

<sup>a</sup>For comparison: Thermally aged TT-101 - 5376 h time interval: Procedure A = 67 N, Procedure B = 161 N

The ASTM D7158 uplift pressure coefficients for the four shingle roofs are unknown; therefore an exact examination of the total uplift resistance of the naturally-aged sealant strip is not possible. Absent this information, the pressure coefficient data provided by TT-101 in the thermal aging tests (Table 12) were used. The corresponding total uplift resistance results for ORM-02 and ORM-03 are given in Table 20 along with a comparison to the minimum uplift resistance required by ASTM D7158 to meet a Class H wind resistance. The approximated wind uplift resistances for both ORM-2 and ORM-3 are over five times the required mean uplift values to achieve ASTM D7158 Class H. This is a significant finding because these products have naturally aged for over nine years in the hot and humid climate of Florida. An inspection of the Procedure B mean uplift resistance result on ORG-01 indicated that its wind resistance would likely surpass the requirements of ASTM D7158 Class H, whereas house ORM-01 would likely be close to the ASTM D7158 Class H requirement. Procedure A tests for ORG-01 and Procedure B tests for ORM-01 were not performed, therefore, the conclusions made regarding these homes are weaker than the conclusions for ORM-02 and ORM-03. The sealant strength at the time of installation could not be determined, therefore, conclusions on the degradation of the shingle tab's sealant strength over time cannot be made.

**Table 20. Estimated ASTM D7158 total uplift resistances for ORM-02 and ORM-03**

House ID	Roof Age (years)	Shingle Type	Mean Total Uplift Resistance of Naturally-Aged Shingles <sup>a</sup> (N) [lbf]	Minimum Required Mean Uplift Resistance for ASTM D7158 Class H <sup>a</sup> (N) [lbf]
ORM-02	13	Three-Tab	133 [30]	24 [5.5]
ORM-03	10	Three-Tab	130 [29]	

<sup>a</sup>Using TT-101's ASTM D7158 uplift pressure coefficients (Section 2.2.3.7)

Three failure modes were observed during the in-situ ASTM D6381 tests:

1. Cohesive failure in the sealant – this is characterized by loss of adhesion within the sealant, with portions of the sealant on the upper and lower shingle visible. This failure mode was not observed in the artificially aged shingle tests, and has only been identified in field aging.
2. Cohesive failure in the adherend – this is characterized by a loss of adhesion within the shingle matrix, leaving the complete sealant strip and a portion of the separated shingle matrix adhered to the other shingle surface (Figure 32a)
3. Combined failure – partial cohesive failure in the sealant and a partial cohesive failure in adherend (Figure 32b).



**Fig. 32. Example of failure modes for mechanically uplifted shingles: (a) cohesive failure in the adherend (ORM-01) and (b) combined cohesive failures in the sealant and adherend (ORG-01).**

The distribution of observed failure modes is presented in Figure 33. Examining the failure modes for ORM-2 and ORM-3, it is apparent that the dominant failure mode obtained by Procedure A testing does not match the dominant failure mode obtained by Procedure B testing. This observation is consistent with thermal aging failure mode results (Section 2.2.3.8). For house ORM-01, the internal strength of the shingle matrix was the controlling factor in the uplift resistance of the sealant strip. Thus, the adhesive bond sealing the shingle's leading edge down was stronger than the internal strength of the shingle's asphalt matrix.

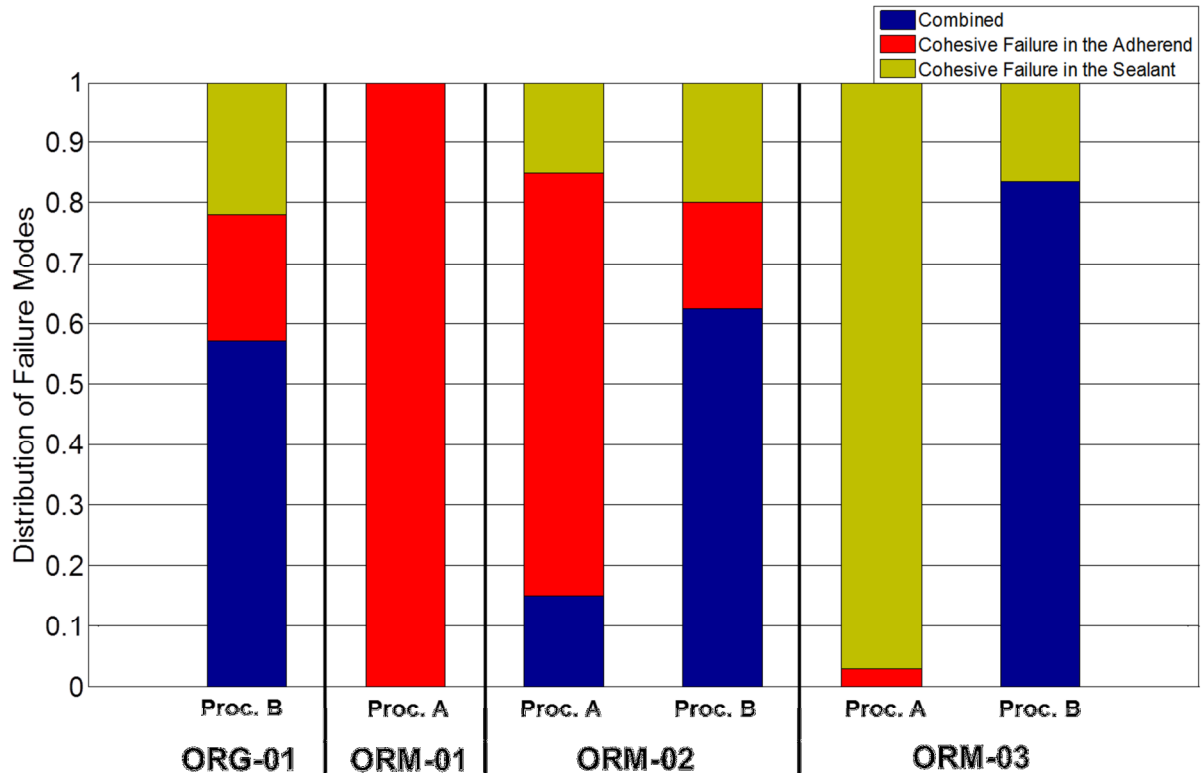


Fig. 33. Distribution of failure modes for in-situ ASTM D6381 mechanical uplift tests.

## 2.4.5 Findings

1. ASTM D6381 Procedure A and B tests were conducted on two roofs, ORM-02 and ORM-03. For both, the estimated mean total wind uplift resistance of the naturally-aged shingles was over five times the minimum mean wind uplift resistance required by ASTM D7158 to meet a wind resistance rating of Class H (the highest rating). While the uplift strength of the shingle's sealant strip at the beginning of the roof's life is unknown, clearly natural aging has not degraded the sealant's performance below the highest wind rating available to shingles as of the writing of this report. Finally, both products were manufactured before the adoption of ASTM D7158, thus, their wind resistance was likely established using the older ASTM D3161 wind test standard. For both shingles investigated, the test data indicated that they would likely meet ASTM D7158 Class H requirements after at least nine years of natural aging.
2. The two remaining roofs, ORG-01 and ORM-01, were each subjected to only one ASTM D6381 test procedure. The mean ASTM D6381 Procedure B uplift resistance of ORG-01 was within 6 N (1.5 lbf) of ORM-01 Procedure B's mean uplift resistance. The mean ASTM D6381 Procedure A mean uplift resistance for ORM-01 shingles was 83% lower than the 5376 h time interval of TT-101 - Procedure A.

3. The variability of the mean uplift resistances for three of the four homes is on the higher end of the range variability obtained from mechanical uplift tests on thermally aged shingles. The data set with the most variability, ORG-01, is likely exaggerated due to the sensitivity of variability measurements at the lower mean values.
4. We observed different dominant failure modes between Procedure A and B mechanical uplift tests. This is consistent with the failure mode results from mechanical uplift tests performed on thermally aged shingles.

#### **2.4.6 Future Work**

We recommend future work continue on in-situ mechanical uplift tests on naturally-aged roofs. At present, testing naturally-aged shingles in their installed state is the best available method of evaluating an aged shingle's wind resistance. Additional tests would provide further ground-truth to observations made during accelerated laboratory methods. However, these tests present logistical difficulties. This is a destructive test and requires the shingle roof to be located either on a home scheduled for demolition or a roof that will be replaced just after uplift testing. This investigation utilized homes slated for demolition, but these homes are rarely offered. If testing is performed on a roof just prior to replacement, it is likely that the roof is: (a) old enough to require replacement, (b) damaged due to a manufacturing/installation error or (c) has become damaged due to weather phenomena (e.g., a wind or hail storm). Option (c) provides an interesting opportunity for several stakeholder groups. If an asphalt shingle roof were damaged as a result of a wind storm, ASTM D6381 mechanical uplift tests could be performed on several shingles throughout the roof in order to establish wind uplift resistance of the shingles. Similar to the method of analysis presented above, conservative ASTM D7158 pressure coefficient values could be established for the type of shingle (i.e., three-tab or laminate) and an estimated total uplift force of the damaged roof could be compared to ASTM D7158 uplift resistance requirements. If the uplift resistance of the roof were greater than the uplift required by ASTM D7158, it is likely that the damage was not initiated by the unsealing of a fully sealed shingle strip. Further discussion about the sealing performance of naturally-aged asphalt shingle roofs is provided in the next section of this report.

## 2.5 Survey of Existing Asphalt Shingle Roofs for Unsealed Asphalt Shingles

### 2.5.1 Introduction

As the main wind load resistance for a shingle is provided by the sealant strip, the lack of adhesion of the shingle's leading edge to the underlying shingle will increase the vulnerability of the shingle to wind damage. Peterka et al. (1997) observed a 50% increase in wind uplift pressure coefficient from a fully-unsealed shingle tab that was raised 5 mm (0.2 in) above the underlying shingle. As will be shown later, even a partial unsealing along the sealant strip line can increase the total uplift load generated on the sealant strip beyond a shingle's predicted ASTM D7158 uplift forces.

Recent work by Marshall et al. (2010) reported patterns of partially unsealed shingles observed on existing residential structures throughout the United States. The patterns, shown in Figure 34, were reportedly located near end-joint regions and it was postulated that shear forces generated from long-term cyclical thermal expansion and contraction of the shingle system caused the unsealing. As a shingle temperature increases through the day, the shingle will expand. Conversely, as a shingle temperature decreases through the night, the shingle material will contract. Asphalt shingle roofs are installed with lateral offsets between shingle courses (rows). Therefore, the leading edge of each shingle strip is adhered to two shingle strips below. Thermal cycling will cause a differential movement between the two adjacent shingle strips, resulting in the application of shear stress through the sealant strip. It is theorized that, over time, the sealant strip becomes unable to resist this shear stress resulting in unsealing of the leading edge of the shingle.

Thermal expansion and contraction of the shingle system was also the reported cause of three-tab fiberglass reinforced shingle splitting and cracking issues discovered in the late 1980's (Koontz, 1990). In response, ARMA and Western States Roofing Contractors Association initiated research into increasing the splitting resistance of the fiberglass reinforcement material to resist the tensile forces that are generated inside the shingle during thermal cycling (Noone and Blanchard, 1993). Given the observations by Marshall et al. (2010) it appears that the failure mode of the shingle due to thermal cycling may have transitioned from cracking of the shingle's surface to unsealing of the shingle near the end joint. However, at present, there are no reports on the extent of this pattern of unsealing and a definitive cause for the unsealing remains unknown.



**Fig. 34. Patterns of partially unsealed asphalt shingles reported in Marshall et al. (2010). (© American Meteorological Society. Used with permission).**

The purpose of this investigation was to quantify the unsealing of asphalt shingles on existing residential roofs using a non-destructive forensic survey method. The method, detailed in Section 2.5.2, provided the investigators the ability to efficiently survey a roof’s complete shingle system, including hips, ridges, and eaves, while maintaining the existing wind resistance of the roof. The surveys were conducted on 27 existing residential structures throughout Florida (Figure 35). Homes were acquired through a Florida Department of Emergency Management home acquisition grant and through personal contacts of the investigators. The roof ages investigated ranged from 1 month to 20+ years and included three-tab and laminate shingle systems.



**Fig. 35. Locations of the unsealed asphalt shingle surveys conducted in Florida.**

### 2.5.2 Survey Procedure

For each roof investigated, the following procedures were conducted:

1. For each shingle, the investigator used their fingertips to gently lift up on the shingle tab/strip, running their fingers along and lifting up on the face of the

leading edge of the tab (Figure 36). The investigator took caution when applying the uplift force to ensure that the tab seal bond was not broken. Compared to a sealed shingle, an unsealed shingle tab provided a significantly lower resistance to finger uplift.

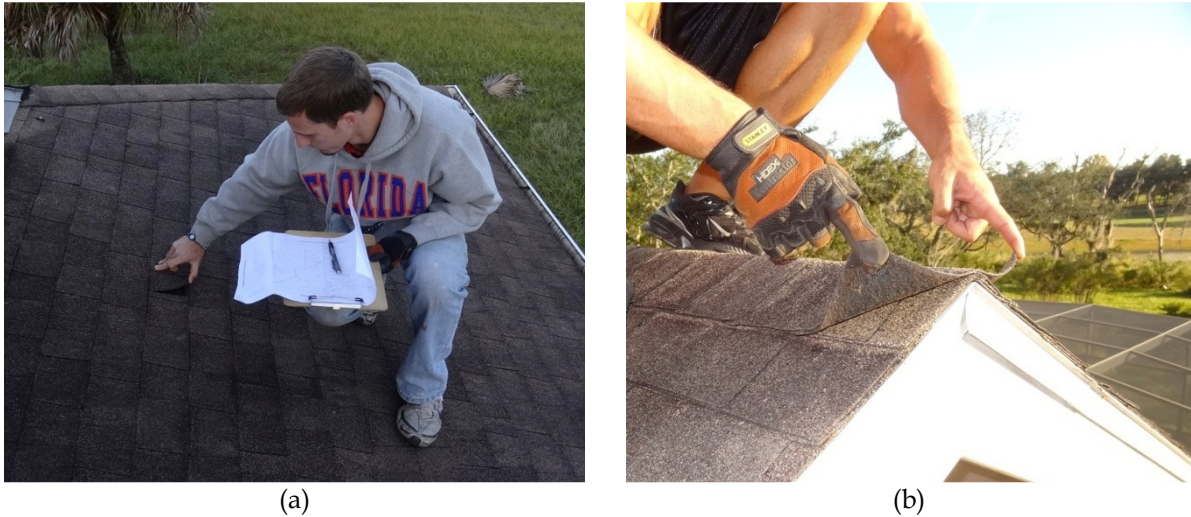


**Fig. 36. UF investigators conducting an unsealed shingle survey: (a) unsealed field shingle and (b) unsealed ridge shingle.**

2. For each shingle that was not fully sealed, the investigator:
  - a) Measured the length of the unsealed portion of the sealant. If the unsealed portion was less than 50 mm (2 in.) it was not marked as an unsealed area.
  - b) Small strips of colored tape were placed on each unsealed shingle in order to identify its location in photographs. This tape was removed once the investigation was completed.
  - c) The location of unsealed shingles on the roof was recorded on roof plan. The location of the unsealed area on the strip/tab shingle (i.e. left, middle, or right side of strip/tab) and length of unsealed sealant was also recorded on the roof plan.
  - d) The failure mode of the sealant directly under the unsealed shingle was documented along with any installation/ manufacturing issues that may have potentially caused the observed unsealing (e.g., a high fastener that prohibited the two shingles from bonding to each other).
  - e) Photos were taken of the sealant strip for each of the observed unsealed conditions.
3. When possible, the investigator recorded the shingle manufacturer, product name, installation age, and time of year when the shingles were installed.
4. Detailed photos were taken to show the following roof conditions:
  - a) A full field shingle strip to identify color and shingle type (three-tab or laminated shingle).

- b) Hip and ridge shingle attachment methods (when possible).
  - c) The shingle's self-seal sealant pattern (when possible).
  - d) The surfacing of any shingles that are directly impacted by sun inhibitors.
  - e) Elevation shots showing all roof slope exposures.
  - f) Photographs of the sealant condition for unsealed shingles.
5. Detailed notes were taken to record the following items:
- a) A field shingle's width, exposure length, full length (when possible), and tab width (if three-tab).
  - b) A typical hip/ridge shingle's width, exposure length, and full length (when possible).
  - c) The width and location of shingle tab's self-seal relative to the leading edge of the shingle (when possible).
  - d) The horizontal offset distance between the shingle's courses.
  - e) Typical fasteners, fastening location and pattern of fastening for both field and hip/ridge shingles (when possible).
  - f) Installation methods for starter strips along the eave (when possible).
  - g) The weather conditions at the time of the survey, including: ambient temperature, sun exposure (i.e., partly cloudy), and temperature of the asphalt shingles throughout the duration of the roof survey.
6. The survey continued until all shingles installed on the roof were surveyed.

### **2.5.3 Analysis Procedures**

For the following analysis, any shingle located on the roof (e.g., field, hip, or ridge) with an unsealed length greater than 50 mm (2 in) was referred to as an "unsealed" shingle. For each roof investigated, a total percentage of unsealed field shingles was calculated by dividing the total number of unsealed field shingles by the total number of shingles located in the field. The total number of shingles was estimated by dividing the total exposed area of the field of roof by the total area of a single shingle strip. A total percentage of unsealed hip and ridge shingles was calculated by dividing the total number of unsealed hip or ridge shingles by the total number of hip or ridge shingles located on the roof. Each home was given a unique identification code with the first three letters corresponding to the city location of the home (Table 21).

**Table 21. City locations for each identification code**

<b>Identification Code</b>	<b>City</b>
SAR	Sarasota, FL
GNV	Gainesville, FL
ORM	Ormond Beach, FL
ORG	Orange City, FL
ALT	Altamonte Springs, FL

## **2.5.4 Results**

### **2.5.4.1 Field Shingles**

Figures 37 and 38 depict typical patterns and amount of unsealing that was observed with blue tape marking the location of unsealed shingle strips. The patterns are not random in nature and were observed on both three-tab and laminate systems with the pattern conforming to the shingle's installation method (i.e., racked or diagonally installed).

**86% Unsealed**



(a)

**39% Unsealed**



(b)

**Fig. 37. Example of unsealing patterns for (a) raked three-tab system with 86% unsealing and (b) diagonally installed laminate system with 39% unsealing.**

**17% Unsealed**

(a)

**1% Unsealed**

(b)

**Fig. 38. Example of unsealing patterns for (a) diagonally installed laminate system with 17% unsealing and (b) diagonally installed laminate system with 1% unsealing.**

For three-tab shingles, the partial unsealing occurred on the tab directly above the end joints of the two shingle strips on the course below (Figure 39). Typically, one-half of the tab width, approximately 152 mm (6 in) was unsealed up to the end joint, while the other half remained fully-sealed. The one-half tab that was unsealed was always located on the half of the tab nearest its own end joint. Fully-unsealed tabs over end joints were observed on older roof systems; however, this was not a frequent observation. The two other tabs not near an end joint were typically well-sealed.

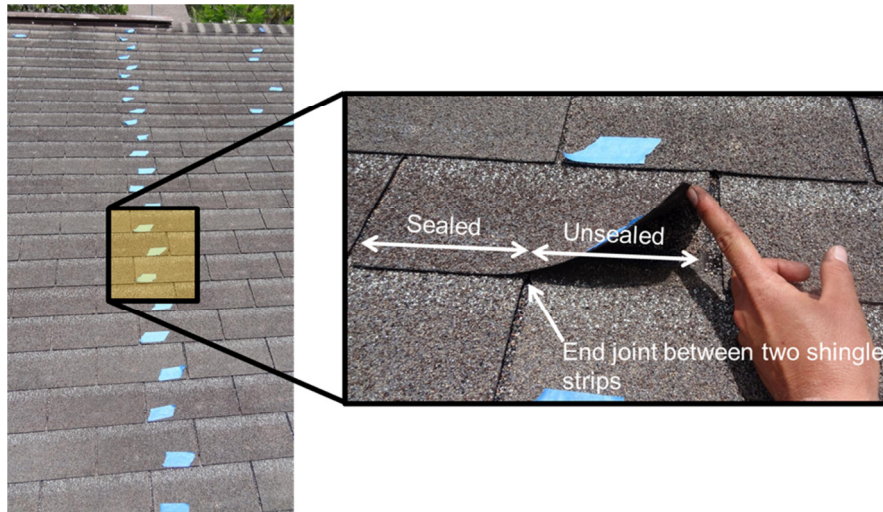


**Fig. 39. Typical unsealing pattern of three-tab shingles that are vertically installed.**

Laminate shingles exhibited similar patterns of partial unsealing (Figure 40). As with the three-tab system, the laminate shingles were typically unsealed from their own end joint to the end joint of the laminate shingle on the course below. With the exception of one older roof, this observed partial unsealing did not extend beyond the end of the course below. Therefore, the length of unsealing for a given laminate shingle strip was controlled by the offset placed between shingle courses. Laminate systems are specified to be installed in a diagonal fashion with offsets ranging from 102 - 178 mm (4 - 7 in). Thus, the percentage of unsealing for each laminate strip can range from 10 - 18% of the total width, for a standard 991 mm (39 in) wide laminate shingle.

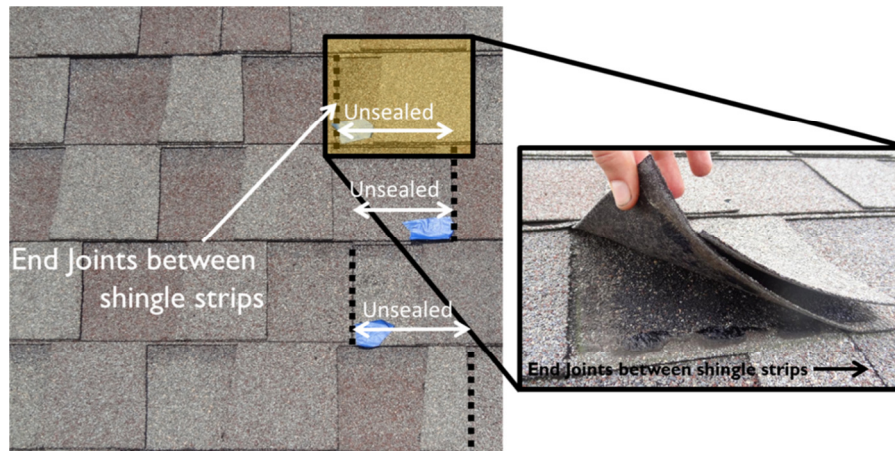


**Fig. 40. Typical unsealing pattern of laminate shingles showing a transition between diagonal directions.**

The analysis of sealant strip failure modes is an important step towards defining the cause of the patterns of unsealing. For all shingles exhibiting unsealing patterns, both three-tab and laminate, the plane of unsealing occurred cohesively within the sealant. As shown in Figure 41, this failure mode is defined by the presence of sealant on the upper and lower

shingles. In the manufacturing process, the sealant is placed on either the top or bottom of the shingle only. Therefore, the presence of sealant on the underside of the top shingle and the top surface of the bottom shingle would indicate that the upper shingle's leading edge was sealed down prior to unsealing. This consistency in failure mode is important because it suggests that the unsealing of shingles is independent of shingle type, installation procedure, roof contractor, and shingle manufacturer. Therefore, we conclude that the observed partially unsealed shingles were a result of a systematic failure of the shingle's sealant strip rather than a random unsealing event. The effects of aging on unsealing will be discussed later in this analysis.



**Fig. 41. All unsealed shingles near the end joint failed cohesively within the sealant strip, suggesting that shingles were previously adhered.**

Newer shingle systems contained a minimal amount of unsealing. Their unsealing was due to installation errors that prevented the shingle from sealing to the course below, rather than the patterns of unsealing noted above. These errors included: under-driven nails in the sealant strip, debris in the sealant strip, and release tape that was inadvertently stuck to the shingle's sealant strip due to packaging errors.

The final analysis of unsealed field shingles will focus on the effects of aging. Table 22 provides a summary of results for each roof investigation and includes information on the roof's age, where possible, the total roof area investigated, the percentage of unsealed field shingles, and whether or not patterns of unsealing were observed. Two observations can be made:

1. 10 of the 27 roofs (37%) had at least 15% of their shingle strips partially unsealed, and 44% had at least 5% of their shingle strips unsealed. Almost every observation of unsealing indicated that the strip was originally sealed, and became unsealed sometime after installation. This indicates that the issue of post-installation unsealing is significant, and it will be shown in Section 3.3 that unsealing elevates the risk of additional (e.g., progressive) unsealing on the adhered portion of the sealant strip due to increased wind uplift forces.
2. A distinct pattern of partial unsealing was observed on 70% (19 out of 27) of the roofs surveyed, including both laminate and three-tab systems. The eight roofs that did not exhibit a pattern had less than or equal to 1% unsealed shingles. There were no cases where widespread unsealing was observed with no pattern.

Unsealing is clearly not random, and strongly associated with the location of the end joint.

It appears that a correlation exists between roof age and the total amount of unsealed shingles strip for a given roof (Figure 42). For roofs with less than six years of aging, no patterns of unsealing were observed and the total percentage of unsealed field shingle strips was less than 1%. The first observation of unsealing patterns was made on a six-year-old laminate roof (SAR-03) that contained 1.4% unsealed shingle strips. The percentage of unsealing was variable for roofs with greater than or equal to six years of aging; however, 15 out of the 18 roofs in this category had visible unsealing patterns.

By grouping the homes of known ages into three age categories (0-6, 7-13, 14-20) the increase in unsealed shingle strips through the aging process is evident, as shown in the boxplot of Figure 43. Also evident is the increase in the variability of the data set for homes older than seven years. A statistical test to evaluate the significance of differences in the amount of observed unsealing between the three age groups is summarized in Table 23. The variance of each age group is not equal; therefore a single sided T-test assuming unequal variances at a 95% confidence interval ( $\alpha = 0.05$ ) was selected for this analysis. From these results we conclude that there is a statistically significant difference between the 0-6 and 7-13 age groups and between the 0-6 and 14-20 age groups. No statistical significance was established between the 7-13 and 14-20 age groups. The results indicate that the unsealing of asphalt shingles may occur after only six year of aging. However, due to the relatively small sample set and the lack of surveys outside of Florida, the trends observed within this report should be confirmed through additional surveys throughout the United States. Marshall et al. (2010) indicates they have seen this pattern in a number of areas of the US.

**Table 22. Summary of results from unsealed asphalt shingle survey - unsealed field shingles**

ID	Roof Age (Years)	Shingle Type	Shingle Color	Roof Slope	Roof Area (m <sup>2</sup> ) [ft <sup>2</sup> ]	Percent of Unsealed Field Shingle Strips	Observed Patterns of Unsealing
SAR-01	9	Laminate	Grey/Light Red	7:12	262 [2820]	39.0	Yes
SAR-02	7	Laminate	Light Brown	6:12	154 [1654]	32.3	Yes
SAR-03	6	Laminate	Light Brown	6:12	154 [1654]	1.4	Yes
SAR-04	16	Laminate	Grey	6:12	232 [2500]	26.4	Yes
SAR-05	15	Laminate	Grey	6:12	266 [2863]	16.9	Yes
SAR-06	17	Laminate	Grey	6:12	251 [2700]	21.2	Yes
SAR-07	0.1	Laminate	Grey	4:12	80 [860]	0.5	No
SAR-08	10	Three-Tab	Light Brown	4:12	149 [1600]	3.5	Yes
SAR-09	20	Three-Tab	Light Green	4:12	67 [716]	56.0	Yes
SAR-10	19	Laminate	Grey	7:12	134 [1447]	79.5	Yes
SAR-11	0.2	Laminate	Brown	4:12	191 [2056]	0.6	No
SAR-12	N/A	Three-Tab	Light Brown	4:12	217 [2340]	86.7	Yes
SAR-13	9	Laminate	Grey	6:12	245 [2640]	4.0	Yes
SAR-14	8	Laminate	Grey	6:12	245 [2640]	23.1	Yes
SAR-15	19	Laminate	Brown	4:12	424 [4567]	4.0	Yes
SAR-16	7	Laminate	Light Grey	7:12	163 [1866]	0.4	No
SAR-17	5	Laminate	Light Brown	7:12	150 [1615]	0.6	No
SAR-18	N/A	Three-Tab	Light Brown	7:12	227 [2444]	66.1	Yes
GNV-01	N/A	Three-Tab	Grey	4:12	324 [3494]	2.7	Yes
GNV-02	3	Laminate	Grey	4:12	419 [4509]	0.6	No
GNV-03	18	Three-Tab	Brown	4:12	321 [3453]	3.5	Yes
ORM-01	13(+) <sup>1</sup>	Three-Tab	Brown	4:12	221 [2375]	7.7	Yes
ORM-02	13	Three-Tab	Brown	4:12	194 [2089]	1.0	No
ORM-03	10	Three-Tab	Brown	4:12	192 [2067]	5.1	Yes
ORG-01	9	Laminate	Light Brown	6:12	378 [4070]	6.3	Yes
ALT-01	N/A	Three-Tab	Grey	4:12	233 [2505]	0.6	No
ALT-02	2	Laminate	Grey	6:12	240 [2586]	0.2	No

<sup>1</sup>Roof was installed prior to 1999 (not used in Figure 42)

**Total Roof Area Investigated**  
**(m<sup>2</sup>) [ft<sup>2</sup>]**  
**6144**  
**[66130]**

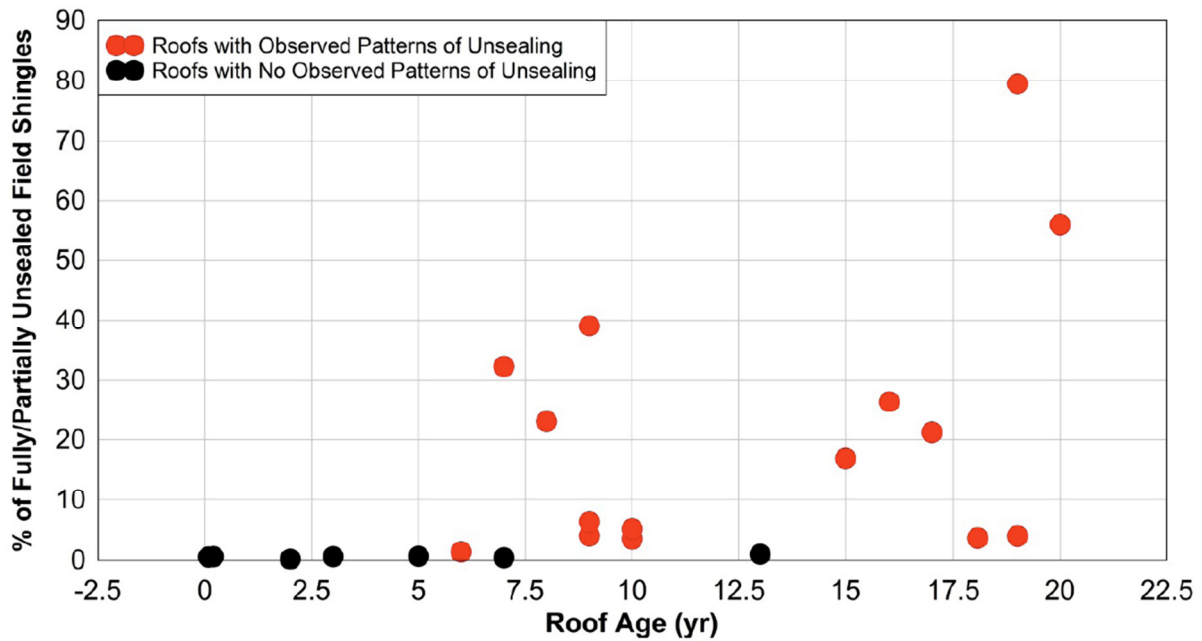


Fig. 42. Percent of unsealed shingle strips located in the field of the roof (hip and ridge shingles not included) versus roof age at the time of investigation.

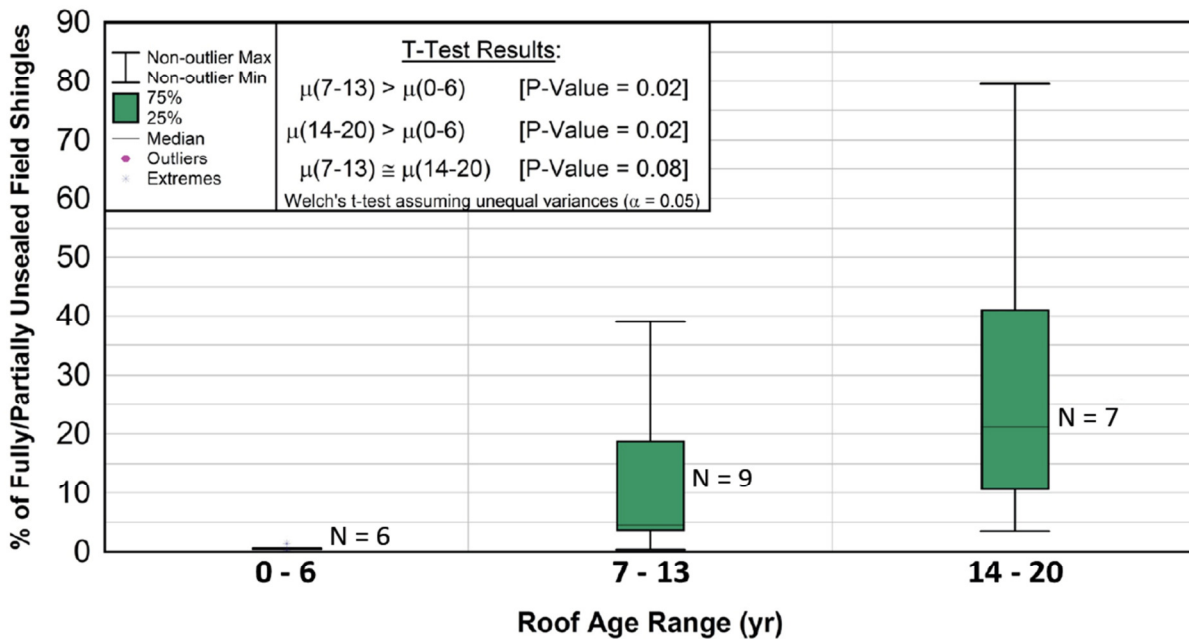


Fig. 43. Boxplot of unsealed shingle strips located in the field of the roof versus roof age at the time of investigation.

Table 23. Statistical comparison between grouped roof ages

Roof Age Range (Years)	Mean Amount of Observed Unsealing (%) [ $\sigma$ ]	Statistically Significant Difference Between 0-6 Year Old Roofs (P-Value) <sup>1</sup>	Statistically Significant Difference Between 7-13 Year Old Roofs (P-Value) <sup>1</sup>
0-6	0.7 [0.4]	--	--
7-13	12.7 [14]	Yes (0.02)	--
14-20	29.6 [28]	Yes (0.02)	No (0.08)

<sup>1</sup>Statistical significance determined using T-Test single sided test with unequal variance with  $\alpha = 0.05$

#### 2.5.4.2 Hip and Ridge Shingles

The analysis of field shingle unsealing highlights the potential for thermal cycling causing overstrain on the sealant near the end joint, and shows a correlation of unsealing with roof age. However, a different cause was identified for hip and ridge shingle unsealing. Two unsealing conditions were observed during the surveys:

1. Completely unsealed hip and ridge shingles due to a lack of sealant strips below the leading edge (Figure 44a). This error occurred when the installer used shingles that did not contain sealant strips. This unsealing condition was observed on three of the 27 homes investigated.
2. Adhesive failure between the shingle's sealant strip and the shingle above. Partial unseal was observed on one or both sides of the roof slope, starting from the edge of the shingle and extending towards the hip/ridge line (Figure 44b). The adhesion along the ridge/hip line was significantly better than the edges of the shingle.



(a)

(b)

**Fig. 44. Typical partially unsealed ridge and hip shingle conditions: (a) fully unsealed ridge shingle due to lack of sealant strip below cap and (b) poor adhesion on edges of shingle.**

Unsealed Condition 1 is considered to be an avoidable error in installation where the installer used asphalt shingles that did not have sealant strips. This condition will not be discussed further in this report. Condition 2, however, may be a system-level design issue in addition to an installation quality issue. Hip and ridge shingles can be purchased either pre-manufactured or cut from three-tab shingles. Both pre-manufactured and cut three-tabs are originally flat shingle strips that are folded over the hip/ridge line and nailed to the substrate with two fasteners per shingle. Similar to field shingles, the leading edge of hip and ridge shingles rely on the sealant strip to restrain the shingle from lifting in the wind. It appears the action of folding the shingle over the roofline may interfere with the proper sealing of the shingle. The lack of sealant transfer suggests that a weak or no bond existed between the sealant strip and shingle's leading edge. Nails in the sealant strip line and high nailing was observed on several partially unsealed shingles, which may have influenced the adhesion performance. The sealant performance directly along the hip/ridge line was significantly better than the edges of the shingle. Further evidence of design issues can be found in Table 24 and Figure 45 where the aging effects noted in field shingles are not evident in the hip and ridge shingle data sets. Newer roof systems (< 10 years) appear to be as vulnerable to unsealed hip and ridge shingles as older roofs ( $\geq 10$  years) (Figure 45).

Unsealed hip and ridge shingles will be susceptible to lifting due to near roof surface wind flow that can enter the underside of the unsealed shingle. For unsealed ridge shingles, the vulnerability to blow off is further increased because the highest wind speeds on a roof occur at the ridgeline (see Section 3.2). A full analysis on the wind performance of unsealed hip and ridge is addressed in Section 5.

Table 24. Summary of results from unsealed asphalt shingle survey - unsealed ridge and hip shingles

ID	Roof Age (Years)	Shingle Type	Total Length of Ridge Shingles (ft)	Percent of Unsealed Ridge Shingles	Total Length of Hip Shingles (ft)	Percent of Unsealed Hip Shingles
SAR-01	9	Laminate	61	23.9	164.5	20.5
SAR-02	7	Laminate	42	0.0	N/A	N/A
SAR-03	6	Laminate	42	6.7	0	N/A
SAR-04	16	Laminate	38	5.0	138	20.0
SAR-05	15	Laminate	34	2.7	160	1.7
SAR-06	17	Laminate	37	11.1	141	23.4
SAR-07	0.08	Laminate	27	3.4	N/A	N/A
SAR-08	10	Three-Tab	49	3.4	N/A	N/A
SAR-09	20	Three-Tab	30	23.9	35	8.0
SAR-10	19	Laminate	85	100.0	N/A	N/A
SAR-11	0.2	Laminate	63	2.2	N/A	N/A
SAR-12	N/A	Three-Tab	67	18.7	N/A	N/A
SAR-13	9	Laminate	52	9.0	79	8.9
SAR-14	8	Laminate	52	2.6	79	0.0
SAR-15	19	Laminate	65	0.0	179	10.8
SAR-16	7	Laminate	32	100.0	74	100.0
SAR-17	5	Laminate	38	0.0	58	0.0
SAR-18	N/A	Three-Tab	84	19.8	N/A	N/A
GNV-01	N/A	Three-Tab	50	0.0	139	3.0
GNV-02	3	Laminate	170	2.8	N/A	N/A
GNV-03	18	Three-Tab	100	5.8	N/A	N/A
ORM-01	13(+) <sup>1</sup>	Three-Tab	57	0.0	N/A	N/A
ORM-02	13	Three-Tab	48	0.0	N/A	N/A
ORM-03	10	Three-Tab	48	3.5	N/A	N/A
ORG-01	9	Laminate	72	12.1	63	22.6
ALT-01	N/A	Three-Tab	45	0.0	N/A	N/A
ALT-02	2	Laminate	48	17.6	142.3	30.0

<sup>1</sup>Roof was installed prior to 1999 (not used in Figure 45)

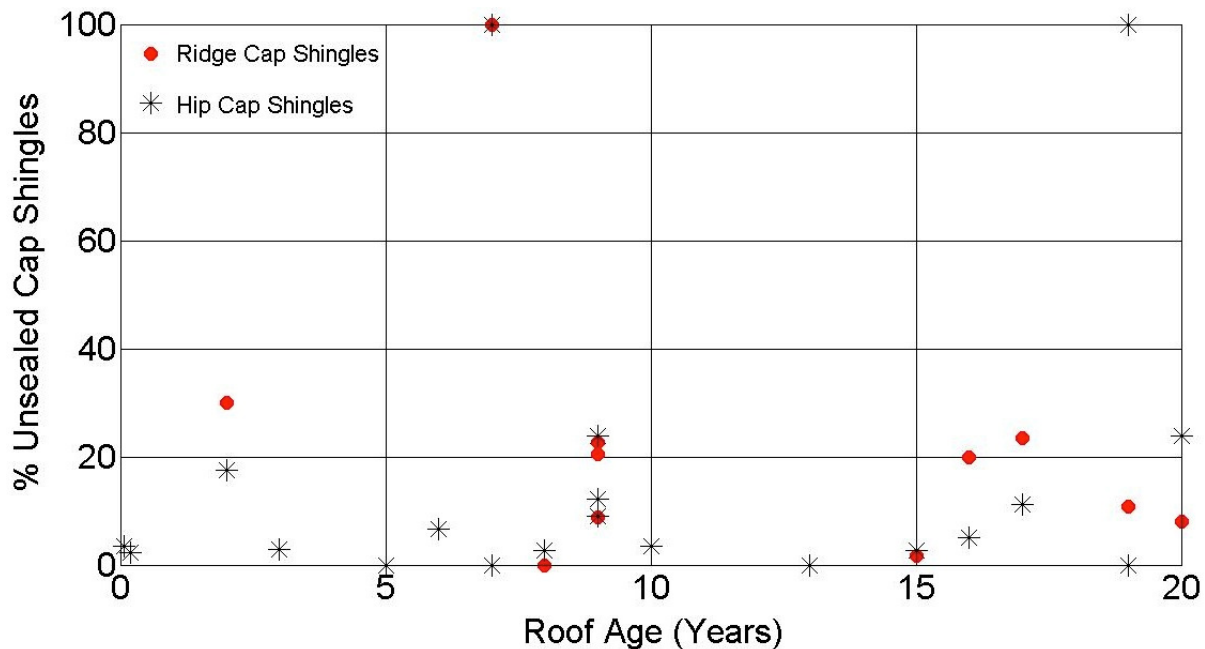


**Fig. 45. Percent of partially unsealed cap shingles versus roof age at the time of investigation. (Note: 100% unsealed ridge shingles represent a lack of sealant strips below the caps)**

### 2.5.5 Findings

1. Observed patterns of partially unsealed asphalt shingles on 19 out of 27 roofs surveyed.
  - a. Thermal expansion and contraction of the shingle system may cause unsealing. Shingles are installed with a lateral offset between courses (rows). Therefore, each shingle strip is bonded to two different shingles on the course below. As each shingle expands and contracts due to thermal fluctuations, a differential movement may occur between each shingle. An in-plane shear stress will be exerted on the tab seal due to a differential movement of the bonded shingles. Over time, the tab sealant may not be able to resist this cyclical shear application and its bond to the shingle tab may break cohesively, leaving it unsealed.
  - b. For all shingles where this pattern unsealing was observed, the failure mode of the tab sealant was a cohesive failure within the sealant. A visible transfer of sealant between the top and bottom shingle was noted for all shingles, indicating that the shingles were sealed at one time before their bond was broken.
  - c. For laminate shingle systems, the unsealing occurred from the end joint of shingle strip to end joint of shingle strip on the course below. The resultant unsealed length is controlled by the offset between shingle

courses; typically ranging from 102 – 178 mm (4 – 7 in). This represents an unsealed length of approximately 10 – 18% of the total length of sealant per shingle strip.

- d. For three-tab shingle systems, the unsealing occurred on one-half of the shingle tab above the end joint of the shingle course below. The unsealing always occurred on the half of the tab closest to its own end joint. The adhesive performance of shingle tabs not above an end joint was excellent, even on older roof coverings.
  - e. A statistically significant difference was established between 0-6 and 7-13 year old roofs and between 0-6 and 14-20 year old roofs. This indicates that an increase in roof age may cause an increase in the amount of unsealed shingles, depending upon the aged physical properties of the tab sealant.
  - f. The amount of unsealing, either fully or partially unsealed, ranged from 1.4% to 86% of the shingle strips on a given roof.
  - g. The amount of unsealing on a given roof appears to be independent of shingle type (three-tab or laminate), roof slope, and house orientation. The investigation was only conducted in Florida, therefore, it is unknown if there are any additional effects from climate variability (e.g., significance of freeze/thaw cycles).
  - h. Observations of partial unsealing exhibiting vertical or diagonal patterns occurred on roofs as new as six years old.
2. Observed hip and ridge cap adhesion issues on 22 out of the 27 homes (81%) surveyed. These patterns correlate to damage observations noted in several FEMA post-hurricane reports (FEMA 2005a, 2005b, 2006, and 2009).
    - a. Unsealing typically occurred on either side of the hip or ridge. Good adhesion was noted along the ridgeline itself, but it appears the folding over of the cap to join the roof slope may be problematic for sealing. Installation issues such as high nailing, overdriven fasteners, and fasteners in the sealant strip can also contribute to lack of edge adhesion. This unsealing exposes the shingle to wind flow that will travel perpendicular to the cap's sealant line, potentially increasing the risk of blow off.
    - b. The total percentage of unsealed hip and ridge shingles for a given roof appears to be independent of the age of the roof.
    - c. The dominant failure mode of this unsealing was an adhesive failure between the sealant and the shingle. This is in contrast to the cohesive

failure mode observed in (1), above, and suggests that the hip and ridge caps may not be fully sealing at the beginning of their installation.

### 2.5.6 Future Work

The data gathered from the 27 roof surveys provided essential information on potential issues in the existing residential building stock. However, these data only represent a small cross-section of existing homes in Florida. Future work should:

1. Expand the roof surveys to include more residential structures throughout the United States. This research studied roofs in Florida's subtropical climate, however, it is unknown if this issue is found in other climates.
2. Investigate the cause of the unsealing patterns. This work should first explore the link between thermal cycling and the unsealing of asphalt shingles. Cullen (1963) reported the linear expansion of fiberglass-reinforced built-up roofing (a somewhat similar construction to asphalt shingles) was non-linear over a temperature range of -51 to 60°C (-60 to 140°F). The greatest rate of expansion was reported at lower temperatures with the rate of change decreasing with increasing temperature. This observation was attributed to the visco-elastic nature of asphalt at elevated temperatures. Cullen (1963) reported two different values of the linear expansion of the fiberglass-reinforced built-up roofing; however, these two values were off by three orders of magnitude between each other and, therefore, the correct value is unknown. Future work should first characterize the rate of expansion and contraction of a modern fiberglass-reinforced asphalt shingle during daily heating and cooling cycles. Using this change rate, the work should then quantify the shear stresses generated on the sealant strip and fasteners during the thermal cycling in order to develop product modifications that can account for these stresses over time.

### 3. ASSESSMENT OF THE ASPHALT SHINGLE WIND LOAD MODEL

#### 3.1 Introduction

Prior to 2003, the wind resistance of asphalt shingles was determined by the ASTM D3161/UL 997 standardized test method based on experimental research conducted by Cullen (1960). The test method consists of passing air across asphalt shingle specimens installed on a 1.27 m by 1.68 m (50 in by 66 in) wood test deck angled at a slope of 2:12. Prior to the test, the shingle decks were conditioned for 16 hours at an ambient temperature of 57-60°C (135-140°F) to activate the thermally sensitive self-sealing sealant strip that restrains the leading edge of the shingle from lifting. Originally the shingles were evaluated as wind resistant if they could successfully withstand a 2 hour wind test at 27 m/s (60 mph) without unsealing of the shingle's sealant strip. In response to observations of shingle damage made in post-storm reports, the test's maximum wind speeds were increased in 2003 to 49 m/s (110 mph) and the shingle's wind resistance was classified according to the following rubric:

*Class A* - The shingles passed at a test velocity of 27 m/s (60 mph)

*Class D* - The shingles passed at a test velocity of 40 m/s (90 mph)

*Class F* - The shingles passed at a test velocity of 49 m/s (110 mph)

In the early 1980s, independent testing performed by Owens Corning found that ASTM D3161/UL 997 did not accurately differentiate the resistance of different shingle systems. Following this study, Colorado State University and Cermak, Peterka and Petersen, Inc. was retained by ARMA to develop a wind uplift model for asphalt shingles in order to provide a more realistic standardized wind test method. The asphalt shingle wind load model and the ASTM D7158 standardized test method were the products of their work.

The asphalt shingle wind load model proposed by Peterka et al. (1997) states that the main wind uplift mechanism for asphalt shingles is caused by a local wind flow separation over the leading edge of the shingle (Figure 46). A region of negative pressure, relative to the ambient, is contained in the separated flow region, and a positive pressure is exerted on the underside of the shingle caused by wind flow under the top shingle. If a shingle's leading edge is fully sealed along the sealant strip, this underside wind flow is restricted from flowing past the sealant strip. Wind uplift forces are applied on the surface of the shingle with the load path continuing directly through the sealant strip line to fasteners in the underlying shingle located near the sealant strip. The lack of sealing along the shingle's sealant strip leaves the shingle vulnerable to lifting in the wind and transfers the main wind load path to the shingle's fasteners upslope of the shingles leading edge.

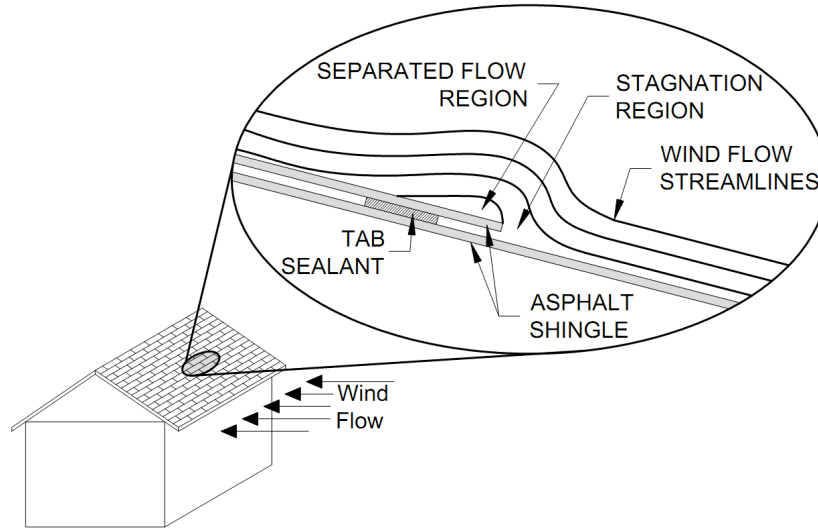


**Fig. 46. Wind uplift forces on asphalt shingles are generated from the separation of wind over the shingle's leading edge.**

Peterka et al (1997) proposed the magnitude of the uplift force is defined by the magnitude of near roof surface wind flow and the geometric composition of the shingle. Model and full-scale measurements of wind flow near the roof surface and in the approach wind flow indicated that the behavior of the near-roof surface wind flow, 25 mm (1 in) above the shingles surface (full-scale), on steep slope roofs is modulated by the upstream approach wind flow (i.e. quasi-steady wind flow) (Peterka et al., 1997). Flow accelerations between the mean near-roof wind speed and approach wind flow at eave height were observed with mean flow acceleration ratios ranging from 0.2 - 1.6. The experiments also determined the peak instantaneous gust near the roof surface was no greater than 2.5 times the mean wind approach wind flow at eave height.

Following the experiments of Peterka and Cermak, the ASTM D7158/UL 2390 standard test method was developed based upon the new asphalt shingle wind uplift model. The method adapted the test deck and fan arrangement of ASTM D3161/UL 997, but modified the evaluation procedure. Instead of subjecting asphalt shingle specimens to high wind flows, the shingles are instrumented with pressure taps on the upper and lower surface of the shingle (Figure 47) and subjected to mean wind speed of 15.6 m/s (35 mph).

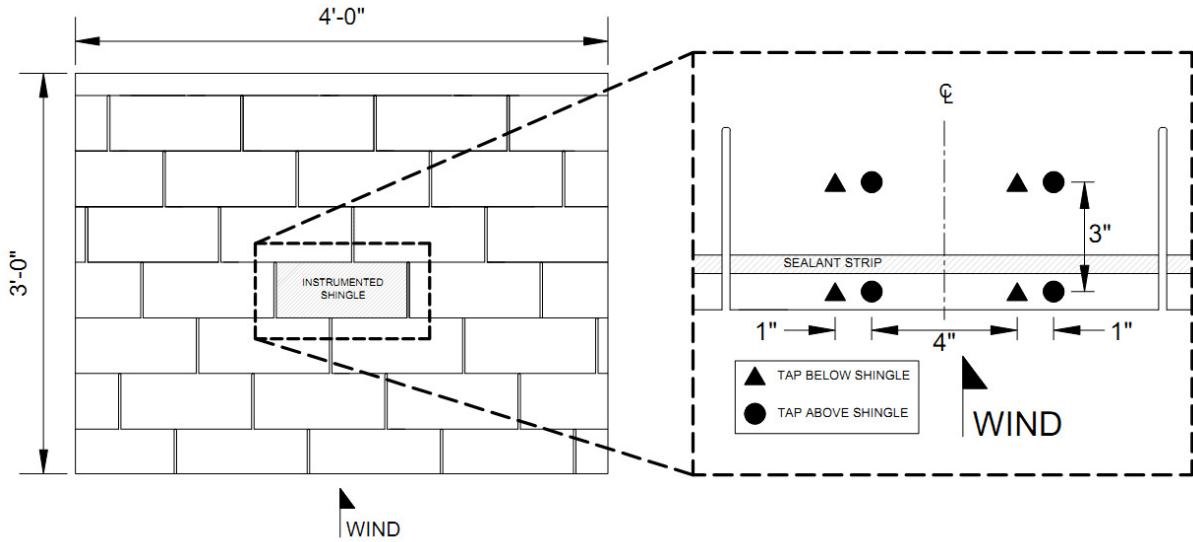


Fig. 47. ASTM D7158 test deck arrangement and pressure tap layout. (1 in = 25.4 mm)

During wind uplift, the shingle deforms at a rate proportional to its stiffness and wind speed. That is, the higher the wind speed, the greater the deformation the stiffer the shingle, the lower the rate of deformation. As the wind speeds used for testing are significantly lower than design-level, small shims are placed under the shingles leading edge to introduce a vertical displacement of the leading edge that would be expected at the design-level speed. This height is estimated by a pre-test measurement of the shingles stiffness and selection of design-level wind speed. The pressure measurements are highly sensitive to changes of the shingle’s leading edge height. Thus, errors of shim placement or height calculation can under- or over-predict pressure at design level.

The pressure measurements capture the absolute mean pressure above and below the shingle’s surface. A dimensionless differential mean pressure coefficient at each tap location is then calculated by subtracting the mean pressure on the top of the shingle’s surface from the mean pressure on the lower surface and normalized by the mean reference velocity pressure measured during the wind test at 25 mm (1 in) above the shingle’s surface [Equation (7)]. An example result of ASTM D7158 testing on a three-tab shingle is given in Table 22. Thus, using the mean pressure data captured in 15.6 m/s (35 mph) near shingle surface wind and converting to mean pressure coefficients, the mean uplift pressure exerted on a shingle’s surface may be scaled to any mean near-roof surface wind velocity of interest.

From Peterka et al. (1997):

$$D\bar{C}_p = \frac{\bar{P}_{Top} - \bar{P}_{Bottom}}{\frac{1}{2}\rho\bar{V}_{ref}^2} \quad (7)$$

Where:

$D\bar{C}_p =$  Mean differential uplift pressure coefficient

- $\bar{P}_{Top}$  = Mean pressure measured on the top of the shingle
- $\bar{P}_{Bottom}$  = Mean pressure measured on the top of the bottom shingle
- $\rho$  = Air density
- $\bar{V}_{ref}$  = Mean air velocity measured 25 mm (1 in) above the instrumented shingles surface

**Table 25. ASTM D7158 test result from shingle product TT-101 in the Thermal Aging experiment**

Test No.	Windward Side			Leeward Side		
	$P_{top} - P_{bottom}$ (Pa)	V (m/s)	DCp1	$P_{top} - P_{bottom}$ (Pa)	V (mph)	DCp2
1	-56.5	14	-0.45	-10.5	14	-0.09
2	-73.3	15	-0.51	-26.8	15	-0.19
<b>Average</b>			-0.48			-0.14

However, peak uplift pressures exerted on the shingle are of most interest for design-level calculations. The calculation of peak pressures is accomplished by utilizing the 2.5 upper bound ratio of the peak roof wind speed by the mean approach wind speed in combination with the uplift differential pressure coefficients measured by ASTM D7158. As shown in Equation (8), the upper bound 2.5 factor is a squared quantity within this equation; therefore, it is imperative the upper bound on peak wind velocities over the roof plane envelopes all steep-slope roofs.

From Peterka et al. (1997):

$$D\hat{P} = \frac{1}{2} \rho \bar{V}_{ref} \left( \frac{\hat{V}_{roof}}{\bar{V}_{ref}} \right)^2 D\bar{C}_p \quad (8)$$

where:

$$\frac{\hat{V}_{roof}}{\bar{V}_{ref}} = 2.5 \quad (9)$$

and

$D\hat{P}$  = Peak differential uplift pressure exerted on the shingles surface

$\rho$  = Air density

$\bar{V}_{ref}$  = Mean velocity measured in the approach flow and eave height

$\hat{V}_{roof}$  = Peak velocity on the roof measured at 25 mm (1 in) above the surface

$D\bar{C}_p$  = Mean differential uplift pressure coefficient

Wind uplift forces acting on the shingle's surface are assumed to be transferred through shingle's sealant strip and down to the shingle below. Yet, direct measurements on the sealant strip were not performed during the development of the wind model to validate this load path assumption. Further complicating this issue is the role of the loading mechanism on asphalt shingles. Wind uplift forces are not uniform over the shingle's surface and the load exerted on the sealant strip is not necessarily one of pure uplift. Adhesives, such as the one used for asphalt shingles, generally have a lower resistance to peel stress than pure tensile stress (i.e., uplift only) (Shiao et al., 2003b). ASTM D7158 attempts to quantify this loading mechanism by measuring the pressure exerted ahead of the sealant strip and behind the sealant strip (Figure 47). The uplift resistance of a shingle is quantified using the ASTM D6381 mechanical uplift test. As described in Section 2.2.2, the test has two procedures with one that simulates a peel-type loading mechanism (Procedure A) and one that simulates a direct tensile loading mechanism (Procedure B). The resistance of the shingle is then determined using a fraction of the shingle's resistance to Procedure A loading in combination with a fraction of the shingle's resistance to Procedure B loading. This fraction is determined by the magnitude of the uplift force ahead of and behind the sealant strip as measured by ASTM D7158.

In total, the wind resistance of an asphalt shingle is defined by ASTM D7158 as the ability of the shingle's sealant strip to resist design-level wind uplift forces. Failure is defined as the loss of the sealant strip's adhesion. The test only evaluates fully sealed shingles; yet, it was shown in Section 2.5 that in-service shingles may be partially unsealed as the shingle's age. The uplift loads exerted on the sealant strip are assumed based on point measurements along the shingle's surface, rather than direct measurement along the sealant strip. These point loads are derived from wind speeds well below design-level and artificial deformation of the shingle is required to produce the estimate of design-level geometric shape. Further, peak forces on the roof are calculated from mean pressures scaled by a squared dimensionless speed-up factor.

The next section summarizes UF research that addresses the speedup factor in the asphalt shingle wind load model and, by default, the ASTM D7158 test standard. The UF work also expanded the knowledge of asphalt shingle wind uplift by quantifying the effect of partial unsealing and the effects of wind direction. Three experiments were conducted:

- 1) A model-scale boundary layer wind tunnel experiment at UWO
- 2) A full-scale boundary layer wind tunnel experiment at the IBHS Research Center
- 3) A full-scale near roof surface wind tunnel experiment at UF

The methods and results of experiments 1 and 2 were detailed in the SERRI Phase I Report. This report will provide a brief overview of the experimental methods and a summary of the key findings and recommendations. Experiment 3 was conducted in Phase II of this project and its experimental methods and results will be fully detailed in this report.

## 3.2 Characterization of Velocity above the Roof Plane

### 3.2.1 Model-Scale Measurement of Near Roof Surface Wind Flow

This experiment used a Time Resolved – Particle Image Velocimetry (TR-PIV) technique to obtain high-fidelity wind velocity measurements over the roof plane of 1:50 scale-model gable roof buildings. The plan dimensions for the two-story rectangular buildings were 893 mm (4.5 m at full-scale) by 720 mm (3.6 m at full-scale). Six models were built with the following roof pitches: flat, 4:12, 5:12, 6:12, 7:12, 9:12 and 12:12. Dr. Greg Kopp at the Boundary Layer Wind Tunnel II at the University of Western Ontario (UWO) led this experiment.

As shown in Figure 48, each building was placed on the wind tunnel’s floor with the mean wind velocity normal to the building’s eave. Smoke particles were injected in the flow field upwind of the building model. A laser projected a light swath perpendicular to the building’s eave edge to create an illuminated section over the building’s roof plane (Figure 48a). A high-speed camera filmed the laser, and the particles’ movement was used to calculate the speed and trajectory of the wind flow in the laser’s plane.

Further details of the measurement system and the methods for velocity calculation may be found in the SERRI Phase I Report Section 8.3.2 and in Taylor et al. (2010). For this report, Section 3.2.3 will detail the significant findings and recommendations of this experiment and the full-scale experiment described in the ensuing section.

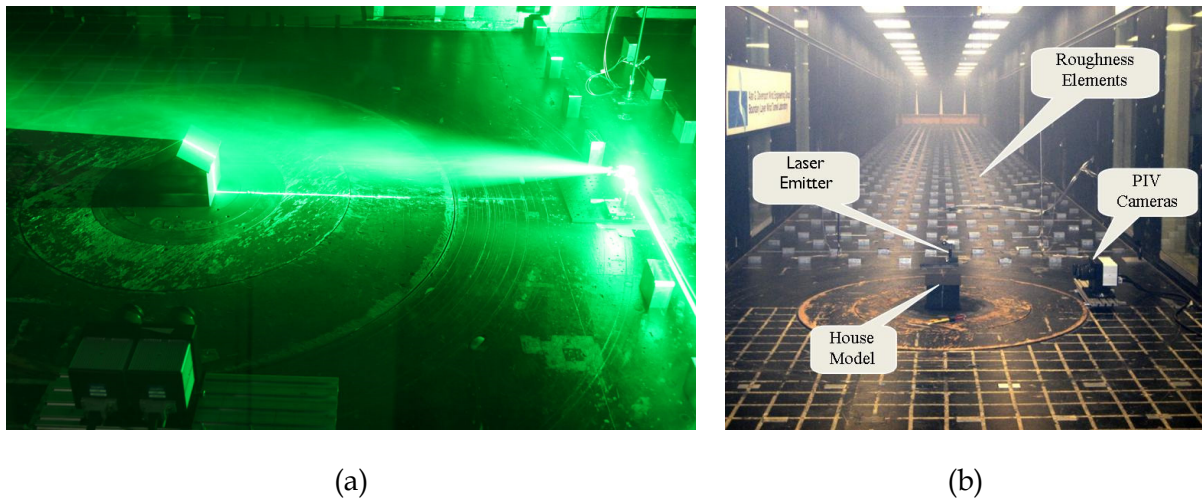


Fig. 48. (a) Particle Image Velocimetry test setup and (b) downwind view of Particle Image Velocimetry test setup components.

### 3.2.2 Full-Scale Measurement of Near Roof Surface Wind Flow

The second experiment, led by UF, was conducted at the IBHS Research Center's full-scale test facility in Richburg, SC. This facility has the capability of subjecting full-scale one- or two-story buildings to Saffir-Simpson Category 3 hurricane wind forces (Simpson 1974, Saffir 1973). Wind is generated by 105 vane-axial fans that have a combined maximum 30 MW draw. The fans are grouped into cells that are individually ducted to form a jet that drives air into the test chamber. At the exit of the jet, a horizontal array of vertically spanning airfoils redirects the air in the horizontal plane to recreate the effects of wind directionality. The test building used in this experiment was attached to a 17 m (55 ft) diameter turntable capable of supporting distributed loads up to 1300 kN (300 kips). The objective of the experiment was to quantify the peak near-roof surface wind speeds relative to a given mean approach wind speed measured at roof height.

The test subject was a 111 m<sup>2</sup> (1200 ft<sup>2</sup>) full-scale rectangular building with a 6:12 half-gable and half-hip roof (Figure 49a). Five Turbulent Flow Instruments (TFI) Cobra Probes simultaneously measured the wind speed above the roof plane. The velocity sensors were placed at heights of 25 mm (1 in) and 305 mm (12 in) at the fifteen locations shown in Figure 49b. The purpose of the 25 mm height was to correlate the peak wind speed measured at this height to the results of Peterka et al. (1997). The purpose of the 305 mm height was to correlate the peak wind speed measured at this height to the results of the PIV experiment described above. This report will focus on the results of the 25 mm height measurements.

Characteristics of the Cobra Probe includes an ability to measure flow within a +/- 45 degrees cone, a maximum sampling frequency of 2000 Hz and a general accuracy of better than  $\pm 0.5$  m/s and  $\pm 1$  degree yaw up to 30% turbulence intensity. Four of the probes were connected to a single data acquisition system. The fifth probe was connected to a standalone unit. The Cobra Probe data acquisition systems contain a trigger input which allows for syncing of multiple data acquisition systems. For this experiment, a trigger was linked between the two acquisition boxes and the RM Young anemometer. A separate computer controlled the trigger function through National Instruments LabVIEW.

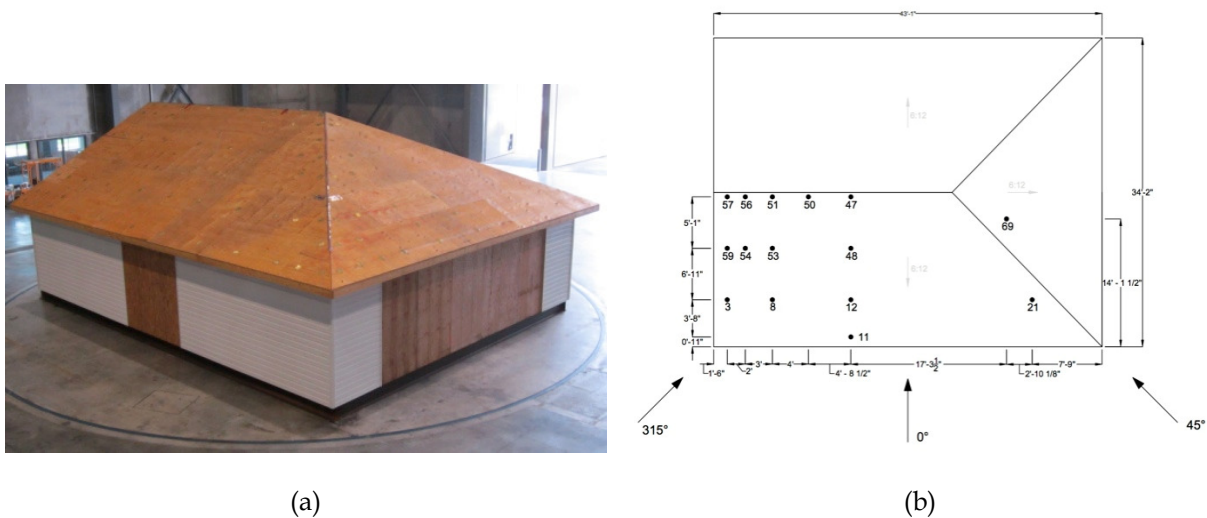
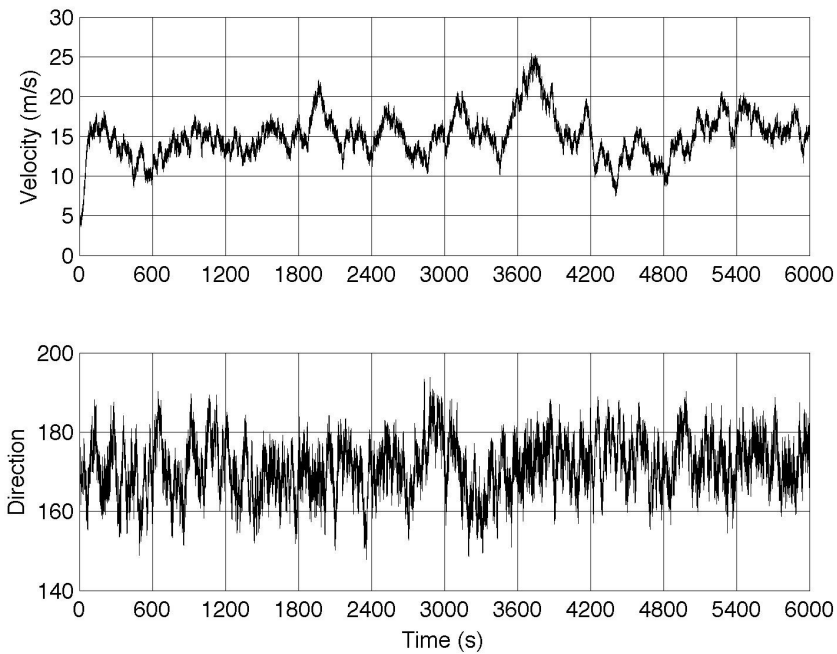


Fig. 49. (a) Aerial view of the test building and (b) roof plan with near roof surface wind measurement locations and experiments wind directions shown.

Approach flow conditions were measured using an RM Young wind monitor (Model Number 05103V) located at the intersection of the exit of the jet and the centerline of the test chamber 5 m (16.4 ft) above the floor. The Cobra Probes and RM Young anemometer were synchronized for a majority of the tests.

Three wind directions were used for the test, as shown in Figure 49b:  $315^\circ$ ,  $0^\circ$ , and  $45^\circ$ . The wind test sequence simulated the mean velocity profile and turbulence characteristics of a flat, open country exposure, corresponding to Exposure C in ASCE 7-10. More information on the turbulence and mean velocity characteristics may be found in SERRI Phase I Report Section 8.5.2. An example record of the wind speed and direction test sequence is shown in Figure 50. Section 3.2.3 will detail the significant findings and recommendations of this experiment and the model-scale experiment described in the previous section.



**Fig. 50. Wind velocity and direction measured at the eave height of the subject home.**

### 3.2.3 Findings and Recommendations

#### Finding

The design “speed-up” ratio used within the ASTM D7158 design load calculation appears to be conservative (Figures 51 and 52). For all roof slopes evaluated, the observed peak near roof to mean approach wind velocity “speed-up” ratio was within 2% of the ASTM D7158 design “speed-up” ratio.

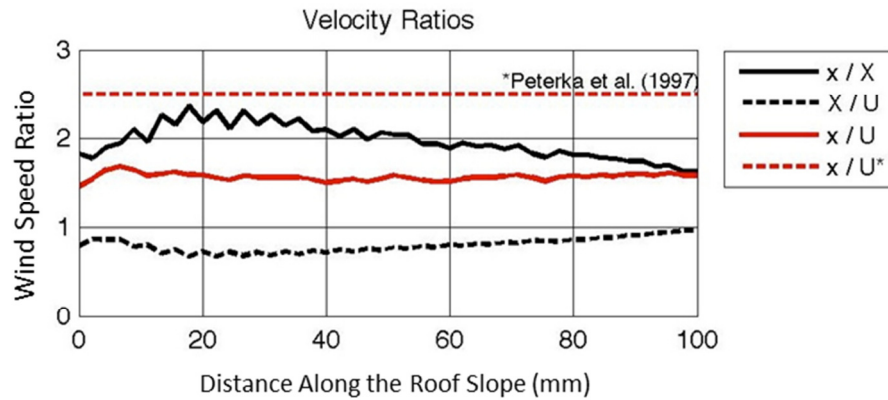


Fig. 51. Particle Image Velocimetry measured “speed-up” factor ( $x/U$ ) compared to Peterka et al. (1997) factor ( $x/U^*$ ).

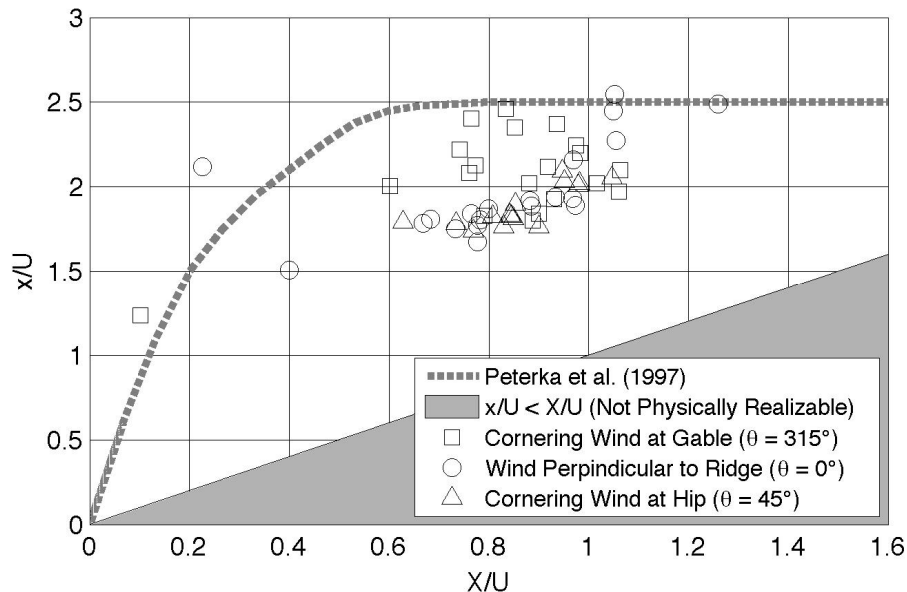


Fig. 52. Comparison of peak speed-up ( $x/U$ ) versus mean speed-up ( $X/U$ ) over the full-scale building roof tested in the IBHS Research Center and wind tunnel modeling results performed by Peterka et al. (1997).

## Recommendation

Based upon the data, we believe the 2.5 “speed-up” ratio to be an appropriate design-level factor in ASTM D7158 for wind flow over “plane” gable and hip roof structures. However, we recommend that future work focus on near surface wind flow on roofs containing complex geometries, valleys, or roof projections (i.e., chimneys) in order to characterize the potential increase in peak gusts that may arise from these additions. This recommendation was also suggested by Peterka et al. (1997) in their original presentation of the wind uplift model for asphalt shingles.

## Finding

Outside of the separated flow region, the highest PIV measured “speed-up” occurred near the ridgeline for a 6:12 roof slope (Figure 53). The highest measured “speed-up” during the full-scale was also near the ridgeline for wind flow perpendicular to the ridgeline on a 6:12 roof. This matches the location of highest “speed-up” observed by Cochran et al. (1999).

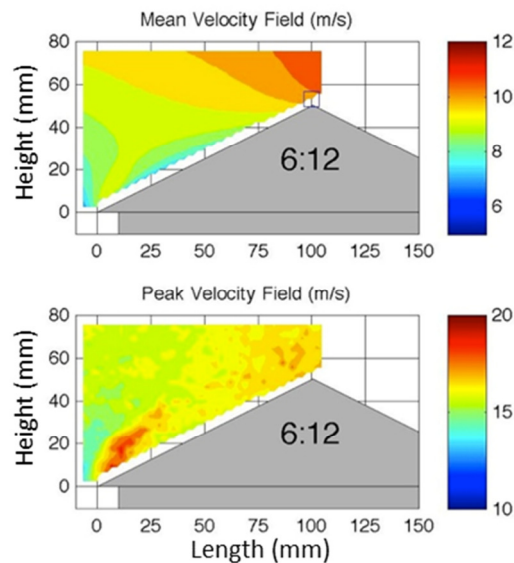


**Fig. 53. Particle Image Velocimetry measured mean velocity field (top plot) and measured peak velocity field (bottom plot).**

## Recommendation

This finding highlights the increased wind vulnerability of ridge shingles. Their location along the ridge line subjects them to the highest wind speeds. Combining this finding with design deficiencies of the ridge shingles (shown later in Section 5), we recommend that future work focus on a new design methodology for the ridge and hip shingle components.

## Finding

As shown in Figure 54, the near roof surface wind flow measured at Location 57 (i.e., the location of highest measured “speed-up”, shown on Figure 49) was well correlated to the approach flow at eave height. Similar results were found at other measurement locations.

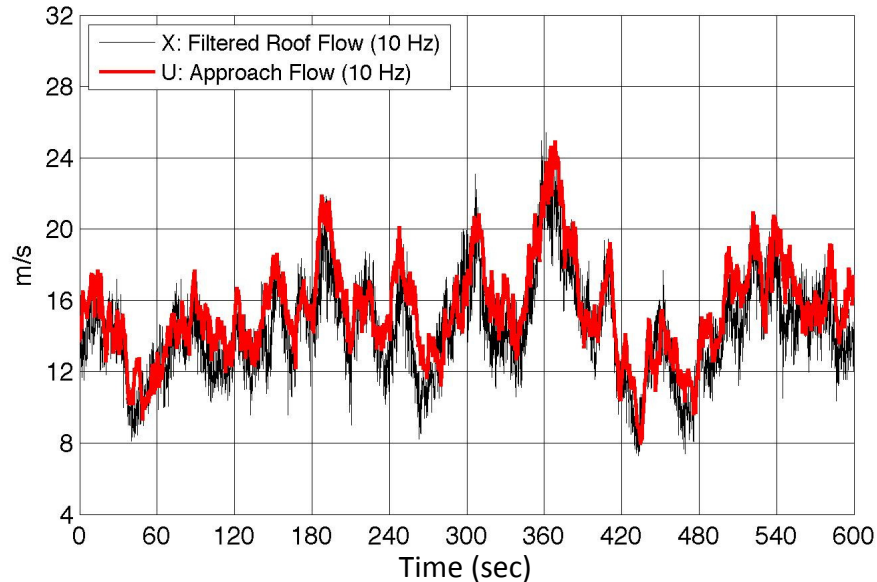


**Fig. 54. Low-pass filtered (10 Hz) velocity record of Location 57 compared to approach flow measured at eave height.**

## Recommendation

None presently. The results indicate the speed-up factor is conservative, although there remain several outstanding issues that could not be addressed inside of the performance period of this research project. The unfiltered measurements (1250 Hz) near the roof surface measurements produced peaks consistent with the speed-up factor used in ASTM D 7158. We have not determined the exact cause of the high frequency components, but it may be attributed to:

1. Turbulence generated by the separated flow at the windward edge of the building.
2. High frequency components in the approach flow not captured by the RM Young wind monitor. The instrument uses a propeller to measure wind speed. Mechanical filtering is a well-known issue. The attenuation increases with frequency (inverse of the wavelength).
3. Vibration and/or instrument error, despite efforts to secure the probe rigidly to the roof.
4. A combination of factors (1) - (3).

### 3.3 Validation and Extension of the Shingle Wind Uplift Model

#### 3.3.1 Overview

The research objectives of this experiment were to:

1. Validate the Peterka et al. (1997) asphalt shingle wind load model (henceforth Peterka model) through direct measurement of the wind uplift forces generated on a fully sealed asphalt shingle's tab sealant subjected to flow up the roof plane.
2. Extend the Peterka model to quantify the effect of the following variables not explicitly addressed in the Peterka model: angle of attack and partial unsealing of the tab sealant.

To achieve these objectives, the investigators developed a Dynamic Flow Simulator (DFS) to replicate near roof surface wind conditions at speeds up to 95 m/s (212 mph). Test specimens included new ASTM D3462 three-tab and laminate fiberglass reinforced asphalt shingles with an ASTM D7158 Class H wind rating. An asphalt shingle's sealant strip, henceforth "test shingle", was instrumented with up to three multi-axis loads cells attached to decking below the shingle. The load cells directly measure the wind uplift forces generated along the shingle's load path. The test deck consisted of an outer stationary 2.43 m (8 ft) long by 1.82 m (6 ft) bare fiberglass composite deck with an inner 1.52 m (5 ft) wood turntable capable of 360° rotation. The test shingle was installed on the test deck turntable with surrounding shingles permanently sealed. Wind velocity was measured at 25 mm (1 in) above the test shingle top surface with a Turbulent Flow Instruments Cobra Probe.

The research evaluated how the variation in mean wind speed, angle of attack, and partial unsealing of a shingle's tab sealant affect the resulting wind uplift loads generated on a shingle's tab sealant. The test shingle was tested in both fully sealed and partially unsealed configurations. Each test shingle replicate was subjected to a total wind exposure of 50 minutes, consisting of five angles of attack for 10 minutes. Within each 10-minute exposure two test wind speeds were applied; 20 m/s (45 mph) for 5 minutes, and 40 m/s (89 mph) for 5 minutes. The longitudinal turbulence intensity of the wind flow was 2.5%, measured 25 mm (1 in) above the shingle's top surface. The wind angles of attacks were: 0° (perpendicular to the leading edge), 22.5°, 45°, 67.5°, and 90° (parallel to the leading edge).

#### 3.3.2 Experimental Methods

This experiment was conducted in the Dynamic Flow Simulator (DFS), which is designed to generate user-defined, turbulent, high wind simulations up to a 100 m/s (224 mph) peak velocity. Wind conditions in the test chamber simulated near-roof surface winds that discontinuous roofing systems, such as asphalt shingles, would encounter in-service.

##### 3.3.2.1 Dynamic Flow Simulator

The DFS has seven main components (Figures 55-57). Air entered the DFS through a 1.5 m (5 ft) diameter inlet and passed through an actively controlled opposed-blade damper system, which control the wind speed. The air was pulled through a 1340 kW (1800 HP) centrifugal blower and then passed through two 90° elbow bends and traveled into a settling chamber to remove undesired fine-scale turbulence and to improve flow uniformity

across the duct cross-section. The settling chamber consisted of a wide-angle diffuser, turbulence screens and a honeycomb, and a duct contraction. Flow uniformity was controlled by three separate mesh screens of 68% porosity in the diffuser. The duct contraction caused the wind to accelerate to its target velocity at the entrance to the test section. The cross-sectional area at the entrance to the test section was 213 cm (7 ft) wide by 38 cm (1.25 ft) tall. A steel turbulence grid, conforming to ASTM D7158 Section 8.2.2.1, was installed upwind of the shingle deck at the junction of the duct contraction and test section (Figure 57). This grid was used to develop a small-scale boundary layer characteristic of near-roof surface wind flow. Vertical and lateral profiles of mean wind speed above the test shingle deck will be discussed in Section 3.3.3.1. The width of the test section did not vary, however the height was adjusted to regain static pressure lost by friction. In other words, the configuration was ‘tuned’ to achieve a zero pressure gradient along the test section. The nominal size of the test specimen plus surrounding deck was 243 cm (8 ft) long by 182 cm (6 ft). A pneumatic lift raised the test specimen into place through an opening in the bottom floor of the test section (Figure 55). Air was exhausted to the free atmosphere through a diffuser at the exit.

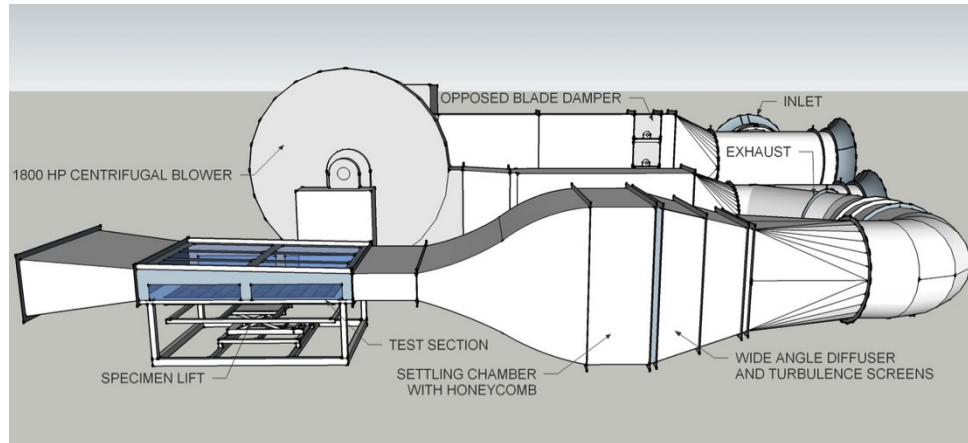


Fig. 55. Rendering of the Dynamic Flow Simulator componentry.



Fig. 56. Dynamic Flow Simulator, as constructed.



**Fig. 57. Test specimen in the Dynamic Flow Simulator test section with upstream turbulence grid shown.**

### **3.3.2.2 Instrumentation / Hardware**

Six-axis load cells were used to measure wind forces on the asphalt shingle tab sealant. The load cells resolve forces and moments in the X-, Y-, and Z-planes (Figure 58b and 58c). Measurements in the three coordinate axes were required because the wind direction was varied. Six-axis load cells, as opposed to single or three-axis load cells, were chosen because of the attachment detail between the top of the load cell and the bottom of the shingle, which introduced a moment arm. This eccentricity would cause in-plane forces on the shingle to be read as moments by the load cell. Without the ability to measure moments, the in-plane forces would not be properly captured by the load cell.

Three ATI Industrial Automation model Nano25 (IP65) six-axis loads cells were distributed along the shingle's self-seal strip. Each load cell consisted of a 28 mm (1.1 in) diameter by 28 mm (1.1 in) tall steel cylinder with silicon strain gauges fixed on the interior face. The sensing ranges and resolutions for each load axis are given in Table 26. The load readings were captured via National Instruments Labview 2010 and a National Instruments 6218 DAQ analog-to-digital converter. Installation of the load cells is provided in Section 3.3.2.6.

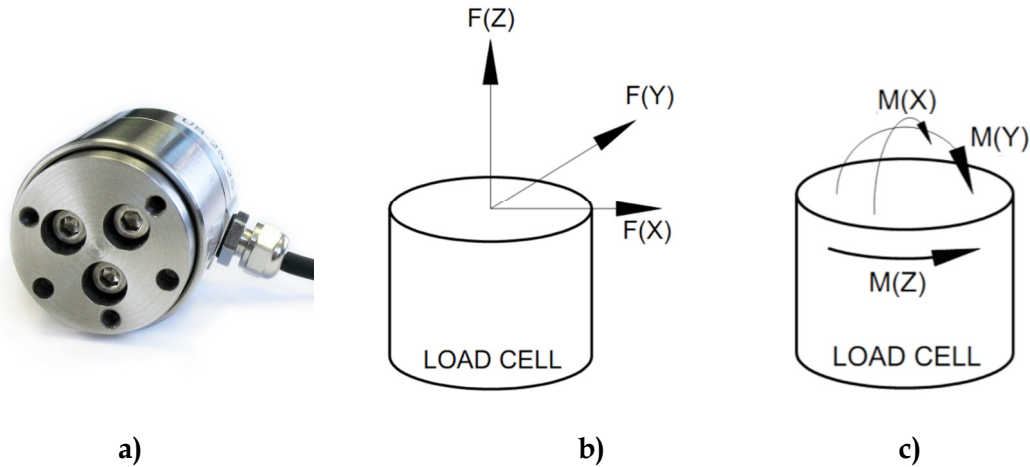
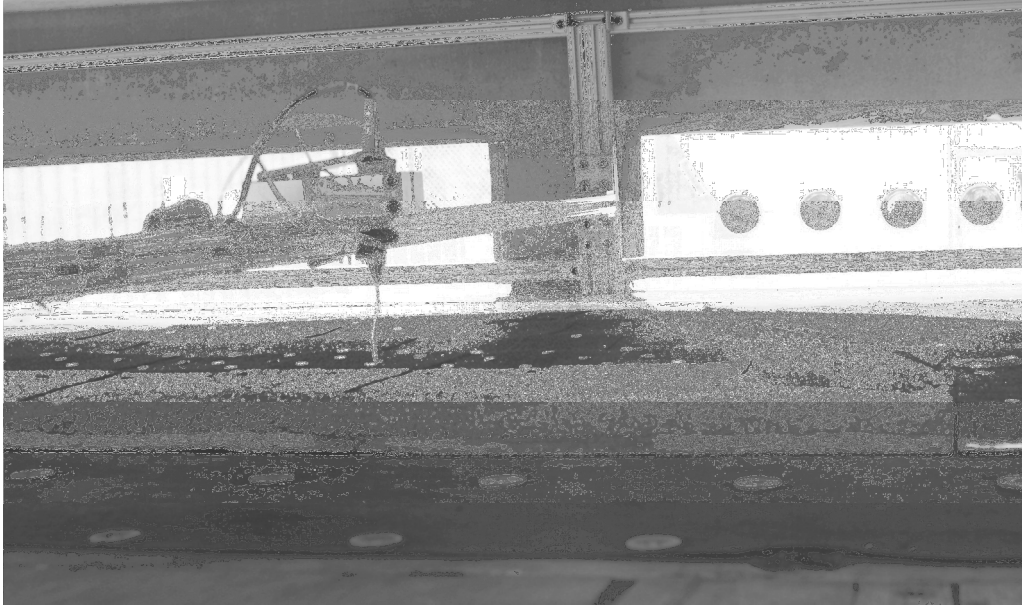


Fig. 58. a) Six-axis load cell measured: b) three forces and c) three moments.

Table 26. Six-axis load cell sensing ranges and resolutions

Measurement Axis (see Figure 58)	F(X) (N) [lbf]	F(Y) (N) [lbf]	F(Z) (N) [lbf]	M(X) (N-m) [lbf-in]	M(Y) (N-m) [lbf-in]	M(Z) (N-m) [lbf-in]
Sensing Range	222 [50]	222 [50]	890 [200]	5.6 [50]	5.6 [50]	3.4 [30]
Sensing Resolution	1/112	1/112	3/112	1/80	1/19	1/60

TFI Cobra Probes were used to capture the 3-axis wind velocity within the test chamber (Figure 59). The probe was mounted to a t-slotted aluminum frame and reference pressure was measured outside the test section. Characteristics of the probe include an ability to measure flow within a  $\pm 45^\circ$  cone, a maximum sampling frequency of 2000 Hz and a general accuracy of better than  $\pm 0.5$  m/s and  $\pm 1^\circ$  yaw up to 30% turbulence intensity. For this experiment, the probes were set to a sampling frequency of 1250 Hz.



**Fig. 59. TFI Cobra Probe measuring wind velocity inside the DFS during testing.**

### **3.3.2.3 Test Specimen Construction**

Each test specimen consisted of an asphalt shingle system installed on a 1.5 m (5 ft) diameter circular wood test deck (Figure 61). This deck was then raised into the test section using a pneumatic lift. The shingle systems consisted of a “test shingle” with surrounding “dummy shingles,” as shown in Figure 60. The test shingle served as the shingle of interest for this experiment and was instrumented with the six-axis load cells along the self-seal strip, while the dummy shingles remained in place throughout all tests. The dummy shingles were the same product as the test shingle. The test deck components are outlined in Section 3.3.2.4. The composition of the asphalt shingle systems is provided in Section 3.3.2.5. The installation of the shingle system and instrumentation is detailed in Section 3.3.2.6.

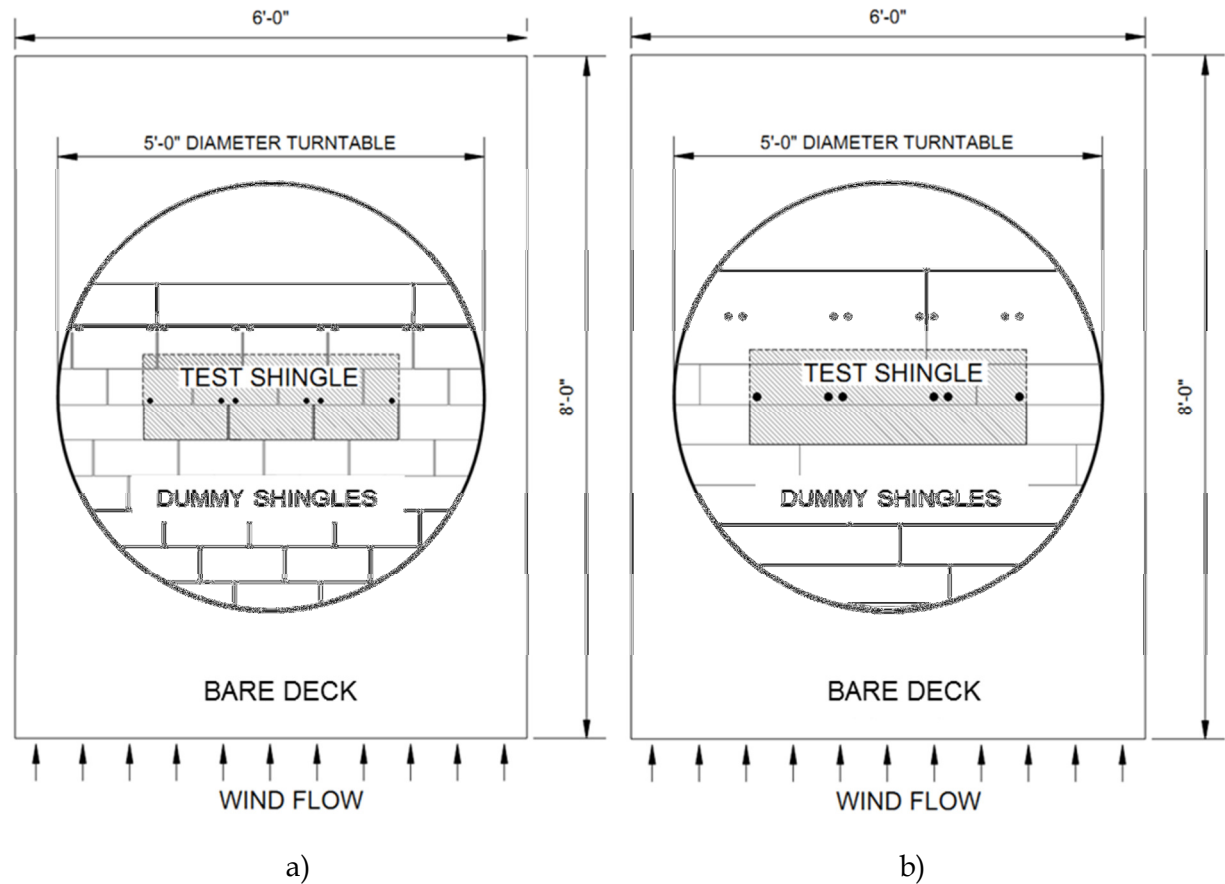
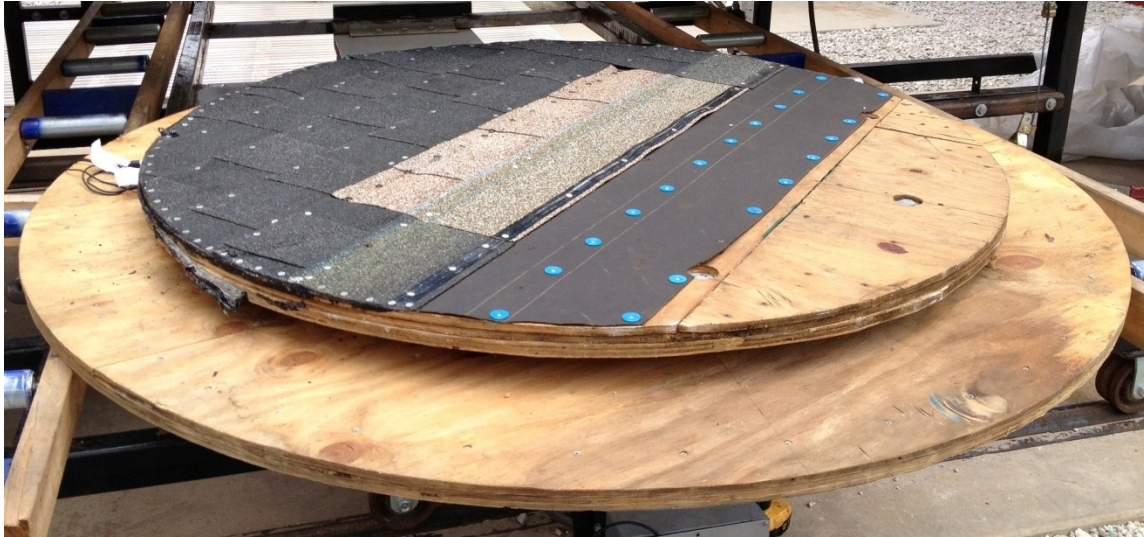


Fig. 60. Plan view of the test specimens: a) three-tab and b) laminate asphalt shingle system. (1 in = 25.4 mm)

### 3.3.2.4 Test Deck Construction

The test deck was composed of two circular wood decks separated by wood spacers (Figure 61). The asphalt shingle system was installed on the upper deck, while the bottom deck served as the support deck for the upper wood deck and six-axis load cells. The 1.5 m (5 ft) circular upper deck was composed of three laminated layers of 19 mm (0.75 in) thick plywood sheathing. The lower 2 m (6.5 ft) deck was composed of four laminated layers of 19 mm (0.75 in) thick plywood sheathing. The decks were spaced 51 mm (2 in) apart to account for the height of the six-axis load cells. A bare 51 mm (2 in) thick fiberglass composite deck with a 1.5 m (5 ft) circular opening was permanently installed in the test section. The test decks were raised into the circular opening with the upper deck top surface flush with the composite deck (Figure 57).



**Fig. 61. Wood test deck with laminate test shingle installed (light colored shingle).**

Two upper test decks were constructed for this experiment: one test deck each for a three-tab and laminate asphalt shingle system. Six-axis load cells were installed below the test shingle on the lower deck to measure the wind loads on the test shingle's self-seal strip. The location of the test shingle for both shingle systems is shown in Figure 60 (See Section 3.3.2.6 for additional shingle installation and instrumentation details). To accommodate the load cell's connection to the test shingle, 35 mm (1.4 in) rectangular strips of wood decking were removed along the test shingle's sealant strip (Figure 64).

### **3.3.2.5 Asphalt Shingle System**

One three-tab and one laminate fiberglass-reinforced asphalt shingle product was used for this experiment. Both products were ASTM D7158 Class H (67 m/s [150 mph]) shingles that conformed to ASTM D3462. The three-tab shingle system was the same TT-101 product used in the thermal aging experiment discussed in Section 2.4, while the laminate shingle product was a new product purchased from a local distributor.

The three tab asphalt shingle consisted of a 914 mm (3 ft) wide by 305 mm (12 in) strip with three, 305 mm (12 in) wide by 127 mm (5 in) tall tab cutouts (Figure 62). Six fasteners were used on all test shingles. For the three-tab test shingles, fasteners were placed 143 mm (5.625 in) up from the leading edge of the shingle with two fasteners spaced 25 mm (1 in) from the edge of the shingle strip and two fasteners above each tab cutout line as shown in Figure 63. See Section 3.3.2.4 for fastener specifications.

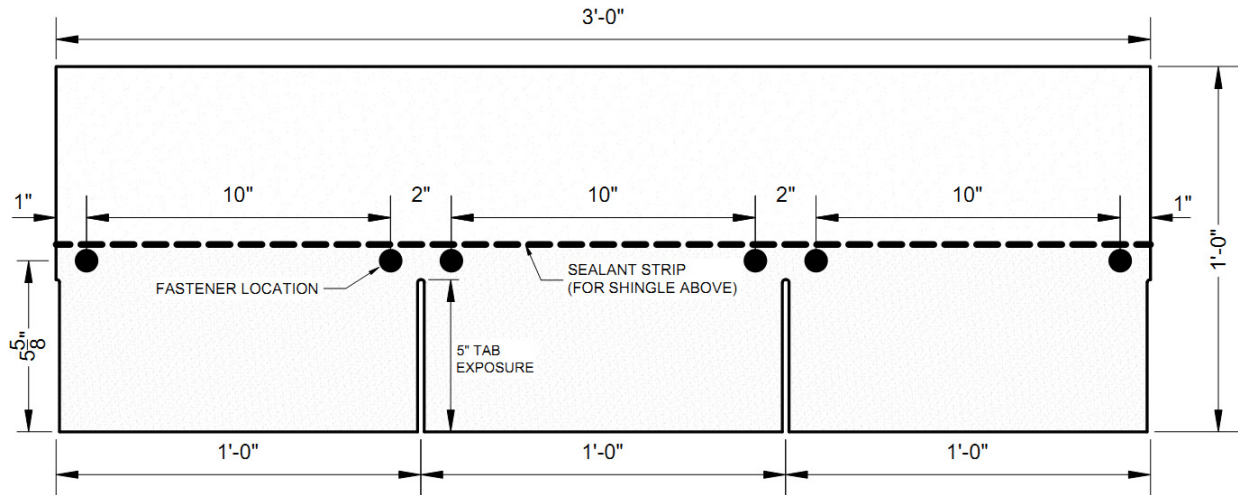


Fig. 62. Plan view, 3-tab asphalt shingle with six fasteners per strip. (1 in = 25.4 mm)

The laminate asphalt shingle consisted of a continuous 984 mm (38.75 in) wide by 324 mm (12.75 in) tall strip (Figure 63). The laminate test shingle's fasteners were placed 171 mm (6.75 in) up from the leading edge of the shingle with two fasteners spaced 25 mm (1 in) from the edge of the shingle strip and four interior fasteners located as shown in Figure 63. See Section 3.3.2.4 for fastener specifications.

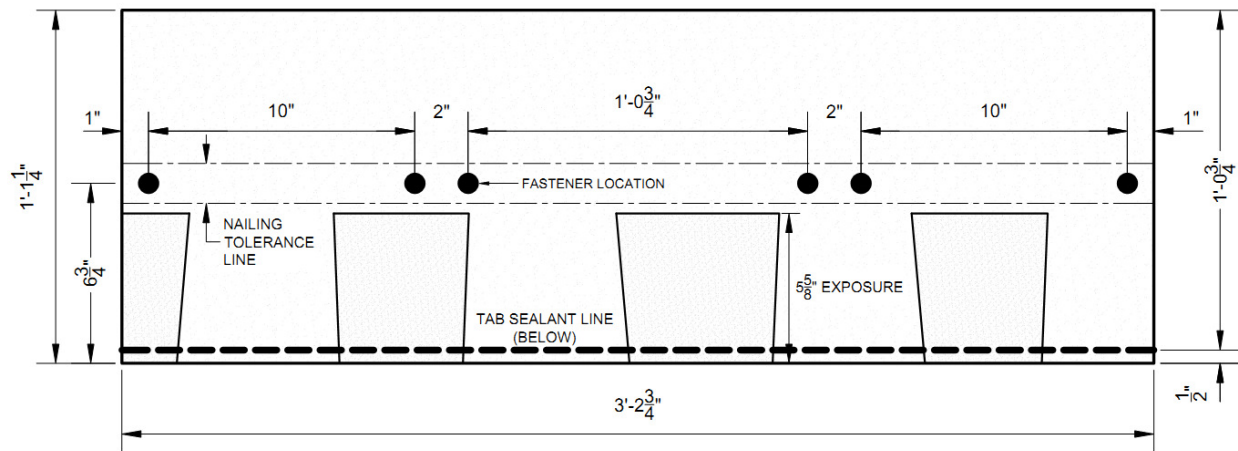


Fig. 63. Plan view, laminate shingle with six fasteners per strip. (1 in = 25.4 mm)

### 3.3.2.6 Asphalt Shingle Installation

This section describes the installation of the test specimens. Asphalt shingles and related components (e.g., roofing felt) were new products stored within the laboratory from the time of acquisition through the time of testing. A single layer of #30 roofing felt, conforming to ASTM D4869 - Type IV, was installed over the wood turntable using hand-driven 25 mm (1 in) long plastic cap nails. The felt had a 51 mm (2 in) sidelap and 102 mm (4 in) endlap.

The three-tab shingles were installed over the roofing felt following a diagonal "twelve up, five off" pattern resulting in a half-tab width offset between succeeding shingle courses.

The laminate shingle system were installed following a “five course diagonal” method, resulting in a 152 mm (6 in) offset between succeeding shingle courses. The dummy shingles and underlayment underneath the test shingle had a rectangular section cut out to match the section cut out from the wood decking (Figure 64). Plastic sheeting was installed over the rectangular openings to restrict air flow from passing through this void, while still allowing a connection between the test shingle and load cells (Figures 67 and 69). Both three-tab and laminate dummy shingles were fastened to the decking using six hand-driven roofing nails (3.06 mm [0.12 in] shank with 9.5 mm [3/8 in] head diameter) per strip with their location shown in Figures 62 and 63, respectively. The leading edges/tabs of the dummy shingles were hand-sealed using asphalt roof cement and additional fasteners were placed on the surface of the shingle to restrain movement.

Three load cells were installed underneath the test shingle’s sealant strip (Figure 67) with each load cell measuring a portion of the sealant strip’s length. The three-tab shingle arrangement had one load cell for every one-half tab width (i.e, 149 mm [5.875 in]) (Figure 65). The laminate shingle arrangement had one load cell measurement for a 152 mm (6 in) length on the left side of the self-seal strip, while the remaining two load cells each measured a 416 mm (16.4 in) length (Figure 66). The 152 mm (6 in) length corresponded to the mean unsealed length observed on laminate shingles during the roof survey experiment discussed in Section 2.5.

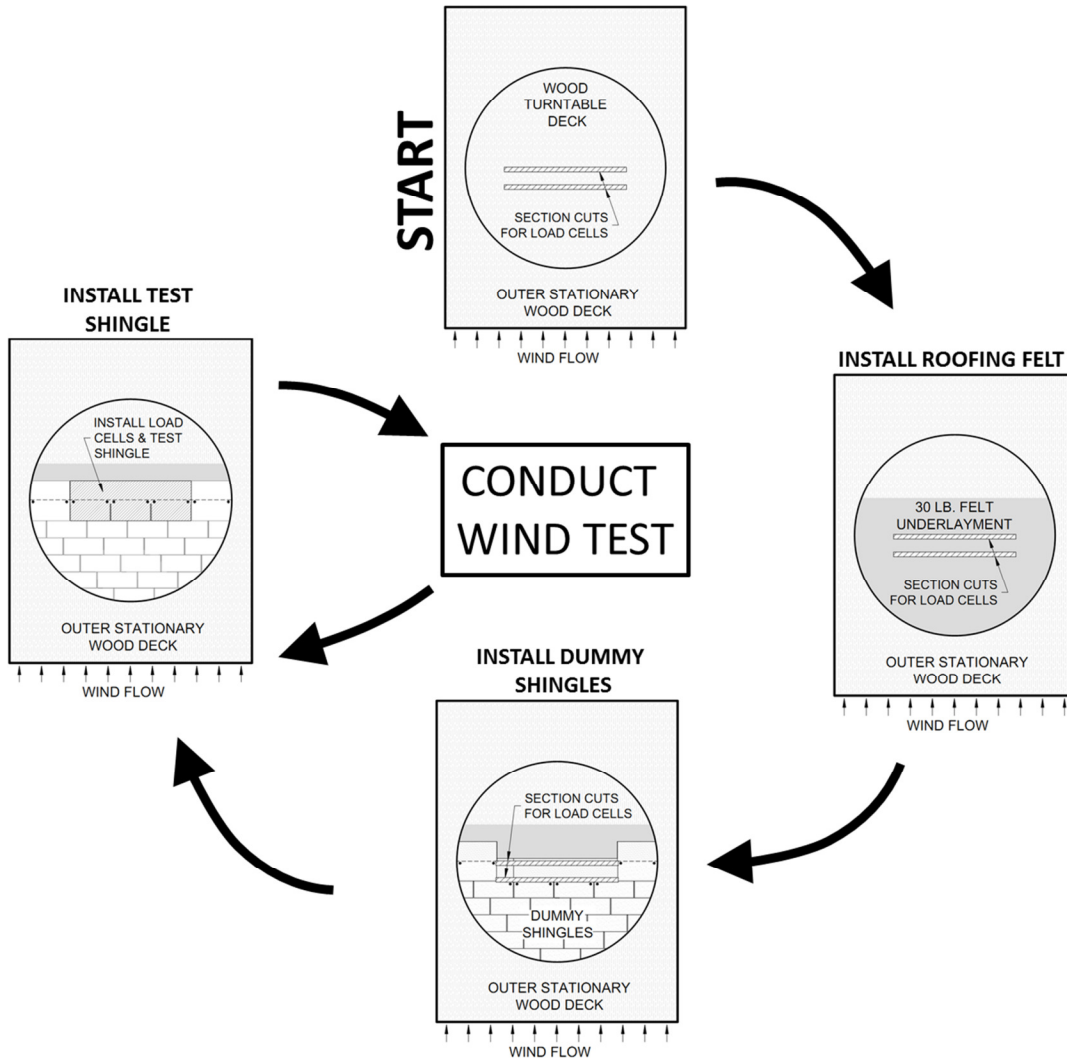


Fig. 64. Installation and wind test procedure. (Note: Three-tab shingle system shown. Laminate shingle system follows same procedure)

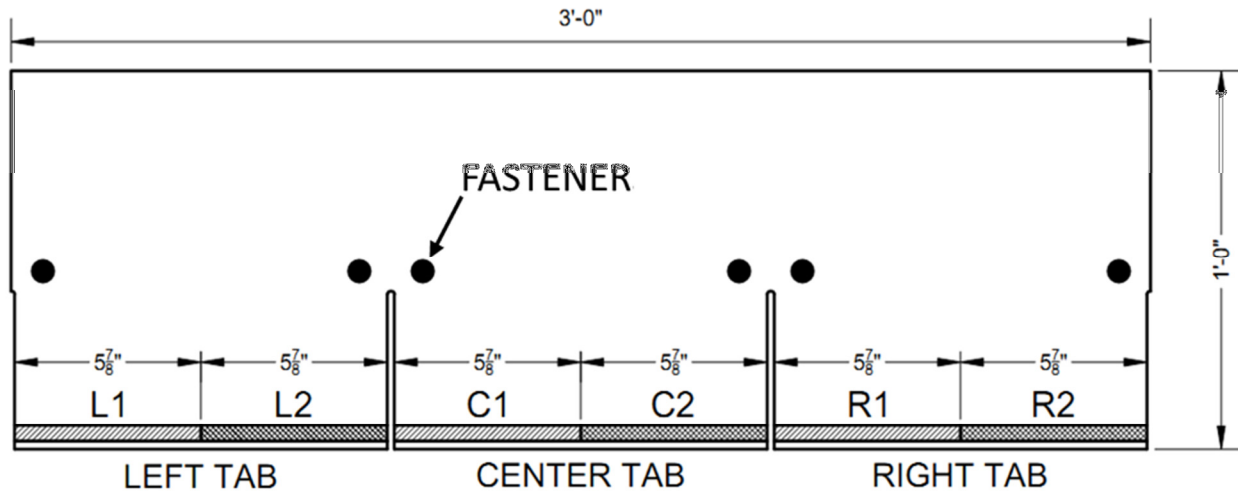


Fig. 65. Load cell measurement locations for three-tab, six fastener test shingle (L1-R2 = sealant strip measurement) (1 in = 25.4 mm)

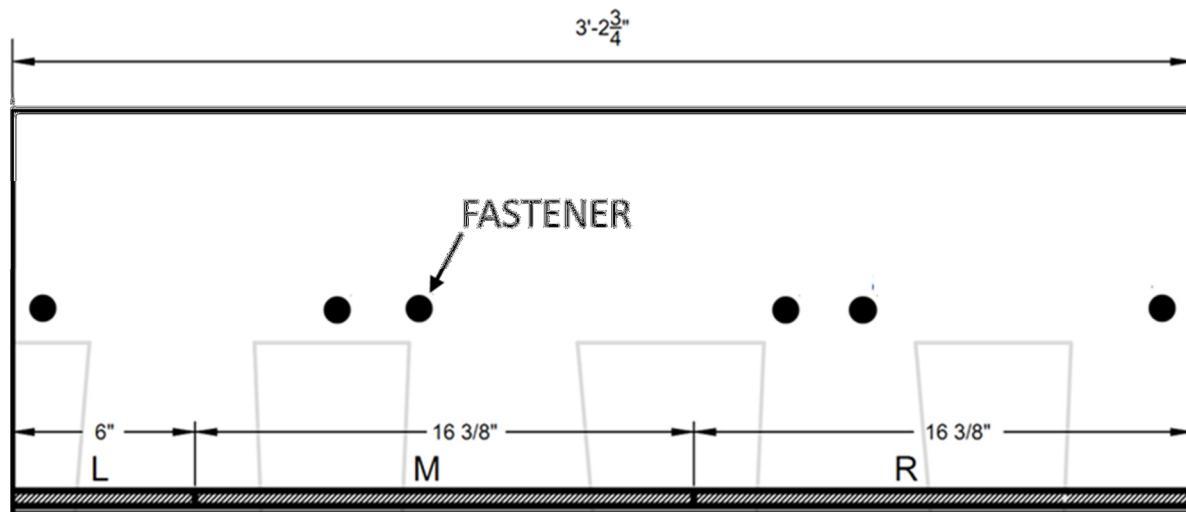
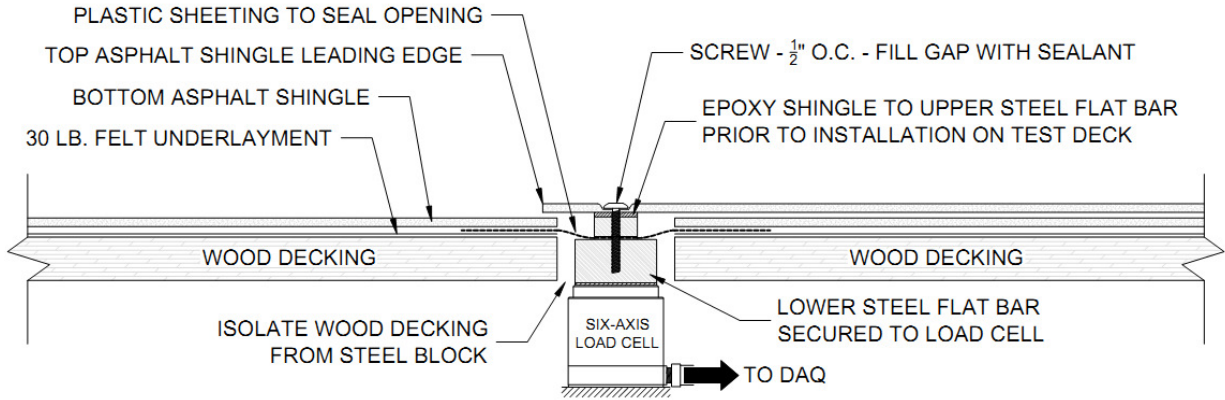


Fig. 66. Load cell measurement locations for laminate, six fastener test shingle (L, M, R = sealant strip measurement) (1 in = 25.4 mm)

For each sealant length selected for measurement, a thin steel flat bar matching the width of the shingle's tab sealant was adhered to the underside of the test shingle using high-strength epoxy (Figure 68). The load cell was installed on the lower test deck below the test specimen and a 6 mm (0.75 in) deep steel flat bar was secured on the top face of the load cell (Figure 67). The length of this flat bar matched the length of the adjoining flat bar adhered to the test shingle. Prior to the installation of the test shingle, a layer of plastic sheeting was installed over the gap created along the tab sealant line to prevent airflow traveling through the void (Figure 69d). The test shingle was then placed into position with the plastic sheeting sandwiched between the two steel flat bar sections (Figure 67). The flat bars were then secured together with low profile screws installed at 13 mm (0.5 in) on center (Figure 67).



**Fig. 67.** Connection detail to measure the six-axis wind loads on an asphalt shingle’s tab sealant. Note: A differential pressure was measured in the test section causing the plastic sheeting to displace upwards and imparting a load on the load cell. This inappropriate load was experimentally estimated and described in further detail in Section 3.3.3.3.



(a)



(b)

**Fig. 68.** Epoxied steel flat bars on (a) underside of three-tab test shingle and (b) underside of laminate test shingle.



(a)



(b)



(c)



(d)

**Fig. 69. Laminate test specimen deck and test shingle installation procedure: (a) lower deck with load cells, (b) closer view of load cell arrangement, (c) top deck with cutout for load cells shown and (d) test shingle placed over the cutout to produce a complete test specimen.**

### 3.3.2.7 Test Matrix

The test matrix is given in Table 27 and a reference plan view of the instrumentation layout is provided in Figure 70. For each test, a new test shingle was installed on the test specimen deck with a total of three test shingle replicates tested for each unsealed location and sealant strip measurement combination (Table 27). Section 3.3.2.6 details installation procedure for the test shingle and instrumentation.

**Table 27. Sealed and partially unsealed asphalt shingle test matrix**

Test	Type	Unsealed Location	Measurement on Sealant Strip
1-3	Three-Tab	---	L2, C1, C2
4-6	Three-Tab	C1	L2, C2
7-9	Laminate	---	L, M, R
10-12	Laminate	L	M, R

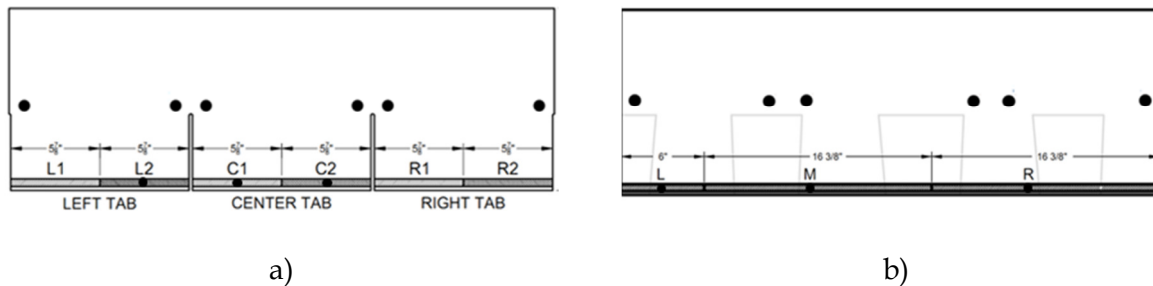


**Fig. 70. Load cell locations for a) three-tab system and b) laminate system. (1 in = 2.54 mm) The load cells were placed at the center of each measurement location (black nodes along the sealant strip on figure).**

For each test, the test shingle was subjected to a wind scenario at five wind azimuths ( $\theta = 0, 22.5, 45, 67.5, 90^\circ$ ) (Figure 71). The wind scenario consisted of two mean wind velocities (20 m/s [45 mph] and 40 m/s [89 mph]) with a longitudinal turbulence intensity of 2% at each mean wind speed (Figure 72). Following ASTM D7158, wind speeds were measured using the Cobra Probe located 25 mm (1 in) above the test shingle and 51 mm (2 in) downwind of the test shingle's leading edge. The probe head was oriented into the flow for all wind azimuths. The duration of each wind test was 10 minutes. The turbulence intensity ( $I_u$ ) is defined as a ratio of the along wind velocity standard deviation ( $\sigma_u$ ) and the mean along wind velocity ( $\bar{U}$ ) measured by the Cobra Probe 25 mm (1 in) above the test specimen. The test started with  $\theta = 0^\circ$ . After completion of the wind scenario, the test deck was then rotated to the new angle of attack and retested. This process continued until all angles of attack were tested. A new test shingle was then installed on the test specimen deck and the process recycled. Wind loads on the sealant strip (sampling frequency = 100 Hz) and wind velocities (sampling frequency = 1250 Hz) above of the test shingle were recorded throughout the test regime.

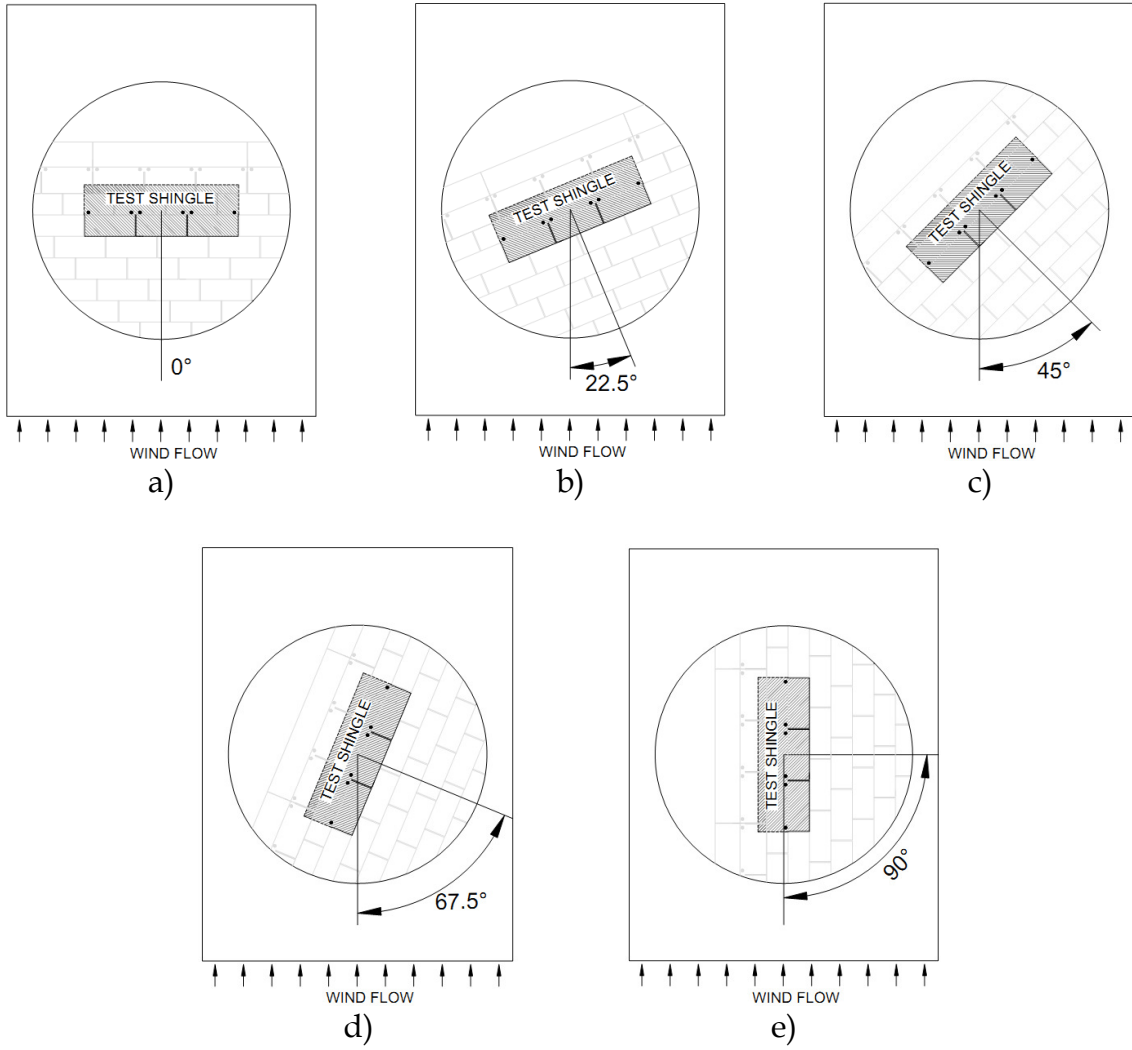


Fig. 71. Wind azimuths.

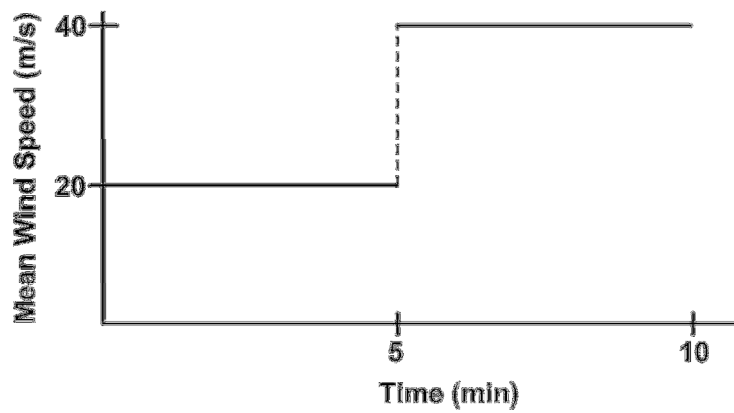


Fig. 72. Wind test sequence for each wind angle of attack.

### 3.3.3 Preliminary Results

#### 3.3.3.1 Wind Characteristics

The analysis of results began by characterizing the wind conditions inside the test chamber. The aluminum frame mount for the Cobra Probe experienced vertical oscillations due to vortex shedding off of the horizontal frame spanning the test sections width. This transfer of vibration likely contributed to the 9.0% longitudinal turbulence intensity that was measured for the raw wind speed data (Table 28). Using a 3<sup>rd</sup> order Butterworth filtering technique, the wind speed record was filtered to a frequency cutoff of 50 Hz and 12 Hz. The 12 Hz cutoff frequency corresponds to the highest frequency component that will satisfy the quasi-steady approximation for asphalt shingle wind uplift (Peterka et al., 1997). The  $I_u$  for the 50 Hz cutoff was 5.7% and the  $I_u$  for the 12 Hz cutoff was 2.3% (Table 28), while the mean wind speed between the 1250 Hz, 50 Hz, and 12 Hz records was identical. Given no difference in mean wind speed records between the raw and filtered records, the measurement of mean wind speeds and mean uplift forces on asphalt shingles was conducted on filtered wind and load records using a 3<sup>rd</sup> order Butterworth filter with a cutoff frequency of 12 Hz.

**Table 28. Comparison of raw wind speed record vs. filtered wind speed record**

Filtering Cutoff Frequency <sup>a</sup>	Mean Wind Speed (m/s) [mph]	$I_u$ (%)
None (Fs = 1250 Hz)	21.27 [47.6]	9.0
100 Hz	21.27 [47.6]	5.7
12 Hz	21.27 [47.6]	2.3

<sup>a</sup>Filtering = 3<sup>rd</sup> order Butterworth low-pass filter

Measurements of mean wind speeds above the test shingle were taken at eight points above the test shingle's top surface (Figure 73). A boundary layer growth emanating from the test shingle's surface is apparent in Low and High Wind Level vertical profiles. The development of the boundary layer is likely caused by the turbulence grid installed upwind of the test deck (Figure 57), and agrees with the vertical wind profile described in ASTM D7158 Section 8.2.1.6.

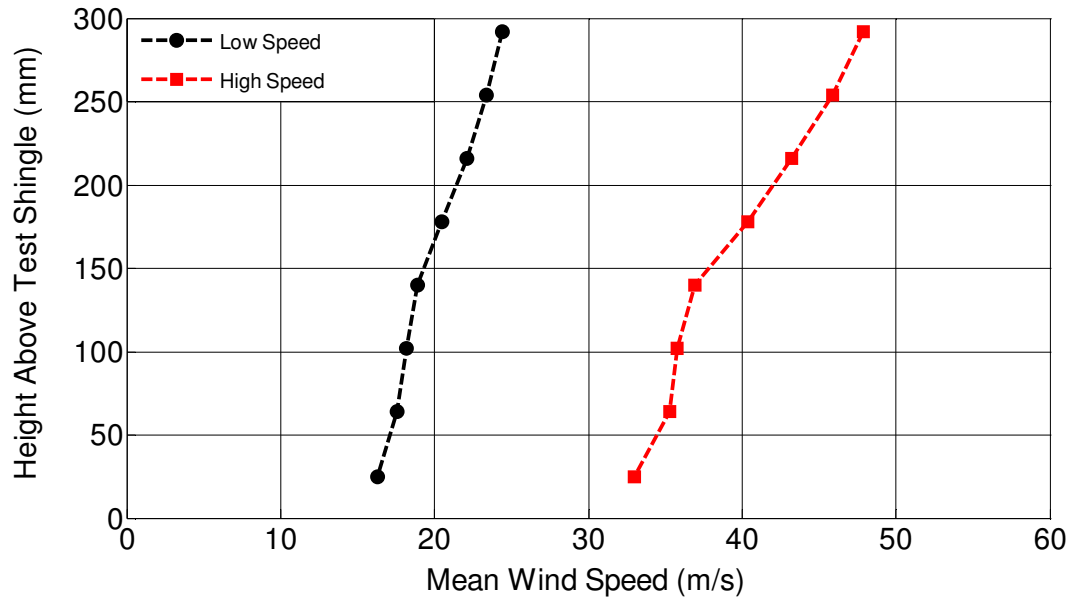


**Fig. 73. Vertical profile of mean longitudinal wind speeds. Note: wind speeds were adjusted during testing to match target wind speeds measured at 25 mm (1 in) above the shingle surface.**

Measurements of mean longitudinal wind speeds across a three-tab test shingle were captured using the Cobra Probe at the seven points shown in Figure 74 at a height of 25 mm (1 in) above the test shingle’s surface. These points are also shown on the laminate shingle in Figure 75. Mean wind speeds were determined using the same five minute wind records used for the wind uplift testing described below. Position 0 corresponds to the measurement location used for all wind uplift tests. A plot of the mean wind speed for each position is shown at the top of Figure 74. All mean wind speeds across the test shingle are within  $\pm 5\%$  of the benchmark set by ASTM D7158 Section 8.2.1.6. The results of the vertical and lateral wind profiles described above indicate that the wind behavior in the DFS test section is representative of the conditions set forth by ASTM D7158.

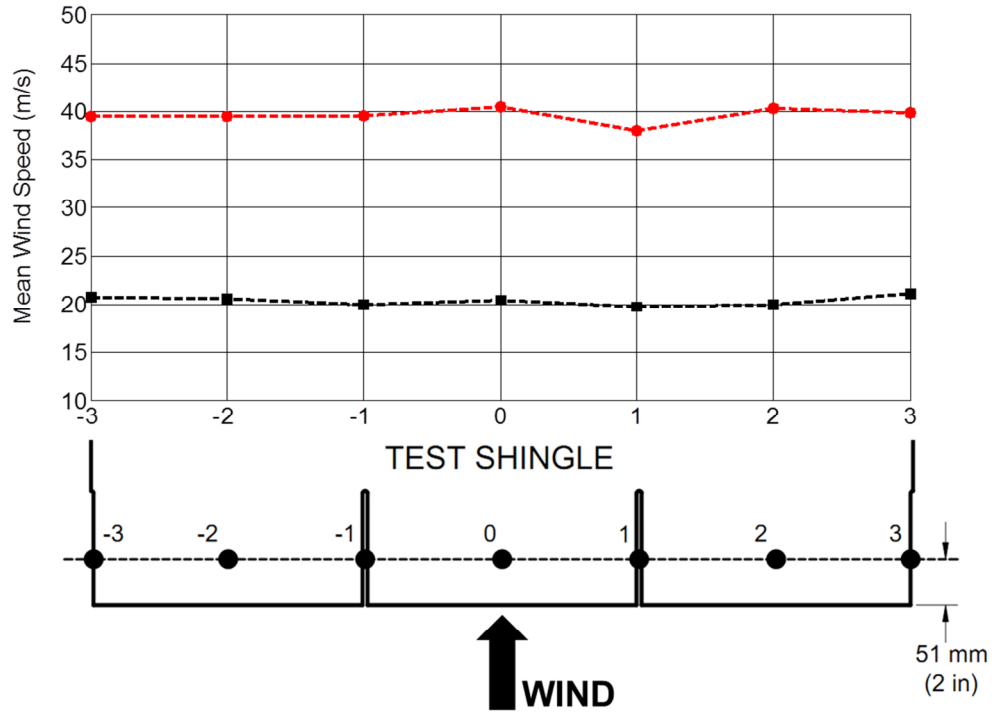


Fig. 74. Lateral mean wind speed profiles for High (red) and Low (black) Wind Levels on three-tab specimens.

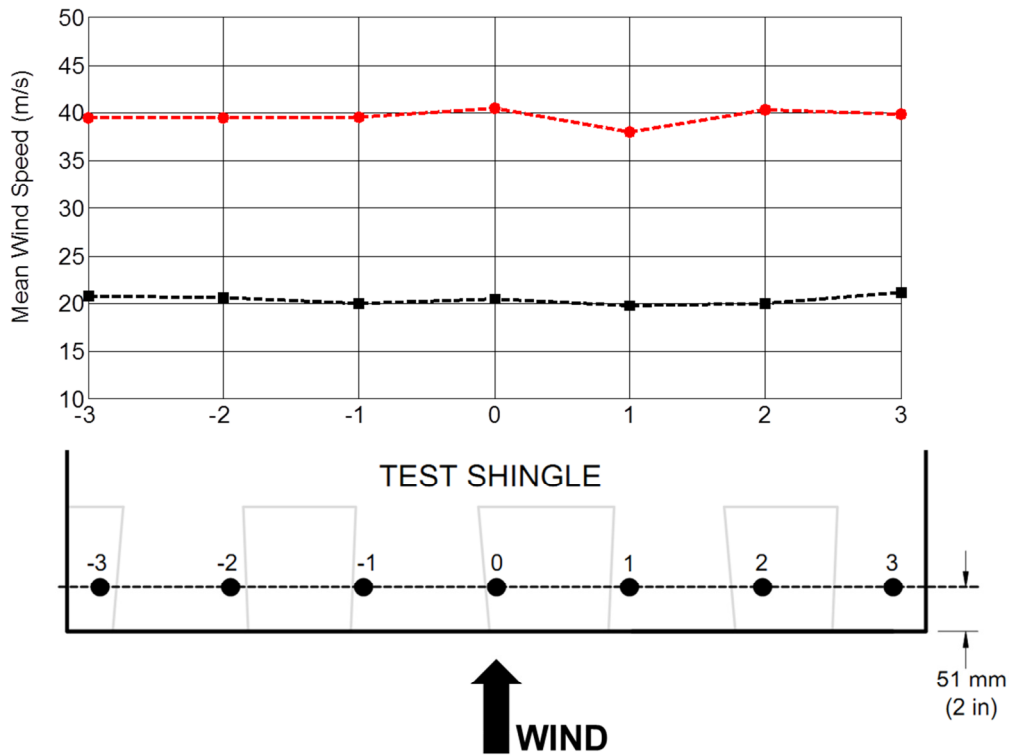


Fig. 75. Lateral mean wind speed profiles for High (red) and Low (black) Wind Levels on laminate specimens.

### 3.3.3.2 Characteristics of Asphalt Shingle Wind Uplift

The wind uplift forces on the laminate and three-tab shingles will be presented in Sections 3.3.3.4 and 3.3.3.5, respectively.

An example of the five minute 20 m/s (45 mph), henceforth 'Low Wind Level', and 40 m/s (89 mph), henceforth High Wind Level, records is shown in Figure 76 and 77, respectively. The DFS system was held at idle prior to the initiation of each wind test, producing the ~ 3 m/s wind speeds observed at the beginning and end of the two wind records shown. Once started, the engine RPM was then increased to set points corresponding to the Low and High Wind Levels. Once acquired, the RPM was held constant for the remainder of the test. Modulation of the upstream opposed blade damper system was not performed for this experiment. Wind speed and load cell readings were recorded just prior to the initiation of the test through the entire test sequence and were stopped after the DFS acquired its idle state. Therefore, the load response of the shingle during the increase and decrease of wind speed was captured for all tests.

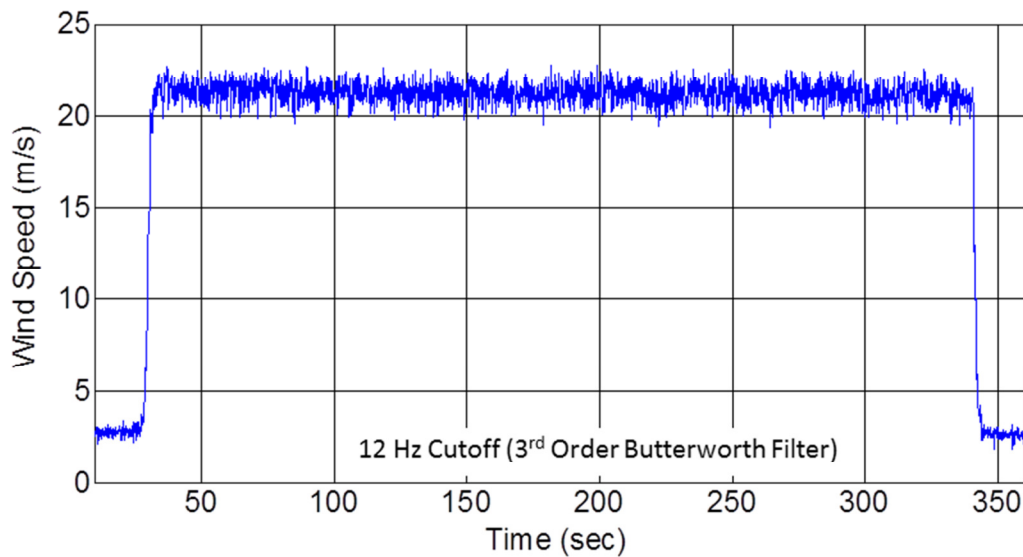


Fig. 76. Example wind speed time-history for Low Wind Level test.

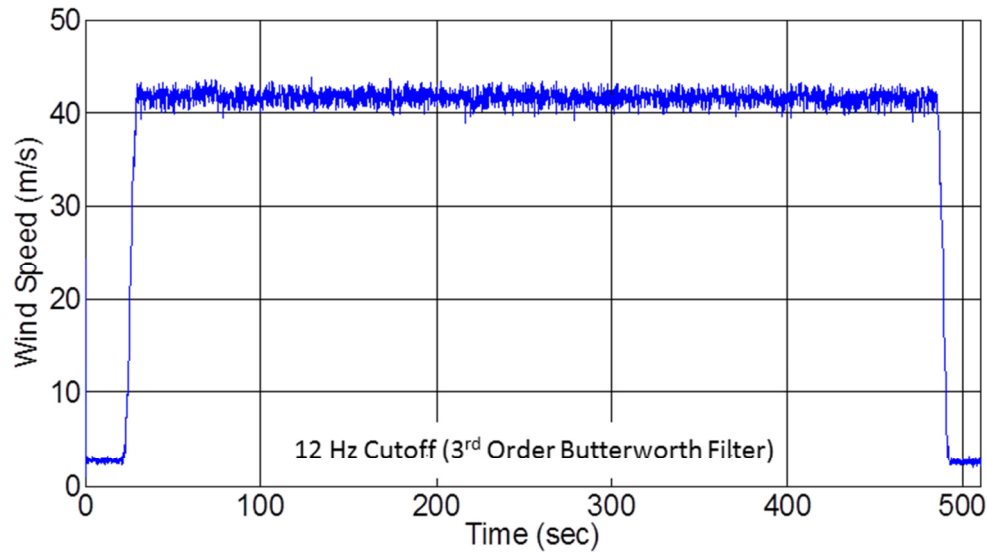
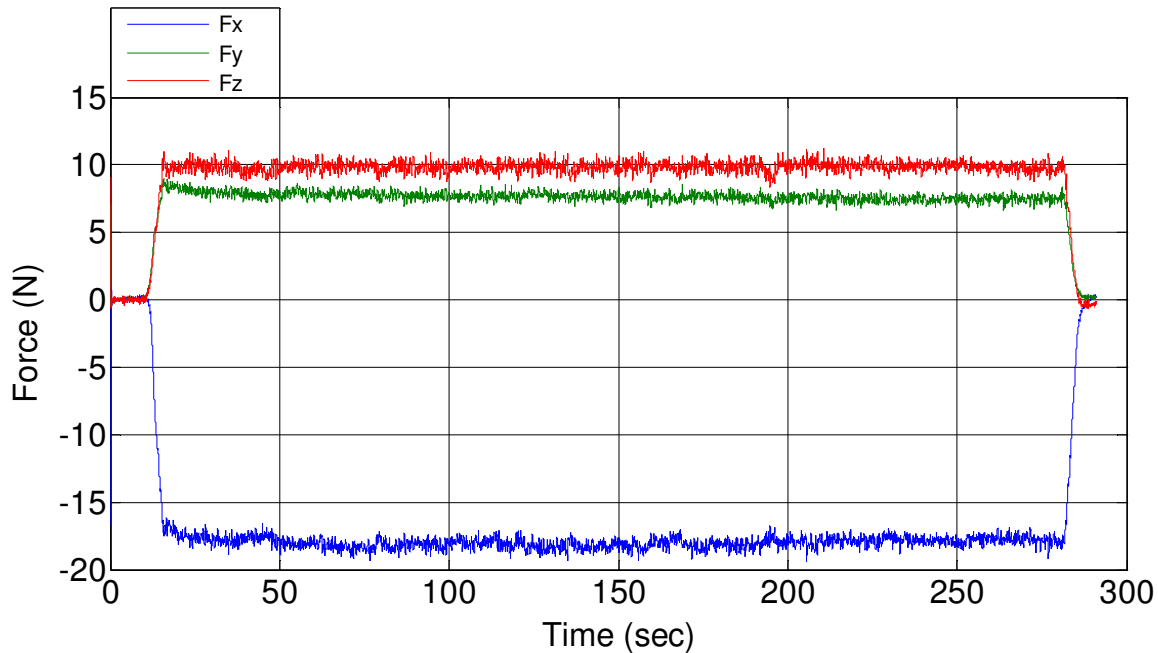


Fig. 77. Example wind speed time-history for High Wind Level test.

Load cell data were captured and recorded at a 100 Hz sampling frequency. As previously stated, the mean loads reported here were acquired using a filtered record set to a 12 Hz cutoff frequency. For each wind test, a plot of all forces and moments measured by the load cell were produced for analysis. The moment response of the shingle will not be discussed in this report. During testing, loads were recorded by the NI data acquisition system as raw load output values without a bias factor (i.e., the loads were not zeroed prior to the initiation of the test). The loads were then biased during the analysis period conducted after the test. An example of a biased wind record used for mean load analysis is given in Figure 78. Wind uplift forces were near zero during the idling period, and then increased with wind speed increase. Uplift force was generally constant on all three measurement axes throughout the test duration and returned back to zero after the conclusion of the test. For the case of constant load readings, mean loads were determined by calculating the time average load on each axis across the entire constant wind speed duration.



**Fig. 78. Force time-history record for Measurement Location C2 on fully sealed three-tab Test Shingle Specimen 3 - 90° wind azimuth - High Wind Level.**

There were several tests where the uplift loads measured by the load cells were not constant through the test duration. After consultation with the load cell manufacturer and independent testing of load cell response to constant load at varying temperatures, it was determined that the load cell's readings were sensitive to changes of temperature within the load cell's steel body. The air flowing through the test chamber was approximately 8 – 17°C (15 – 30°F) greater than the ambient outdoor air temperature. During testing, the load cell body was heated by thermal conduction from the steel plates attached to the load cell, causing an expansion of the load cell body. As load readings are based upon the amount strain exhibited within the load cell's body, changes in the load cell's dimensional size due to thermal expansion produced a change in load reading. Therefore, for a load cell experiencing a constant application of wind uplift by the shingle and a change in temperature, the load cell time-history readings showed a change in load over time. Other potential factors influencing the load readings included creep of the shingle.

An example of the behavior described above is given in Figure 79. The loads are initially stable at zero prior to the initiation of the wind test and respond to the increase in wind speed. However, a change in load is observed on all three measurement axis throughout the wind test as the load cell is heated by the chamber's air. Once the wind test stops, the measured loads do not return back to their original, zero force, values, rather, they return to an offset value created by the temperature change. In general, the net difference between the zero value and load acquired at the start of the wind test matched the net difference between the last point recorded during the wind test and the offset value acquired after the test stopped. Therefore, the wind uplift load was constant throughout the test sequence and the change in load during the test was caused by temperature fluctuations. For the case where temperature effects were observed, the mean values reported for this analysis represent net change between the pre-test load and the load acquired once the target wind

speed has been achieved. If the net differences between the pre-test and post-test change in load were not similar or could not be determined, the mean load values were not reported.

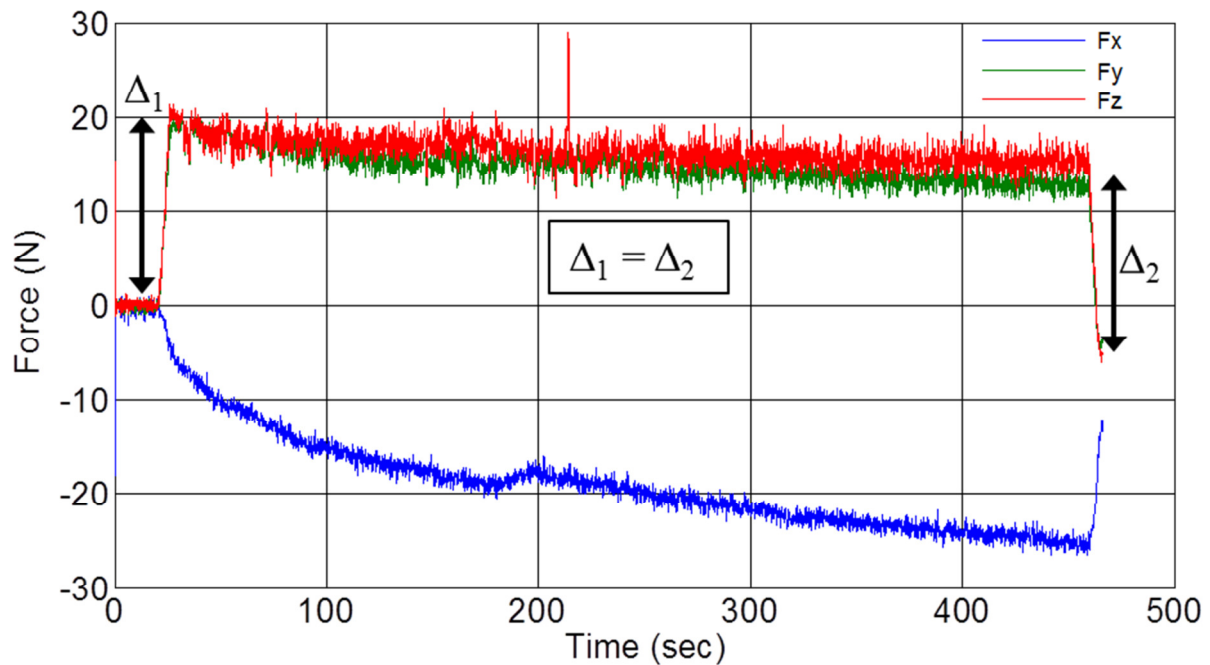


Fig. 79. Example of temperature effects on load cell output – force time-history record for Measurement Location C2 on fully sealed three-tab Test Shingle Specimen 3 - 45° wind azimuth - High Wind Level.

In-plane load readings ( $F_x$  and  $F_y$ ) captured during wind testing indicate that a significant amount of in-plane load is placed on the tab sealant during wind uplift (Figure 78), at all wind directions. Figure 80 shows a visual representation of the in-plane coordinate axis for in-plane load readings for all wind tests. For this report, the in-plane loads have been resolved into a single resultant in-plane load vector using Equation (10) and a single in-plane resultant load angle using Equation (11) (Figure 80).

$$F_{IP} = \sqrt{F_x^2 + F_y^2} \quad (10)$$

Where:

$F_{IP}$  = In-plane resultant force on the tab sealant

$F_x$  = In-plane force in the x-direction, as shown in Figure 80

$F_y$  = In-plane force in the y-direction, as shown in Figure 80

$$\theta_{IP} = 30 - \tan^{-1} \left( \frac{-F_x}{F_y} \right) \quad (11)$$

Where:

$\theta_{IP}$  = In-plane resultant wind angle in degrees, see Figure 80 for reference

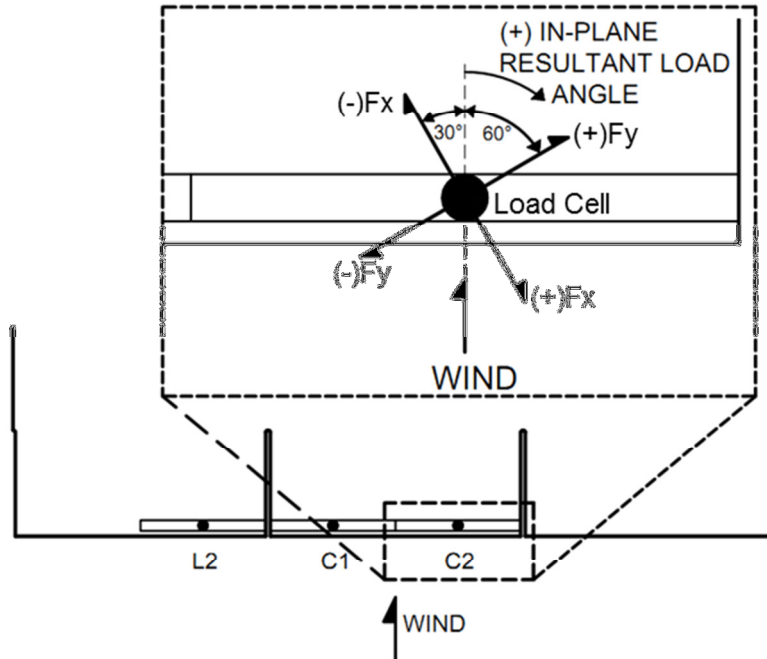


Fig. 80. In-plane force orientation for six-axis load cells.

Using the uplift ( $F_z$ ) load in combination with the in-plane resultant load calculated above, the total resultant force on the tab sealant was calculated using Equation (12) and the resultant vertical load angle was calculated using Equation (13). This report will summarize the uplift only loads and the total force loads for each shingle product.

$$F = \sqrt{F_{IP}^2 + F_z^2} \quad (12)$$

Where:

$F$  = Total resultant force on the tab sealant

$F_z$  = Uplift force on the tab sealant in the z-direction, refer to Figure 58

$$\theta_{TF} = \tan^{-1}\left(\frac{F_z}{F_{IP}}\right) \quad (13)$$

Where:

$\theta_{TF}$  = Total force resultant vertical wind angle in degrees

For a comparison of measured uplift forces to ASTM D7158 predicted forces, the loads are reported below in three forms: distributed loads, force coefficients, and predicted seal strip loads at various wind speeds. The distributed loads reported below were calculated by dividing the load measured by the load cell by the total measurement length of the load cell. For each shingle product, the mean uplift pressure coefficients determined from ASTM D7158 testing (Table 29) was used to calculate the predicted distributed load. This procedure is outlined below.

The distributed load measured on the test shingles was calculated using the following equation:

$$F_D = \frac{F}{L} \quad (14)$$

Where:

$F_D$  = Distributed Load

$F$  = Load measured by the load cell

$L$  = Measurement length for load cell

The distributed uplift load predicted by ASTM D7158 is calculated using the mean pressure coefficients reported in Table 29 and Equation (15):

**Table 29. ASTM D7158 mean uplift pressure coefficients for laminate and three-tab test shingles**

Shingle Product	$D\bar{C}p_1$	$D\bar{C}p_2$	$L_1$ (mm) [in]	$L_2$ (mm) [in]
Laminate	-1.03	-0.27	22 [0.875]	121 [4.75]
Three-Tab	-0.48	-0.14	32 [1.25]	95 [3.75]

$$F_{DP} = [(D\bar{C}p_1 * L_1) + (D\bar{C}p_2 * (L_2/2))] * \left(\frac{1}{2}\rho V^2\right) \quad (15)$$

Where:

$F_{DP}$  = ASTM D7158 predicted force coefficient

$D\bar{C}p_1$  = Mean differential uplift pressure coefficient ahead of the sealant strip

$D\bar{C}p_2$  = Mean differential uplift pressure coefficient behind the sealant strip

$L_1$  = Length from the center of the seal strip to the leading edge of the shingle

$L_2$  = Length from the center of the seal strip to the top of the shingle's exposure

Force coefficients for both the measured and ASTM D7158 predicted loads were calculated by normalizing the distributed loads acquired above by the velocity pressure measured by the Cobra Probe velocity sensor 25 mm (1 in) above the test shingle’s surface (Equation (16)). This normalization scheme reports distributed loads that are independent of wind speed, and, assuming quasi-steady behavior, allows the distributed loads to be scaled to any desired mean wind speed by multiplying the force coefficient by the velocity pressure of interest.

$$F_c = \frac{(F_D \text{ or } F_{DP})}{\frac{1}{2} \rho V^2} \quad (16)$$

Where:

$F_c$  = Force Coefficient (1/m)

$F_D$  = Distributed Load (N/m)

### 3.3.3.3 Correction for Static Pressure Effects

Static pressure inside the test section (i.e., the pressure difference between the inside of the DFS and ambient conditions) was measured during each test 25 mm (1 in) above the shingle test specimen using the TFI Cobra Probe. The mean static pressure from the Low Wind Level was -115 Pa (-2.4 psf), while the mean static pressure from the High Wind Level test was 369 Pa (-7.7 psf) (Table 30). Thus, the pressure in the test section was lower than the ambient atmospheric pressure. A vertical profile of static pressure at the test specimen was also measured, showing that the static pressure at the test specimen surface was approximately 90% of the static pressure measured at 25 mm (1 in) above the test specimen. This finding was used in the conversion of static pressure measured 25 mm (1 in) above the shingle to the predicted static pressure induced force measured by the load cells (Equation 18).

**Table 30. Static pressure in DFS test section 25 mm (1 in) above the test shingle specimen**

Wind Speed Level	Static Pressure in Test Section <sup>a</sup>	
	Mean (Pa) [psf]	$\sigma$ (Pa) [psf]
Low	-115 [-2.4]	19 [0.4]
High	-369 [-7.7]	67 [1.4]

<sup>a</sup>Measured 25 mm (1 in) above test specimen

The plastic sheeting used in the connection of the test shingle’s sealant strip to six-axis load cell creates an air barrier between two load cell connection plates, making it susceptible to static pressure induced forces (Figure 81). Thus, the readings on the load cells will have a contribution from the uplift forces produced on the shingle surface transferring down through the sealant strip and uplift forces produced by the suction pressure on the plastic

sheeting. As will be shown later in this section, asphalt shingles rapidly vent air on their underside, which prevents a differential pressure caused by global static pressure changes between the upper and lower surface of the shingle. Therefore, forces generated on the load cell due to static pressure are a result of the connection detail and do not exist on shingles. An experiment was conducted to quantify the forces measured by the six-axis load cells in the presence of only static pressure. The static pressure forces were then subtracted from the forces obtained during DFS testing to produce the measured wind loads on an asphalt shingle – absent the static pressure induced forces.

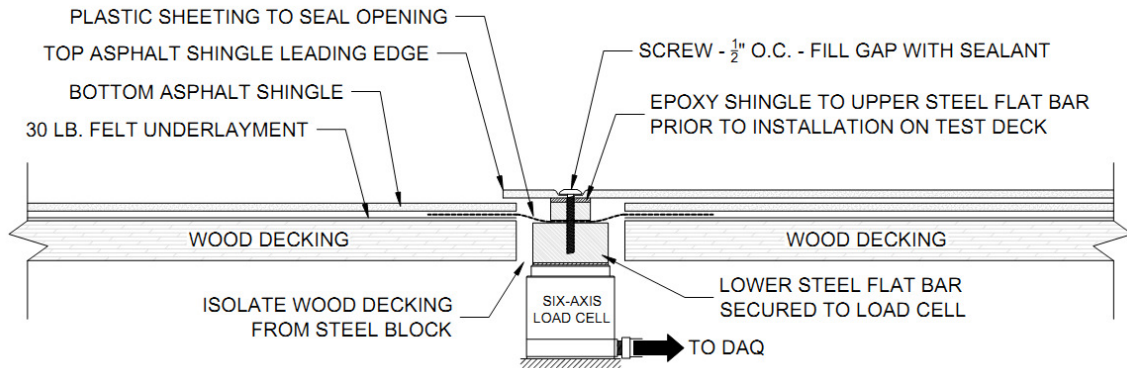


**Fig. 81. Connection detail for specimen's sealant strip to six-axis load cell.**

The static pressure experiment was conducted on an instrumented test deck with similar construction to the test deck used during the DFS testing (Figure 82a and 82b). Three decks were constructed for this experiment: 1) laminate shingle, 2) three-tab shingle, and 3) laminate pressure tap. Decks 1 and 2 utilized the same test specimen construction and connection detail to six-axis load cells as the DFS experiment. For the laminate shingle specimens, two six-axis load cells were installed on locations M and R, while the six-axis load cells were installed on C1 and C2 for the three-tab specimens. Deck 3 (Figure 85) was constructed to evaluate the pressures exerted on the top and bottom surface of the shingle when subjected to rapidly fluctuating static pressure. The wood sheathing substrate that the shingle specimens were installed to was 19 mm (0.75 in) thick plywood, as opposed to a three layer laminated plywood deck with a total thickness of 57 mm (2.25 in).

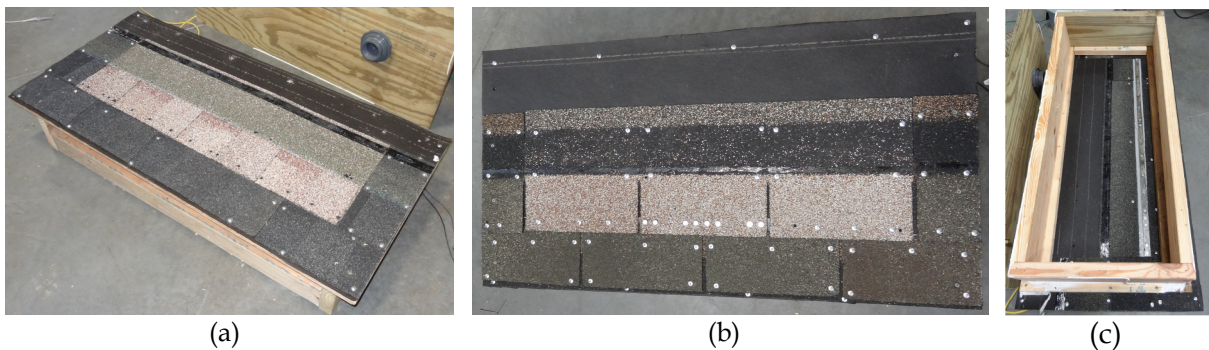


**Fig. 82. Static pressure test specimens: (a) laminate, (b) three-tab, and (c) no shingle.**

Static pressure was generated above the test shingle using a wood pressure chamber that surrounded the test shingle. The pressure was applied and controlled by a single Pressure Load Actuator (PLA), developed by UWO (Figure 83). Each pressure test consisted of a step and 20 second hold at 5% step sizes of the PLA's control valve. Pressures up to 5300 Pa (111 psf) were achieved during the test. One specimen of each shingle type was used for this experiment with three pressure tests conducted on each specimen. Simultaneous chamber pressure and six-axis load cell forces and moments were recorded using NI-6281 hardware and NI LabVIEW 8.5 software.

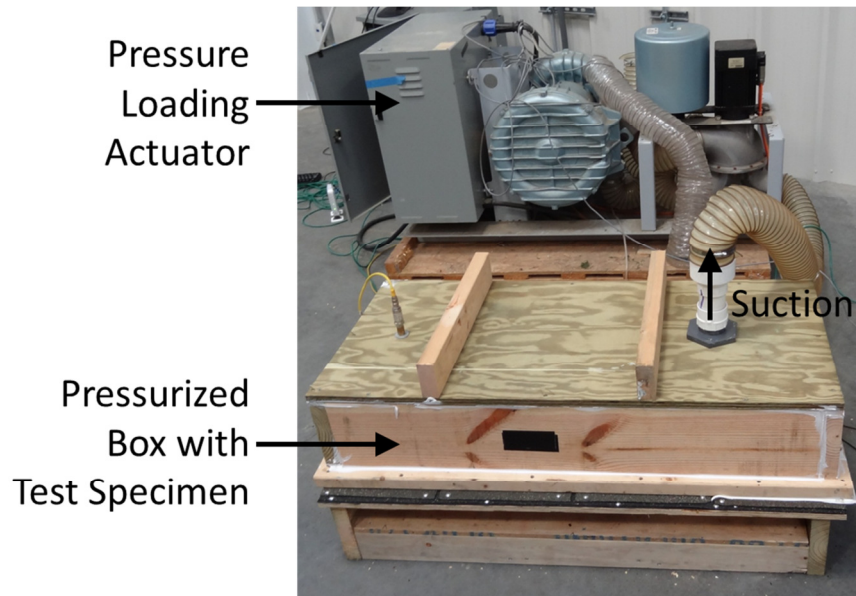


Fig. 83. Static pressure test setup.

The forces measured at each hold portion of the test were constant, thus mean forces at each hold were calculated by averaging each axis force over the entire hold period. An example of this averaging result at each hold is given in Figure 84 for the laminate shingle specimen. As static pressure in the chamber decreases, the  $F_z$  and  $F_y$  loads increase, while  $F_x$  decreases. An increase in the  $F_z$  load was expected, as the plastic sheeting billows upward in response to the suction pressure induced in the chamber. The direction and magnitude of  $F_x$  loads indicates an in-plane shear force perpendicular to the sealant strip directed towards the shingle's fasteners. From previous small-scale experiments, this in-plane shear was found to be caused by pressures on the shingle surface leeward of the sealant strip. The likely cause of this leeward pressure is the plastic sheeting's upward response to pressure imparting a force on the underside of the shingle surface on the leeward portion of the shingle. The response of  $F_z$  is generally linear throughout the range of pressure, while  $F_x$  and  $F_y$  are linear for pressures greater than 210 Pa (4.4 psf). The results shown in Figure 84 are typical for the three-tab and laminate specimens.

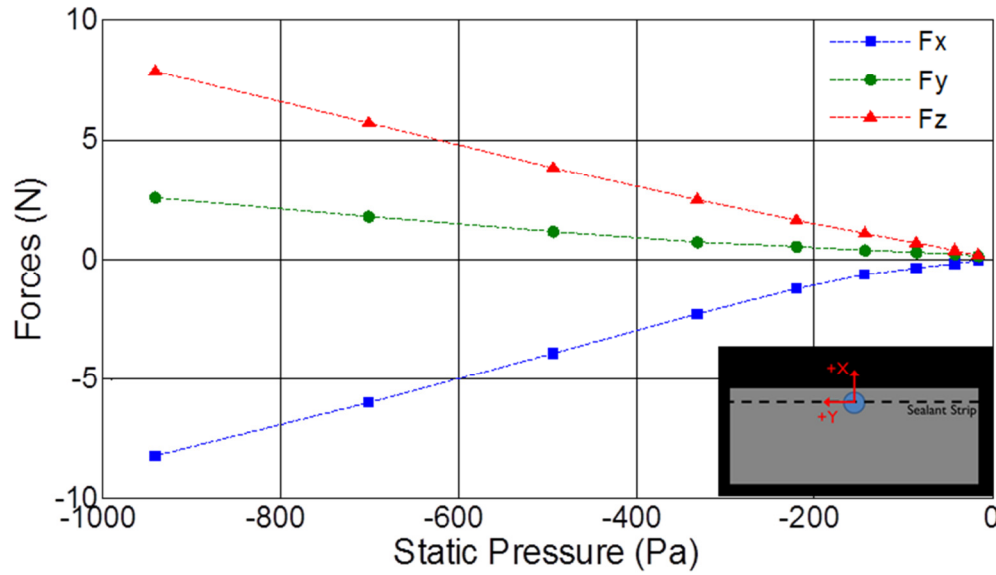


Fig. 84. Force measurements of six-axis load cell attached to laminate shingle specimen in response to static pressure.

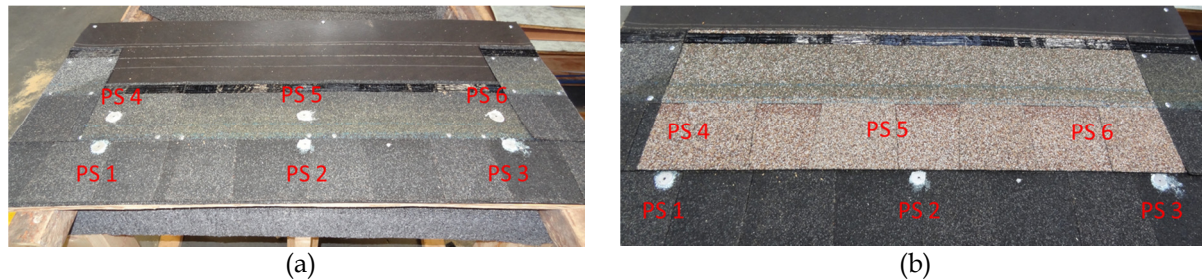
Table 31 summarizes the average distributed force at each measurement axis normalized by the static pressure in the chamber for each condition. The load response for the laminate and three-tab shingles are the same in the x-direction, and similar for the y- and z-direction loads. The No Shingle condition represents the force measurement of the load cells in response to static pressure when there is no shingle present and only the upper steel flat bar is sandwiching the plastic sheeting. Given the significant reduction in loads measured during the No Shingle condition, it appears that the presence of the shingle with the plastic sheeting between the load cell and shingle has a significant effect on the forces measured by the six-axis load cells due to static pressure.

Table 31. Static pressure induced force measurements normalized by static pressure

Condition	Fx (N/m/Pa)	Fy (N/m/Pa)	Fz (N/m/Pa)
Laminate	0.037	-0.006	-0.082
Three-Tab	0.037	0.010	-0.088
No Shingle (Bar Only)	-0.007	-0.002	-0.041

A final experiment measured the pressure difference between the top and bottom surface of a laminate shingle subjected to a negative static pressure, relative to ambient. Peterka and Cermak (1983) conducted a similar experiment with a three-tab shingle. This experiment utilized a laminate shingle fully sealed along its sealant strip, as it represents a more closed surface leeward of the sealant strip. The test deck consisted of 19 mm (0.75 in) thick plywood decking with No. 30 felt and dummy laminate shingles surrounding the test specimen – similar to the DFS experiment. Six 6.35 mm (0.25 in) diameter steel pressure taps were utilized with three taps located in front of the test shingle to represent the top surface pressure and three taps located on the underside of the test shingle (Figure 85). The barb

end of each tap was located on the underside of the plywood decking and sealed around its perimeter to prevent airflow through the drilled opening. The pressure at each tap was measured with a Dwyer MS-321-LCD pressure sensor relaying an analogue signal to an NI-6218 data acquisition system. The sensor has a maximum pressure reading of 150 Pa (3.1 psf) and an accuracy of 2 Pa (0.04 psf). Pressure was applied in the same wooden box utilized for the force measurement tests and the pressure test sequence consisted of actuating the valve to various openings from zero followed by a minimum 20 second hold.



**Fig. 85. Pressure tap layout for static pressure test on laminate shingles.**

The results of the pressure test suggest that a differential pressure between the top and bottom shingle surface may exist on laminate shingles; however, the magnitude of this differential is only ~6% of the static pressure. As shown in Figure 86, as the static pressure is rapidly decreased, the pressures measured below the shingle at PS 5 and PS 6 are approximately 6% lower than the pressures measured on the top of the shingle (PS 2 and PS 3). The underside pressure at PS 4 is closer to the top surface, likely caused by the single layer thickness of the shingle at the left end joint of the shingle near PS 4. Whereas, the double thickness of end joint near PS 6 may provide additional restriction from air movement below the shingle. The pressure difference between measurements at PS 5/6 and PS 2/3 is also greater than the accuracy of the sensor. Three-tab shingles were not evaluated, however, given the use of cutouts to separate the strip; it is likely that the laminate shingle with its continuous surface represents a conservative estimate of a shingle's ability to equalize pressure. The 6% difference in pressure is not, however, the primary cause of the load cell readings when the shingle is subjected to only static pressure and can be attributed to the use of the plastic sheeting imparting a force on the shingle and, subsequently, a force reading on the load cell.

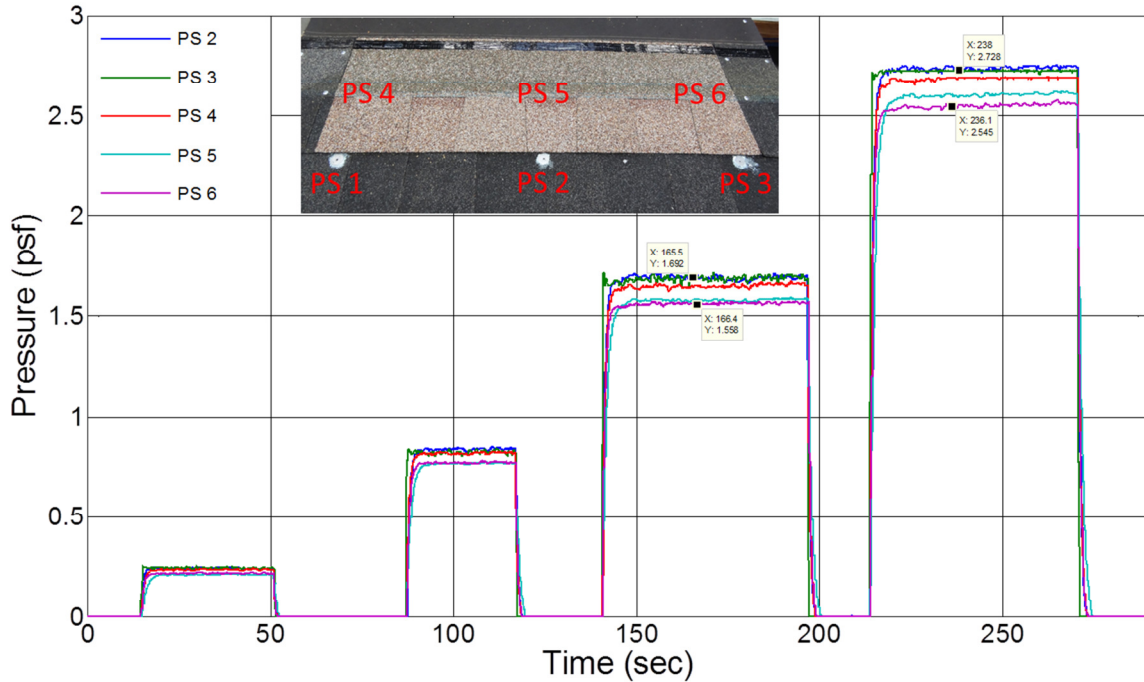


Fig. 86. Measured static pressures on top and bottom surface of laminate shingle. (1 psf = 47.8 Pa)

Given the results of this section, the wind uplift forces on asphalt shingle data presented in the following sections were calculated by subtracting the total force measured by the load cells along each axis subtracted from the load produced at each axis as a result of static pressure in the chamber (Equation (17)).

$$F_i = F_{lci} - F_{spi} \quad (17)$$

Where:

$$F_{spi} = P_s * C_{spi} * L * 0.90 \quad (18)$$

And where:

$F_i$  = Mean wind force exerted on the asphalt shingle along the axis of interest

$F_{lci}$  = Mean force measured by the load cell along the axis of interest

$F_{spi}$  = Mean force exerted on load cell as a result of static pressure in the test section

$P_s$  = Static pressure measured by the TFI Cobra Probe 25 mm (1 in) above shingle

$C_{spi}$  = Mean force coefficient along the axis of interest given in Table 31

$L$  = Measurement length

Using the calculation method above, several measurements on the laminate and three-tab specimens reported a negative mean vertical ( $F_z$ ) force on the sealant (i.e., a downward force). This is in counter to the anticipated positive (i.e., uplift)  $F_z$  forces along the sealant strip and indicates that the experimental procedure utilized to determine the effect of static pressure may have produced greater than estimated static pressure induced forces. Sources of this overestimation may reside in the use of a thinner substrate for the test shingles, producing a more flexible structure than the DFS test deck. Other sources of error include the arrangement of the plastic sheeting and the cutout size in the decking for the load cells. Given the amount of negative  $F_z$  load measurements, it appears that the results presented below are lower than the actual wind uplift exerted on the test shingles. Load cell readings on the x, y, and z axis were not used in the reporting of data below where negative z-axis loads were observed, but may be found in Tables A-1 through A-6 in Appendix A.

The process of experimentally quantifying the static pressure load then modifying the raw measurement made during wind testing likely introduces significant error into the final results. This error can be sourced both to the experimental estimate technique and to the interaction matrix built into the software for the six-axis load cells. The data presented herein represent initial results and future experiments are scheduled, using a modified connection detail that will not respond to static pressure.

#### **3.3.3.4 Wind Uplift Forces on Laminate Shingles**

A tabular summary of results for mean uplift loads ( $F_z$  only) measured on each laminate test shingle compared to the ASTM D7158 predicted uplift is located in Tables A-1 through A-6 in Appendix A. A graph of the results is given in Figure 87. The measured mean uplift loads for the fully sealed laminate shingles - for all wind azimuths (directions) - were less than the ASTM D7158 predicted loads with the exception of one measurement at a 22.5° wind azimuth. This highest recorded mean uplift load was 9% greater than the ASTM D7185 predicted, occurring on Measurement Location L for the High Wind Level. The measured mean uplift loads for the partially unsealed laminate shingles - for all wind azimuths - was less than the ASTM D7158 predicted. The highest recorded mean uplift load for the partially unsealed case was 21% less than the ASTM D7185 predicted, occurring on Measurement Location L for the High Wind Level at a 22.5° wind azimuth. Comparing the results of the fully and partially unsealed cases, the data indicates that partial unsealing does not cause an increase in pure uplift load on the shingle's self-seal strip. Interestingly, when the shingle was partially unsealed, higher uplift loads were recorded on Measurement Location R than the measurement location adjacent to the unsealing (M). The highest uplift loads were measured at the 22.5° wind azimuth, however, the spread of the data indicates that wind direction does not induce a significant change in mean uplift loads.

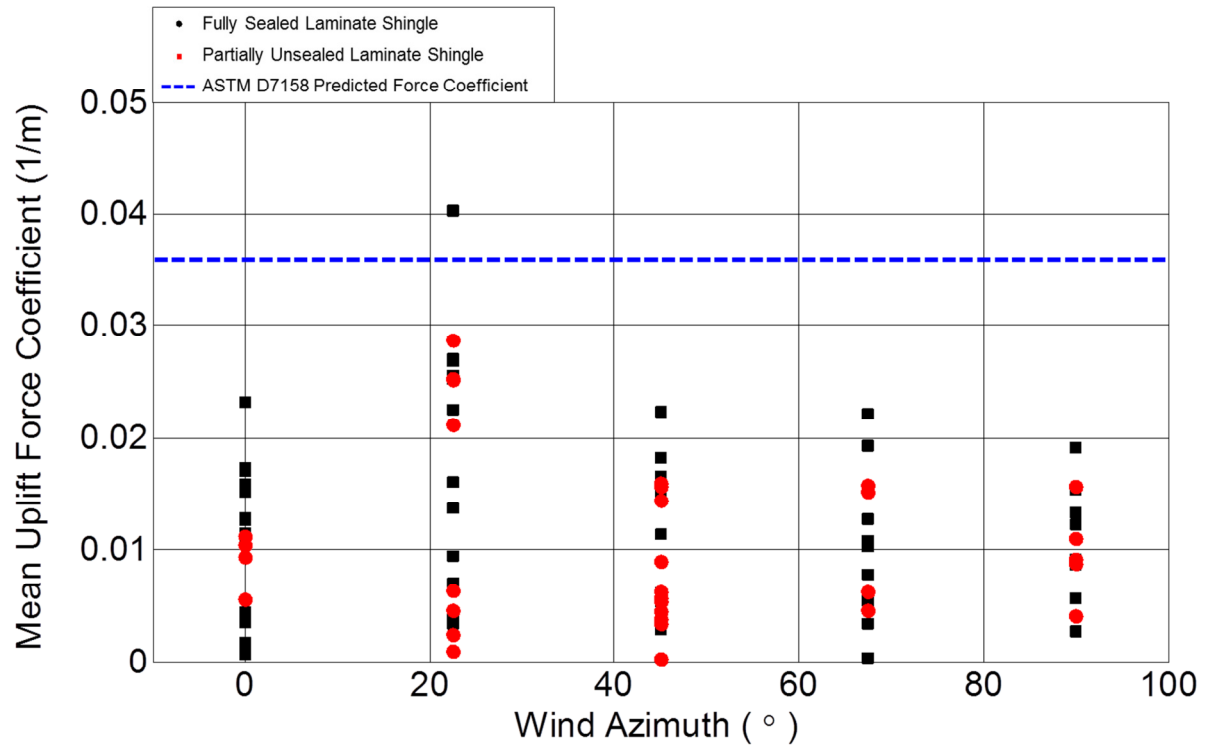


Fig. 87. Mean uplift force coefficient for laminate shingle specimens versus wind azimuth. Note: blue dashed line is uplift component only.

The average of the mean uplift loads for the three laminate replicates at each wind azimuth – Wind Level – Measurement Location combination are summarized in Table 32. Measurement Location R produced the most consistent measurements with COVs as low as 5%, whereas the shorter length Measurement Location L produced COVs up to 70%. For both the fully and partially sealed case, no averaged uplift force coefficient measurements were greater than the ASTM D7158 predicted. As with the individual results, the averaged results suggest that unsealing 152 mm (6 in) of the laminate shingle’s sealant strip does not cause an increase in uplift force on the remaining strip.

The total force measured on the laminate shingle’s self-sealing strip is summarized in Tables A-1 through A-6 of Appendix A and Figure 89. For the fully sealed laminate shingle case, the percentage of measurements above the ASTM D7158 prediction increased from 2% for the uplift force only measurements to 25% of the total force measurements. For the partially unsealed laminate shingle case, this percentage increased from 0% for the uplift force only measurements to 30% of the total force measurements. The highest measured force for the fully sealed laminate shingle increased from a force coefficient of  $0.040 \text{ m}^{-1}$  for uplift only to  $0.068 \text{ m}^{-1}$  when accounting for in-plane forces. The effects of the in-plane force are particularly noticeable for the partially unsealed shingles, whereby the highest mean force coefficient increased from  $0.028 \text{ m}^{-1}$  for uplift only to  $0.059 \text{ m}^{-1}$  for total force. These results indicate that in-plane forces play a significant role in the overall wind loading of a shingle’s self-seal strip. The mean load vertical angle above the horizontal plane of the roof for the fully sealed shingles was  $22^\circ$  ( $\sigma = 13^\circ$ ), while mean load vertical angle for the partially unsealed was  $18^\circ$  ( $\sigma = 17^\circ$ ). Therefore, the in-plane loading on the self-seal strip dominates the pure uplift, z-direction, loading.

**Table 32. Laminate - measured mean uplift (combined)**

Wind Azimuth (°)	Wind Speed Level (High/Low)	Measurement Location	Measured Mean Uplift Force Coefficient (1/m) [COV]				Predicted Mean Uplift Force Coefficient (1/m)
			Fully Sealed		Partially Unsealed		
			Mean (1/m)	COV (%)	Mean (1/m)	COV (%)	
0	Low	L	0.012	--	Unsealed	Unsealed	0.037
		M	0.006	90	--	--	
		R	0.006	75	--	--	
	High	L	0.014	58	Unsealed	Unsealed	
		M	0.011	52	0.006	--	
		R	0.015	12	0.010	8	
22.5	Low	L	0.014	77	Unsealed	Unsealed	0.037
		M	0.018	48	--	--	
		R	0.028	43	0.017	73	
	High	L	0.013	70	Unsealed	Unsealed	
		M	0.010	33	0.003	70	
		R	0.018	58	0.024	8	
45	Low	L	--	--	Unsealed	Unsealed	0.037
		M	0.011	--	0.005	46	
		R	0.011	42	0.005	17	
	High	L	0.003	0	Unsealed	Unsealed	
		M	0.008	67	0.004	67	
		R	0.019	13	0.015	5	
67.5	Low	L	--	--	Unsealed	Unsealed	0.037
		M	0.011	--	--	--	
		R	0.010	--	--	--	
	High	L	0.005	--	Unsealed	Unsealed	
		M	0.008	109	0.007	29	
		R	0.014	42	0.015	9	
90	Low	L	--	--	Unsealed	Unsealed	0.037
		M	0.015	--	--	--	
		R	0.009	--	--	--	
	High	L	0.003	--	Unsealed	Unsealed	
		M	0.011	52	0.010	49	
		R	0.012	16	0.010	10	

**Table 33. Laminate - measured mean total force (combined)**

Wind Azimuth (°)	Wind Speed Level (High/Low)	Measurement Location	Measured Mean Total Force Coefficient (1/m) [COV]				Predicted Mean Uplift Force Coefficient (1/m)
			Fully Sealed		Partially Unsealed		
			Mean (1/m)	COV (%)	Mean (1/m)	COV (%)	
0	Low	L	0.033	20	Unsealed	Unsealed	0.037
		M	0.023	68	--	--	
		R	0.028	18	--	--	
	High	L	0.026	46	Unsealed	Unsealed	
		M	0.031	47	0.034	--	
		R	0.038	11	0.032	6	
22.5	Low	L	0.041	21	Unsealed	Unsealed	0.037
		M	0.041	17	--	--	
		R	0.058	6	0.028	35	
	High	L	0.034	44	Unsealed	--	
		M	0.039	38	0.044	25	
		R	0.044	--	0.047	17	
45	Low	L	--	--	Unsealed	Unsealed	0.037
		M	0.026	29	0.024	33	
		R	0.027	--	0.022	38	
	High	L	0.022	16	Unsealed	Unsealed	
		M	0.029	24	0.022	20	
		R	0.029	--	0.030	19	
67.5	Low	L	--	--	Unsealed	Unsealed	0.037
		M	0.032	--	0.053	--	
		R	0.039	--	0.067	--	
	High	L	0.018	25	Unsealed	Unsealed	
		M	0.024	15	0.024	21	
		R	0.029	--	0.034	40	
90	Low	L	--	--	Unsealed	Unsealed	0.037
		M	0.023	--	--	--	
		R	0.021	--	0.092	--	
	High	L	0.028	14	Unsealed	Unsealed	
		M	0.033	8	0.028	51	
		R	0.037	16	0.037	42	

The combined uplift and total force coefficient results of Tables 32 and 33, respectively, suggest that a 152 mm (6 in) unsealing does not cause an increase in measured total load along the sealant strip. However, progressive unsealing was observed in one laminate specimen at the interface of shingle's lower surface and the left side of the steel flat bar connecting the shingle to the load cell, as shown in Figure 88. The specimen began unsealing during tests at the 22.5° wind azimuth and continued unsealing throughout the test sequence. It appears that an unsealing of this type exposes the adjacent sealed portion of the sealant strip to a concentration of peel-type stresses. Further discussion of the implications of this finding is provided in the Significant Findings and Conclusions Section 3.3.4 below.



Fig. 88. Progressive unsealing observed on partially unsealed laminate shingle specimen.

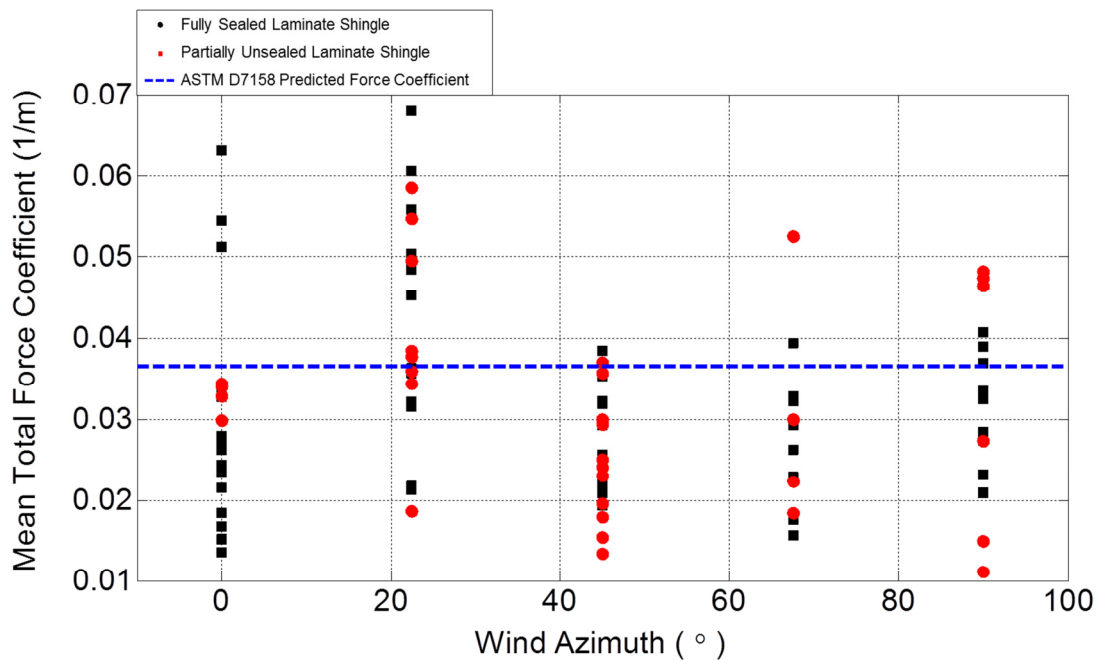


Fig. 89. Mean total force coefficient for laminate shingle specimens versus wind azimuth.

Table 33. Laminate - measured mean total force (combined)

Wind Azimuth (°)	Wind Speed Level (High/Low)	Measurement Location	Measured Mean Total Force Coefficient (1/m) [COV]				Predicted Mean Uplift Force Coefficient (1/m)
			Fully Sealed		Partially Unsealed		
			Mean (1/m)	COV (%)	Mean (1/m)	COV (%)	
0	Low	L	0.033	20	Unsealed	Unsealed	0.037
		M	0.023	68	--	--	
		R	0.028	18	--	--	
	High	L	0.026	46	Unsealed	Unsealed	
		M	0.031	47	0.034	--	
		R	0.038	11	0.032	6	
22.5	Low	L	0.041	21	Unsealed	Unsealed	0.037
		M	0.041	17	--	--	
		R	0.058	6	0.028	35	
	High	L	0.034	44	Unsealed	--	
		M	0.039	38	0.044	25	
		R	0.044	--	0.047	17	
45	Low	L	--	--	Unsealed	Unsealed	0.037
		M	0.026	29	0.024	33	
		R	0.027	--	0.022	38	
	High	L	0.022	16	Unsealed	Unsealed	
		M	0.029	24	0.022	20	
		R	0.029	--	0.030	19	
67.5	Low	L	--	--	Unsealed	Unsealed	0.037
		M	0.032	--	0.053	--	
		R	0.039	--	0.067	--	
	High	L	0.018	25	Unsealed	Unsealed	
		M	0.024	15	0.024	21	
		R	0.029	--	0.034	40	
90	Low	L	--	--	Unsealed	Unsealed	0.037
		M	0.023	--	--	--	
		R	0.021	--	0.092	--	
	High	L	0.028	14	Unsealed	Unsealed	
		M	0.033	8	0.028	51	
		R	0.037	16	0.037	42	

### 3.3.3.5 Wind Uplift Forces on Three-Tab Shingles

The mean uplift force coefficients obtained on all load cell measurements is presented in Figure 90, stratified by wind azimuth. Tabular results of the distributed loads and force coefficients for all replicates are located in Tables A-7 through A-12 in Appendix A. The measured mean uplift force coefficients for the fully sealed specimens were less than the ASTM D7158 predicted force coefficients on all measurements, while the measured mean uplift force coefficients for the partially unsealed specimens were greater than the ASTM D7158 predicted force coefficients on 25% of the measurements. The plot of Figure 90 clearly shows that the unsealing of one-half tab width of the shingle produces consistently higher uplift force when compared to the fully sealed. As expected, the highest loads on the unsealed shingle were measured on the remaining sealant strip of the unsealed tab (i.e., C2). Uplift forces on the fully sealed specimens do not appear to be sensitive to changes in wind direction (Figure 90). Given the variability within the data, a definitive conclusion cannot be made on the effects of wind direction on the uplift forces generated on a fully sealed shingle. The uplift force measured on the partially unsealed shingle indicates that these forces increase for wind azimuths of 22.5° and greater. The distribution and peak measured force coefficients for the 22.5° through 90° wind azimuths produce similar uplift force coefficients. This is likely caused by wind flow entering underneath the shingle specimen on the leeward side of the sealant strip, causing an increase in positive pressure exerted on the shingle's underside.

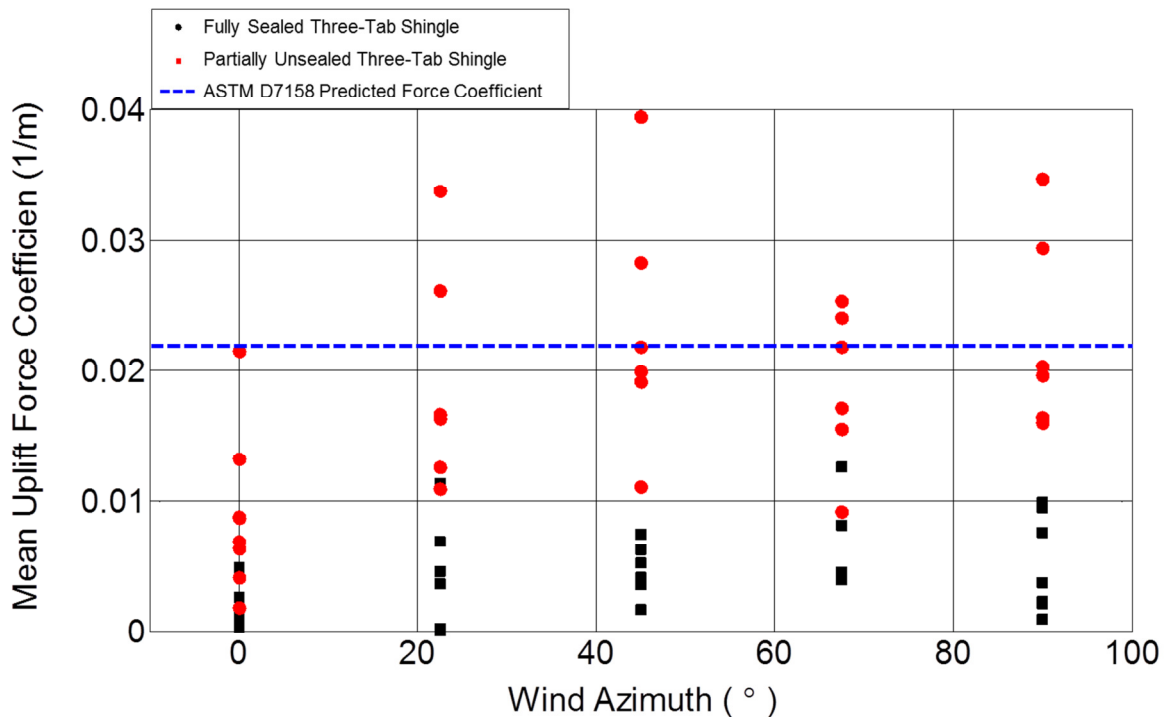
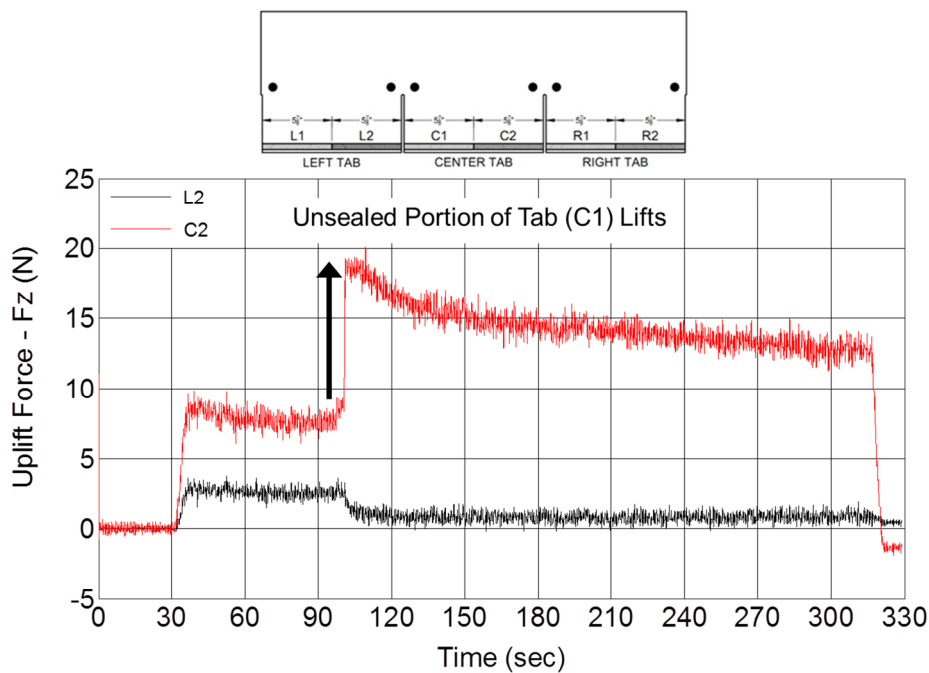


Fig. 90. Mean uplift force coefficient for three-tab specimens versus wind azimuth.

**Table 34. Three-Tab - measured mean uplift force (combined)**

Wind Azimuth (°)	Wind Speed Level (High/Low)	Measurement Location	Measured Mean Uplift Force Coefficient (1/m) [COV]				Predicted Mean Uplift Force Coefficient (1/m)
			Fully Sealed		Partially Unsealed		
			Mean (1/m)	COV (%)	Mean (1/m)	COV (%)	
0	Low	L	--	--	0.022	0	0.022
		M	--	--	Unsealed	Unsealed	
		R	0.004	29	0.006	21	
	High	L	--	--	0.002	0	
		M	--	--	Unsealed	Unsealed	
		R	0.002	84	0.010	21	
22.5	Low	L	--	--	--	--	0.022
		M	0.002	100	Unsealed	Unsealed	
		R	0.007	--	0.024	40	
	High	L	--	--	--	--	
		M	--	--	Unsealed	Unsealed	
		R	0.005	85	0.015	12	
45	Low	L	--	--	--	--	0.022
		M	--	--	Unsealed	Unsealed	
		R	0.003	43	0.020	35	
	High	L	--	--	--	--	
		M	--	--	Unsealed	Unsealed	
		R	0.006	23	0.026	36	
67.5	Low	L	0.003	100	--	--	0.022
		M	0.002	100	Unsealed	Unsealed	
		R	0.005	--	0.017	38	
	High	L	--	--	--	--	
		M	--	--	Unsealed	Unsealed	
		R	0.008	43	0.020	18	
90	Low	L	--	--	--	--	0.022
		M	0.001	88	Unsealed	Unsealed	
		R	0.005	56	0.027	29	
	High	L	--	--	--	--	
		M	--	--	Unsealed	Unsealed	
		R	0.008	37	0.019	10	

An example of the effect of wind uplift on a partially unsealed shingle is given in the uplift load time-history plot of Figure 91. This test was conducted at the High Wind Level (40 m/s) with the specimen oriented to a 45° wind azimuth. The test initialized 30 seconds into the record with the uplift forces at measurement locations C2 and L2 approximately 8 N and 3 N, respectively. The unsealed portion of the tab (C1) remained in a horizontal position during the initial period of the wind test. However, 70 seconds into the test (t = 100 sec) the unsealed portion of the shingle tab lifted and folded backwards, causing the uplift force at C2 to increase by 10 N, while the uplift force at L2 decreased by 2 N. This time-history indicates that as the shingle's unsealed tab lifts it exposes the interior of the shingle to additional wind flow, thereby, increasing the wind uplift force on the remaining portion shingle's sealant strip. Further discussion on the implications of this observation is provided in Section 3.3.4.



**Fig. 91. Lifting of the unsealed portion of a three-tab specimen increased the uplift force on the sealed portion of the tab.**

The mean total force coefficient results for the fully sealed and partially unsealed three-tab shingle specimens are plotted in Figure 92 and tabulated in Appendix A. The averaged results of the three replicates for each sealed condition are summarized in Table 35. The measured mean total force coefficients for the fully sealed shingles were greater than the ASTM D7158 predicted on 33% of the measurements. While 97% of the partially sealed shingle measurements were greater than ASTM D7158 predicted. The highest measured mean total force coefficient for the fully sealed case was approximately 2.5 times greater than the ASTM D7158 predicted. Whereas, the highest measured mean total force coefficient for the partially unsealed case was 4.5 times greater than the ASTM D7158 predicted. Similar to the uplift (z-direction) results, the mean total force coefficients measured on the unsealed shingles were generally higher than the fully sealed. The COVs of the averaged results ranged from 3% to 100% with the most consistent measurements captured at

Measurement Location C2 (Table 35). The mean vertical angle for the fully sealed shingle was  $12^\circ$  ( $\sigma = 9^\circ$ ), where, the partially unsealed vertical angle was  $24^\circ$  ( $\sigma = 10^\circ$ ). As with the laminate shingle specimens, it appears that in-plane forces play a significant role on asphalt shingle wind loading.

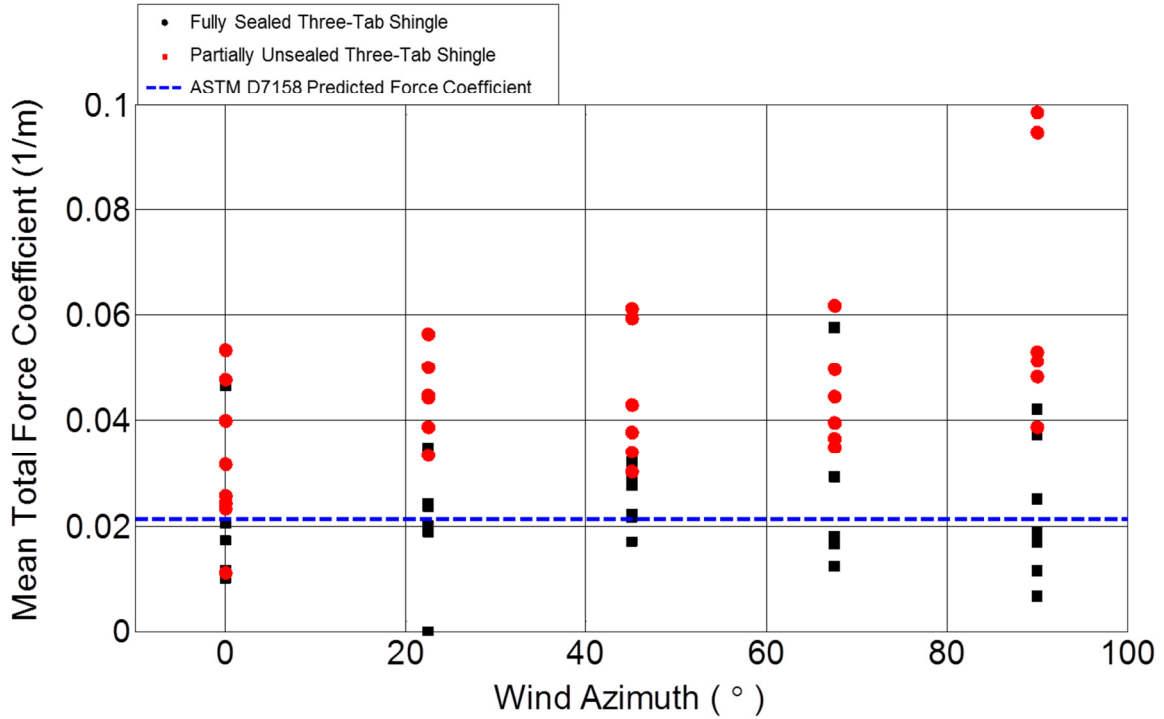


Fig. 92. Mean total force coefficient for three-tab specimens versus wind azimuth.

Table 35. Three-Tab - measured mean total force (combined)

Wind Azimuth (°)	Wind Speed Level (High/Low)	Measurement Location	Measured Mean Total Force Coefficient (1/m) [COV]				Predicted Mean Uplift Force Coefficient (1/m)
			Fully Sealed		Partially Unsealed		
			Mean (1/m)	COV (%)	Mean (1/m)	COV (%)	
0	Low	L	--	--	0.040	--	0.022
		M	--	--	Unsealed	Unsealed	
		R	0.010	3	0.036	35	
	High	L	--	--	0.011	--	
		M	--	--	Unsealed	Unsealed	
		R	0.016	23	0.033	33	
22.5	Low	L	--	--	--	--	0.022
		M	0.012	100	--	Unsealed	
		R	0.020	--	0.045	21	
	High	L	--	--	--	--	
		M	--	--	Unsealed	Unsealed	
		R	0.026	26	0.044	11	
45	Low	L	--	--	--	--	0.022
		M	--	--	Unsealed	Unsealed	
		R	0.028	15	0.042	29	
	High	L	--	--	--	--	
		M	--	--	Unsealed	Unsealed	
		R	0.022	20	0.046	25	
67.5	Low	L	0.075	100	--	--	0.022
		M	0.006	100	Unsealed	Unsealed	
		R	0.058	--	0.045	28	
	High	L	--	--	--	--	
		M	--	--	Unsealed	Unsealed	
		R	0.021	27	0.045	9	
90	Low	L	--	--	--	--	0.022
		M	0.008	89	Unsealed	Unsealed	
		R	0.024	53	0.077	35	
	High	L	--	--	--	--	
		M	--	--	Unsealed	Unsealed	
		R	0.029	34	0.051	4	

### 3.3.4 Preliminary Findings

The initial results of the experiment indicate the current surface pressure measurements utilized in the ASTM D7158 test standard may not be an appropriate method for predicting uplift forces on a shingle's sealant strip. The pressure coefficient results from ASTM D7158 were obtained from a shingle that was artificially uplifted along the shingle's leading edge to match the predicted design-level wind speed deflection. Thus, these coefficients should be conservative for all winds below design-level. Considering uplift forces only, three-tab and laminate products exceeded ASTM D7158 on only 0% and 2% of the measurements, respectively (Table 36). When measured in-plane forces were added to the uplift, the three-tab and laminate products exceeded ASTM D7158 on 33% and 25% of the measurements, respectively (Table 36). In-plane forces had an effect on the overall loading of the shingle's sealant strip.

**Table 36. Comparison of measured force coefficients above ASTM D7158 prediction**

Shingle Type	Force Component	% of Measured Force Coefficients Above ASTM D7158 Prediction
Laminate	Uplift Only (Fz)	2
	Total (Fx+Fy+Fz)	25
Three-Tab	Uplift Only (Fz)	0
	Total (Fx+Fy+Fz)	33

At present, this finding is not conclusive due to the presence of negative static pressure (relative to the atmospheric pressure) in the test section that produced uplift of the plastic sheeting and a subsequent load interaction on the instrumented shingle. Therefore, the forces measured by the load cells were a combination of realistic wind uplift forces on the shingle produced by wind flowing over the shingle and unrealistic forces exerted on instrumented shingle by the plastic sheeting. As reported, an experiment was conducted to quantify the static pressure-induced force imparted on the instrumented shingle by isolating the instrumented shingle on a replicate test deck and applying static pressure over the shingle in absence of wind velocity. The load response of the shingle was physically correct in all measurement axes (X-, Y-, and Z-axis). The results presented in Sections 3.3.3.4 and 3.3.3.5 were calculated by subtracting the predicted static pressure-induced force on each axis from the raw load readings measured during wind testing to produce the wind uplift force exerted on the instrumented shingle from near-roof wind flow. However, a near majority of these filtered results showed a mean negative Z-component (downward) force. Measurements with a mean negative Z-component were not included in the results presented above because negative Z-component forces are not physically realizable within the wind load model for asphalt shingles (Peterka et al. 1997). Thus, the method utilized for predicting the static pressure effects may be too high in the Z-axis, while the X- and Y-axis predicted forces may or may not be appropriate. Given the implications for these results to impact the ASTM D7158 test method, it is imperative that further validation of these results be conducted.

The second finding of increased loads on partially unsealed shingles is significant, but also requires further validation. Comparing the results of the fully sealed and partially unsealed three-tab specimens, the uplift forces exerted on the sealed portion of the sealant strip are greater for the partially unsealed than the fully. As hypothesized, when the unsealed portion of the shingle lifts in the wind, the shingle is exposed to increased wind flow behind the shingle's sealant strip. This leeward pressurization not only increases the vertical (Z-axis) component of the load on the sealant strip, but also increases the in-plane forcing on the sealant strip due to the membrane response of the shingle under pressure. This was confirmed in an unpublished experiment conducted by the authors where pressure was applied to the instrumented shingle's surface behind the sealant strip.

When compared to the fully sealed laminate specimens, increased forces on the sealant strip were not observed on the partially unsealed laminate shingle specimens. As previously stated, this is likely due to the length over which the load cells were measuring, whereby, any increased forces due to partial unsealing were likely concentrated near the interface of the sealed and unsealed portion of the laminate specimen. Progressive unsealing from peel-stresses was observed in one specimen, but increased loads were not measured.

## 4. SYSTEM-LEVEL WIND RESISTANCE OF ASPHALT SHINGLES

### 4.1 Introduction

Current standardized test methods evaluate performance of shingles in isolation and do not consider rake, eave, hip, ridge, or valley details, nor roof penetrations despite results from post-storm reports that show wind related damage to these components (Figure 93) (FEMA, 2005a; FEMA, 2005b; FEMA, 2006; FEMA, 2009). Fastener pull-through, lifting, and unsealing initiated at roof edge details have been shown to progress upslope causing extensive damage to field shingles and underlayment - exposing the interior of the building to moisture intrusion. Hip and ridge shingle blow off are common in below design-level windstorms, leaving the secondary water barrier to provide waterproofing (Figure 93b) (FEMA, 2011). These post-storm reports provide valuable information on how in-service shingle systems are performing in windstorms, yet their conclusions contain uncertainty. Unknown variables such as damage progression, wind speeds at the building site, and the pre-storm condition of the roof can influence the interpretation of these observations. In short, damage to system-level shingle roofing components has been observed, but the direct cause of damage is not well defined.

It logically follows that an investigation on the wind resistance of asphalt shingles must include a holistic investigation of the complete roof system. The objective of this experiment was to assess the system-level performance of asphalt shingle roofs subjected to hurricane force winds. Utilizing the unique capabilities of the IBHS Research Center, the investigators evaluated the wind resistance of three shingle systems installed on full-scale hip and gable style roofs. One ASTM D7158 Class H three-tab product - henceforth TT-201 - and two ASTM D7158 Class H laminate products - henceforth LAM-201 and LAM-202 - were tested in this investigation. A single professional roofing contractor performed installation of the shingle roofing systems. UF specified to the installer that all shingle roofs should be installed in accordance with Florida Building Code 2010 Section R905.2 and manufacturer guidelines. During post-wind test investigations of the roof specimens, UF noted deviations from Florida Building Code and manufacturer specifications that may have adversely contributed to the shingle's performance during wind testing. Specific instances of nonconformance to code and/or manufacturer specifications are noted in the results presented below.

The shingle roof specimens were constructed outdoors at the IBHS Research Center summer 2011. Following an 11 month outdoor conditioning period, the roofs were individually brought inside the wind tunnel and installed on a base structure to form a complete one-story residential building. The building was then subjected to three 30 minute stochastic wind simulations of increasing intensity, followed by one 17 minute low turbulence ramp and hold wind scenario. The peak eave height approach wind speeds were 53 m/s (119 mph) - the maximum achievable wind speed by the Research Center. During testing, the behavior of the shingle system was recorded using seven high definition cameras. After testing, the post-test condition of the roof was documented. This section will detail the experimental methods, summarize the performance of the shingle systems, and provide recommendations with the goal of improving the system-level wind resistance of asphalt shingle roofs.



(a)



(b)



(d)



(c)

**Fig. 93. Post-storm observations of shingle roof systems: (a) rake edge shingle blow off [Photo from FEMA (2011)], (b) hip shingle blow off [Photo from FEMA (2011)], (c) rake shingle and underlayment blow off [Photo from FEMA (2005a)], and (d) eave shingle blow off [Photo from FEMA (2009)]**

## 4.2 IBHS Research Center

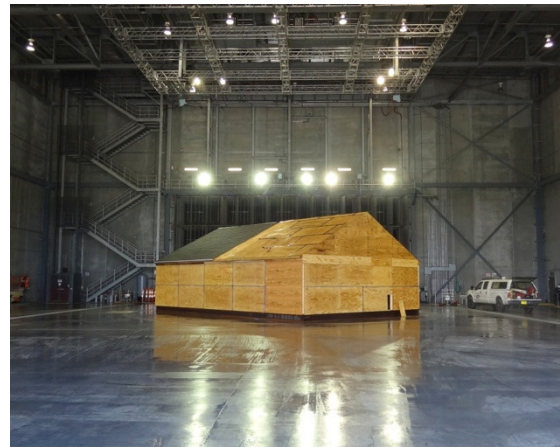
The IBHS Research Center has a full-scale test facility capable of subjecting one- and two-story buildings to Saffir-Simpson Hurricane Wind Scale Category 3 hurricane wind-induced pressure loading (Simpson 1974, Saffir 1973) (Figures 94 and 95). More detail of the facility may be found in Section 3.2.2.



Fig. 94. Google Earth image of the IBHS Research Center with shingle roof specimens located at conditioning site (shown on right).



(a)



(b)

Fig. 95. IBHS Research Center (a) exterior view showing the fan arrays and (b) interior of test chamber with test specimen installed on the base structure.

## 4.3 Experimental Methods

The experimental methods are presented in five parts:

- Section 4.3.1- Experiment Overview
- Section 4.3.2 - Construction of Asphalt Shingle Roof Specimens
- Section 4.3.3 - Conditioning Phase Temperature Profiles
- Section 4.3.4 - Base Structure
- Section 4.3.5- Installation of Asphalt Shingle Roof Specimens
- Section 4.3.6 - Test Sequence Procedure

### 4.3.1 Experiment Overview

This experiment evaluated the wind performance of 17 full-scale ASTM D7158 Class H asphalt shingle roof systems. The test matrix consisted of three different shingle products comprised of two laminate shingle products (LAM-201 and LAM-202) and one three-tab product (TT-201) (Table 37). For each manufacturer, three hip roofs and six mono-slope roofs were constructed for a total of nine roofs per manufacturer. All roofs were constructed with a 6:12 roof slope. The third hip roof for TT-201 was constructed, but not tested due to time constraints encountered during testing. The shingle roof specimens were constructed at the IBHS Research Center in summer 2011 and were conditioned outdoors for 11 months (Figures 94 and 98).

The complete test building, Figures 96 and 97, consisted of a base structure (Section 4.3.4) and asphalt shingle roof specimen (Section 4.3.2). The base structure was a 9.1 m W x 12.2 m L x 2.4 m H (30 ft W x 40 ft L x 7 ft 10 in H) steel frame sheathed with wood-framed wall panels on the exterior of the structure. One half of the base structure's roof was a permanent 6:12 gable roof with bare plywood roof decking. The base structure was installed on the chamber's turntable throughout the experiment. For a hip roof test, each roof was driven from the conditioning site using an 18 ton crane and installed on the open half of the base structure (Figure 96). For the mono-slope roof sections, two mono-slope roofs were installed for each test to form one complete gable roof section (Figure 97). Once wind testing was completed, the roof sections were driven back to the conditioning site and reinstalled on their support structures.

**Table 37. Asphalt shingle roof specimen test matrix**

Asphalt Shingle ID	Shingle Type (Color)	Number of Hip Roofs	Number of Mono-Slope Gable Roofs
LAM-201	Laminate (Black)	3	6
LAM-202	Laminate (Black)	3	6
TT-201	Three-Tab (Black)	3	6
<b>Total</b>		<b>9</b>	<b>18</b>

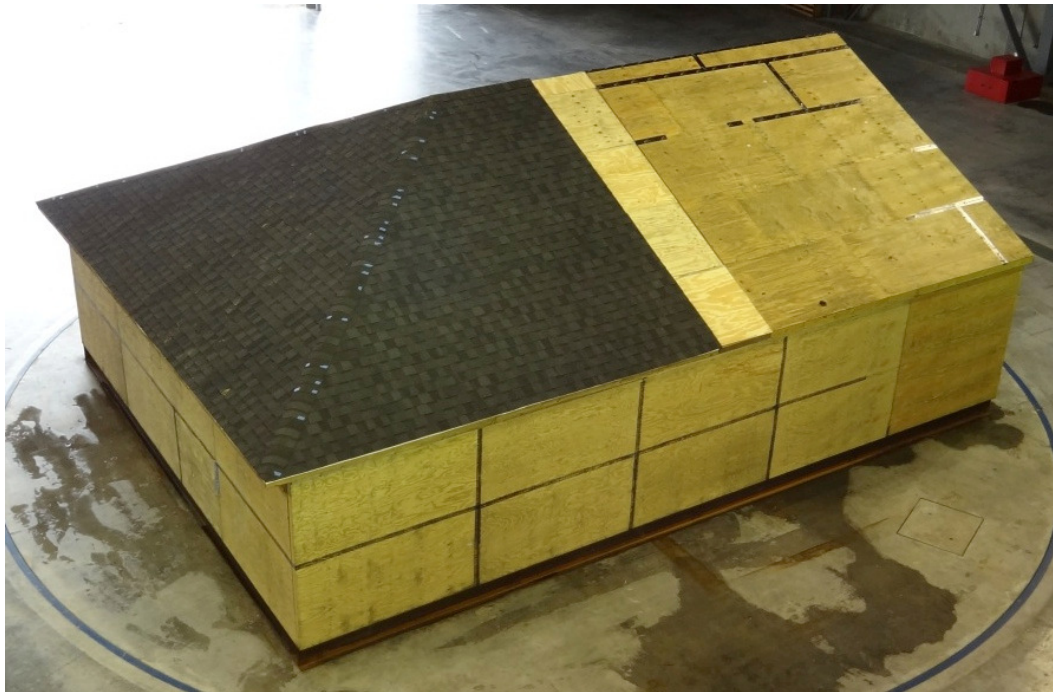


**Fig. 96. Test building with hip roof specimen. The blue marks note the location of partially/fully unsealed shingles.**

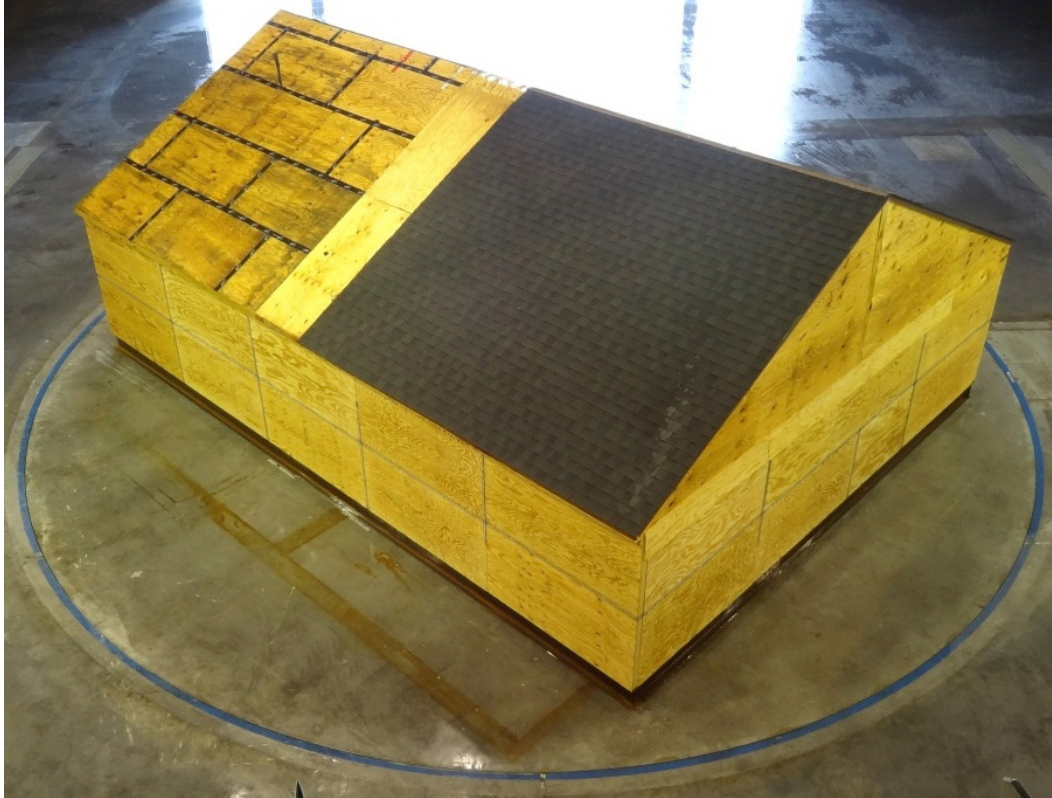


**Fig. 97. Test building with gable roof specimen.**

### **4.3.2 Construction of Asphalt Shingle Roof Specimens**

The asphalt shingle roof specimens were constructed at the IBHS Research Center from July 2011 to mid-August 2011. UF constructed the roof specimen's wood support structures, erected the roof trusses, and installed the wood roof sheathing. A professional roofing contractor installed the asphalt shingle roof coverings and roof accessories (e.g., drip edge flashings). The roof slopes on all mono-slope and front faces of the hip roof sections were oriented south to maximize the amount of sun exposure on the shingle systems (Figure 98). The roof specimens were conditioned on this site for an 11 month period prior to wind testing to allow the self-sealing adhesive on the shingle to fully adhere and to subject the roofs to four seasons.



**Fig. 98. Aerial view of the completed asphalt shingle roof sections at the IBHS Research Center. The roofs were located at this field site throughout their 11 month conditioning phase.**

#### **4.3.2.1 Roof Specimen Support Structures**

The support structure for each roof section consisted of a pressure-treated 4x6 wood frame secured to isolated reinforced concrete piers. The wood support beams braced the bottom truss chords of the roof specimens along their natural wall support lines, as shown in Figures 99a and 100a. The shingle roof specimens were secured to the support beams via one Simpson Strong-Tie H2.5Z per roof truss.

#### **4.3.2.2 Mono-Slope Roof Construction**

Each mono-slope gable roof specimen (18 in total) consisted of 11 mono-sloped metal plate connected southern yellow pine trusses with a bottom chord length of 4.7 m (15.5 ft) and height of 2.4 m (7.75 ft) for a roof slope of 6:12 (Figure 99). The trusses were spaced at 2 ft on center, with the exception of one gable end truss that was spaced at 0.36 m (1.2 ft) to give an overall specimen width of 5.8 m (19.2 ft). The truss system was internally braced with dimensional lumber along the bottom, strut, and top chords, where necessary (Figure 99b). The roof sheathing consisted of 1.2 m by 2.4 m (4 ft by 8 ft) oriented strand board (OSB) exterior grade 11 mm (7/16 in) thick roof sheathing panels. The panels were staggered at 1.2 m (4 ft) spacing between panel rows with 3.2 mm (0.13 in) spacing between panels achieved using Simpson Strong-Tie PSCA Panel Sheathing Clips. Following FBC 2010 Section R803.2.3.1, sheathing panels were pneumatically fastened to each roof truss using 8d ring shank nails at a spacing of 152 mm (6 in) field and 152 mm (6 in) edge (Figure 99c). The specifications of the nails included: 2.9 mm (0.113 in) shank diameter, 51 mm (2 in) nail length, and 7 mm (0.28 in) full round head diameter. The specimen's fascia board consisted of a single 2x4 lumber board fastened to each truss with two 8d ring shank nails. The gable ends, back side, and underside were not sheathed. Two thermocouples were

installed between shingles on one mono-slope roof per manufacturer to record the temperature of the shingles throughout conditioning phase in order to evaluate the effect of the exposed underside of the roof on shingle temperature. These measurements are discussed in Section 4.3.3.



**Fig. 99. (a) - (c) Construction of the mono-slope gable roof sections. (d) Completed mono-slope gable roof section.**

#### **4.3.2.3 Hip Roof Construction**

Each hip roof specimen (9 in total) consisted of metal plate connected southern yellow pine roof trusses with overall plan dimensions of 9.7 m (32 ft) wide by 6.2 m (20.2 ft) long with a roof slope of 6:12 (Figure 100). Similar to the mono-slope gable sections, 11 mm (7/16 in) thick exterior grade OSB sheathing panels were secured to the roof trusses using 8d ring shank nails at a spacing of 152 mm (6 in) field and 152 mm (6 in) edge. As with the mono-slope specimens, the gable end and bottom chords of each hip roof were not sheathed. No shingle temperatures were measured on the hip roofs as the temperature measurements obtained on mono-slope roof specimens were assumed to match the hip specimens.

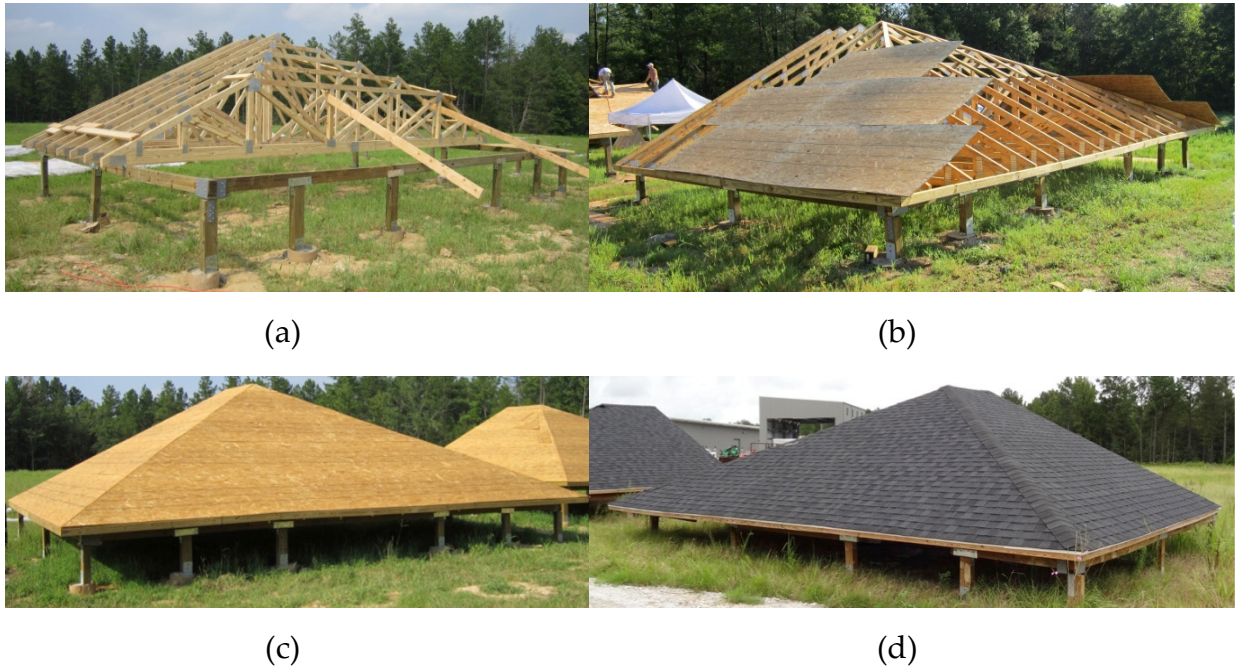


Fig. 100. (a) - (c) Construction of the hip roof sections. (d) Completed hip roof section.

#### 4.3.2.4 Asphalt Shingle Installation

The type of asphalt shingle, rather than a specific manufacturer or product, was of interest to this experiment. Therefore, the test matrix utilized two laminate (architectural) style shingles, LAM-201 and LAM-202, and one three-tab fiberglass-reinforced shingle, TT-201. All three manufacturers' products were wind rated as ASTM D7158 Class H. LAM-201 and LAM-202 shingle products carried a "lifetime" warranty, while TT-201 carried a "25-year" warranty. Asphalt shingle products and accessories were purchased by UF from Richburg, SC contractor supply stores and all products remained anonymous throughout the investigation. A Richburg (SC) professional roofing company installed the asphalt shingle roof systems with the installation procedures conforming to 2010 Florida Residential Building Code Section R905.2 and manufacturers' guidelines. Installation of all roofing and associated components was performed by one individual, to achieve consistency in workmanship.

Galvanized Type-D profile metal drip edge flashing was installed along all eave edges and 76 mm by 76 mm (3 in by 3 in) galvanized angle flashing was installed along all gable ends and mono-slope backsides. The flashings were secured with pneumatically driven, 12 gauge, 9.5 mm (3/8 in) diameter head, 31 mm (1.25 in) length, galvanized steel roofing nails at 25 mm (4 in) on center.

The roof underlayment consisted of a single layer of ASTM D226 Type II (No. 30) roofing felt with 152 mm (6 in) laps at all seams. The underlayment was not set in roofing cement around the roof's perimeter. Hand-driven, 31 mm (1.25 in) long galvanized steel button cap type fasteners secured the felt to the decking at a maximum spacing of 914 mm (36 in) on center.

Starter strips were installed along the eave edges of all roofs. Each manufacturer's guidelines specified that the starter strips and first course of shingles contain an overhang of 6.3 - 19mm (0.25 - 0.75 in) beyond the eave drip edge and rake edge metal. A median overhang of 12.7 mm (0.5 in) was used for this installation. In accordance with each manufacturer's installation specifications, the starter strips consisted of the manufacturer's three-tab shingles with the exposed tabs cut from the shingle. Each strip was installed such that the self-seal strip was closest to the eave edge. All starter strips were secured to the roof with six pneumatically driven, 12 gauge, 9.5 mm (3/8 in) diameter head, 31 mm (1.25 in) length, galvanized steel roofing nails. Following ARMA (2006) and manufacturer specifications, UF specified that the fasteners be placed at a maximum 76 mm (3 in) upslope of the butt end of the starter strip. These directions were also printed on the packaging of each shingle bundle. However, post-test investigations of lifted eave edge shingles showed several areas where the nail placement was higher than the specified limit. More discussion on the impacts of this high nailing is given in Section 4.4.1. For LAM-201 and LAM-202, starter strips were also placed along the rake edges of the mono-slope gable sections with the self-seal closest to the rake edge. TT-201 did not contain the rake edge starter strips due to error of the installation contractor. The eave and rake edge shingles for all manufacturers were not set in asphalt roof cement.

Asphalt shingle systems were installed following a "six up, six off" method conforming to manufacturer recommendations. It was specified that six nails per shingle strip should be used with the location of the nails conforming to each manufacturer's nail placement specification. Post-test investigations of lifted field shingles showed that the six nails were used and properly placed for LAM-201 and LAM-202. However, only four nails were used on TT-201's shingles. FBC 2010 Section R905.2.6 allows the use of four nails. The impact of four vs. six nails on sustained damage will be discussed in Section 4.4.1.

Hip and ridge shingles were installed on all hip roof specimens. The traditional method of creating a hip/ridge shingle consists of cutting a three-tab shingle vertically at each cutout to create individual tabs. A more recent product introduced by manufacturers is the pre-manufactured hip/ridge cap. Typically, the pre-manufactured product has a greater thickness and/or a different self-seal strip than a three-tab shingle. Manufacturers can require the customer to use pre-manufactured hip/ridge shingles to get the highest wind resistance warranty, and the cost of using the pre-manufactured product is greater than the traditional three-tab method. In order to evaluate the performance differences between these two methods, cut three-tab shingles were used on TT-201's hip roofs, while the pre-manufactured hip/ridge shingles were used on LAM-201 and LAM-202's hip roofs. The hip and ridge shingles were secured using two pneumatically driven, 12 gauge, 9.5 mm (3/8 in) diameter head, 31 mm (1.25 in) length, galvanized steel roofing nails at a location specified by the manufacturer.

### **4.3.3 Conditioning Phase Temperature Profiles**

The temperatures of the asphalt shingle systems were recorded during the condition period to assess the thermal loads encountered by the shingle roof specimens and to evaluate the effects of the exposed underside of the roof decking. UF installed two thermocouples on one mono-slope gable roof per manufacturer. It was assumed that the thermal loads for each manufacturer would be equivalent on all roofs. The thermocouples were Omega SA1XL-T-SRTC copper-constantan (Type T) thermocouples with a

temperature range of -250 C to 350 C (-328 F to 662 F). Each sensor was located approximately 1.2 m (4 ft) from the eave and 1.5 m (5 ft) from either gable end. The thermocouples were embedded between two asphalt shingles during the shingle installation with the wire lead running below the roof decking via a small hole in the roof sheathing and underlayment created prior to the shingle installation (Figure 101a). Temperature data were collected at 3 minute intervals by an Omega OM-CP-TC101A solid state single channel data logger which was sealed within PVC housing and secured to the underside of the roof decking (Figure 101b). The temperature data were downloaded to a computer just prior to wind performance testing.

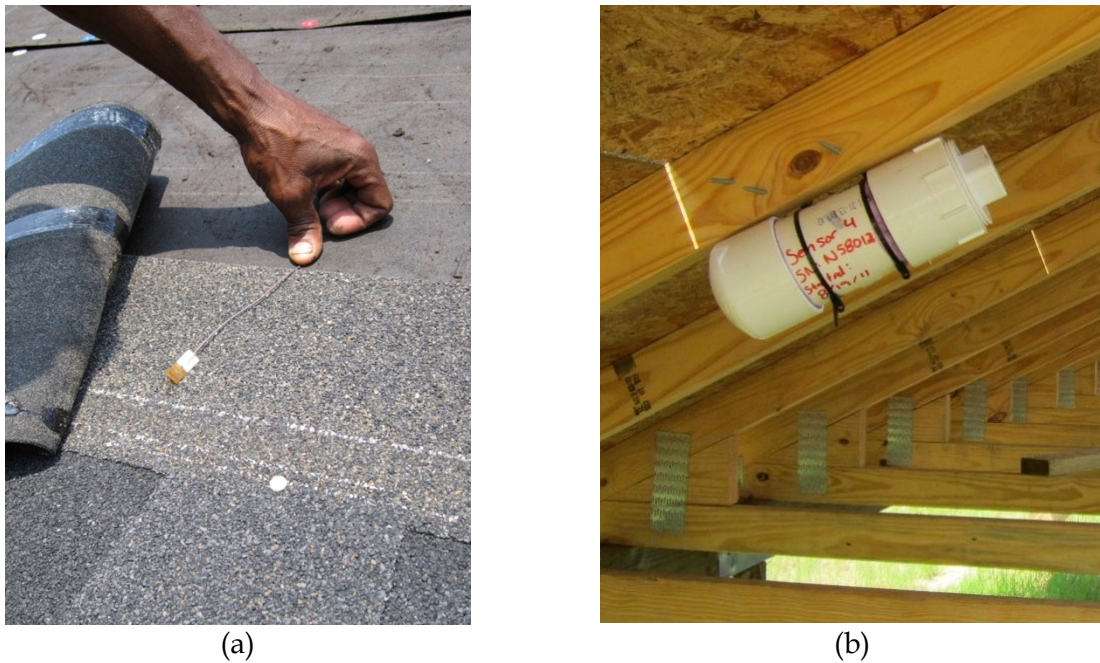


**Fig. 101. (a) Omega copper-constantan thermocouple was sandwiched between two shingles and recorded thermal loads encountered during conditioning period. (b) Thermocouple data loggers were installed in PVC housing and secured to roof trusses for weather protection.**

Table 38 provides a summary of each manufacturer's peak and minimum temperatures recorded during the conditioning phase. The peak recorded temperature was 82°C (180°F), obtained on TT-201's shingles on September 8<sup>th</sup>, 2011 at 12:45 Eastern Standard Time. Figure 103 shows a temperature time history of all three manufacturers' shingles at that date. LAM-201 and LAM-202's peak temperatures were within 2°C (6°F) of TT-201. The lowest shingle temperature was -16°C (3°F), obtained on TT-201's shingles. The lowest temperatures for LAM-201 and LAM-202 were within 2°C (3°F) of TT-201.

Parker and Sherwin (1998) measured the temperature of a black three-tab shingle roof installed over a conventionally constructed ventilated attic in Central Florida during the summer of 1997. Their reported peak shingle temperature of 81.8°C (179.3°F) is only 0.2°C (0.7°F) less than the measured peak temperature of TT-201. Therefore, we conclude that the shingle specimens at IBHS obtained a peak temperature that would be expected for dark color shingles installed on a residential structure in the Southeast United States.

Also shown in Table 38 is the percentage of time the shingle temperatures were at or above 70°C (158°F). This threshold matches the set-point temperature used in the Thermal (Section 2.2) and UV+Heat+Water Spray (Section 2.3) accelerated aging experiments. An empirical cumulative distribution plot of the measured temperatures is shown in Figure 102. These data indicate that the set-point temperature used in the accelerated aging experiments is greater than approximately 98% of the temperature measurements recorded during the 11 month conditioning phase and 12°C (22°F) less than the peak recorded temperature. The temperature used for the accelerated aging experiments was selected based upon recommendations from the Oversight Committee and matches temperatures used in previous shingle accelerated aging studies (Terrenzio et al., 1997). Based upon these data it appears that the temperatures used in the accelerated aging studies represent an appropriate upper bound for accelerated studies of shingle aging.

**Table 38. Summary of recorded asphalt shingle temperatures during the 11 month conditioning phase**

Shingle ID	Peak Shingle Temperature (°C) [°F]	Lowest Shingle Temperature (°C) [°F]	Percentage of Time Above 70°C [158°F]
LAM-201	80 [174]	-14 [6]	0.7%
LAM-202	82 [179]	-15 [5]	2.0%
TT-201	82 [180]	-16 [3]	2.3%

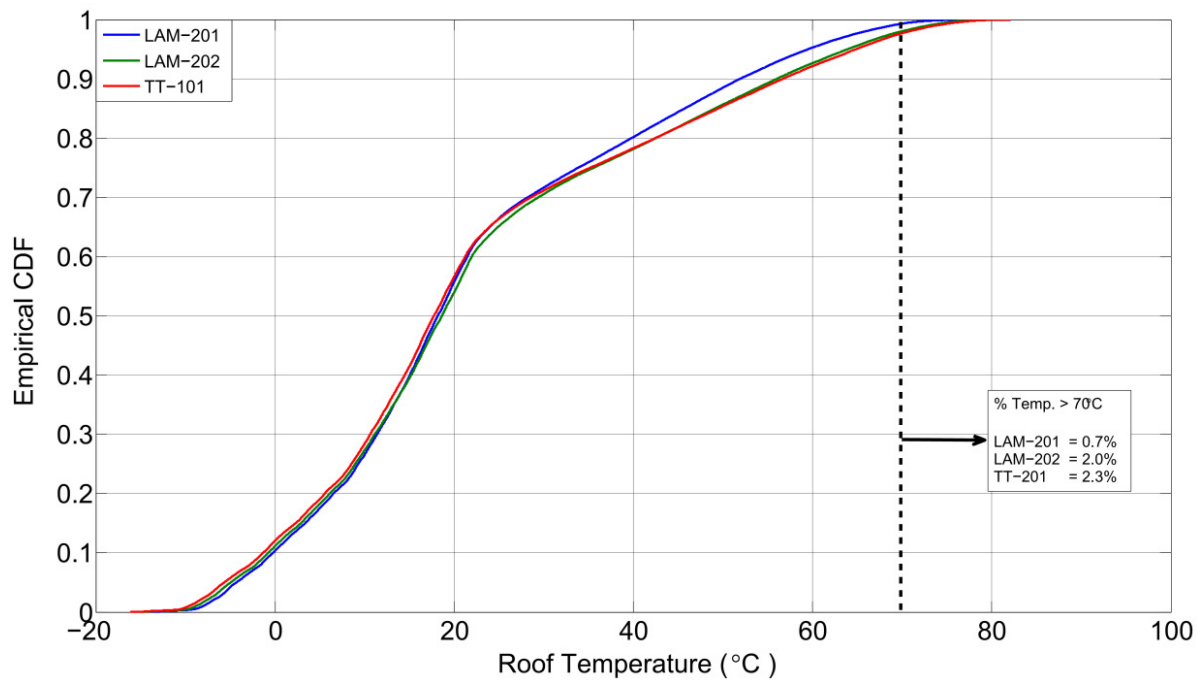


**Fig. 102. Empirical cumulative distribution function (CDF) for measured roof temperatures during the condition phase.**

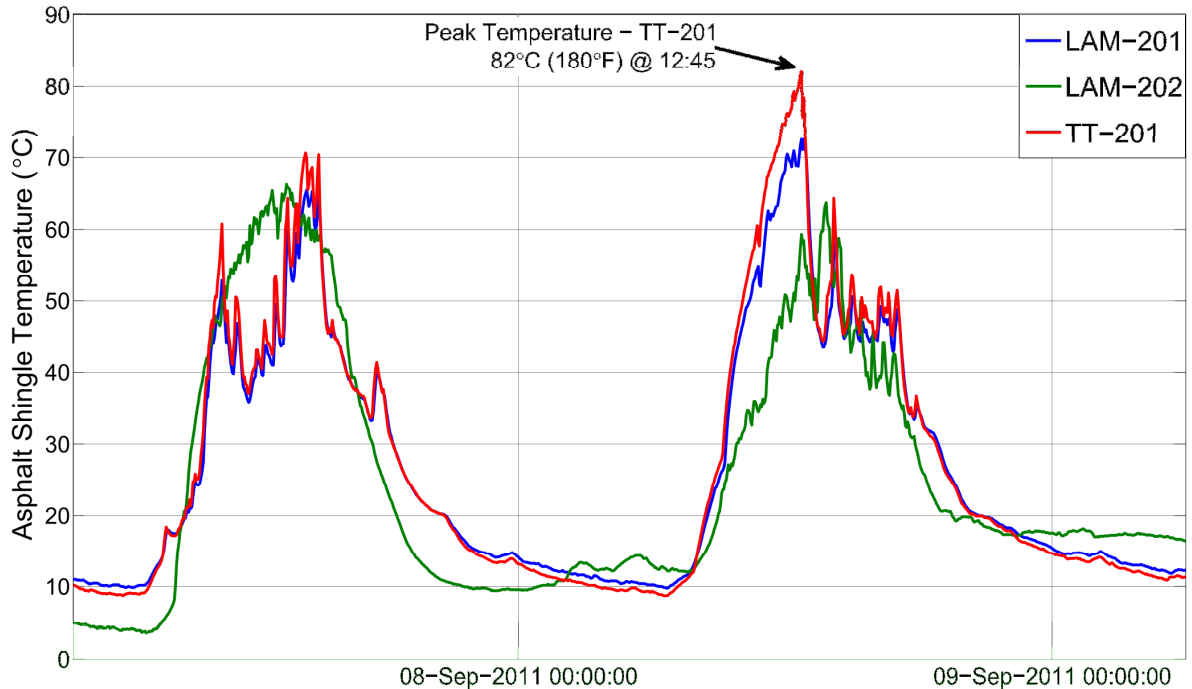


Fig. 103. Example temperature time history generated from thermocouples embedded between shingles during the conditioning phase. The peak observed temperature during the conditioning phase is shown.

#### 4.3.4 Base Structure

The base structure was composed of two parts:

1. An internal 9.1 m W x 12.2 m L x 2.4 m H (30 ft W x 40 ft L x 7 ft 10 in H) steel moment resisting frame with exterior wood wall panels.
2. A permanent gable half-roof with a 6:12 roof slope and 203 mm (8 in) eave overhangs on both sides.

Each shingle roof specimen was installed on the remaining half-roof to form a complete test building (Figures 96 and 97). The steel frame was originally erected by IBHS and modifications to the frame were completed by UF in July 2012 (Figure 104). Two interior steel beams were added at the top of the frame to provide a wall line to accept the backsides of the mono-slope gable roofs (Figure 104a). A 2x4 double top plate was installed along the top of each wall line to provide an installation point for the permanent half-roof and shingle roof specimen. The wood wall panels were fastened along the bottom of the wall into the lower steel framing beams and along the 2x12 header beams at the top of the wall. The top steel framing on the gable end of the test specimen was lowered 0.3 m (1 ft) to allow the steel lifting beams that carried the shingle roof specimen to rest on the side of the structure during testing. The exposed gap between the top of the wall and the shingle roof specimen was covered with wood panels prior to wind testing.

The permanent gable half-roof consisted of 10 roof trusses with a total bottom chord length of (32 ft) and 6: 12 roof slope (Figure 104b). The trusses were spaced at 0.6 m (2 ft) on

center and secured to the base structure's frame using one Simpson Strong-Tie H2.5Z hurricane strap per truss member per wall line. The roof was sheathed with 11.9 mm (0.47 mm) thick structural grade 1.2 m by 2.4 m (4 ft by 8 ft) plywood panels fastened to the roof trusses using 8d ring shank nails at a spacing of 152 mm (6 in) field and 152 mm (6 in) edge. No roof covering was installed over the plywood sheathing, but the seams were taped.

The permanent roof's overall width provided a 0.9 m (3 ft) gap between the interior gable end of the permanent roof and the interior gable end of the shingle roof specimen. The shingle roof specimens were hoisted with steel lifting beam located on the bottom of the roof sections and rigging attached overhead (Figure 105a). Therefore, the gap allowed the roof to be installed on the roof structure by the crane using the existing rigging setup. Once installed, the crane rigging was removed and gap was covered with 11.9 mm (0.47 mm) thick structural grade plywood sheathing bearing on 4x4 dimensional lumber located on the top chords of the interior gable ends of the permanent half-roof and shingle roof specimen.

The investigators originally anticipated that the test building would have to be driven out of the test chamber to exchange shingle roof specimens. An internal house moving drive system was installed on the interior of the base structure. However, the crane that transported the roof sections from the conditioning site to the base structure had enough clearance to get through the test chamber's door opening. Therefore, once modifications to the base structure frame were completed, the base structure was driven into the test chamber and installed on the turntable (Figure 104c). The base structure remained on the turntable throughout the experiment.

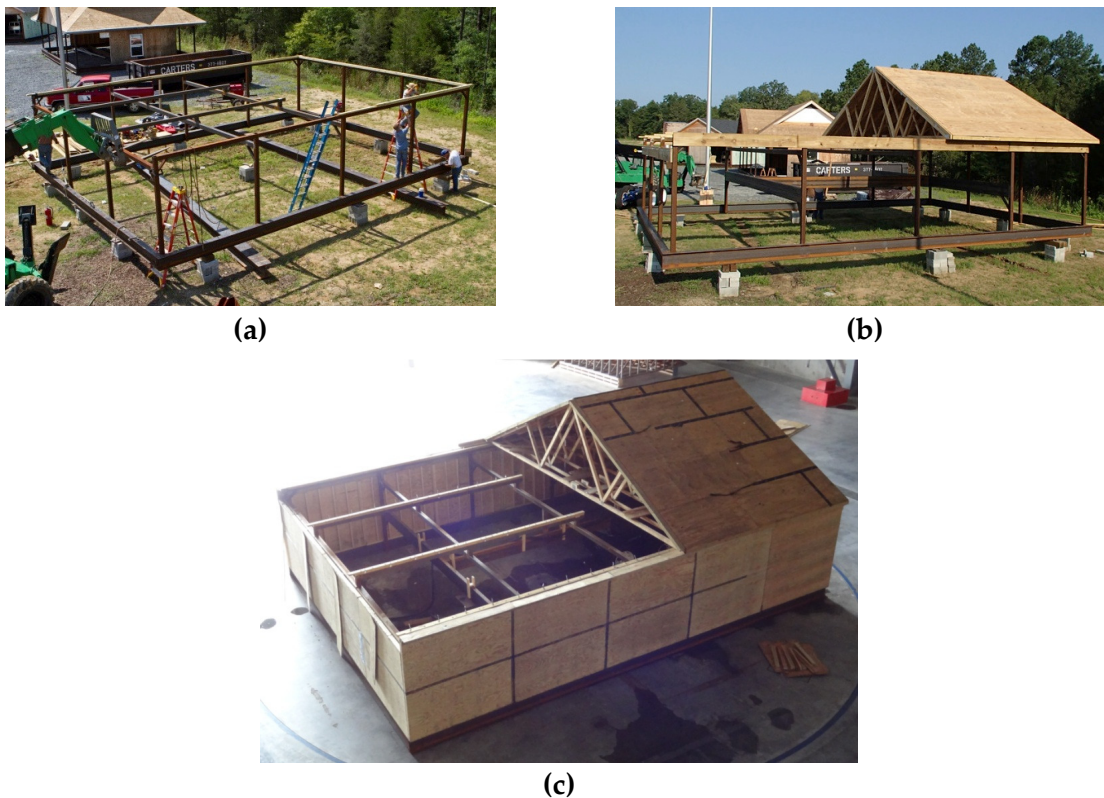


**Fig. 104.** The base structure construction consisted of (a) modifications to the existing steel structural framing, (b) installation of a permanent gable end 6:12 roof and (c) installation of wood-framed exterior walls secured to the steel frame.

### 4.3.5 Installation of Asphalt Shingle Roof Specimens

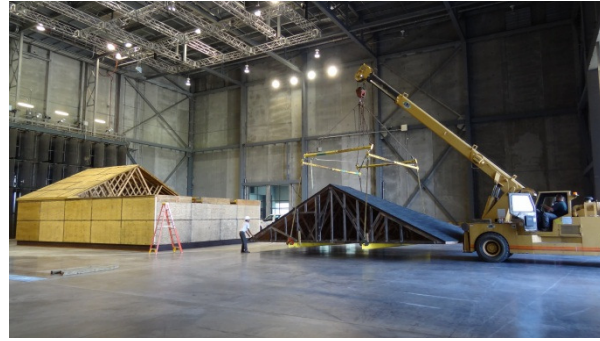
Movement of the roof sections from the conditioning site to the test chamber was achieved by using a Grove 179 kN (36000 lbf) driving crane with hoist rigging. A gravel road was installed from the edge of the Research Centers concrete apron down through the roof sections to provide a solid substrate for the crane. The installation of the hip and gable roof specimens will be described separately in this section.

Each hip roof specimen was installed by the following method:

1. Two 6.7 m (22 ft) long W8x24 steel beams were placed under the hip roof specimen along the lengthwise direction of the roof. Each beam was located approximately 2.4 m (8 ft) from the eave edges of the hip roof. Beam clamps were placed at each beam end for a total of four lifting points. As shown in Figure 105a, the crane was positioned near the roof specimen and the rigging straps were attached to the beam clamps. The roof was then hoisted off of the wood support structure and driven into the test chamber.
2. Once inside the test chamber, 4x4 dimensional lumber was fastened to the top chord of the roof's gable end truss to provide a bearing surface for the plywood sections that fill the gap between the permanent roof and shingle roof specimen (Figure 105b).
3. The crane hoisted the shingle roof specimen over the open end of the base structure and then, once in position, lowered the specimen onto the base structure (Figure 105c).
4. The rigging and beam clamps were then removed from the lifting beams and the beams were pushed into the base structure. Next, the 0.9 m (3 ft) exposed gap between the permanent and specimen's interior gable ends was covered with 11.9 mm (0.47 in) thick structural grade plywood fastened to the 4x4 dimensional lumber using 38 mm (1.5 in) screws at an approximate spacing of 102 mm (4 in) on center.
5. The roof specimen was secured to the base structure's wall top plates using a single Simpson Strong-Tie H2.5Z hurricane strap at each truss along the three wall lines. A completed hip roof test building is shown in Figure 105d.



(a)



(b)



(c)



(d)

**Fig. 105. Hip roof installation procedure: the roof was (a) carried from the conditioning site with crane and rigging, then (b) driven inside the test chamber and (c) hoisted onto the base structure. A survey for the presence of unsealed shingles (following ERP #6) was conducted before testing (d) and blue painter's tape was used to mark the location of unsealed shingles.**

Each gable roof specimen was installed by the following method:

1. Two 6.7 m (22 ft) long W8x24 steel beams were placed under a single mono-slope roof specimen along the lengthwise direction of the roof. Each beam was located approximately 0.9 m (3 ft) from the eave edge and backside of the mono-slope roof. Beam clamps were placed at each beam end for a total of four lifting points. The crane was positioned near the roof specimen and the rigging straps were attached to the beam clamps. The roof was then hoisted off of the wood support structure and driven into the test chamber.
2. Once inside the test chamber, 4x4 dimensional lumber was fastened to the top chord of the roof's interior gable end truss to provide a bearing surface for the plywood sections that fill the gap between the permanent roof and shingle roof specimen. The exterior gable end was sheathed with 11.9 mm (0.47 in) thick structural grade plywood fastened to the gable end truss system using 38 mm (1.5 in) screws at an approximate spacing of 152 mm (6 in) on center.

3. The crane hoisted the mono-slope shingle roof specimen over the open end of the base structure with the eave overhang at 208 mm (8 in) beyond the base structure wall. Once in position, the crane lowered the specimen onto the base structure, with the roof bearing the exterior base structure wall and one interior beam member (Figure 106a).
4. The rigging and beam clamps were then removed from the lifting beams and the beams were pushed out of the base structure. The crane, rigging, and lifting beams were then driven back to the conditioning site to repeat Steps 1-3 for the transport of the mating mono-slope gable roof specimen.
5. The 0.9 m (3 ft) exposed gap between the permanent and specimen's interior gable ends was covered with 11.9 mm (0.47 mm) thick structural grade plywood fastened to the 4x4 dimensional lumber using 38 mm (1.5 in) screws at an approximate spacing of 102 mm (4 in) on center.
6. The roof specimen was secured to the base structure's wall top plates using a single Simpson Strong-Tie H2.5Z hurricane strap at each truss along the three wall lines. A completed gable roof test building is shown in Figure 106b.

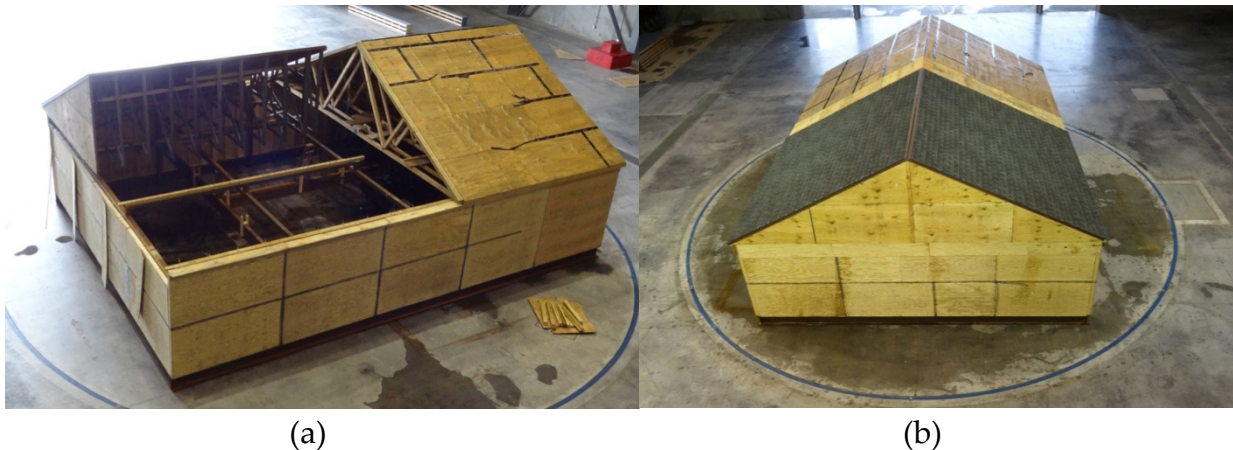


Fig. 106. Similar to the hip roof sections, each mono-slope gable section was (a) individually installed on the base structure to form a (b) complete gable roof section.

### 4.3.6 Test Sequence Procedure

#### 4.3.6.1 Wind Directions

Three wind directions - 0°, 45°, and 90° - were used to evaluate the effect of wind direction on sustained damage (Figure 107). Each shingle roof specimen was subjected to one wind direction during the entire test sequence. Therefore, each manufacturer's product was evaluated with one shingle roof replicate per roof type (i.e., hip and gable) for each wind direction.

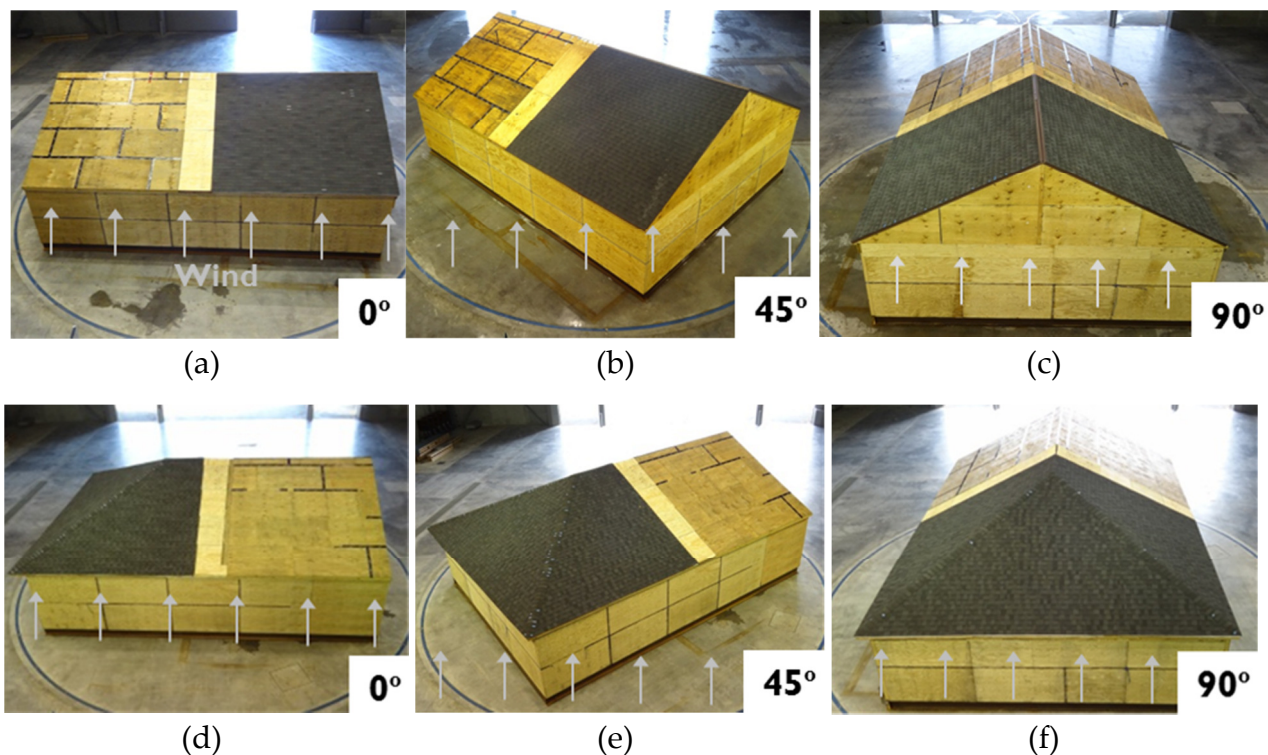


Fig. 107. Wind directions for (a) - (c) gable roof sections and (d) through (f) hip roof sections.

#### 4.3.6.2 Pre-test Condition Analysis

The test sequence flowchart is shown in Figure 108. Prior to the initiation of the wind testing, a roof survey of unsealed field, hip, and ridge shingles was conducted following the procedures specified in Section 2.5.2. Unsealed shingles were defined as any shingle strip that contained greater than 51 mm (2 in) of unsealing. Each unsealed shingle was marked with a small strip of blue painters tape placed on the top surface of the shingle near the leading edge. Once surveyed, photos were taken on the roof, ground-level, and above the test building to record the condition and location of the unsealed shingles. The location of the unsealed shingles was then transferred to a roof plan to evaluate the performance of the unsealed shingles during the wind testing.

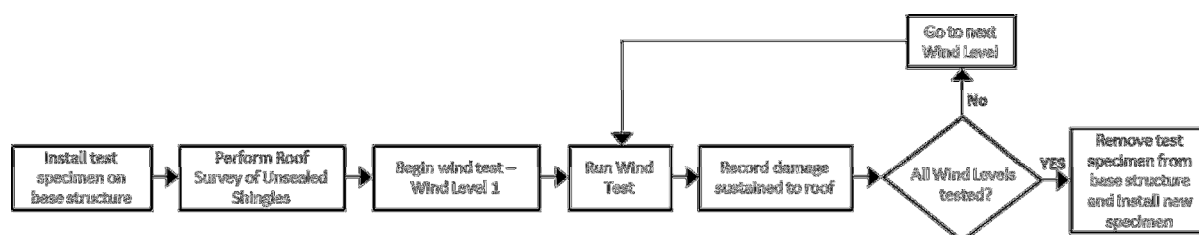


Fig. 108. Test sequence flowchart. (Note: Exposure C wind profile for all wind tests)

### 4.3.6.3 Wind Flow Measurement

Approach wind flow conditions were measured at the intersection of the exit of the jet and centerline of the test chamber at 5 m (16.4 ft) above the floor (Figure 109). Horizontal wind speed and direction were measured by an RM Young wind monitor (Model Number 05103V) at a sampling rate of 100 Hz. Dynamic characteristics of the anemometer's four-blade polypropylene helicoid propellers (Model Number 08234) include a 2.7 m 63% recovery distance constant and a damped natural wavelength of 7.4 m. The wind monitor is rated for a 100 m/s gust survival and has a 50% recovery vane delay distance of 1.3 m. The limitations caused by its frequency response characteristics are detailed in Schroeder and Smith (2003).

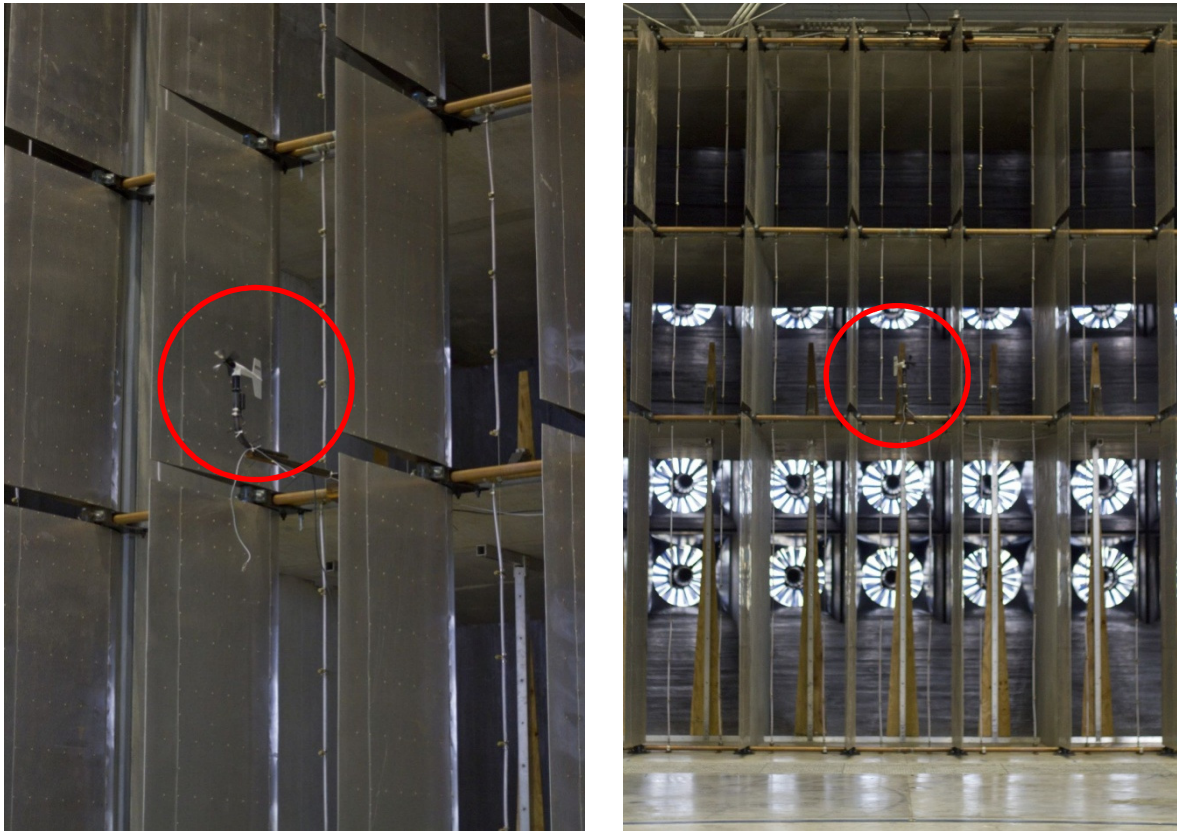


Fig. 109. Wind monitor (shown in red circle).

### 4.3.6.4 Wind Level Characteristics

The test sequence consisted of three 30-minute stochastic wind tests (Wind Levels 1, 2 and 3), followed by a 17-minute low-turbulence wind test (Wind Level 4). The experiment began with LAM-201 – Roof 1 and continued through LAM-201 – Roofs 2 and 3. A statistical summary of the input wind time history of Wind Levels 1-3 for these roofs is given in Table 39 and a 200 s sample showing the wind fluctuations of each Wind Level is shown in Figure 110. Wind Level 4 was not used for LAM-201 – Roofs 1-3.

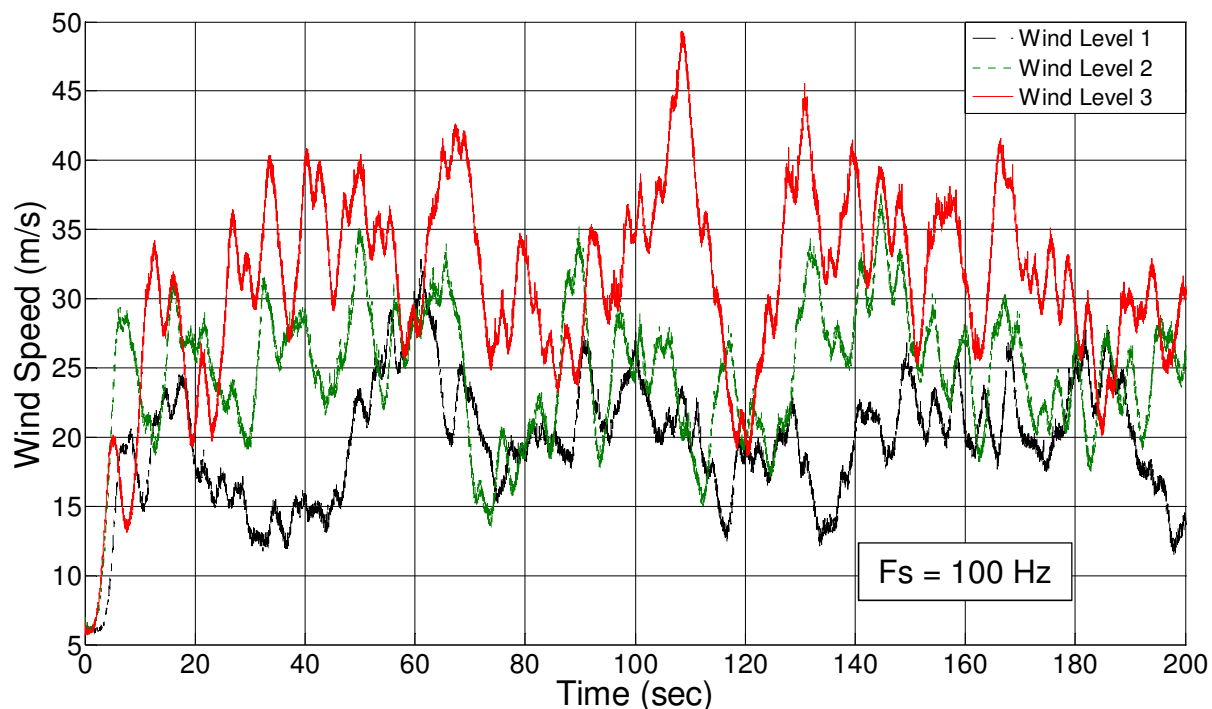


Fig. 110. Example wind speed time history (first 200 s) for Wind Levels 1-3 used for LAM-201 - Roofs 1-3.

Table 39. Statistical summary for Wind Levels 1-3 used on LAM-201 - Roofs 1-3

Wind Level	Test Duration (minutes)	Mean Wind Speed <sup>1</sup> (m/s) [mph]	Peak Instantaneous Wind Speed <sup>1</sup> (m/s) [mph]	Longitudinal Turbulence Intensity (%)
1	30	20 [45]	33 [74]	20
2	30	26 [58]	44 [98]	19
3	30	32 [71]	53 [119]	18

<sup>1</sup>Wind speeds varied approximately +/- 1 m/s (2 mph) per day due to air density fluctuations

The investigators modified Wind Levels 1-3 and added Wind Level 4 for the remaining shingle roof specimens (LAM-201 - Roofs 4-6, LAM-202 - Roofs 1-6, and TT-201 - Roofs 1-5). A statistical summary of the modified Wind Levels 1-3 is given in Table 40 and a 200 s sample showing the wind fluctuations for Wind Levels 1-3 is shown in Figure 111. A complete time history of Wind Level 4 is shown in Figure 112, while the wind speed characteristics used for the five ramps in Wind Level 4 is given in Table 41.

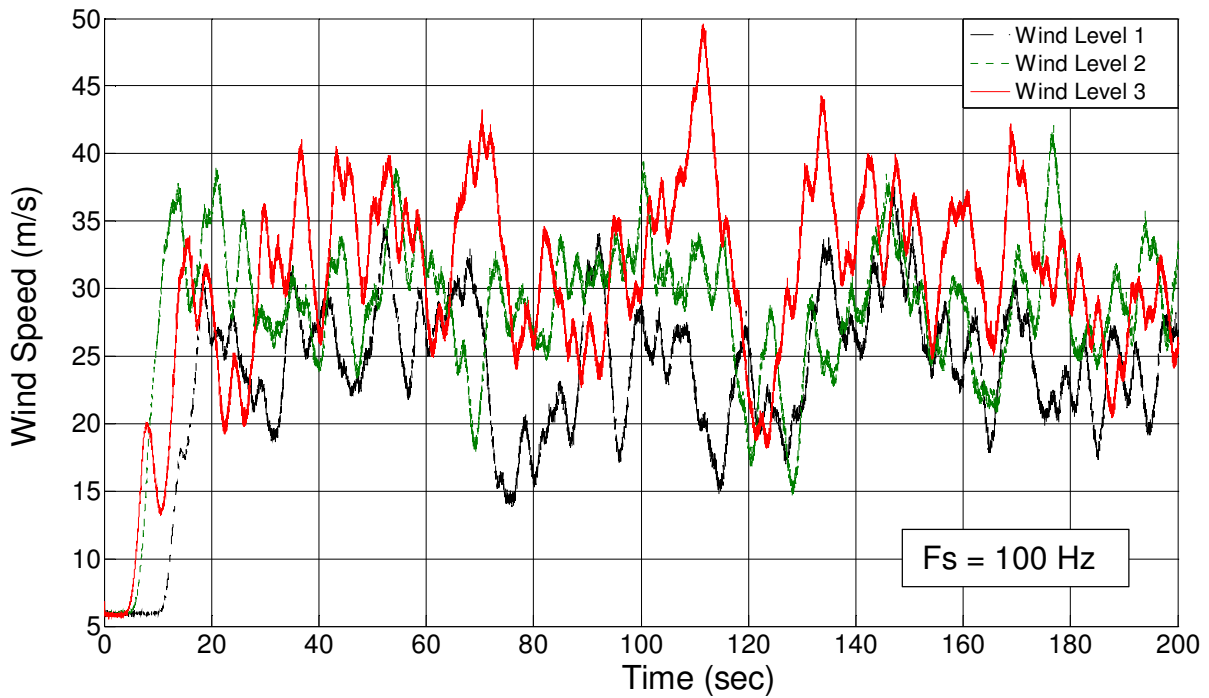


Fig. 111. Example wind speed time history (first 200 s) for Wind Levels 1-3 used for LAM-201 – Roofs 4-6, LAM-202 – Roofs 1-6, and TT-201 – Roofs 1-5.

Table 40. Statistical summary for Wind Levels 1-3 used on LAM-201 – Roofs 4-6, LAM-202 – Roofs 1-6, and TT-201 – Roofs 1-5

Wind Level	Test Duration (minutes)	Mean Wind Speed <sup>1</sup> (m/s) [mph]	Peak Instantaneous Wind Speed <sup>1</sup> (m/s) [mph]	Longitudinal Turbulence Intensity (%)
1	30	26 [58]	44 [98]	21
2	30	29 [65]	43 [96]	18
3	30	32 [72]	52 [116]	18

<sup>1</sup>Wind speeds varied approximately +/- 1 m/s (2 mph) per day due to air density fluctuations

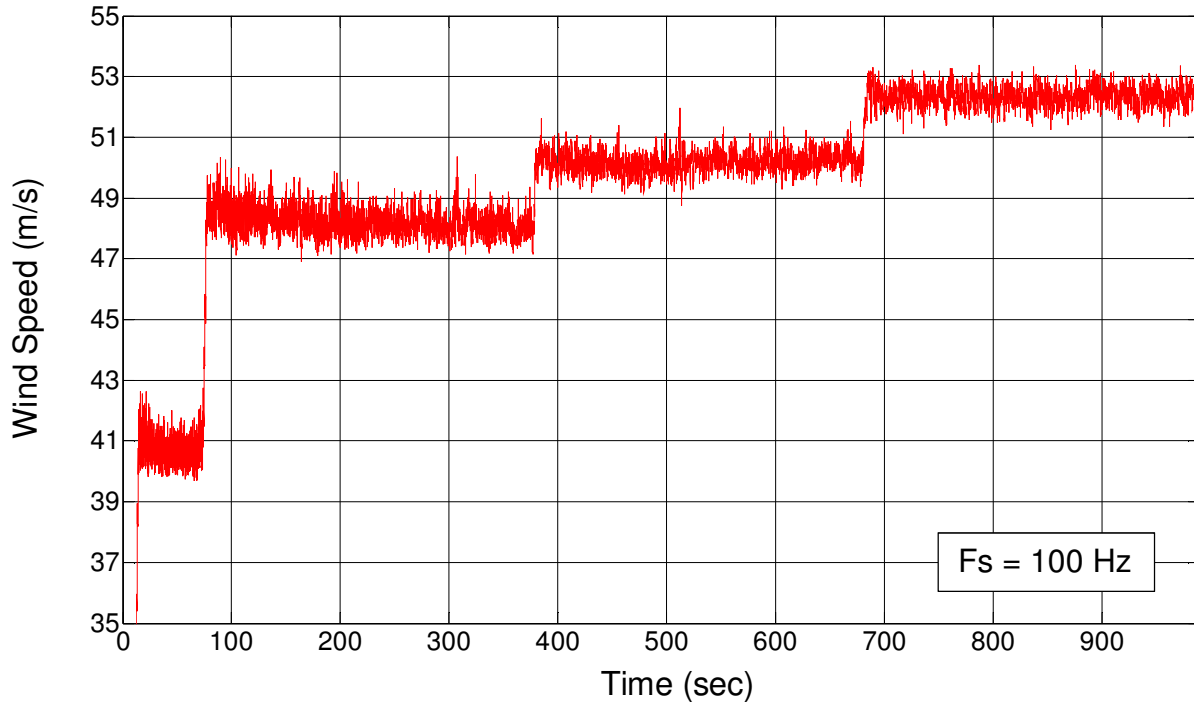


Fig. 112. Wind speed time history for Wind Level 4.

Table 41. Summary of test parameters for Wind Level 4 used on LAM-201 – Roofs 4-6, LAM-202 – Roofs 1-6, and TT-201 – Roofs 1-5

Ramp Number	Duration (minutes)	Mean Wind Speed <sup>1</sup> (m/s) [mph]	Longitudinal Turbulence Intensity (%)
1	1	41 [92]	1
2	5	48 [107]	1
3	5	50 [112]	1
4	5	52 [116]	1

<sup>1</sup>Wind speeds varied approximately +/- 1 m/s (2 mph) per day due to air density fluctuations

Wind-driven rain was simulated at all Wind Levels for the gable roof specimens and Wind Level 1 only for the hip roof specimens. The hip roof specimens were subjected to a shorter duration of rain to minimize road flooding. The test building was subjected to a uniform wetting rate at an estimated 203 mm/h (8 in/h) using an array of spray nozzles located at the exit of the jet.

#### 4.3.6.5 Post-Test Assessment

High definition video was captured on seven cameras located at the ground-level and above the test section for all tests. This video assisted the investigators during the wind testing to locate areas where shingles had lifted or blown off. A visual survey was performed at the ground level and photographs were captured following each Wind Level test. After the completion of Wind Level 4, the roof was surveyed by the investigators to

record the roof's condition. The shingle roof test specimen was then removed from the base structure and installed back on its support structure at the conditioning site. The process of shingle roof specimen installation and testing then repeated with the next specimen.

## **4.4 Results**

The performance of the shingle roof specimens will be summarized in three sections:

Section 4.4.1 – Field, Eave, and Rake Shingle Performance

Section 5.4.2 – Hip and Ridge Shingle Performance

Section 4.4.3 – Estimated Repair Costs

### **4.4.1 Field, Eave, and Rake Shingle Performance**

A summary of the field, eave, and rake shingle performance for LAM-201 and LAM-202 is given in Table 42 and for TT-201 in Table 43. Eave shingles are defined as the first course of shingles, including the starter strips, which were installed along roof's eave. Rake shingles are defined as the shingles installed at the gable end.

**Table 42. Summary of field, eave, rake, and underlayment wind resistance - LAM-201 and LAM-202**

Product ID (Type)	Roof Number	Roof Type	Wind Direction	Field Shingles		Eave Edge	Rake Edge	Underlayment
				Pre-Test Condition	Post-Test Condition	Percentage of Shingles with Surface Cracks or Blown Off (Windward Eave Only)	Percentage of Shingles with Surface Cracks or Blown Off	Percentage of Torn Underlayment
				Percentage of Unsealed Shingles	Percentage of Shingles with Surface Cracks or Blown Off			
LAM-201 (Laminate)	1	Gable	0	0	0	54	0	0
	2	Gable	45	0	0	7	0	0
	3	Gable	90	0	0	0	0	0
	4	Hip	0	0	0	10	--	0
	5	Hip	45	0	0	8	--	0
	6	Hip	90	0	0.4	31	--	0
LAM-202 (Laminate)	1	Gable	0	1	1	48	0	0
	2	Gable	45	2	1	36	0	0
	3	Gable	90	5	2.5	49	0	0
	4	Hip	0	0	0	86	--	0
	5	Hip	45	0	0	0	--	0
	6	Hip	90	0	0.002	50	--	0

#### 4.4.1.1 LAM-201 Field, Eave, and Rake Performance

The overall performance of LAM-201's field shingles was excellent. For all roofs, pre-test roof surveys found that all shingles were fully sealed and post-test assessment found that all shingles remained sealed throughout wind testing. The 0.4 percent damage to Roof 6's field shingles was the result of a pull-through at the eave edge fasteners, causing a progressive lifting of the roofing system (Figure 113).

Conversely, the eave edge performance of LAM-201 was variable. Windward eaves on five out of the six roofs had pull-through of starter strip shingles at their fasteners. In general, this pull-through at the eave caused isolated surface cracking to the starter strip, first, and second shingle courses. Pull-through of leeward eave shingles was not observed. Post-test assessment of the eaves which sustained pull-through indicated that the location of the starter strip fasteners from the eave edge played a significant role in the wind performance of the eave. For all eaves with pull-through, starter strip fasteners were located 102 – 127 mm (4 – 5 in) from the eave edge (Figure 113 and 114). This was a contractor error. ARMA's Asphalt Roofing Residential Manual (2006) specifies that the starter strip fasteners should be located 38 – 76 mm (1.5 – 3 in) from the eave edge. Whereas, FEMA 499 FS 7.3 recommends 25 mm (1 in) to 64 mm (2.5 in) with 25 mm (1 in) preferred if framing conditions permit. As will be noted for the other manufacturers' shingle systems, placing fasteners within ARMA's nailing tolerance may have prevented the pull-through in eave shingles. Inspection of several eave shingles that did not sustain pull-through revealed nail placements within ARMA's specifications.

Reducing eave shingle overhang beyond the drip edge can reduce the load placed on eave shingle fasteners. As wind flow encounters the eave edge it travels vertically, causing a separated air flow region on the roof surface near the eave (Robertson, 1991). This vertical wind flow exerts an uplift force on the shingle's exposed underside, and the magnitude of the force is a function of the total exposed area of shingle. The presence of a gutter would also change the wind flow pattern at the eave and may have changed the outcome.

LAM-201's rake edge shingles remained in place and did sustain pull-through at attachment points. An inspection of fastener placement found that the fasteners were placed within 25 mm (1 in) of the rake edge, as specified. The rake edge for this manufacturer utilized a starter strip running vertically along the rake edge (also known as a bleeder strip), however, it is unknown if the addition of this detail contributed towards the wind resistance of the rake edge. FEMA (2006) observed blown off shingles along rakes containing bleeder strips leading them to conclude that bleeder strips do not significantly increase blow-off resistance. All rake and eave metal flashings were unaffected by the wind tests.



**Fig. 113. Pull-through of the starter strip around fasteners on LAM-201 – Roof 6. The fasteners were placed approximately 102 mm (4 in) from the butt edge of the starter strip.**



**Fig. 114. Pull-through of the starter strip around fasteners on LAM-201 – Roof 2. The fasteners were placed approximately 127 mm (5 in) from the butt edge of the starter strip.**

#### **4.4.1.2 LAM-202 Field, Eave, and Rake Performance**

For LAM-202, pre-test partially unsealed field shingles influenced the performance of the roof specimens. If a shingle was fully sealed before the wind test, it did not unseal during the wind test. The specific cause of the pre-test non-sealing is unknown; however, the failure mode of the tab sealant, in every non-sealed case, was an adhesive failure between the tab sealant and the shingle. For the gable roof specimens, pre-test unsealed shingles were found along the exterior and interior edges of the roof (Figure 115). An example of the progressive unsealing and surface cracking caused by pre-test unsealed shingles is shown in Figures 116 and 117 for Roof 2 (45° wind direction). Five unsealed

shingles of varying lengths along the windward rake were found during the pre-test survey (Figure 115). During the Wind Level 1 test, one shingle with 325 mm (14 in) of unsealed length lifted in the wind, causing an additional 51 mm (2 in) of unsealing (Figure 116a). During the Wind Level 2 test, progressive unsealing continued on the lifted shingle and two additional shingles with smaller unsealed lengths lifted in response to the wind flow (Figure 116b). By Wind Level 3, all pre-test unsealed shingles had lifted (Figure 116c). At the end of Wind Level 4, all pre-test unsealed shingles were permanently deformed causing pull-through and surface cracking in adjacent shingles (Figure 116d). Diagonal cracks were observed on the lifted shingles where they hinged from lifting in the wind (Figure 117). The investigators reassessed the unsealed shingles one week after the roof was tested and placed back in its conditioning site. Several shingle strips showed signs of resealing, however, no attempts were made to assess the uplift resistance of the resealed shingles.

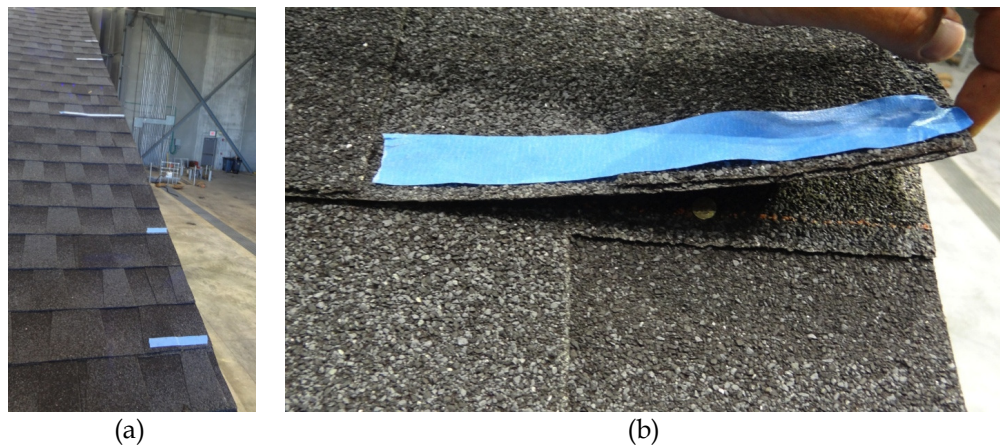


**Fig. 115. Pre-test roof survey of LAM-202 - Roof 2 found five partially unsealed shingles along the windward rake. The blue tape was placed on the leading edge where shingles were found unsealed prior to the wind testing. The cause of the partial unseal is unknown.**





Post- Wind Level 3

(c)



Post- Wind Level 4

(d)

**Fig. 116. Progressive lifting of pre-test unsealed shingles and eave near windward edge for LAM-202 – Roof 2.**

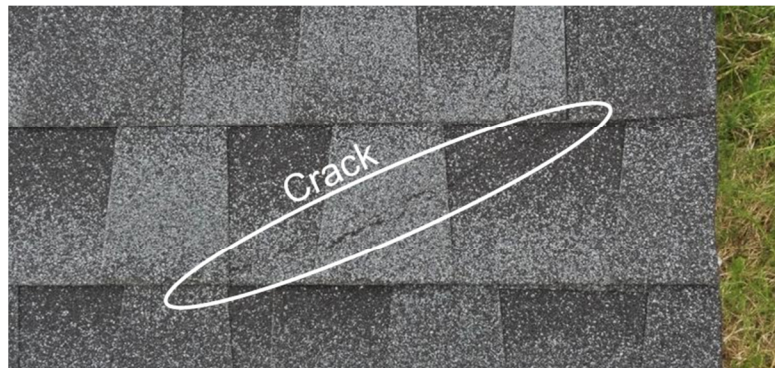
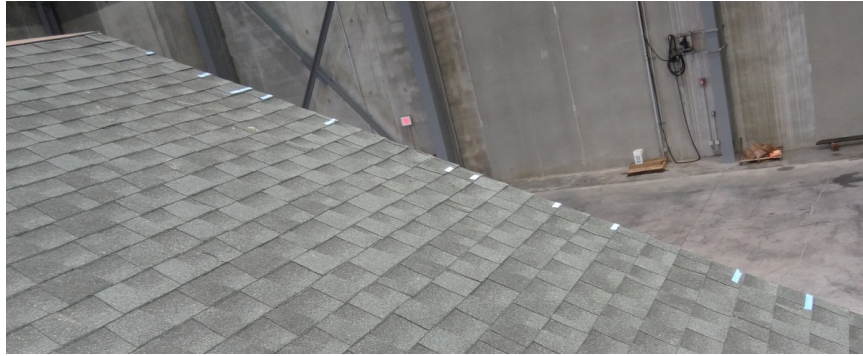
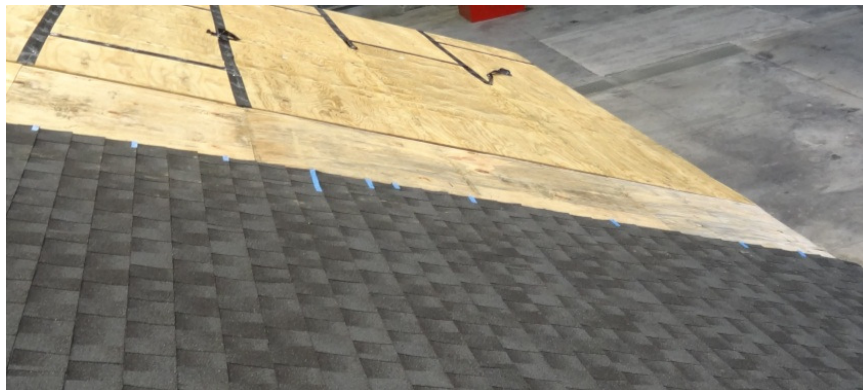


**Fig. 117. Crack on pre-test unsealed shingle caused by the shingle lifting during wind testing.**

Pre-test partially unsealed shingles were also observed on the gable style Roof 3 (90°). Thirteen partially unsealed shingles of varying lengths were found on the windward rake edge (Figure 118a), and ten unsealed shingles of varying lengths were found on the leeward edge of the roof specimen (Figure 118b). Similar to Roof 2, the unsealed shingles lost adhesion by way of an adhesive failure between the sealant strip and shingle surface, as shown in Figure 119. The specific cause of the unsealing is unknown. One partially unsealed shingle was found in the field of the roof prior to wind testing, located on the third course from the eave (Figure 120). For this unsealed shingle, the release tape placed on the shingle did not prevent the shingles from sticking together when bundled in their packaging. As the contractor removed the shingle from the package, the release tape was bonded to the sealant strip and subsequently peeled away from the other shingle, leaving the release tape on the sealant strip. The release tape remained on the sealant strip throughout the conditioning and testing of the roof specimen, resulting in an unsealed length of 711 mm (28 in) out of a total strip length of 1 m (39.4 in).



(a)



(b)

**Fig. 118. Pre-wind test unsealed shingles (marked with blue tape) for LAM-202 – Roof 3 (a) windward rake and (b) interior edge of shingle specimen.**



**Fig. 119. Pre-wind test unsealed rake shingle with an adhesive failure mode – LAM-202 – Roof 3.**



(a)



(b)

**Fig. 120. Shingle with 711 mm (28 in) of unsealed length (a) located on the third course on the interior of the roof section. (b) The non-sealing was caused by a transfer of the release tape onto the sealant strip. This shingle remained on the roof during wind testing and no surface cracks were observed following the test.**

The wind direction for this roof was 90°; therefore, the wind flow was directed perpendicular to the rake (Figure 107c). Five rake unsealed shingles lifted and hinged backwards during the wind testing; however, the interior edge shingles on the leeward side of the roof specimen did not lift. The unsealed shingle located in the field of the roof did not lift during wind testing and, therefore, was not affected by the wind.

The building was then rotated to the 0° building orientation (wind flow perpendicular to the eave) and an additional Wind Level 4 test was conducted to investigate the effect the response of unsealed shingles located within the separated flow region. Recall that the interior 711 mm (28 in) unsealed shingle was located on the third course of the roof, approximately 457 mm (18 in) from the eave edge. Therefore, the interior unsealed shingle was likely within the separated flow region; where negative (uplift) pressures on non-porous materials (e.g., wood roof sheathing) are the greatest. Peterka et al. (1997) states that the layout of asphalt shingles permits air pressure to rapidly equalize between their upper and lower surface. This renders shingles unaffected by the negative pressures produced within the separated flow region. The interior unsealed shingle did not sustain surface cracking due to lifting or blow off from the Wind Level 4 test. However, a small amount of

periodic “fluttering” of the shingle was observed during the wind test; likely in response to the turbulent wind flow contained within the separated region. This indicates that unsealed shingles located within separated flow are not affected by negative pressure (relative to ambient) generated within the separated region. All unsealed shingles along the rake of the windward roof slope (11 in total) lifted during the Wind Level 4 test. A 152 mm (6 in) section of an unsealed shingle was blown off of the roof (Figure 121a), while the remaining ten unsealed shingles had horizontal cracks on their top surface due to lifting (Figure 121d). Progressive unsealing was observed on several pre-test unsealed shingles and this impacted the performance of adjacent shingles. However, the fasteners of the adjacent shingles prevented additional surrounding shingles from surface cracks or blow off. The hip roof field shingles were fully sealed and the only field shingles that would require repair or replacement were impacted by the pull-through and lifting of eave starter strip shingles.

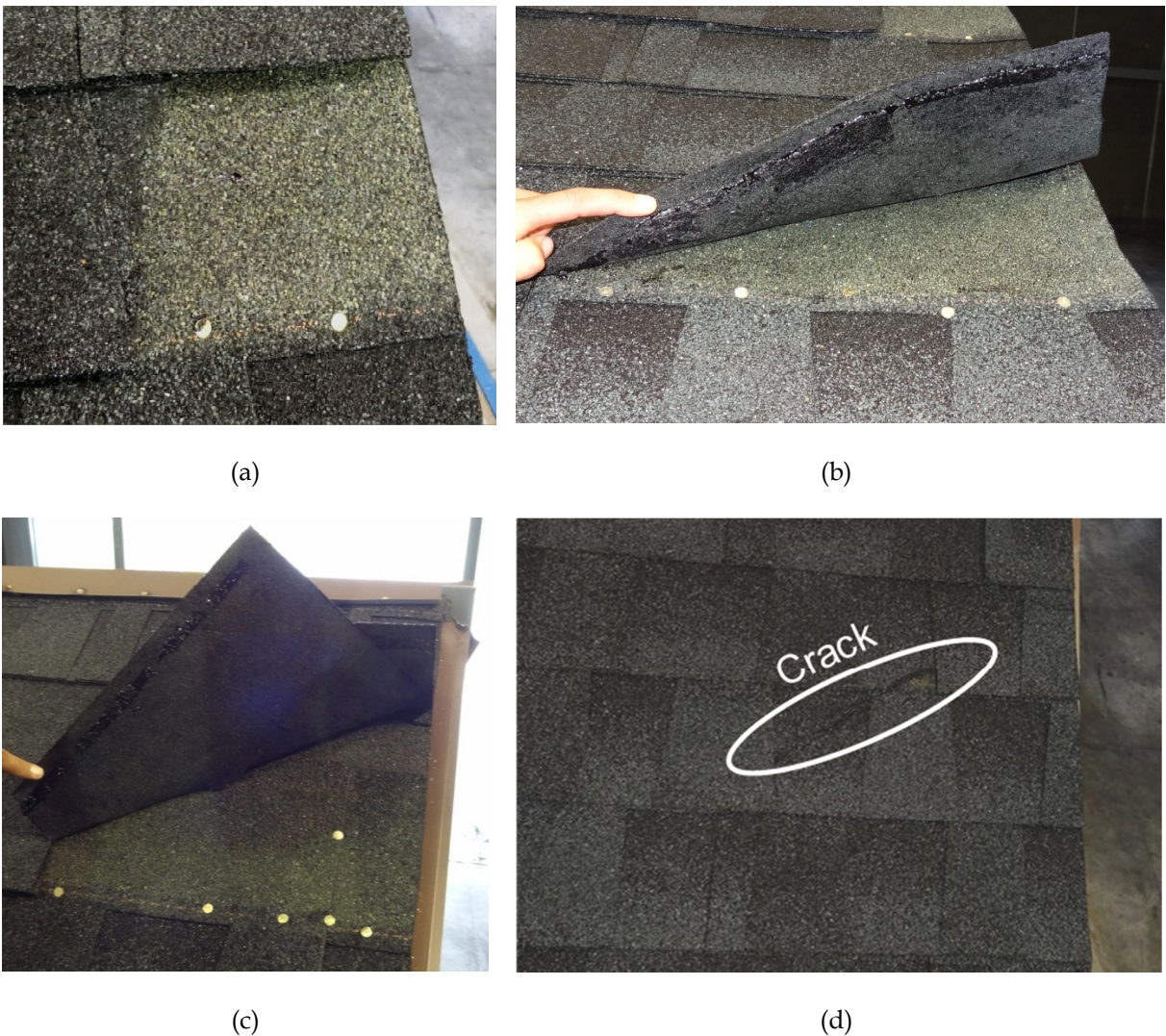


**Fig. 121. LAM-202 – Roof 3 pre-test unsealed shingles: (a) loss of shingle during wind tests, (b) and (c) pre-test unsealed shingles that lifted during wind testing, (d) crack formed on shingle surface due to pre-test unsealed shingle lifting during wind test.**

The performance of the eave for LAM-202 and LAM-201 were similar. Five out of the six roofs sustained pull-through of windward eave starter strips at their attachment points (Figure 122). In general, a small section of eave shingles pulled through their fasteners during Wind Level 1 or 2. As wind speeds increased in Wind Levels 3 and 4, additional pull-through and lifting of eave shingles occurred. A visual example of the progressive lifting is given above in Figure 116. Eave lifting caused surface cracking on adjacent shingles the starter strip, first, and second shingle courses. For the eaves with shingle pull-through, starter strip fasteners were located 89 – 127 mm (3.5 – 5 in) from the eave edge. Recall, ARMA (2006) specifies that starter strip fasteners should be placed a maximum of 76 mm (3 in) from the eave edge. A combination of fasteners placed closer to the eave, additional fasteners, and a reduction of eave overhang would likely have increased the eave wind resistance.



**Fig. 122.** Pull-through of the shingle system’s eave starter strips around the fasteners on LAM-202 – Roof 2. The fasteners were placed approximately 127 mm (5 in) from the butt edge of the starter strip.

#### 4.4.1.3 TT-201 Field, Eave, and Rake Performance

Of the three products compared in this experiment, TT-201’s three-tab field shingles had the greatest amount of shingles that would require either replacement or repair. As shown in Table 43, all five roofs had field shingles that would require replacement/repair with the percentage of shingles ranging from 1% to 55% of the total amount of shingles on the roof. This occurred for two reasons:

1. Pre-wind test fully and partially unsealed shingle tabs. The unsealed shingles lifted in the wind and either folded backwards, causing horizontal cracking near the top of their exposure, or blew off the roof due to fatigue from fluttering in the wind (Figure 127). More pre-wind test unsealing was evident on TT-201's three-tab shingles than the laminate shingles of LAM-201 and LAM-202.
2. Pull-through around rake edge fasteners or eave starter strip fasteners. Fasteners were placed outside of ARMA (2006) edge distance tolerance. Unlike the eave starter strip pull-through at fasteners on LAM-201 and LAM-202 roofs, the pull-through of TT-201's eave starter strips and rake shingles caused larger areas of surrounding field shingles to unseal, blow off, or sustain surface cracks.

The greatest amount of pre-test unsealing occurred on Roof 5 (45°) with 12% of the roof's shingles either partially or fully unsealed (Figure 124). In contrast to the adhesive mode of unsealing noted on the unsealed shingles of LAM-201 and LAM-202, a majority of TT-201's pre-test unsealed shingles failed cohesively within the sealant strip (Figure 123). This indicates that the shingles were, at one time, fully sealed and became unsealed either due to natural weathering or due to stresses caused by the transport of the roof specimen from the conditioning site to the test chamber. The progression lifted and blown off shingles caused by the unsealed shingles is presented in Figure 125. During Wind Level 1, several unsealed shingle tabs lifted and larger "sheeting" type lifting and blow off occurred near the ridge where several unsealed shingles were adjacent to one another. Additional shingle tabs lifted throughout Wind Levels 2-4, producing the final result shown in Figure 126. Post-test assessment of Roof 5 found that 9% of the field shingles were blown off or damaged to the point where repair or replacement would be required. The assessment also found that pre-test unsealed shingles with a minimum unsealed length of 152 mm (6 in) (i.e., one-half tab width) became unsealed during the wind test. This is a significant finding because this shows that partially unsealed shingles can become fully unsealed during wind storms. Recall that the roof surveys conducted on naturally-aged roofs in Section 2.5.4 found patterns of partially unsealed three-tab shingles containing an unsealed length of one-half tab width. Therefore, given the results of Roof 5, it appears that the partially unsealed three-tab shingles observed on the naturally-aged homes can become unsealed in below design-level wind events.



**Fig. 123. TT-201 – Roof 5 pre-test unsealing was caused by a cohesive failure in the tab sealant for both (a) partially and (b) fully unsealed shingles.**

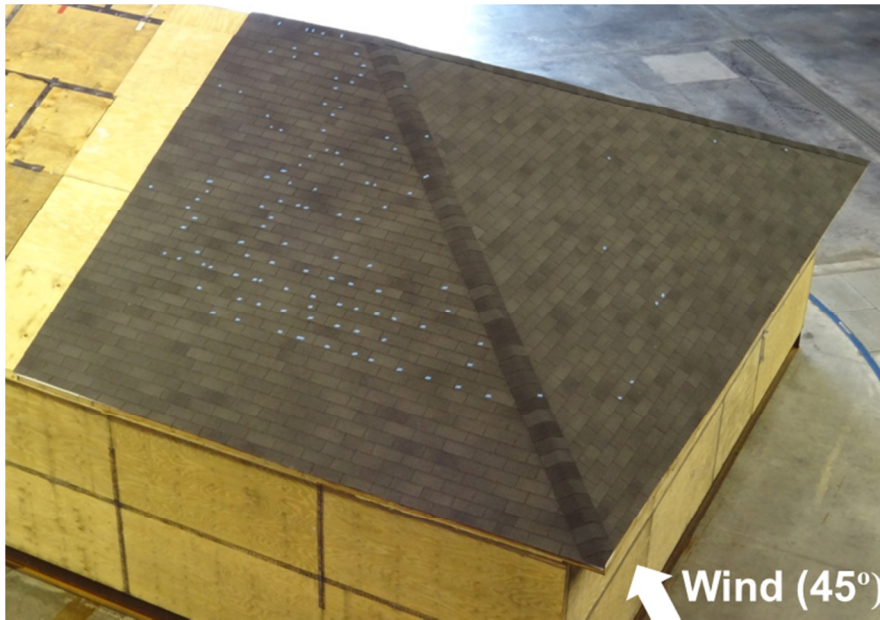
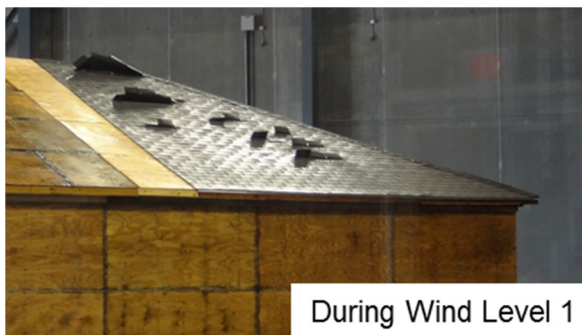


Fig. 124. Unsealed shingles found on TT-201 – Roof 5 prior to wind testing. Blue marks denote the location of full/partially unsealed shingle.



(a)



(b)



(c)



(d)

Fig. 125. Progression of shingles lifting, folding, and blowing off during wind testing of TT-201 – Roof 5.

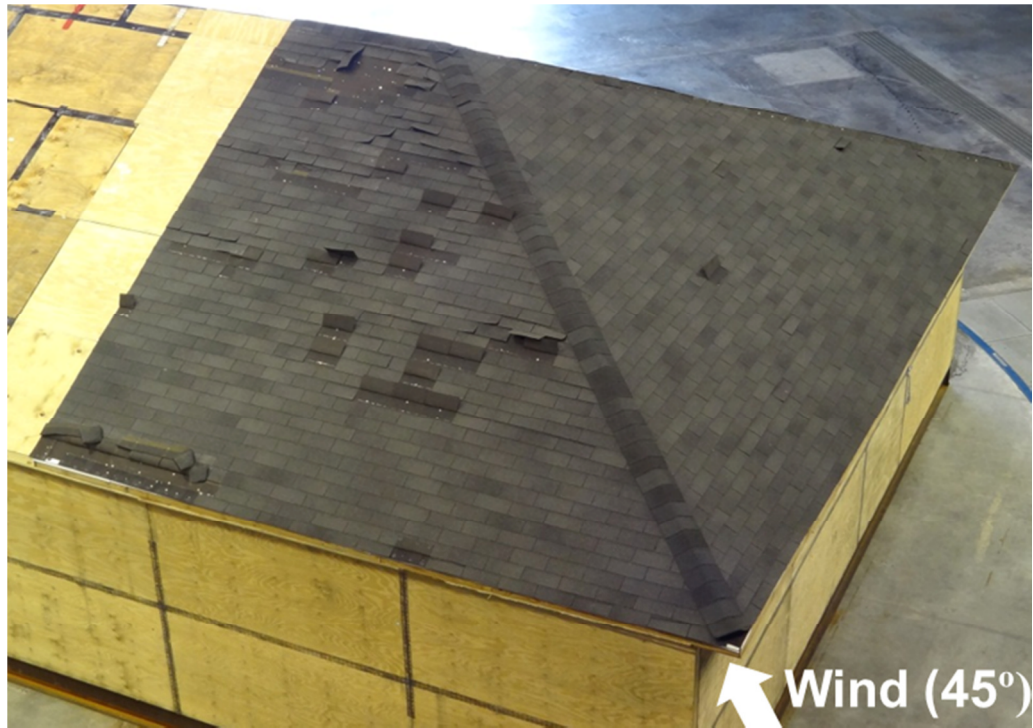


Fig. 126. Post-Level 4 wind test photo of TT-201 - Roof 5.



(a)



(b)

Fig. 127. TT-201 - Roof 5 (a) blow off of shingles caused by a group of pre-test unsealed shingles. (b) Horizontal crack formed by lifting of the unsealed tab during wind testing.

Pull-through of eave starter strip shingles were observed on all roofs, while pull-through of rake shingles at their rake fasteners were observed on Roof 2 (45°) and Roof 3 (90°). The greatest amount of field shingles that were either blown off, unsealed, or cracked (55%) was caused by a combined pull-through of the rake shingle and eave starter strip fasteners on Roof 3 (90°). Figure 128 shows Roof 3 at the end of Wind Level. The fasteners restraining the rake shingles were located 76 mm (3 in) from the rake, which is 51 mm (2 in) further than the specified limit. The fasteners restraining the eave starter strips were located 127 mm (5 in) from the eave edge, which is 51 mm (2 in) further than the specified limit. The pull-through at the edge fasteners may have been prevented if: (1) the fasteners were located closer to the roof edges and (2) six nails were used per strip rather than the four that

were placed on this specimen's shingles. Once pull-through and subsequent blow off of shingles initiated at the eave and rake edges, the blow off progressed towards the interior of the roof with the amount of blown off shingles increasing with increasing wind speed (Figure 128). A 0.93 m<sup>2</sup> (10 ft<sup>2</sup>) section of No. 30 underlayment felt was also torn during Wind Level 4 (Figure 128d), exposing the wood decking. The final condition of the test specimen is given in Figure 129.

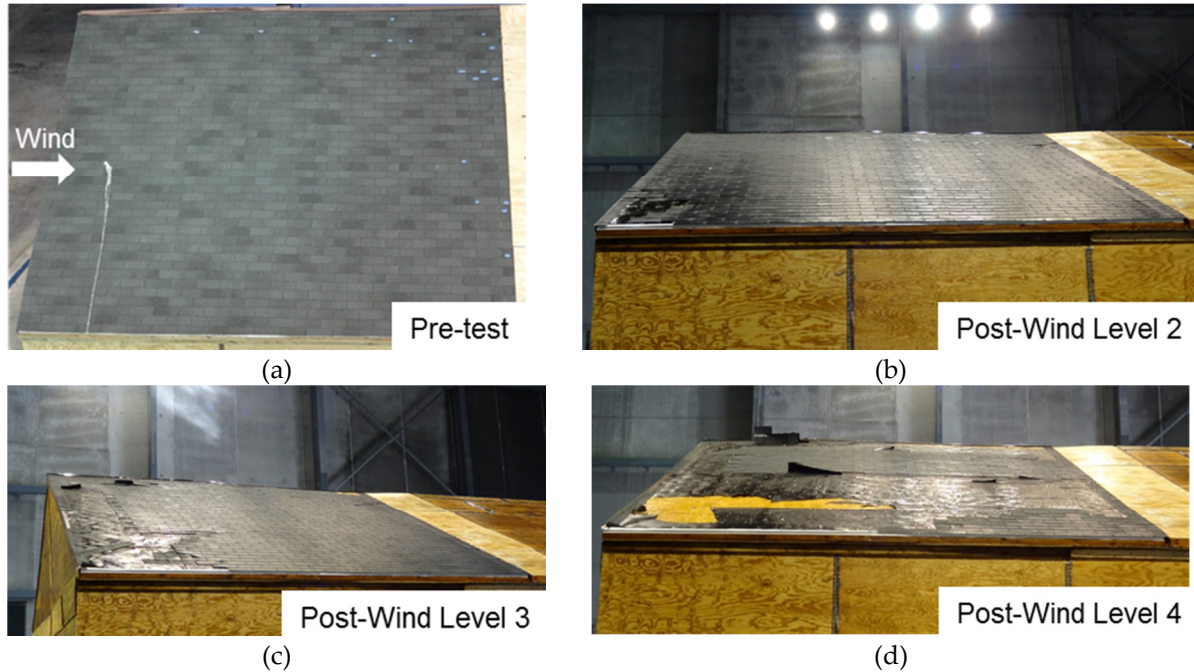


**Fig. 128. Progression of shingle blow off for TT-201 - Roof 3. Fasteners placed further from the roof's edges than recommended by ARMA (2006).**



**Fig. 129. TT-201 - Roof 3 with blown off shingles caused by eave and rake shingles that pulled-through their edge fasteners. Note: The location of fasteners was not within ARMA (2006) specification.**

TT-201's three-tab shingles were fastened to the roof deck using four fasteners per shingle, while LAM-201 and LAM-202's laminate shingles were fastened with six fasteners per shingle. In addition, laminate shingles are constructed with two shingle layers and their resistance to pull-through at the fastener heads is likely greater than a single layer three-tab shingle. The combination of additional nails and additional pull-through resistance most likely contributed to the laminates' better performance when edge detail pull-through occurred.

#### 4.4.2 Hip and Ridge Shingle Performance

The wind performance of the hip and ridge shingles for each roof specimen is summarized in Table 44. The results of the ridge shingle performance may not be relevant for discussion as the shingled portion of the hip roof's ridge was only 2 m (6.5 ft). Therefore, the results of the ridge shingle performance are reported, but this section's discussion will focus on the hip shingle performance only.

Hip shingle blow off was observed on all roofs at a rate ranging from 41-86% of total number of hip shingles installed on the roof. Interestingly, the results indicate no discernible performance differences between the field prepared three-tab hip/ridge shingles (TT-201) and the more expensive pre-manufactured hip/ridge shingles (LAM-201 and LAM-202). Manufacturers often require the installation of pre-manufactured hip/ridge shingles in order to obtain a higher wind resistance warranty; yet these results suggest that their resistance is no better than the traditional cut three-tab method. The results also show a clear correlation between the rate of blow off and wind direction, with the 90° wind direction producing roughly twice the amount of blown off hip shingles as compared to the other test directions. Blow off of hip shingles did not impact adjacent field shingles, likely due to the placement of the hip shingles over the field shingles.

Pre-test partially and fully unsealed hip and ridge shingles were found on all hip roof specimens and the rate of unsealing was higher in the pre-manufactured hip/ridge shingles than the cut three-tabs. A visual reference of the different levels of unsealed hip shingles is given in Figure 130. Hip shingles were typically sealed along the centerline of the hip line, but unsealed at the edges of the shingle, either on one or both sides of the hip line (Figure 130). Inspection of unsealed hip shingle's sealant strip showed adhesive failures between the sealant strip and the bottom of the shingle. This indicates that the hip shingles were likely not sealed from the time of installation to the time of inspection. Similar results of unsealed hip shingles were obtained on the roof surveys detailed in Section 2.5.4.2.

**Table 43. Summary of field, eave, rake, and underlayment wind resistance – TT-201**

Product ID (Type)	Roof Number	Roof Type	Wind Direction	Field Shingles		Eave Edge	Rake Edge	Underlayment
				Pre-Test Condition	Post-Test Condition	Percentage of Shingles with Surface Cracks or Blown Off (Windward Eave Only)	Percentage of Shingles with Surface Cracks or Blown Off	Percentage of Torn Underlayment
				Percentage of Unsealed Shingles (Fully/Partially)	Percentage of Shingles with Surface Cracks or Blown Off			
TT-201 (Three-Tab)	1	Gable	0	5	1	5	0	0
	2	Gable	45	4	5	5	41	4
	3	Gable	90	3	55	61	83	6
	4	Hip	0	1	2	16	--	0
	5	Hip	45	12	9	19	--	0



10% Unsealed Hip Shingles

(a)



31% Unsealed Hip Shingles

(b)

Fig. 130. Example of partially unsealed hip shingles (marked with blue tape): (a) LAM-201 – Roof 6 (10% unsealed) and (b) LAM-202 – Roof 4 (31 % unsealed)

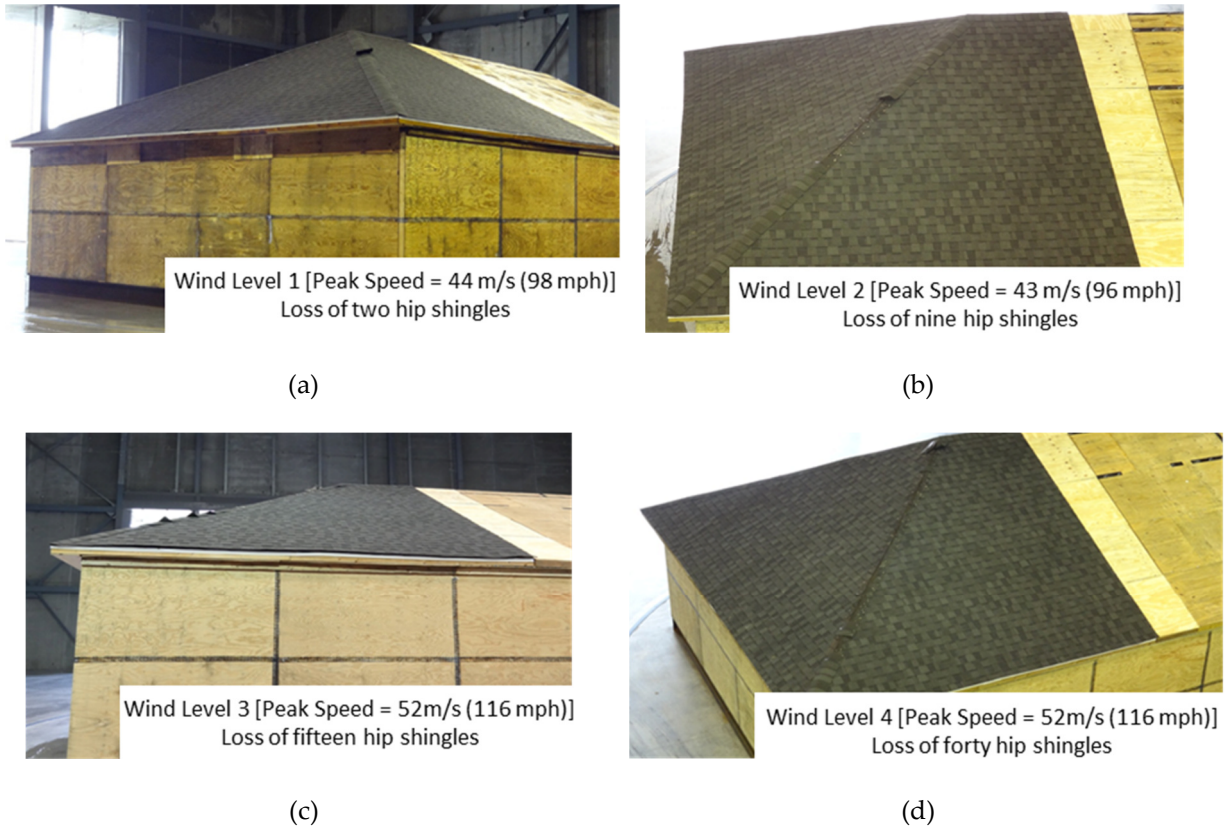


Fig. 131. Example of unsealed hip shingle on LAM-201 – Roof 5. The shingle was unadhered at the edge of the hip shingle and adhered closer to the center of the hip line. (Note: this photo was taken after wind testing.)

While hip shingle blow off rate statistics appear to be independent of the amount of pre-test partially unsealed hip shingles, the vulnerability of the hip system to wind related blow off likely increased with the mere presence of partially unsealed hip shingles. This conclusion is illustrated in the series of photos shown in Figure 132 for LAM-201 – Roof 4 (0°). The first loss of hip shingles occurred during Wind Level 1 with the blow off of two shingles (Figure 132a). The first shingle to lift was an unsealed hip shingle located during the pre-test survey (Figure 132a). The blow off then progressed upwards during Wind Levels 2 and 3 (Figures 132a and 132b). An unsealed shingle also blew off towards the bottom of the roof during Wind Level 3 causing progressive blow off through Wind Level 4 (Figure 132d). By the end of the wind test, only 10 out of the 44 hip shingles on the windward hip line remained on the roof.

**Table 44. Summary of ridge and hip shingle pre-test adhesion condition and resulting wind resistance**

Product ID (Type)	Roof Number	Wind Direction (°)	Pre-Test Condition	Post-Test Condition	Pre-Test Condition	Post-Test Condition
			Partially/Fully Unsealed Hip Shingles (%)	Blown Off Hip Shingles (%)	Partially/Fully Unsealed Ridge Shingles (%)	Blown Off Ridge Shingles (%)
LAM-201 (Laminate)	4	0	31	44	0	0
	5	45	30	50	0	0
	6	90	10	84	0	0
LAM-202 (Laminate)	4	0	37	41	0	0
	5	45	45	42	8.3	0
	6	90	51	86	88	0
TT-201 (Three-Tab)	4	0	4	50	33	0
	5	45	5	49	67	0



**Fig. 132. Progression of hip shingle blow off through the wind test sequence for specimen LAM-201 - Roof 4.**

The critical wind direction for hip shingle wind loading is evident in the photos shown in Figures 133 – 135. These patterns were consistent with all manufacturers. It appears that wind flow roughly perpendicular to the hip line produces the greatest wind load on hip shingles and the load is magnified for hip shingles that are unsealed on their windward edges. This is particularly evident in the 45° wind direction (Figure 134). For this direction, the wind flow is parallel to the windward hip line and perpendicular to the leeward. The resultant blow off occurs on the leeward hip line, while the hip shingles on the windward hip line remained intact on the roof with no lifting. For an unsealed hip shingle with wind flow perpendicular to the hip line, the wind is able to enter the underside of the unsealed shingle, generating uplift on the shingle.

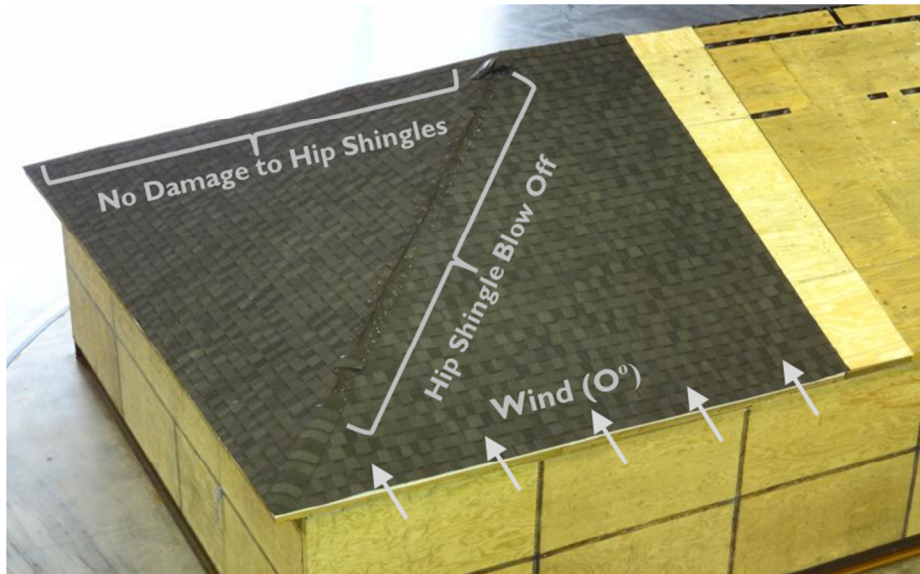


Fig. 133. Typical hip shingle blow off for 0° wind azimuth (photo of LAM-201 - Roof 4 specimen).

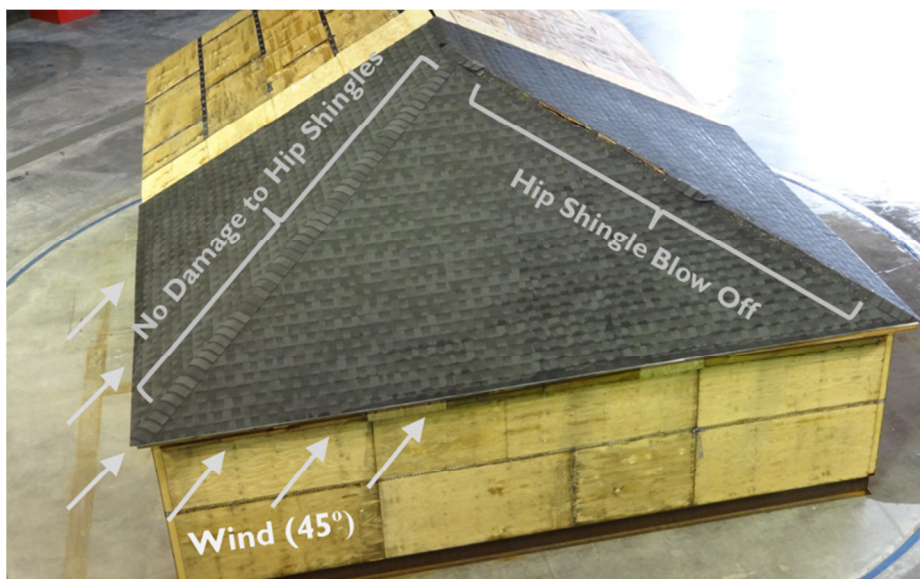


Fig. 134. Typical hip shingle blow off for 45° wind azimuth (photo of LAM-202 - Roof 5 specimen).



**Fig. 135. Typical hip shingle blow off for 90° wind azimuth (photo of LAM-201 – Roof 6 specimen).**

Hip shingles provide a flashing over an exposed gap caused by intersection of two roof slopes, and the underlayment felt sheet should wrap over the hip line to provide a secondary water barrier (Figure 136a). The investigators found evidence of tears in wrapped No. 30 felt underlayment where hip shingles blew off of specimen LAM-202-Roof 6 (Figure 136b). This was likely caused during the process of cutting the field shingles at the hip line using a hooked or straight blade knife. If an underlayment is torn or not wrapped over the hip line and hip shingles are blown off, the hip line is then susceptible to moisture intrusion.



**Fig. 136. Underlayment wrapped over hip line: (a) likely water-resistant (LAM-201 – Roof 4) and (b) torn underlayment likely due to roof installers cutting field shingles at the hip line causing exposure of hip line to moisture intrusion (LAM-202 – Roof 6).**

#### 4.4.3 Estimated Roof Repair Costs

The purpose of this section is to detail the estimated cost that a homeowner or insurer would incur as a result of each roof specimen's wind damage. Repair estimates were performed by Oversight Committee member John Minor using Xactware (current price list) cost estimation software. Model inputs were based on post-test photos provided by UF and the damage statistics given in Tables 39 - 44. The reported estimates were for repair of the asphalt shingle roof covering systems only, and do not attempt to quantify any potentially negative impacts to the roof sheathing or interior components (e.g., drywall, insulation, etc.) caused by loss of the roof covering. The estimate's repair materials were selected for each roof based upon the type and quality that were originally installed. The dye used to color the shingle granules can vary between lots and a roof's color will change throughout the aging process. For this estimate, it was assumed that the homeowner possessed a single bundle of the same shingles that were used for the original installation. Therefore, repair of individual sections could be replaced using up to this amount. Beyond this area, complete replacement was required. We believe this represents a conservative estimate of repair costs.

The labor and materials costs associated with roof repair and replacement will vary based upon the location of the residence. Therefore, the repair estimates given in Tables 45 and 46 are reported for six cities in the Southeast United States: Charleston (South Carolina), Galveston (Texas), Gulfport (Mississippi), Miami (Florida), Tampa (Florida), and Wilmington (North Carolina). These cities represent major metropolitan areas located in hurricane-prone regions. Overall, the cost of repair in Miami is the most expensive of the set, while the cost of repair in Gulfport is the least expensive. A line item cost of repair for each roof specimen is given in Tables B-1 through B-17 in Appendix B for Miami, FL.

For the gable roofs, the average estimated repair costs to LAM-201's (\$136.77 - Miami, FL) roofs was approximately one-half the cost of LAM-202's (\$306.88 - Miami, FL) (Table 45). The repair costs for both LAM-201 and LAM-202's gable roofs were attributed to labor, re-nailing, and resealing of uplifted eave shingles. However, the damage to the three TT-201 gable roof specimens was so extensive that they required complete replacement of their shingle roof systems: shingles, felt underlayment, and edge metal (Table 46). The cost of replacing one TT-201 three-tab gable roof specimen ranged from \$1529.64 in Gulfport, MS to \$2781.18 in Miami, FL.

The main cost difference between LAM-201 and LAM-202's gable and hip roofs can be attributed to the hip shingle blow off that occurred on the hip roof specimens. The blow off sustained on one hip line in the 0° and 45° wind azimuths required replacement of all of the hip/ridge shingles. The estimated cost of replacing the 16 linear meters (52 linear ft) of the high profile pre-manufactured hip/ridge shingles that were on LAM-201 and LAM-202's hip roofs was \$416.52 (Miami, FL). Similar to TT-201's gable roof specimens, the hip roof blow off on both roofs required replacement of the complete roof covering system. This cost ranged from \$1710.09 in Gulfport, MS to \$3109.25 in Miami, FL.

The eave pull-through and lifting on LAM-201 - Roof 6 is one example of a repair decision that a claims adjuster would have make following a wind event (Figure 137). A 2 m (7 ft) section of starter strips lifted, pulled through their fasteners, and folded backwards; causing surface cracks on three shingles upslope of the eave. This was estimated to require a replacement of a 9.3 m<sup>2</sup> (100 ft<sup>2</sup>) section of roofing. However, if the homeowner did not have extra shingles in storage or if a best match color could not be found, replacement of the complete roofing system would be required.



**Fig. 137. Pull-through eave starter strip shingles at fasteners causing cracking to the surface of first and second shingle courses (LAM-201 – Roof 6).**

The effect of wind direction on estimated roof covering repair costs for Miami, FL (i.e., the most expensive repair city of the six examined) is shown in Figure 138. The results indicate that wind direction was not a controlling factor in required repair costs. As previously noted for orientations at 0° and 45°, blow off of hip shingles was generally isolated to one hip line on the three manufacturer's hip roof specimens. However, blow off in this one line required replacement of all of the hip/ridge shingles. Also evident, are performance differences between the laminate shingle systems (LAM-201 and LAM-202) and the three-tab shingle system (TT-201). The estimated cost of repair to the laminate systems was under \$1000.00 per roof, with exception of LAM-201 – Roof 6, while the three-tab roof repair costs were all over \$2500.00. These results may be skewed as the three-tab roofs were installed with four fasteners, as opposed to six fasteners per strip in the laminate. The products evaluated within the test represent a small fraction of the total asphalt shingle market and, therefore, weaker and/or stronger shingle products likely exist.

**Table 45. Summary of estimated repair and replacement costs – LAM-201 and LAM-202**

Product ID (Type)	Roof Number	Roof Type	Wind Direction	Estimated Cost of Repairing/Replacing Damaged Roofing in Six Southeast United States Cities (\$USD) <sup>a</sup>					
				Charleston, SC	Galveston, TX	Gulfport, MS	Miami, FL	Tampa, FL	Wilmington, NC
LAM-201 (Laminate)	1	Gable	0	\$167.67	\$155.03	\$149.40	\$281.88	\$180.40	\$163.49
	2	Gable	45	\$73.21	\$70.64	\$68.07	\$128.44	\$82.20	\$74.50
	3	Gable	90	No Repairs Necessary					
	4	Hip	0	\$397.38	\$383.43	\$369.49	\$697.15	\$446.18	\$404.35
	5	Hip	45	\$315.61	\$304.54	\$293.47	\$553.71	\$354.37	\$321.15
	6	Hip	90	\$963.20	\$929.41	\$895.61	\$1689.83	\$1081.49	\$980.10
LAM-202 (Laminate)	1	Gable	0	\$174.92	\$168.78	\$162.65	\$306.88	\$196.40	\$177.99
	2	Gable	45	\$174.92	\$168.78	\$162.65	\$306.88	\$196.40	\$177.99
	3	Gable	90	\$174.92	\$168.78	\$162.65	\$306.88	\$196.40	\$177.99
	4	Hip	0	\$490.54	\$473.32	\$456.11	\$860.59	\$550.78	\$499.14
	5	Hip	45	\$490.54	\$473.32	\$456.11	\$860.59	\$550.78	\$499.14
	6	Hip	90	\$490.54	\$473.32	\$456.11	\$860.59	\$550.78	\$499.14

<sup>a</sup>Costs estimated using Xactware (October 2012 price list) software

**Table 46. Summary of estimated repair and replacement costs - TT-201**

Manufacturer (Type)	Roof Number	Roof Type	Wind Direction	Estimated Cost of Repairing/Replacing Damaged Roofing in Six Southeast United States Cities (\$USD) <sup>1</sup>					
				Charleston, SC	Galveston, TX	Gulfport, MS	Miami, FL	Tampa, FL	Wilmington, NC
TT-201 (Three-Tab)	1	Gable	0	\$1585.29	\$1529.64	\$1474.02	\$2781.18	\$1779.97	\$1613.08
	2	Gable	45	\$1585.29	\$1529.64	\$1474.02	\$2781.18	\$1779.97	\$1613.08
	3	Gable	90	\$1585.29	\$1529.64	\$1474.02	\$2781.18	\$1779.97	\$1613.08
	4	Hip	0	\$1772.27	\$1710.09	\$1647.90	\$3109.25	\$1989.92	\$1803.37
	5	Hip	45	\$1772.27	\$1710.09	\$1647.90	\$3109.25	\$1989.92	\$1803.37

<sup>1</sup>Costs estimated using Xactware (October 2012 price list) software

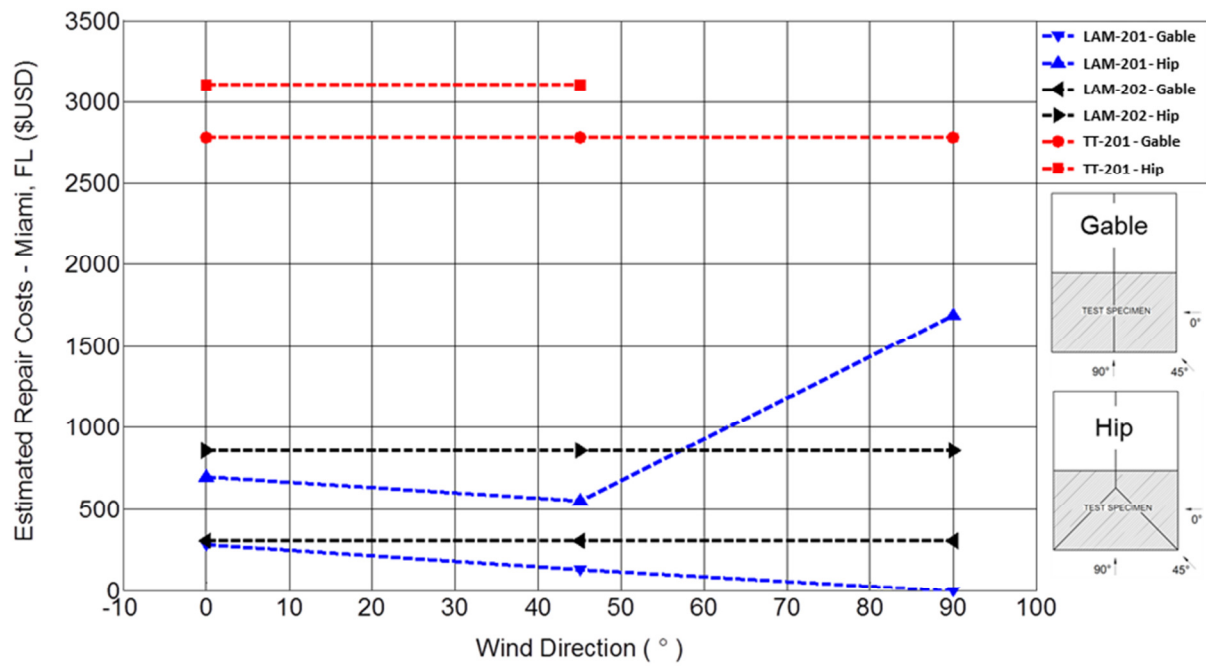


Fig. 138. Estimated cost of roof repairs in Miami, FL versus wind direction. (Costs estimated using Xactware 2012 software and October 2012 price list)

## 4.5 Findings and Recommendations

### Finding

Fully sealed asphalt shingles located in the field of the roof remained sealed down throughout testing, unless disturbed by the lifting of edge details or lifting of adjacent shingles that were partially or fully unsealed prior to wind testing. Shingles which were partially or fully unsealed before the wind tests had an increased susceptibility to folding or tearing that caused surface cracking or blow off of shingle.

### Recommendation

All shingle products used in this experiment were classified as ASTM D7158 Class H [150 mph nominal design wind speed (Vasd)]. This standardized test method is only valid for a fully sealed shingle and its wind uplift resistance is defined for new shingles in a laboratory setting. While the experiment discussed in Section 5 did not achieve the design level wind speeds that these products are designed for, the results of this experiment suggests that fully sealed shingles can resist hurricane force winds. This positive conclusion is significant as it appears that fully sealed shingles should be expected to perform well during high wind storms, assuming that edge details remain intact.

However, partially and fully unsealed (or non-bonded) asphalt shingles that exist on a roof prior to a high wind event pose a significant issue that is in need of attention. We recommend that future work should focus first on the mechanics behind the systematic unsealing, as described in Section 2.5.4, or lack of initial sealing of shingles and on a potential solution for new shingle products. As for the existing residential stock, we recommend that immediate work be conducted on investigating potential retrofit methods that can be easily performed by roofing professionals. The use of roofing cement to reseal unsealed shingles is an obvious solution; however, the long-term performance of roofing cement is unknown. The focus of the future work should be on long-term solutions that will ensure shingles will remain adhered throughout their life.

Installation errors, particularly nailing location at the eave and rake, most likely contributed to the edge detail pull-through sustained in the experiments. While the installation errors might be dismissed as the product of one installer, evidence from field investigations has shown similar installation errors. We believe that additional training, or a certification program, for roof installers might provide significant cost benefits.



**Fig. 139. (a) Shingle blow off obtained from system-level performance test caused by pre-test non-bonded shingles and (b) blown off shingles observed by FEMA after Hurricane Charley [Photo from FEMA (2011)]**

### Finding

Localized pull-through of eave and rake shingles at attachment points were observed on 15 out of the 17 roofs tested in this experiment. This impacted surrounding shingles in the field of the roof.

### Recommendation:

FEMA 499 Fact Sheet recommends dabs of asphalt roof cement between the starter and first course shingles. Future work should evaluate the wind resistance of this detail. The location of the fasteners relative to the edge likely plays a large role in the overall wind resistance of the edge system. Fasteners located approximately 13 – 51 mm (0.5 – 2 in) above manufacturer’s guidelines likely caused the pull-through of shingles. Our first recommendation for edge details calls for more stringent guidance on the proper installation of details. Locating fasteners closer to the edge of the roof (as per FEMA 2012), increasing the number of fasteners in the starter strips, and reducing the overhang of the rake and eave shingles beyond the edge condition will most likely improve the wind resistance of the edge detail. However, there are no standard test methods currently available to evaluate the wind resistance of an edge system; therefore, future work should focus on defining the wind resistance of edge details in order to provide a wind resistant installation method. We also recommend that a shingle’s overhang beyond the edge condition be kept to a minimum. The overhang used for this experiment was set to 13 mm (0.5 in) beyond the drip edge. ARMA (2006) recommends an overhang beyond the edge conditions ranging from 6 – 19 mm (0.25-0.75 in). Reducing a shingle’s overhang from the edge to the FEMA (2012) recommended 6 mm (0.25 in) will reduce the uplift loads placed on the edge detail.

The loss of restraint at the eave caused surface cracking to an isolated area of shingles adjacent shingles for the laminate systems (LAM-201 and LAM-202). However, rake and edge pull-through at fasteners on one three-tab system (TT-201) initiated a progressive lifting and blow off of shingles located in the field of the roof (Figure 140a). The cause of this

performance gap between the laminate and three-tab system as a result of pull-through at the edge fasteners is likely due to (1) an increased pull-through resistance of the laminate system's material and (2) use of six nails in the laminate as opposed to the four nails that were used in the three-tab. Post-storm reports have also repeatedly shown the loss of eave and rake shingles with similar blow off and surface cracking results to adjacent field shingles (Figure 140b). The use of six-nails on all shingle strips will decrease the amount of stress on the nail/shingle connection that occurs when edge details lose their restraint. However, fastener loads for uplifted shingles are not currently defined. We recommend that work should be conducted to quantify loads generated on a shingle's fasteners with a range of fastener densities (e.g., 4 or 6 nails per shingle). For rake edges, the addition of roofing cement on the edges of rake shingles, as shown in FEMA P-499 Fact Sheet 7.3 (Figure 141), may significantly improve the performance of the rake edge detail. However, we also recommend that further investigation should be conducted to evaluate the long-term effects of asphalt roof cement use. This includes the measurement of its wind uplift capacity. Residential structures located in High-Velocity Hurricane Zones in Florida (Miami-Dade and Broward counties) require asphalt roof cement for edge details. We recommend that inspections of homes with roof cement use be conducted to assess its long-term performance.

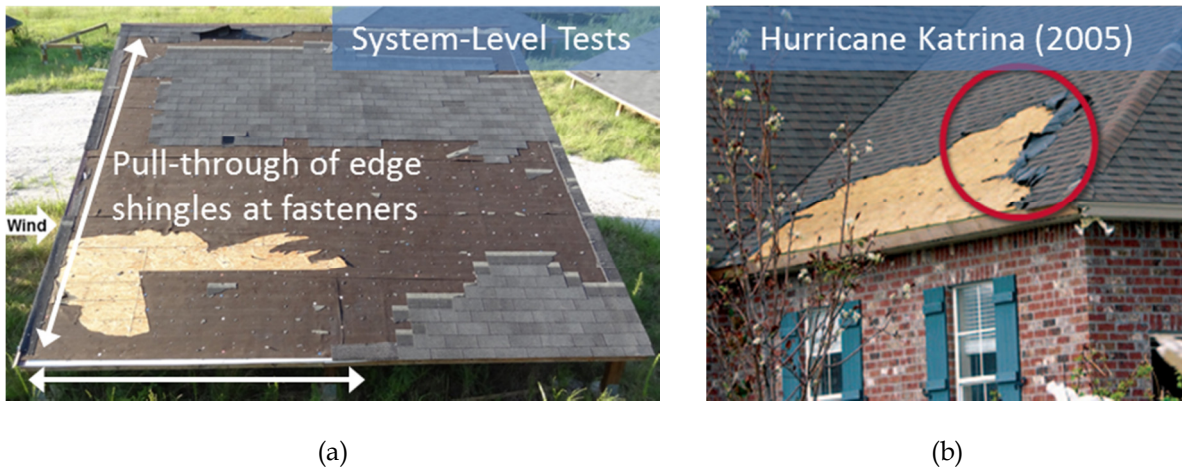


**Fig. 140. (a) Shingle blow off observed during System-Level wind tests caused by pull-through of edge details at their fasteners. (b) Roof from FEMA post-storm assessment teams after Hurricane Katrina [Photo from FEMA (2011)].**

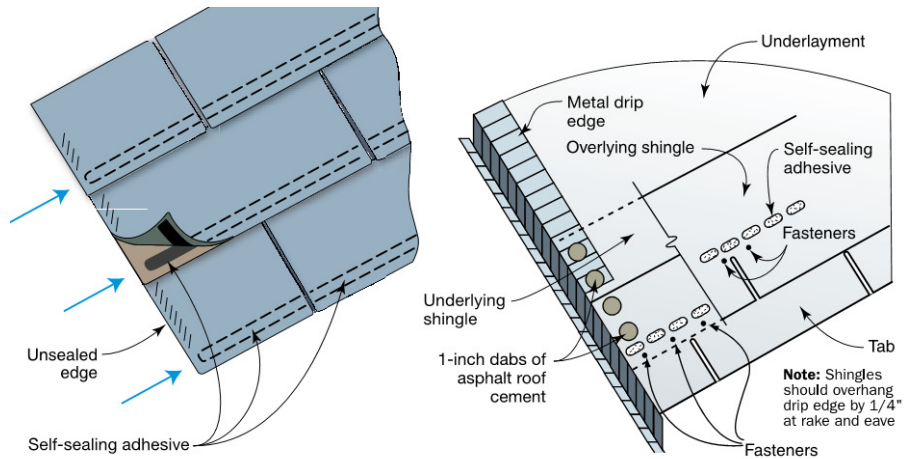


**Fig. 141. FEMA P-499 recommended installation method for rake details. Further work is necessary to define wind resistance of this method and to ensure long-term performance of asphalt roof cement. [Figure from FEMA (2012)]**

### Finding

Hip shingle blow off was observed on all roofs at an equivalent rate for pre-manufactured hip/ridge shingles used in products LAM-201 and LAM-202 and cut three-tab shingles used for hip/ridge shingles in product TT-201. The lack of adhesion on hip/ridge shingles observed both in this experiment and field surveys (Section 2.5) demonstrates that hip/ridge shingle products may be unable to provide the adhesive performance required to resist high wind. It is hypothesized that the partial unseal is caused by the inability of the hip/ridge shingle's edges to remain folded over the roofline, preventing adhesion at the corner of the hip/ridge shingle's leading edge. Once partially unsealed, hip/ridge shingles in high winds are subjected to increased pressurization on the underside of the hip/ridge shingle - leading to an increased likelihood of blow off.

### Recommendation:

We strongly recommend further study of the wind resistance of hip/ridge shingles with emphasis on the adhesive performance on the edges of the hip/ridge shingles. A second recommendation relates to existing shingle roofs with hip/ridge shingles. The roof surveys conducted in Section 2.5.4.2 demonstrated that partially unsealed hip/ridge shingles could occur on roofs of all ages. Given the susceptibility of partially unsealed hip/ridge shingles to blow off, as shown in the System-Level wind tests, it appears that the existing hip/ridge shingles may be vulnerable to blow off in high winds. We recommend immediate development of adequate retrofit methods to increase the wind resistance of existing hip/ridge shingles. Potential retrofit methods may follow the guidelines given in FEMA P-499 Technical Fact Sheet 7.3, shown in Figure 142. This FEMA recommendation is for new construction, however, future work should first focus on the application of this guideline as a retrofit method. As part of this work, the improvement of wind resistance using this retrofit method should be quantified along with the long-term performance of this retrofit method.

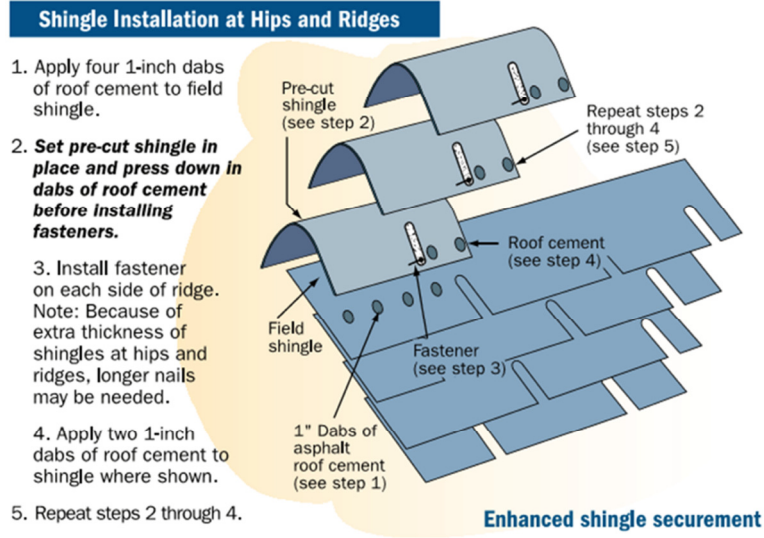


Fig. 142. FEMA P-499 Technical Fact Sheet 7.3 – new construction installation guideline for enhanced hip and ridge shingle wind resistance. Further work is necessary to define wind resistance of this method and to ensure long term performance of asphalt roof cement. [Figure from FEMA (2012)]

## 5. REFERENCES

- ARMA (2006). *Asphalt Roofing Residential Manual*. Asphalt Roofing Manufacturers Association, Washington, DC.
- ASTM D3161 (2005). *Standard Test Method for Wind-Resistance of Asphalt Shingles (Fan-Induced Method)*. ASTM International, West Conshohocken, PA.
- ASTM D3462 (2010a). *Standard Specification for Asphalt Shingles Made from Glass Felt and Surfaced with Mineral Granules*. ASTM International, West Conshohocken, PA.
- ASTM D6381 (2008). *Standard Test Method for Measurement of Asphalt Shingles Mechanical Uplift Resistance*. ASTM International, West Conshohocken, PA.
- ASTM D7158 (2011). *Standard Test Method for Wind Resistance of Asphalt Shingles (Uplift Force/Uplift Resistance Method)*. ASTM International, West Conshohocken, PA.
- ASTM E145-94 (2001). *Standard Specification for Gravity-Convection and Forced-Ventilation Ovens*. ASTM International, West Conshohocken, PA.
- Baskaran, A. (1999). "Wind uplift model for asphalt shingles (discussion)." *Journal of Wind Engineering and Industrial Aerodynamics*, pp. 67-69.
- Cochran L., Peterka J.A., and Derickson, R. (1999). "Roof surface wind speed distributions on low-rise buildings." *Architectural Science Review*.
- Corbin, R.L. (2000). "New method for measuring the wind resistance of asphalt roofing shingles." *RCI Interface*. RCI, Inc., pp. 9-11.
- Cullen, W. (1960). "Wind resistance of asphalt shingle roofing." *Fall Conferences of the Building Research Institute*, National Academy of Sciences, Washington D.C., pp. 33-42.
- Dixon, C.R., Masters, F.J., Prevatt, D.O., Gurley, K.R. (2012). "An historical perspective on the wind resistance of asphalt shingles." *RCI Interface*. RCI, Inc., pp. 4-14.
- Fedor, G.R., Brennan, P.J. (1996). "Comparison between natural weathering and fluorescent UV exposures: UVA-340 test results." *Durability Testing of Non-Metallic Materials - ASTM STP 1294*, American Society for Testing and Material.
- FEMA (2005a). "Hurricane Charley in Florida." *FEMA 488*, Federal Emergency Management Agency.
- FEMA (2005b). "Summary report on building performance: 2004 hurricane season." *FEMA 490*, Federal Emergency Management Agency.
- FEMA (2006). "Hurricane Katrina in the Gulf Coast." *FEMA 549*, Federal Emergency Management Agency.
- FEMA (2009). "Hurricane Ike in Texas and Louisiana." *FEMA 757*, Federal Emergency Management Agency.
- FEMA (2011). "Coastal construction manual: principles and practices of planning, siting, designing, constructing, and maintaining residential buildings in coastal areas (4<sup>th</sup> ed.)" *FEMA P-55*, Federal Emergency Management Agency.
- FEMA (2012). "Home builder's guide to coastal construction." *FEMA P-499*. Federal Emergency Management Agency.
- Gurley, K. and Masters, F. (2011). "Post 2004 hurricane field survey of residential building performance." *ASCE Natural Hazards Review*, to appear November 2011.
- Hubard, G.A. and Decker, D.S. (1995) *Engineering Properties of Asphalt Mixtures and the Relationship to Performance*, ASTM International, West Conshocken, PA.
- Insurance Institute for Business & Home Safety. (2009). "Hurricane Ike: nature's force vs. structural strength." IBHS.

- Koontz, J.D. (1990) "Shingle splitting problem." *Western Roofing Magazine*.
- Liu, Z., Pogorzelski, H., Masters, F.M., Tezak, S. and Reinhold, T.A. (2010). "Surviving nature's fury: performance of asphalt shingle roofs in the real world." *RCI Interface Magazine*, RCI.
- Marshall, T.P., Morrison, S.J., Herzog, R.F., Green, J.R. (2010). "Wind effects on asphalt shingles." *29<sup>th</sup> Conference on Hurricanes and Tropical Meteorology*. American Meteorological Society.
- Nichols, T. (2010). "A stronger bond." *National Roofing Contractors Association Professional Roofing Magazine*.
- Noone, M.J. and Blanchard, W.K. (1993). "Asphalt shingles – a century of success and improvement." *10<sup>th</sup> Conference on Roofing Technology*, National Roofing Contractors Association.
- Ott, R. L. and Longnecker, M.T. (2004). *A First Course in Statistical Methods*. Brooks/Cole, Belmont, CA.
- Parker, D., Sherwin, J. (1998). "Comparative summer attic thermal performance of six roof constructions." *The 1998 ASHRAE Annual Meeting*, Toronto, Canada.
- Peterka, J.A. and Cermak, J.E. (1983). "Wind-tunnel study of wind resistance of roofing shingles." *Colorado State University*, Fort Collins, Colorado.
- Peterka, J.A., Cermak, J.E., Cochran, L.S., Cochran, B.C., Hosoya, N., Derickson, R.G., Jones, J., Metz, B. (1997). "Wind uplift model for asphalt shingles." *Journal of Architectural Engineering*, pp. 147-155.
- Peterka, J.A., Cermak, J.E. and Hosoya, A. (1983). "Wind-tunnel study of wind pressures on roofing shingles." *Colorado State University*, Fort Collins, Colorado.
- Peterka, J.A. and Esterday (2000). "Development of a shingle uplift coefficient test standard." Cermak Peterka Petersen, Inc. (*Not publically available*)
- Robertson, A.P. (1991). "Effect of eaves detail on wind pressures over an industrial building." *Journal of Wind Engineering and Industrial Aerodynamics*, pp. 325-333.
- RICOWI (2006). "Hurricanes Charley and Ivan investigation report." *Roofing Industry Committee on Weather Issues*, McDonough, Georgia.
- Saffir, H.S., (1973). "Hurricane wind and storm surge, and the hurricane impact scale." *The Military Engineer*, Alexandria, Virginia.
- Shiao, M.L., Nester, D.A. and Terrenzio, L.A. (2003a). "On the kinetics of thermal loads for accelerated aging." *ASTM Roofing Research and Standards Development*.
- Shiao, M.L., Snyder, R.A., Livsey, R.D. and Kalkanoglu, H.M. (2003b). "Measuring uplift resistance of asphalt shingles." *ASTM Special Technical Publication*, pp. 3-18.
- Simpson, R., (1974). "The hurricane disaster potential scale." *Weatherwise*, 27, 169-186.
- Taylor, Z.J., Gurka, R., Kopp, G.A., and Liberzon, A. (2010). "Long duration, time- resolved PIV to study unsteady aerodynamics." *Instrumentation and Measurement*, pp. 3262-3269.
- Terrenzio, L.A., Harrison, J.W., Nester, D.A. and Shiao, M.L. (1997). "Natural vs. artificial aging: use of diffusion theory to model asphalt and fiberglass-reinforced shingle performance." *Fourth International Symposium on Roofing Technology*, NRCA.
- UL 997 (1995). *Wind Resistance for Prepared Roof Covering Materials*. Underwriters Laboratory.
- UL 2390 (2003). *Test Methods for Wind Resistant Asphalt Shingles with Sealed Tabs*. Underwriters Laboratory.
- US Census Bureau (2003). "Census of population and housing (2000)." US Dept. of Commerce, Economics and Statistics Administration, Washington, D.C.



## **APPENDIX A. SUMMARY OF MEASURED WIND FORCES**

A summary of the total force coefficients measured on each test shingle specimen is given in the following tables in this appendix.

**Table A-1. Comparison of measured forces versus ASTM D7158 predicted uplift results for Fully Sealed Laminate Specimen 1**

Wind Azimuth (°)	Mean Wind Speed (m/s)	Measurement Location	Mean Distributed Loads (N/m)			Total Resultant Distributed Load	Vertical Load Angle (°)	Force Coefficients		
			F <sub>x</sub>	F <sub>y</sub>	F <sub>z</sub>			Uplift	Total	Predicted
0	20.3	L	-3.3	-7.1	2.9	8.4	20.2	0.011	0.033	0.037
		M	-6.5	0.2	2.8	7.1	23.0	0.011	0.028	
		R	-13.2	1.3	3.2	13.7	13.4	0.013	0.054	
	39.5	L	-21.9	0.4	22.1	31.1	45.3	0.023	0.033	
		M	-38.3	25.5	16.5	48.9	19.8	0.017	0.051	
		R	-56.8	12.0	15.2	60.0	14.6	0.016	0.063	
22.5	20.3	L	-3.1	-8.7	0.9	9.3	5.3	0.003	0.036	0.037
		M	-7.7	1.4	2.4	8.2	17.0	0.009	0.032	
		R	-11.5	1.4	4.1	12.3	19.4	0.016	0.048	
	39.5	L	-25.5	-7.1	21.4	34.0	39.0	0.022	0.036	
		M	-30.4	41.8	13.1	53.3	14.2	0.014	0.056	
		R	-48.7	17.0	25.5	57.5	26.3	0.027	0.060	
45	20.3	L	2.3	-0.4	-0.2	2.4	-5.2	-0.001	0.010	0.037
		M	-3.9	3.8	2.7	6.1	26.5	0.011	0.026	
		R	-7.6	0.4	3.5	8.4	25.0	0.015	0.035	
	39.5	L	4.0	-20.4	2.7	21.0	7.5	0.003	0.022	
		M	-0.9	27.0	14.3	30.5	27.9	0.015	0.032	
		R	-29.0	-7.2	21.3	36.7	35.6	0.022	0.038	
67.5	20.3	L	2.5	-0.4	2.7	3.7	46.9	0.011	0.015	0.037
		M	-3.0	7.0	2.7	8.0	19.5	0.011	0.032	
		R	-9.4	0.3	2.5	9.7	15.1	0.010	0.039	
	39.5	L	-9.1	-12.9	5.1	16.6	17.9	0.005	0.018	
		M	-2.0	20.6	18.3	27.6	41.4	0.019	0.029	
		R	-21.4	-4.8	20.8	30.2	43.5	0.022	0.032	
90	20.3	L	-1.6	-2.8	-0.2	3.2	-4.0	-0.001	0.013	0.037
		M	1.0	4.2	3.9	5.8	41.6	0.015	0.023	
		R	-4.8	0.0	2.1	5.2	24.1	0.009	0.021	
	39.5	L	-21.2	-18.8	2.7	28.4	5.4	0.003	0.028	
		M	8.1	18.1	19.3	27.6	44.3	0.019	0.027	
		R	-23.1	-20.2	13.3	33.5	23.5	0.013	0.033	

Table A-2. Comparison of measured forces versus ASTM D7158 predicted uplift results for Fully Sealed Laminate Specimen 2

Wind Azimuth (°)	Mean Wind Speed (m/s)	Measurement Location	Mean Distributed Loads (N/m)			Total Resultant Distributed Load	Vertical Load Angle (°)	Force Coefficients		
			F <sub>x</sub>	F <sub>y</sub>	F <sub>z</sub>			Uplift	Total	Predicted
0	20.0	L	-23.3	8.2	-0.4	24.7	-0.9	-0.002	0.101	0.037
		M	-4.5	-0.3	0.1	4.5	1.8	0.001	0.018	
		R	-3.7	-0.4	0.4	3.7	6.3	0.002	0.015	
	40.0	L	14.8	1.6	14.8	21.0	44.8	0.015	0.022	
		M	-21.3	10.0	10.6	25.8	24.1	0.011	0.026	
		R	-19.6	8.0	16.6	26.9	38.1	0.017	0.028	
22.5	18.5	L	-6.6	-4.2	5.3	9.4	34.4	0.025	0.045	0.037
		M	-8.4	2.0	5.7	10.4	33.2	0.027	0.049	
		R	-8.3	7.8	8.4	14.2	36.4	0.040	0.068	
	40.0	L	-30.0	5.3	3.9	30.7	7.3	0.004	0.031	
		M	-16.0	12.3	6.8	21.3	18.7	0.007	0.022	
		R	-23.1	35.7	24.5	49.1	30.0	0.025	0.050	
45	21.0	L	3.6	-0.6	-0.8	3.7	-13.2	-0.003	0.014	0.037
		M	-2.5	2.9	-0.7	3.9	-9.9	-0.002	0.014	
		R	-4.9	-0.5	1.6	5.2	18.3	0.006	0.019	
	41.2	L	1.7	1.7	-5.3	5.8	-65.8	-0.005	0.006	
		M	7.9	21.4	3.1	23.0	7.7	0.003	0.022	
		R	-5.7	-11.8	17.2	21.6	52.7	0.017	0.021	
67.5	21.1	L	-1.6	-1.7	-3.4	4.1	-55.4	-0.012	0.015	0.037
		M	-2.4	1.9	-2.4	3.9	-37.8	-0.009	0.014	
		R	-0.5	-4.5	-1.1	4.6	-13.5	-0.004	0.017	
	41.2	L	-23.0	14.5	-8.0	28.3	-16.4	-0.008	0.027	
		M	7.8	26.2	0.3	27.3	0.6	0.000	0.026	
		R	-4.3	-21.8	8.0	23.7	19.9	0.008	0.023	
90	21.6	L	-4.2	1.8	-2.4	5.1	-27.4	-0.008	0.018	0.037
		M	3.6	3.2	-1.5	5.1	-17.3	-0.005	0.018	
		R	4.2	-0.7	-0.4	4.3	-5.9	-0.002	0.015	
	41.6	L	-25.1	15.8	-3.6	29.9	-6.9	-0.003	0.028	
		M	28.7	16.5	9.4	34.4	15.8	0.009	0.032	
		R	6.9	-41.4	9.6	43.0	12.9	0.009	0.041	

**Table A-3. Comparison of measured forces versus ASTM D7158 predicted uplift results for Fully Sealed Laminate Specimen 3**

Wind Azimuth (°)	Mean Wind Speed (m/s)	Measurement Location	Mean Distributed Loads (N/m)			Total Resultant Distributed Load	Vertical Load Angle (°)	Force Coefficients		
			F <sub>x</sub>	F <sub>y</sub>	F <sub>z</sub>			Uplift	Total	Predicted
0	21.0	L	-4.1	-3.9	-1.9	6.0	-19.0	-0.007	0.022	0.037
		M	-5.6	-1.0	0.0	5.7	-0.3	0.000	0.021	
		R	-3.4	-0.4	1.2	3.6	18.6	0.004	0.013	
	41.0	L	-22.6	-9.8	3.6	24.9	8.2	0.003	0.024	
		M	-14.7	-8.0	3.9	17.2	13.1	0.004	0.017	
		R	-20.1	1.2	13.1	24.0	33.1	0.013	0.023	
22.5	21.3	L	-0.9	-1.7	-4.4	4.8	-66.7	-0.016	0.017	0.037
		M	-3.0	3.6	-1.6	4.9	-18.9	-0.006	0.018	
		R	1.3	10.9	-1.4	11.1	-7.4	-0.005	0.040	
	41.0	L	-32.2	-2.0	-12.3	34.6	-20.9	-0.012	0.034	
		M	11.0	-6.2	-10.5	16.4	-39.7	-0.010	0.016	
		R	-12.1	17.6	3.5	21.7	9.2	0.003	0.021	
45	21.5	L	2.6	-9.8	-4.7	11.2	-24.9	-0.017	0.040	0.037
		M	0.9	-3.2	-2.4	4.1	-35.7	-0.008	0.015	
		R	4.2	-0.7	0.2	4.2	2.1	0.001	0.015	
	41.1	L	-7.1	-14.4	-7.7	17.8	-25.6	-0.007	0.017	
		M	32.2	6.4	5.5	33.3	9.5	0.005	0.032	
		R	11.4	20.7	18.7	30.1	38.5	0.018	0.029	
67.5	20.1	L	-3.3	1.0	-3.1	4.6	-42.2	-0.013	0.019	0.037
		M	-3.8	1.1	-2.1	4.5	-27.7	-0.008	0.018	
		R	-1.3	-4.0	-0.9	4.3	-11.8	-0.004	0.017	
	41.0	L	-29.0	11.6	-3.9	31.5	-7.1	-0.004	0.031	
		M	15.6	1.7	3.5	16.0	12.5	0.003	0.016	
		R	-8.0	-30.0	13.0	33.6	22.8	0.013	0.033	
90	21.4	L	-1.9	-1.3	-3.5	4.1	-56.6	-0.012	0.015	0.037
		M	1.0	3.6	-0.9	3.8	-14.2	-0.003	0.014	
		R	0.0	-2.1	-0.7	2.2	-18.1	-0.002	0.008	
	41.0	L	-20.4	-2.4	-2.5	20.7	-7.0	-0.002	0.020	
		M	37.8	12.3	5.7	40.2	8.2	0.006	0.039	
		R	-0.8	-35.5	12.6	37.7	19.5	0.012	0.037	

Table A-4. Comparison of measured forces versus ASTM D7158 predicted uplift results for Partially Sealed Laminate Specimen 1

Wind Azimuth (°)	Mean Wind Speed (m/s)	Measurement Location	Mean Distributed Loads (N/m)			Total Resultant Distributed Load	Vertical Load Angle (°)	Force Coefficients		
			F <sub>x</sub>	F <sub>y</sub>	F <sub>z</sub>			Uplift	Total	Predicted
0	21.1	L	--	--	--	--	--	--	--	0.037
		M	-3.0	-0.9	-0.2	3.1	-4.1	-0.001	0.011	
		R	4.6	-0.7	-10.0	11.0	-65.2	-0.037	0.041	
	41.1	L	--	--	--	--	--	--	--	
		M	-33.8	8.4	5.7	35.3	9.3	0.005	0.034	
		R	-29.1	3.0	9.5	30.7	18.1	0.009	0.030	
22.5	20.3	L	--	--	--	--	--	--	--	0.037
		M	-3.8	-9.6	-1.0	10.4	-5.5	-0.004	0.041	
		R	-6.3	-4.2	-1.5	7.7	-11.6	-0.006	0.031	
	40.5	L	--	--	--	--	--	--	--	
		M	-30.1	15.5	6.3	34.5	10.6	0.006	0.034	
		R	-40.4	13.5	25.2	49.5	30.6	0.025	0.050	
45	20.7	L	--	--	--	--	--	--	--	0.037
		M	-0.8	-4.0	2.3	4.7	29.8	0.009	0.018	
		R	-0.5	3.7	-0.1	3.7	-1.2	0.000	0.014	
	41.0	L	--	--	--	--	--	--	--	
		M	15.1	4.8	0.2	15.9	0.7	0.000	0.015	
		R	5.2	24.8	16.1	30.0	32.5	0.016	0.029	
67.5	21.0	L	--	--	--	--	--	--	--	0.037
		M	-28.8	10.8	-9.2	32.1	-16.6	-0.034	0.119	
		R	7.4	-1.2	-8.6	11.4	-48.9	-0.032	0.043	
	41.0	L	--	--	--	--	--	--	--	
		M	-21.8	-20.6	9.6	31.5	17.7	0.009	0.031	
		R	15.5	1.7	13.0	20.3	39.8	0.013	0.020	
90	21.5	L	--	--	--	--	--	--	--	0.037
		M	18.9	6.7	-18.9	27.5	-43.3	-0.067	0.097	
		R	12.5	-2.0	-20.5	24.1	-58.2	-0.073	0.085	
	41.0	L	--	--	--	--	--	--	--	
		M	-22.7	-3.6	16.2	28.2	35.1	0.016	0.027	
		R	-0.3	-12.5	8.9	15.3	35.6	0.009	0.015	

**Table A-5. Comparison of measured forces versus ASTM D7158 predicted uplift results for Partially Sealed Laminate Specimen 2**

Wind Azimuth (°)	Mean Wind Speed (m/s)	Measurement Location	Mean Distributed Loads (N/m)			Total Resultant Distributed Load	Vertical Load Angle (°)	Force Coefficients		
			F <sub>x</sub>	F <sub>y</sub>	F <sub>z</sub>			Uplift	Total	Predicted
0	21.3	L	--	--	--	--	--	--	--	0.037
		M	1.1	-2.2	-4.5	5.1	-61.2	-0.016	0.018	
		R	-1.1	-3.5	-2.2	4.3	-30.7	-0.008	0.016	
	41.1	L	--	--	--	--	--	--	--	
		M	-17.1	-1.0	-4.6	17.8	-15.1	-0.004	0.017	
		R	-26.4	-21.1	10.7	35.4	17.6	0.010	0.034	
22.5	21.3	L	--	--	--	--	--	--	0.037	
		M	-5.4	-2.0	3.6	6.8	31.6	0.013		0.024
		R	-7.0	0.7	7.9	10.6	48.5	0.029		0.038
	41.0	L	--	--	--	--	--	--		--
		M	-52.0	30.7	1.0	60.4	0.9	0.001		0.059
		R	-49.5	14.5	21.6	56.0	22.7	0.021		0.055
45	21.2	L	--	--	--	--	--	--	0.037	
		M	-5.3	-0.4	0.9	5.4	10.1	0.003		0.020
		R	3.4	7.3	1.7	8.2	12.0	0.006		0.030
	41.0	L	--	--	--	--	--	--		--
		M	-10.2	23.1	5.4	25.9	12.1	0.005		0.025
		R	-32.2	-11.3	16.4	37.9	25.7	0.016		0.037
67.5	20.6	L	--	--	--	--	--	--	0.037	
		M	-10.7	8.0	-8.8	16.0	-33.4	-0.034		0.062
		R	-0.3	-5.0	-7.9	9.4	-57.6	-0.031		0.036
	41.0	L	--	--	--	--	--	--		--
		M	-22.1	0.7	6.4	23.0	16.2	0.006		0.022
		R	-26.2	-4.7	15.5	30.8	30.3	0.015		0.030
90	21.0	L	--	--	--	--	--	--	0.037	
		M	5.1	8.5	-18.8	21.2	-62.3	-0.070		0.079
		R	19.0	-10.0	-19.9	29.3	-42.9	-0.074		0.109
	41.0	L	--	--	--	--	--	--		--
		M	-35.8	30.4	9.4	47.9	11.3	0.009		0.046
		R	-33.5	-33.3	11.2	48.5	13.4	0.011		0.047

**Table A-6. Comparison of measured forces versus ASTM D7158 predicted uplift results for Partially Sealed Laminate Specimen 3**

Wind Azimuth (°)	Mean Wind Speed (m/s)	Measurement Location	Mean Distributed Loads (N/m)			Total Resultant Distributed Load	Vertical Load Angle (°)	Force Coefficients		
			Fx	Fy	Fz			Uplift	Total	Predicted
0	20.1	L	--	--	--	--	--	--	--	0.037
		M	-0.8	-0.9	-3.0	3.2	-67.5	-0.012	0.013	
		R	1.4	-8.1	-2.1	8.5	-14.6	-0.009	0.034	
	40.5	L	--	--	--	--	--	--	--	
		M	-40.4	16.5	-6.7	44.2	-8.7	-0.007	0.044	
		R	-27.1	-14.6	11.2	32.8	19.9	0.011	0.033	
22.5	20.9	L	--	--	--	--	--	--	0.037	
		M	-1.6	-1.0	-1.9	2.7	-44.4	-0.007		0.010
		R	0.7	-4.8	1.2	5.0	13.9	0.004		0.019
	41.0	L	--	--	--	--	--	--		--
		M	-35.0	16.8	2.5	38.9	3.7	0.002		0.038
		R	-26.1	3.6	25.7	36.8	44.3	0.025		0.036
45	21.2	L	--	--	--	--	--	--	0.037	
		M	-6.2	7.6	1.1	9.9	6.2	0.004		0.036
		R	0.0	-3.5	1.2	3.7	19.3	0.004		0.013
	41.0	L	--	--	--	--	--	--		--
		M	-18.2	16.0	5.7	24.9	13.3	0.006		0.024
		R	-15.0	10.7	14.8	23.6	38.8	0.014		0.023
67.5	21.0	L	--	--	--	--	--	--	0.037	
		M	-8.8	0.5	-11.4	14.4	-52.2	-0.042		0.053
		R	3.0	-15.9	-7.7	17.9	-25.6	-0.029		0.067
	41.0	L	--	--	--	--	--	--		--
		M	-16.4	8.3	4.7	19.0	14.2	0.005		0.018
		R	-10.7	-50.1	16.2	53.7	17.6	0.016		0.052
90	20.8	L	--	--	--	--	--	--	0.037	
		M	11.5	0.7	-19.1	22.4	-58.9	-0.072		0.084
		R	12.5	-2.0	-20.6	24.2	-58.4	-0.078		0.092
	41.0	L	--	--	--	--	--	--		--
		M	-9.9	4.0	4.2	11.5	21.6	0.004		0.011
		R	-4.1	-48.4	9.3	49.5	10.8	0.009		0.048

**Table A-7. Comparison of measured forces versus ASTM D7158 predicted uplift results for Fully Sealed Three-Tab Specimen 1**

Wind Azimuth (°)	Mean Wind Speed (m/s)	Measurement Location	Mean Distributed Loads (N/m)			Total Resultant Distributed Load	Vertical Load Angle (°)	Force Coefficients		
			F <sub>x</sub>	F <sub>y</sub>	F <sub>z</sub>			Uplift	Total	Predicted
0	21.0	L2	8.3	1.8	-2.3	8.8	-15.0	-0.008	0.033	0.022
		C1	4.3	-3.0	-3.0	6.0	-30.0	-0.004	0.008	
		C2	-0.3	3.1	-1.0	3.3	-18.5	-0.001	0.004	
	41.0	L2	11.6	37.8	-7.9	40.4	-11.3	-0.008	0.039	
		C1	-39.1	0.7	-7.4	39.8	-10.6	-0.003	0.014	
		C2	-47.4	33.1	3.4	57.9	3.4	0.001	0.021	
22.5	21.0	L2	0.6	1.2	-3.9	4.1	-71.1	-0.014	0.015	0.022
		C1	-1.4	3.7	-1.2	4.1	-17.6	-0.002	0.006	
		C2	-7.1	14.1	-0.7	15.8	-2.4	-0.001	0.021	
	41.0	L2	10.6	51.9	-16.1	55.3	-16.9	-0.016	0.054	
		C1	-62.7	6.6	-4.4	63.2	-4.0	-0.002	0.022	
		C2	-47.0	45.4	13.1	66.7	11.3	0.005	0.024	
45	21.0	L2	3.7	-2.3	-3.3	5.4	-37.4	-0.012	0.020	0.022
		C1	-7.2	4.0	-1.6	8.4	-11.1	-0.002	0.011	
		C2	-18.8	14.4	1.2	23.7	2.8	0.002	0.032	
	41.0	L2	35.1	24.2	-14.9	45.2	-19.3	-0.014	0.044	
		C1	-8.1	2.0	-9.1	12.3	-47.7	-0.003	0.004	
		C2	-46.9	37.5	11.6	61.1	11.0	0.004	0.022	
67.5	21.0	L2	7.4	-1.0	-4.2	8.6	-29.1	-0.015	0.032	0.022
		C1	-6.5	4.6	-3.6	8.8	-24.1	-0.005	0.012	
		C2	-16.5	3.7	-0.4	16.9	-1.2	0.000	0.023	
	41.0	L2	27.5	25.6	-19.0	42.1	-26.9	-0.018	0.041	
		C1	-11.3	13.9	-9.7	20.4	-28.4	-0.003	0.007	
		C2	-48.3	11.1	11.0	50.8	12.6	0.004	0.018	
90	21.0	L2	11.5	6.7	-6.5	14.8	-26.0	-0.024	0.055	0.022
		C1	-6.6	10.4	1.7	12.4	7.8	0.002	0.017	
		C2	-12.7	10.2	-2.4	16.5	-8.4	-0.003	0.022	
	41.0	L2	79.5	46.4	-15.5	93.3	-9.6	-0.015	0.091	
		C1	13.6	20.2	-1.5	24.4	-3.6	-0.001	0.009	
		C2	-50.7	9.8	10.5	52.7	11.4	0.004	0.019	

Table A-8. Comparison of measured forces versus ASTM D7158 predicted uplift results for Fully Sealed Three-Tab Specimen 2

Wind Azimuth (°)	Mean Wind Speed (m/s)	Measurement Location	Mean Distributed Loads (N/m)			Total Resultant Distributed Load	Vertical Load Angle (°)	Force Coefficients		
			F <sub>x</sub>	F <sub>y</sub>	F <sub>z</sub>			Uplift	Total	Predicted
0	21.0	L2	26.0	10.3	-3.8	28.2	-7.7	-0.014	0.104	0.022
		C1	-0.8	-11.6	-5.9	13.0	-26.9	-0.008	0.018	
		C2	-2.7	-6.1	3.4	7.5	27.5	0.005	0.010	
	41.5	L2	51.6	29.3	-12.9	60.7	-12.3	-0.012	0.057	
		C1	-9.5	-29.3	-28.2	41.8	-42.5	-0.010	0.014	
		C2	-35.6	-31.2	14.0	49.3	16.5	0.005	0.017	
22.5	21.4	L2	12.1	8.5	-4.2	15.4	-15.9	-0.015	0.055	0.022
		C1	-17.0	6.7	2.7	18.4	8.5	0.004	0.024	
		C2	-18.0	21.9	-0.8	28.3	-1.6	-0.001	0.037	
	40.9	L2	6.0	94.2	-20.2	96.6	-12.1	-0.020	0.094	
		C1	0.7	-8.2	-12.9	15.3	-57.6	-0.005	0.005	
		C2	-23.0	47.4	0.5	52.7	0.5	0.000	0.019	
45	21.3	L2	13.3	0.2	-5.2	14.3	-21.1	-0.019	0.052	0.022
		C1	10.5	-7.2	-0.6	12.7	-2.9	-0.001	0.017	
		C2	-9.7	13.5	2.6	16.8	9.0	0.003	0.022	
	40.9	L2	34.7	62.3	-21.5	74.5	-16.8	-0.021	0.073	
		C1	50.4	-9.4	-16.6	53.9	-17.9	-0.006	0.019	
		C2	-41.3	9.8	20.6	47.1	25.9	0.007	0.017	
67.5	20.9	L2	--	--	--	--	--	--	--	0.022
		C1	-3.3	7.6	3.1	8.9	20.4	0.004	0.012	
		C2	-3.6	14.8	-0.4	15.3	-1.6	-0.001	0.021	
	40.0	L2	33.2	60.2	-18.4	71.1	-15.0	-0.019	0.072	
		C1	25.5	-11.4	-4.2	28.3	-8.5	-0.002	0.011	
		C2	-37.6	5.9	21.8	43.8	29.8	0.008	0.016	
90	21.2	L2	--	--	--	--	--	--	--	0.022
		C1	-4.8	-0.7	0.7	4.9	8.0	0.001	0.007	
		C2	-27.2	4.8	5.7	28.2	11.7	0.008	0.038	
	39.8	L2	81.1	58.2	-16.3	101.2	-9.2	-0.017	0.104	
		C1	-7.2	-14.9	-11.6	20.2	-35.0	-0.004	0.008	
		C2	-103.8	-31.6	26.4	111.7	13.7	0.010	0.042	

**Table A-9. Comparison of measured forces versus ASTM D7158 predicted uplift results for Fully Sealed Three-Tab Specimen 3**

Wind Azimuth (°)	Mean Wind Speed (m/s)	Measurement Location	Mean Distributed Loads (N/m)			Total Resultant Distributed Load	Vertical Load Angle (°)	Force Coefficients		
			F <sub>x</sub>	F <sub>y</sub>	F <sub>z</sub>			Uplift	Total	Predicted
0	20.4	L2	-10.4	-5.7	0.1	11.9	0.4	0.000	0.046	0.022
		C1	--	--	--	--	--	--	--	
		C2	-7.3	1.0	1.8	7.5	13.6	0.003	0.011	
	38.0	L2	-9.4	-26.4	-7.4	29.0	-14.7	-0.008	0.033	
		C1	--	--	--	--	--	--	--	
		C2	-27.2	3.9	1.5	27.5	3.1	0.001	0.011	
22.5	20.0	L2	-13.8	-8.6	-1.7	16.3	-6.1	-0.007	0.066	0.022
		C1	--	--	--	--	--	--	--	
		C2	-11.7	4.2	4.6	13.3	20.2	0.007	0.020	
	36.8	L2	-24.5	-41.3	-13.1	49.8	-15.2	-0.016	0.060	
		C1	--	--	--	--	--	--	--	
		C2	-74.9	-3.0	25.6	79.2	18.9	0.011	0.035	
45	19.0	L2	-12.4	-1.1	-3.3	12.9	-14.9	-0.015	0.058	0.022
		C1	--	--	--	--	--	--	--	
		C2	-14.3	10.5	3.1	18.0	10.0	0.005	0.030	
	37.3	L2	0.0	-5.9	-10.5	12.1	-60.6	-0.012	0.014	
		C1	--	--	--	--	--	--	--	
		C2	-58.2	24.1	14.4	64.6	12.9	0.006	0.028	
67.5	19.6	L2	-34.3	-8.4	1.6	35.3	2.6	0.007	0.149	0.022
		C1	--	--	--	--	--	--	--	
		C2	-34.7	13.1	2.9	37.2	4.5	0.005	0.058	
	38.2	L2	-19.4	-15.4	-11.0	27.1	-23.9	-0.012	0.030	
		C1	--	--	--	--	--	--	--	
		C2	-63.9	-10.4	30.9	71.7	25.5	0.013	0.029	
90	19.6	L2	-12.2	-1.2	-1.5	12.4	-6.8	-0.006	0.053	0.022
		C1	--	--	--	--	--	--	--	
		C2	-7.2	-0.6	1.4	7.3	10.8	0.002	0.011	
	38.6	L2	20.2	-38.0	-15.2	45.6	-19.4	-0.017	0.050	
		C1	--	--	--	--	--	--	--	
		C2	-47.4	-33.6	23.7	62.7	22.1	0.009	0.025	

Table A-10. Comparison of measured forces versus ASTM D7158 predicted uplift results for Partially Sealed Three-Tab Specimen 1

Wind Azimuth (°)	Mean Wind Speed (m/s)	Measurement Location	Mean Distributed Loads (N/m)			Total Resultant Distributed Load	Vertical Load Angle (°)	Force Coefficients		
			F <sub>x</sub>	F <sub>y</sub>	F <sub>z</sub>			Uplift	Total	Predicted
0	19.8	L2	0.2	6.9	-2.4	7.3	-18.9	-0.010	0.030	0.022
		C1	--	--	--	--	--	--	--	
		C2	-25.4	-23.9	4.1	35.1	6.8	0.006	0.054	
	38.0	L2	-9.6	-1.2	1.6	9.8	9.1	0.002	0.011	
		C1	--	--	--	--	--	--	--	
		C2	-95.0	-62.1	21.0	115.4	10.5	0.009	0.048	
22.5	19.3	L2	18.6	12.8	-1.7	22.6	-4.3	-0.007	0.099	0.022
		C1	--	--	--	--	--	--	--	
		C2	-16.6	-21.4	6.8	27.9	14.0	0.011	0.045	
	37.5	L2	10.7	29.8	-4.4	31.9	-7.9	-0.005	0.037	
		C1	--	--	--	--	--	--	--	
		C2	-92.7	-38.4	29.6	104.6	16.5	0.013	0.044	
45	19.0	L2	9.6	19.4	-3.9	22.0	-10.1	-0.017	0.099	0.022
		C1	--	--	--	--	--	--	--	
		C2	-9.0	-14.4	6.7	18.2	21.6	0.011	0.030	
	38.0	L2	--	--	--	--	--	--	--	
		C1	--	--	--	--	--	--	--	
		C2	-105.7	-41.1	95.3	148.1	40.0	0.039	0.061	
67.5	19.0	L2	2.2	12.5	-3.2	13.1	-14.3	-0.015	0.059	0.022
		C1	--	--	--	--	--	--	--	
		C2	-20.3	-2.4	5.6	21.2	15.2	0.009	0.035	
	38.0	L2	136.4	44.5	-18.5	144.7	-7.3	-0.021	0.163	
		C1	--	--	--	--	--	--	--	
		C2	-75.0	-11.3	57.9	95.4	37.4	0.024	0.039	
90	19.0	L2	40.9	19.5	-5.6	45.7	-7.0	-0.025	0.206	0.022
		C1	--	--	--	--	--	--	--	
		C2	-39.8	-35.4	21.0	57.3	21.5	0.035	0.095	
	38.0	L2	161.2	58.3	-10.5	171.8	-3.5	-0.012	0.194	
		C1	--	--	--	--	--	--	--	
		C2	-28.9	114.8	49.1	128.2	22.5	0.020	0.053	

**Table A-11. Comparison of measured forces versus ASTM D7158 predicted uplift results for Partially Sealed Three-Tab Specimen 2**

Wind Azimuth (°)	Mean Wind Speed (m/s)	Measurement Location	Mean Distributed Loads (N/m)			Total Resultant Distributed Load	Vertical Load Angle (°)	Force Coefficients		
			F <sub>x</sub>	F <sub>y</sub>	F <sub>z</sub>			Uplift	Total	Predicted
0	19.0	L2	--	--	--	--	--	--	--	0.022
		C1	--	--	--	--	--	--	--	
		C2	-13.8	1.0	2.5	14.1	10.3	0.004	0.023	
	38.0	L2	--	--	--	--	--	--	--	
		C1	--	--	--	--	--	--	--	
		C2	-56.4	-15.0	21.3	62.1	20.1	0.009	0.026	
22.5	19.0	L2	--	--	--	--	--	--	--	0.022
		C1	--	--	--	--	--	--	--	
		C2	-27.0	4.1	20.4	34.1	36.8	0.034	0.056	
	38.0	L2	--	--	--	--	--	--	--	
		C1	--	--	--	--	--	--	--	
		C2	-114.3	-2.8	40.1	121.1	19.3	0.017	0.050	
45	19.0	L2	--	--	--	--	--	--	--	0.022
		C1	--	--	--	--	--	--	--	
		C2	-28.7	-13.0	17.1	35.9	28.5	0.028	0.059	
	38.0	L2	--	--	--	--	--	--	--	
		C1	--	--	--	--	--	--	--	
		C2	-91.7	3.6	48.2	103.6	27.7	0.020	0.043	
67.5	19.0	L2	--	--	--	--	--	--	--	0.022
		C1	--	--	--	--	--	--	--	
		C2	-33.4	6.8	15.3	37.4	24.1	0.025	0.062	
	38.0	L2	--	--	--	--	--	--	--	
		C1	--	--	--	--	--	--	--	
		C2	-108.0	6.1	52.8	120.4	26.0	0.022	0.050	
90	19.0	L2	--	--	--	--	--	--	--	0.022
		C1	--	--	--	--	--	--	--	
		C2	-44.2	-35.9	17.8	59.6	17.4	0.029	0.099	
	38.0	L2	--	--	--	--	--	--	--	
		C1	--	--	--	--	--	--	--	
		C2	-103.1	-27.6	47.5	116.8	24.0	0.020	0.048	

**Table A-12. Comparison of measured forces versus ASTM D7158 predicted uplift results for Partially Sealed Three-Tab Specimen 3**

Wind Azimuth (°)	Mean Wind Speed (m/s)	Measurement Location	Mean Distributed Loads (N/m)			Total Resultant Distributed Load	Vertical Load Angle (°)	Force Coefficients		
			F <sub>x</sub>	F <sub>y</sub>	F <sub>z</sub>			Uplift	Total	Predicted
0	19.0	L2	7.2	1.9	4.8	8.8	32.6	0.022	0.040	0.022
		C1	--	--	--	--	--	--	--	
		C2	-16.9	-7.8	4.2	19.1	12.7	0.007	0.032	
	38.0	L2	-6.4	78.8	-6.9	79.3	-5.0	-0.008	0.090	
		C1	--	--	--	--	--	--	--	
		C2	-48.7	8.2	31.9	58.8	32.9	0.013	0.024	
22.5	18.8	L2	1.7	15.3	-3.4	15.7	-12.3	-0.015	0.073	0.022
		C1	--	--	--	--	--	--	--	
		C2	-12.2	-1.8	15.5	19.8	51.5	0.026	0.033	
	38.3	L2	-12.6	76.2	-16.9	79.0	-12.3	-0.019	0.088	
		C1	--	--	--	--	--	--	--	
		C2	-84.8	-15.0	39.9	94.9	24.9	0.016	0.039	
45	18.0	L2	7.2	37.3	-5.1	38.4	-7.7	-0.026	0.193	0.022
		C1	--	--	--	--	--	--	--	
		C2	-16.7	0.7	11.8	20.5	35.3	0.022	0.038	
	36.8	L2	82.0	98.4	-13.4	128.8	-6.0	-0.016	0.155	
		C1	--	--	--	--	--	--	--	
		C2	-56.2	-30.3	43.2	77.1	34.1	0.019	0.034	
67.5	19.0	L2	19.4	38.7	-6.2	43.7	-8.2	-0.028	0.197	0.022
		C1	--	--	--	--	--	--	--	
		C2	-17.6	8.5	10.3	22.1	27.8	0.017	0.037	
	38.0	L2	77.4	59.1	-12.2	98.2	-7.1	-0.014	0.111	
		C1	--	--	--	--	--	--	--	
		C2	-79.0	-62.9	37.5	107.7	20.4	0.015	0.045	
90	19.0	L2	22.2	35.4	-2.9	41.9	-4.0	-0.013	0.189	0.022
		C1	--	--	--	--	--	--	--	
		C2	-20.9	-3.6	9.9	23.4	25.0	0.016	0.039	
	38.0	L2	57.0	23.7	-5.4	62.0	-5.0	-0.006	0.070	
		C1	--	--	--	--	--	--	--	
		C2	-93.5	-71.8	38.7	124.1	18.2	0.016	0.051	



**APPENDIX B. APPRAISAL OF ROOF SPECIMENS TESTED IN THE IBHS  
RESEARCH CENTER**

**Table B-1. Estimated Roof Costs for LAM-201 - Roof 1 (Gable) - Miami, FL**

Description	Quantity	Quantity Unit	Unit Cost (\$USD)	Total Line Cost (\$USD)
Rofer	2	H	\$97.82	\$195.64
Roofing - General Laborer	2	H	\$30.62	\$61.24
Roof Cement, Nails & Use of Hand Tools	1	LS	\$25.00	\$25.00

Total = \$281.88

**Table B-2. Estimated Roof Costs for LAM-201 - Roof 2 (Gable) - Miami, FL**

Description	Quantity	Quantity Unit	Unit Cost (\$USD)	Total Line Cost (\$USD)
Rofer	1	H	\$97.82	\$97.82
Roofing - General Laborer	1	H	\$30.62	\$30.62

Total = \$128.44

**Table B-3. Estimated Roof Costs for LAM-201 - Roof 3 (Gable) - Miami, FL**

Description	Quantity	Quantity Unit	Unit Cost (\$USD)	Total Line Cost (\$USD)
No Repairs Required				

Total = \$0.00

**Table B-4. Estimated Roof Costs for LAM-201 - Roof 4 (Hip) - Miami, FL**

Description	Quantity	Quantity Unit	Unit Cost (\$USD)	Total Line Cost (\$USD)
Remove and Replace Ridge Cap - High Profile	52	LF	\$8.01	\$416.52
Rofer	1	H	\$97.82	\$97.82
Roofing - General Laborer	1	H	\$30.62	\$30.62
Roofing Cement/Hand Tools	1	LS	\$15.00	\$15.00
Haul debris - Per Pickup Truck Load - Including Dump Fees	1	EA	\$137.19	\$137.19

Total = \$697.15

**Table B-5. Estimated Roof Costs for LAM-201 - Roof 5 (Hip) - Miami, FL**

Description	Quantity	Quantity Unit	Unit Cost (\$USD)	Total Line Cost (\$USD)
Remove and Replace Ridge Cap - High Profile	52	LF	\$8.01	\$416.52
Haul debris - Per Pickup Truck Load - Including Dump Fees	1	EA	\$137.19	\$137.19

Total = \$553.71

**Table B-6. Estimated Roof Costs for LAM-201 - Roof 6 (Hip) - Miami, FL**

Description	Quantity	Quantity Unit	Unit Cost (\$USD)	Total Line Cost (\$USD)
Remove and Replace Ridge Cap - High Profile	52	LF	\$8.01	\$416.52
(Material Only) Laminated Shingles w/Felt <sup>a</sup>	1	SQ	\$108.60	\$108.60
Rofer	8	H	\$97.82	\$782.56
Roofing - General Laborer	8	H	\$30.62	\$244.96
Haul debris - Per Pickup Truck Load - Including Dump Fees	1	EA	\$137.19	\$137.19

Total = \$1,689.83

<sup>a</sup>The nature of the body shingle repair could go either way. It could be an expensive repair including the time to procure the best match shingles or could be argued for replacement of that slope especially if the slope was in a high visibility area.

**Table B-7. Estimated Roof Costs for LAM-202 - Roof 1 (Gable) - Miami, FL**

Description	Quantity	Quantity Unit	Unit Cost (\$USD)	Total Line Cost (\$USD)
Rofer	2	H	\$97.82	\$195.64
Roofing - General Laborer	2	H	\$30.62	\$61.24
Roof Cement, Nails & Use of Hand Tools	1	LS	\$50.00	\$50.00

Total = \$306.88

**Table B-8. Estimated Roof Costs for LAM-202 - Roof 2 (Gable) - Miami, FL**

Description	Quantity	Quantity Unit	Unit Cost (\$USD)	Total Line Cost (\$USD)
Roofer	2	H	\$97.82	\$195.64
Roofing - General Laborer	2	H	\$30.62	\$61.24
Roof Cement, Nails & Use of Hand Tools	1	LS	\$50.00	\$50.00

Total = \$306.88

**Table B-9. Estimated Roof Costs for LAM-202 - Roof 3 (Gable) - Miami, FL**

Description	Quantity	Quantity Unit	Unit Cost (\$USD)	Total Line Cost (\$USD)
Roofer	2	H	\$97.82	\$195.64
Roofing - General Laborer	2	H	\$30.62	\$61.24
Roof Cement, Nails & Use of Hand Tools	1	LS	\$50.00	\$50.00

Total = \$306.88

**Table B-10. Estimated Roof Costs for LAM-202 - Roof 4 (Hip) - Miami, FL**

Description	Quantity	Quantity Unit	Unit Cost (\$USD)	Total Line Cost (\$USD)
Remove and Replace Ridge Cap - High Profile	52	LF	\$8.01	\$416.52
Roofer	2	H	\$97.82	\$195.64
Roofing - General Laborer	2	H	\$30.62	\$61.24
Roofing Cement/Hand Tools	1	LS	\$50.00	\$50.00
Haul debris - Per Pickup Truck Load - Including Dump Fees	1	EA	\$137.19	\$137.19

Total = \$860.59

**Table B-11. Estimated Roof Costs for LAM-202 - Roof 5 (Hip) - Miami, FL**

Description	Quantity	Quantity Unit	Unit Cost (\$USD)	Total Line Cost (\$USD)
Remove and Replace Ridge Cap - High Profile	52	LF	\$8.01	\$416.52
Roofer	2	H	\$97.82	\$195.64
Roofing - General Laborer	2	H	\$30.62	\$61.24
Roofing Cement/Hand Tools	1	LS	\$50.00	\$50.00
Haul debris - Per Pickup Truck Load - Including Dump Fees	1	EA	\$137.19	\$137.19

Total = \$860.59

**Table B-12. Estimated Roof Costs for LAM-202 - Roof 6 (Hip) - Miami, FL**

Description	Quantity	Quantity Unit	Unit Cost (\$USD)	Total Line Cost (\$USD)
Remove and Replace Ridge Cap - High Profile	52	LF	\$8.01	\$416.52
Roofer	2	H	\$97.82	\$195.64
Roofing - General Laborer	2	H	\$30.62	\$61.24
Roofing Cement/Hand Tools	1	LS	\$50.00	\$50.00
Haul debris - Per Pickup Truck Load - Including Dump Fees	1	EA	\$137.19	\$137.19

Total = \$860.59

**Table B-1347. Estimated Roof Costs for TT-201 - Roof 1 (Gable) - Miami, FL**

Description	Quantity	Quantity Unit	Unit Cost (\$USD)	Total Line Cost (\$USD)
3-Tab - 25 Yr. Shingle Roofing - w/o Felt	8	SQ	\$253.29	\$2026.32
Remove 3-Tab - 25 Yr. Shingle Roofing - Including Felt	7.15	SQ	\$51.03	\$364.86
Roofing Felt	8	SQ	\$34.75	\$278.00
Remove & Replace Drip Edge	50	LF	\$2.24	\$112.00

Total = \$2781.18

**Table B-14. Estimated Roof Costs for TT-201 – Roof 2 (Gable) – Miami, FL**

Description	Quantity	Quantity Unit	Unit Cost (\$USD)	Total Line Cost (\$USD)
3-Tab – 25 Yr. Shingle Roofing – w/o Felt	8	SQ	\$253.29	\$2026.32
Remove 3-Tab – 25 Yr. Shingle Roofing – Including Felt	7.15	SQ	\$51.03	\$364.86
Roofing Felt	8	SQ	\$34.75	\$278.00
Remove & Replace Drip Edge	50	LF	\$2.24	\$112.00

Total = \$2781.18

**Table B-15. Estimated Roof Costs for TT-201 – Roof 3 (Gable) – Miami, FL**

Description	Quantity	Quantity Unit	Unit Cost (\$USD)	Total Line Cost (\$USD)
3-Tab – 25 Yr. Shingle Roofing – w/o Felt	8	SQ	\$253.29	\$2026.32
Remove 3-Tab – 25 Yr. Shingle Roofing – Including Felt	7.15	SQ	\$51.03	\$364.86
Roofing Felt	8	SQ	\$34.75	\$278.00
Remove & Replace Drip Edge	50	LF	\$2.24	\$112.00

Total = \$2781.18

**Table B-16. Estimated Roof Costs for TT-201 – Roof 4 (Hip) – Miami, FL**

Description	Quantity	Quantity Unit	Unit Cost (\$USD)	Total Line Cost (\$USD)
3-Tab – 25 Yr. Shingle Roofing – w/o Felt	8	SQ	\$253.29	\$2026.32
Remove 3-Tab – 25 Yr. Shingle Roofing – Including Felt	6.67	SQ	\$51.03	\$340.37
Remove and Replace Ridge Cap – Composition Shingles	52	LF	\$6.78	\$352.56
Roofing Felt	8	SQ	\$34.75	\$278.00
Remove & Replace Drip Edge	50	LF	\$2.24	\$112.00

Total = \$3109.25

**Table B-17. Estimated Roof Costs for TT-201 - Roof 5 (Hip) - Miami, FL**

Description	Quantity	Quantity Unit	Unit Cost (\$USD)	Total Line Cost (\$USD)
3-Tab - 25 Yr. Shingle Roofing - w/o Felt	8	SQ	\$253.29	\$2026.32
Remove 3-Tab - 25 Yr. Shingle Roofing - Including Felt	6.67	SQ	\$51.03	\$340.37
Remove and Replace Ridge Cap - Composition Shingles	52	LF	\$6.78	\$352.56
Roofing Felt	8	SQ	\$34.75	\$278.00
Remove & Replace Drip Edge	50	LF	\$2.24	\$112.00

Total = \$3109.25





**Southeast Region Research Initiative**

National Security Directorate

P.O. Box 6242

Oak Ridge National Laboratory

Oak Ridge, TN 37831-6252

[www.serri.org](http://www.serri.org)